

AN ABSTRACT OF THE DISSERTATION OF

Kyung Ho Lee for the degree of Doctor of Philosophy in Civil Engineering presented on September 10, 2004.

Title: Site-Specific Load Models and Hazards for Probability-Based Design

Abstract approved:



David V. Rosowsky

Structural design codes have evolved continuously since modern codes were established. The allowable stress design format has been widely used since the late 19th century. During the past two decades, probability-based limit states design concepts have evolved and are increasingly being used for various material and structural types. Limit state design, such as LRFD in the U.S., has requirements to ensure that structures perform satisfactorily under various loads and load combinations and that properly designed structures have reliable and consistent safety levels. Performance-based design concepts recently have gained interest among designers and researchers as an alternative to traditional (strength) design procedures. Performance-based engineering procedures require reliable predictions of structural response in order to quantify and limit damage to acceptable levels during the service-life of the structure.

The objective of this study is to develop new contributions in performance-based design of engineered woodframe structures. Specially, fragility curves are developed for

structures subjected to various natural hazards (and combinations of hazards) and new site-specific snow load models and hazard models are developed for use in probabilistic design.

To accomplish these objectives, fragility curves are developed for assessing probabilistic response of engineered woodframe structures under wind, snow and earthquake hazards. The fragility curves developed herein can be used to develop performance-based design guidelines for woodframe structures built in high hazard regions as well as to provide information on which to base structural safety or expected structural (and economic loss) assessments. Probabilistic snow load models and snow hazard curves also are developed in this study. Updated snow load models can be used in code calibration studies and in the development of next-generation partial safety factors. The snow hazard curves can be used in a number of reliability-based design and performance-based design applications including assessment of partial safety factors for limit states design, evaluation of load combinations (coincidence) factors considering multiple hazards, evaluation of failure probabilities (by convolving with fragility curves for different performance levels, and development of risk-based assessment procedures for structures (and inventories of structures) under extreme snow loading.

©Copyright by Kyung Ho Lee

September 10, 2004

All Rights Reserved

Site-Specific Load Models and Hazards for Probability-Based Design

by
Kyung Ho Lee

A DISSERTATION

Submitted to

Oregon State University

in partial fulfillment of
the requirement for the
degree of

Doctor of Philosophy

Presented September 10, 2004

Commencement June 2005

Doctor of Philosophy dissertation of Kyung Ho Lee
presented on September 10, 2004.

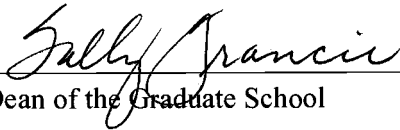
APPROVED:



Major Professor, representing Civil Engineering

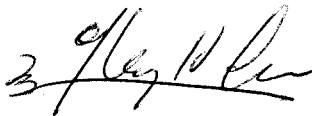


Head of the Department of Civil, Construction and Environmental Engineering



Dean of the Graduate School

I understand that my dissertation will become part of the permanent collection of Oregon State University libraries. My signature below authorizes release of my dissertation to any reader upon request.



Kyung Ho Lee, Author

ACKNOWLEDGEMENTS

This research would not have been possible without the assistance from many people who gave me their support in different ways. To them I would like to convey my heartfelt gratitude and sincere appreciation.

It gives me great pleasure to acknowledge the guidance, suggestions, constructive criticism, encouragements, and financial assistance provided by my major professor, Dr. David Rosowsky. He will always be remembered as a key factor that geared my career towards this path. I also would like to thank my graduate committee members: Dr. Solomon Yim, Dr. Robert Leichti, Dr. Christopher Higgins, and Dr. Jack Higginbotham for their advice and help in completing my graduate program. Many thanks to the Structural Reliability Research Group members, especially Dr. Jun Hee Kim for his valuable assistance with running the computer programs, and the staff in department of Civil Engineering and department of Wood Science and Engineering for their assistance during my graduate program.

I am forever thankful and in debt to my parents, Jae Dal Lee and Min Ja Kim for their love, encouragement, support, and prayer. Also, I would like to thank my brother and sister, and their family for their love. Finally, I wish to thank my lovely wife, Young Mi, my cute daughter, Kay Sun, and my second child who prepares for the world in her mom, for their love, patience, encouragement, and prayer.

CONTRIBUTION OF AUTHORS

Dr. David V. Rosowsky assisted with the writing of Chapter 2, 3, 4, and 5. Dr. Jun Hee Kim assisted with running the structural analysis programs, CASHEW and SAWS, used in Chapter 3 and 5.

TABLE OF CONTENTS

	<u>Page</u>
1. Introduction.....	1
1.1 General.....	1
1.2 Scope and Objectives.....	5
1.3 Organization.....	6
2. Fragility Assessment for Roof Sheathing Failure in High Wind Regions.....	9
2.1 Abstract.....	9
2.2 Introduction.....	10
2.3 LRFD and PBD.....	11
2.4 Fragility Modeling.....	13
2.5 Fragility Model for Roof Sheathing Subjected to Wind Load.....	15
2.5.1 Description of Baseline Structures.....	15
2.5.2 Limit States.....	16
2.5.3 Uplift Capacity (Resistance) Statistics.....	17
2.5.4 Dead Load Statistics.....	18
2.5.5 Wind Load Statistics.....	18
2.5.6 Calculation of Probability of Failure for Individual Sheathing Panel.....	20
2.5.7 Calculation of Roof System Failure Probabilities.....	23
2.6 Results.....	24
2.7 Summary and Conclusions.....	27
2.8 References.....	29
3. Fragility Curves for Woodframe Structures Subjected to Lateral Wind Loads.....	42
3.1 Abstract.....	42

TABLE OF CONTENTS (continued)

	<u>Page</u>
3.2 Introduction.....	43
3.3 Structural Analysis.....	44
3.4 Wind Loads.....	46
3.5 Lateral Wind Fragilities.....	50
3.6 Compound Fragility.....	53
3.7 Summary and Conclusions.....	54
3.8 References.....	56
4. Site-Specific Snow Load Models and Hazard Curves for Probabilistic Design.....	70
4.1 Abstract.....	70
4.2 Introduction.....	71
4.3 Probabilistic Snow Load Model.....	73
4.3.1 Background.....	73
4.3.2 Ground Snow Load Data.....	75
4.3.3 Conversion Factors for Roof Snow Load.....	76
4.3.4 Updated Snow Load Models.....	78
4.4 Oregon Snow Hazard Curves.....	80
4.4.1 Background.....	80
4.4.2 Ground Snow Load Data for Oregon.....	82
4.4.3 Development of Design Ground Snow Load.....	83
4.4.4 Oregon Snow Hazard Curves.....	84
4.5 Summary and Conclusions.....	86
4.6 References.....	88

TABLE OF CONTENTS (continued)

	<u>Page</u>
5. Fragility Analysis of Woodframe Buildings Considering Combined Snow and Earthquake Loading.....	105
5.1 Abstract.....	105
5.2 Introduction.....	106
5.3 Sites Considered.....	108
5.4 Baseline Structures.....	108
5.5 Limit State Probability Calculation by Convolution Integrals.....	110
5.5.1 Limit State Probability Calculation Considering One Hazard.	111
5.5.2 Limit State Probability Calculation Considering Two Hazards.....	113
5.6 Probabilistic Description of Hazards.....	115
5.6.1 Seismic Hazards.....	115
5.6.2 Snow Hazards.....	117
5.7 Structural Analysis.....	120
5.8 Seismic Fragility Surface.....	122
5.9 Evaluation of Snow Load Combination (companion action) Factors...	123
5.10 Summary and Conclusions.....	125
5.11 References.....	128
6. Conclusions and Recommendations.....	142
6.1 Conclusions.....	143
6.2 Recommendations.....	145
Bibliography.....	146
Appendices.....	152

LIST OF APPENDICES

	<u>Page</u>
Appendix A.1 Dimension and panel layouts for other baseline structures.....	152
Appendix A.2 Summary of <i>GC</i> statistics for other baseline structures.....	157
Appendix A.3 Complementary fragility curves for other baseline structures...	162
Appendix B.1 Equivalent wind speed pushover curves for other buildings considering two different load directions.....	171
Appendix B.2 Lateral wind fragilities.....	173
Appendix B.3 Lognormal parameters for lateral wind fragilities determined by quick analysis.....	175
Appendix C.1 Complete results for design ground snow load curves for Oregon.....	177
Appendix C.2 Complete results for ground snow hazard curves for Oregon....	190
Appendix D.1 Plan and section views for Type B Structure.....	203
Appendix D.2 Comparisons of $F_r^{(Y=1,yr)}(x)$ and $F_r^{(Y=50,yr)}(x)$ with the fragility curves $F_r(x)$ in the case of Boston, MA.....	205

LIST OF FIGURES

<u>Figure</u>		<u>Page</u>
2.1	Dimensions and panel layout showing 4 panel locations, Structure Type 1.....	36
2.2	Fragilities for individual roof sheathing failure.....	37
2.3	Lognormal fitted roof system complementary fragilities.....	37
2.4	Comparison of roof system survivorship curves for different wind directions.....	38
2.5	Comparison of roof system survivorship curves for different damage levels.....	38
2.6	Comparison of roof system survivorship curves for different nail types.....	39
2.7	Comparison of roof system survivorship curves for different exposures.....	39
2.8	Comparison of roof system survivorship curves for different baseline structures.....	40
3.1(a)	Detailed wall configurations for Type-I house model.....	61
3.1(b)	Detailed wall configurations for Type-II house model.....	62
3.1(c)	Detailed wall configurations for Type-III house model.....	64
3.2	Pushover curves for Type-III building considering two different load directions.....	65
3.3	Equivalent wind speed pushover curves for Type-III building considering two different wind directions.....	65
3.4	Equivalent wind speed pushover curves considering random wind load.....	66

LIST OF FIGURES (continued)

<u>Figure</u>		<u>Page</u>
3.5	Lognormal-fitted fragility curves for different displacement limits.....	66
3.6	Fragility comparison with and without wind directionality factor.....	67
3.7	Comparison of fragilities using the simulation and the quick analysis..	67
3.8	Example of compound fragility curve.....	68
4.1	84 sites in the continental United States used to develop probabilistic snow load model.....	100
4.2	Lognormal probability paper showing fit of annual maximum ground snow load (Rapid City, SD).....	101
4.3	Lognormal probability paper showing fit of actual-to-nominal 50-year maximum roof snow load (Rapid City, SD).....	101
4.4	Composite statistics for actual-to-nominal 50-year maximum roof snow loads for different regions.....	102
4.5	NRCS and NCDC weather stations and county areas for Oregon snow loads.....	102
4.6	Design ground snow load curves for G-18.....	103
4.7	Ground snow hazard curves for G-18.....	103
5.1(a)	Plan and section views for Type A structure.....	134
5.1(b)	Detailed shearwall configurations for Type A structure.....	135
5.2	Determination of limit state probability (single hazard).....	136
5.3	Determination of limit state probability (two hazards).....	136
5.4	Marginal seismic hazard curves for different reference periods (Carbondale, IL).....	137

LIST OF FIGURES (continued)

<u>Figure</u>		<u>Page</u>
5.5	Marginal ground snow hazard curves for different reference periods (Carbondale, IL).....	137
5.6	Lognormal seismic fragility.....	138
5.7	Seismic fragilities considering various deterministic ground snow loads.....	138
5.8	Alternate presentation: Seismic fragility vs. ground snow load.....	139
5.9	Comparison of $F_r^{Y=1yr}(x)$ with $F_r(x)$	139
5.10	Seismic fragilities convolved with snow hazards.....	140
5.11	Snow load combination factors for determining additional seismic weight to use in seismic fragility analysis.....	140
5.12	Summary of snow load combination factors for determining additional seismic weight to use in seismic fragility analysis.....	141

LIST OF TABLES

<u>Table</u>		<u>Page</u>
2.1	Dimensions and characteristics of baseline houses.....	31
2.2	Summary of resistance statistics.....	31
2.3	Summary of wind load parameters statistics.....	32
2.4	Summary of GC_p statistics for Structure Type 1.....	33
2.5	Lognormal parameters for roof sheathing fragilities.....	34
3.1	Dimensions and construction details for baseline structures.....	58
3.2	Statistics for wind load parameters.....	59
3.3	Lognormal parameters for lateral wind fragilities determined by simulation.....	60
4.1	Statistics for annual maximum ground snow load.....	90
4.2	Statistics for 50-year maximum roof snow load.....	93
4.3	Composite statistics for 50-year maximum actual-to-nominal roof snow loads by geographic groupings.....	95
4.4	Distribution and parameters for Oregon snow hazard.....	96
5.1	Site information.....	131
5.2	Seismic hazard parameters.....	131
5.3	Statistics for annual maximum ground snow load.....	132
5.4	Ground snow hazard parameters.....	132
5.5	Comparison of limit states probabilities.....	133
5.6	Snow loads (in psf) for EQ+S.....	133

LIST OF APPENDIX FIGURES

<u>Figure</u>	<u>Page</u>
A.1(a) Dimensions and panel layouts, Structure Type 2.....	153
A.1(b) Dimensions and panel layouts, Structure Type 3.....	154
A.1(c) Dimensions and panel layouts, Structure Type 4.....	155
A.1(d) Dimensions and panel layouts, Structure Type 5.....	156
A.3.1(a) Comparison of roof sheathing survivorship curves for different wind directions (Structure Type 1 / Exposure C / 8d nail – 6 in./12in. spacing).....	163
A.3.1(b) Comparison of roof sheathing survivorship curves for different damage levels (Structure Type 1 / Exposure C / 8d nail – 6 in./12in. spacing).....	163
A.3.1(c) Comparison of roof sheathing survivorship curves for different nail types (Structure Type 1 / all possible wind directions).....	164
A.3.1(d) Comparison of roof sheathing survivorship curves for different exposures (Structure Type 1 / 6d nail – 6in./12in. spacing / all possible wind directions).....	164
A.3.2(a) Comparison of roof sheathing survivorship curves for different wind directions (Structure Type 2 / Exposure C / 8d nail – 6 in./12in. spacing).....	165
A.3.2(b) Comparison of roof sheathing survivorship curves for different damage level (Structure Type 2 / Exposure C / 8d nail – 6 in./12in. spacing).....	165
A.3.2(c) Comparison of roof sheathing survivorship curves for different nail types (Structure Type 2 / Exposure C / all possible wind directions)....	166
A.3.2(d) Comparison of roof sheathing survivorship curves for different exposures (Structure Type 2 / 8d nail – 6in./12in. spacing / all possible wind directions).....	166

LIST OF APPENDIX FIGURES (continued)

<u>Figure</u>	<u>Page</u>
A.3.3(a) Comparison of roof sheathing survivorship curves for different wind directions (Structure Type 3 / Exposure C / 8d nail – 6 in./12in. spacing).....	167
A.3.3(b) Comparison of roof sheathing survivorship curves for different damage level (Structure Type 3 / Exposure C / 8d nail – 6 in./12in. spacing).....	167
A.3.3(c) Comparison of roof sheathing survivorship curves for different nail types (Structure Type 3 / Exposure C / all possible wind directions)....	168
A.3.3(d) Comparison of roof sheathing survivorship curves for different exposures (Structure Type 3 / 8d nail – 6in./12in. spacing / all possible wind directions).....	168
A.3.4(a) Comparison of roof sheathing survivorship curves for different wind directions (Structure Type 4 / Exposure C / 8d nail – 6 in./12in. spacing).....	169
A.3.4(b) Comparison of roof sheathing survivorship curves for different damage level (Structure Type 4 / Exposure C / 8d nail – 6 in./12in. spacing).....	169
A.3.5(a) Comparison of roof sheathing survivorship curves for different wind directions (Structure Type 5 / Exposure C / 8d nail – 6 in./12in. spacing).....	170
A.3.5(b) Comparison of roof sheathing survivorship curves for different damage level (Structure Type 5 / Exposure C / 8d nail – 6 in./12in. spacing).....	170
B.1(a) Equivalent wind speed pushover curves for Type-I building considering two different load directions.....	172
B.1(b) Equivalent wind speed pushover curves for Type-II building considering two different load directions.....	172
B.2(a) Lateral wind fragility using the simulation [Exposure B, with directionality factor].....	174

LIST OF APPENDIX FIGURES (continued)

<u>Figure</u>	<u>Page</u>
B.2(b) Lateral wind load fragility using the simulation [Exposure C, without directionality factor].....	174
C.1(a) Design ground snow load curves for G-01.....	178
C.1(b) Design ground snow load curves for G-02.....	178
C.1(c) Design ground snow load curves for G-03.....	179
C.1(d) Design ground snow load curves for G-04 (North).....	179
C.1(e) Design ground snow load curves for G-04 (South).....	180
C.1(f) Design ground snow load curves for G-05.....	180
C.1(g) Design ground snow load curves for G-06.....	181
C.1(h) Design ground snow load curves for G-07.....	181
C.1(i) Design ground snow load curves for G-08.....	182
C.1(j) Design ground snow load curves for G-09.....	182
C.1(k) Design ground snow load curves for G-10.....	183
C.1(l) Design ground snow load curves for G-11 (Hood River County).....	183
C.1(m) Design ground snow load curves for G-11 (Rain Shadow – Northeast side of Mountain Hood only).....	184
C.1(n) Design ground snow load curves for G-12.....	184
C.1(o) Design ground snow load curves for G-13.....	185
C.1(p) Design ground snow load curves for G-14.....	185
C.1(q) Design ground snow load curves for G-15.....	186
C.1(r) Design ground snow load curves for G-16.....	186

LIST OF APPENDIX FIGURES (continued)

<u>Figure</u>		<u>Page</u>
C.1(s)	Design ground snow load curves for G-17.....	187
C.1(t)	Design ground snow load curves for G-18.....	187
C.1(u)	Design ground snow load curves for P-01.....	188
C.1(v)	Design ground snow load curves for P-02.....	188
C.1(w)	Design ground snow load curves for G-23.....	189
C.2(a)	Ground snow hazard curves for G-01.....	191
C.2(b)	Ground snow hazard curves for G-02.....	191
C.2(c)	Ground snow hazard curves for G-03.....	192
C.2(d)	Ground snow hazard curves for G-04 (North).....	192
C.2(e)	Ground snow hazard curves for G-04 (South).....	193
C.2(f)	Ground snow hazard curves for G-05.....	193
C.2(g)	Ground snow hazard curves for G-06.....	194
C.2(h)	Ground snow hazard curves for G-07.....	194
C.2(i)	Ground snow hazard curves for G-08.....	195
C.2(j)	Ground snow hazard curves for G-09.....	195
C.2(k)	Ground snow hazard curves for G-10.....	196
C.2(l)	Ground snow hazard curves for G-11 (Hood River County).....	196
C.2(m)	Ground snow hazard curves for G-11 (Rain Shadow – Northeast side of Mountain Hood only).....	197
C.2(n)	Ground snow hazard curves for G-12.....	197
C.2(o)	Ground snow hazard curves for G-13.....	198

LIST OF APPENDIX FIGURES (continued)

<u>Figure</u>		<u>Page</u>
C.2(p)	Ground snow hazard curves for G-14.....	198
C.2(q)	Ground snow hazard curves for G-15.....	199
C.2(r)	Ground snow hazard curves for G-16.....	199
C.2(s)	Ground snow hazard curves for G-17.....	200
C.2(t)	Ground snow hazard curves for G-18.....	200
C.2(u)	Ground snow hazard curves for P-01.....	201
C.2(v)	Ground snow hazard curves for P-02.....	201
C.2(w)	Ground snow hazard curves for G-23.....	202
D.1	Plan and section views for Type B Structure.....	204
D.2(a)	Comparison of $F_r^{Y=1yr}(x)$ with $F_r(x)$ [Type A building / Boston, MA / 2% drift limit].....	206
D.2(b)	Comparison of $F_r^{Y=50yr}(x)$ with $F_r(x)$ [Type A building / Boston, MA / 2% drift limit].....	206

LIST OF APPENDIX TABLES

<u>Table</u>		<u>Page</u>
A.2(a)	Summary of GC_p statistics for Structure Type 2.....	158
A.2(b)	Summary of GC_p statistics for Structure Type 3.....	159
A.2(c)	Summary of GC_p statistics for Structure Type 4.....	160
A.2(d)	Summary of GC_p statistics for Structure Type 5.....	161
B.3	Lognormal parameters for lateral wind fragilities determined by quick analysis.....	176

1. Introduction

1.1 General

In the Middle Ages, large structures (e.g., churches, towers, castles) were constructed by skilled craftsmen. The “margin of safety” was provided by comparison to other existing successful structures. The learning process was based on trial and error. Structural design codes have evolved continuously since the first modern structural design codes (expressed in terms of formulae and procedures) were established in the 19th century. Allowable stress design (ASD) has been widely used in structural design from the late 19th century. In ASD, elastically computed stresses resulting from specified working loads are checked to ensure that they do not exceed certain limiting stresses divided by a safety factor. Safety factors have declined more or less continuously during the past century, reflecting the increasing confidence of the civil engineering profession in its stress calculations as well as the quality of construction materials. While ASD is easy to use and is familiar to structural designers, allowable stress does not correspond to any distinct (or observable) state of structural performance or specific concern to the owner or occupants. In addition, ASD can not ensure reliable and consistent safety levels. During the past two decades, efforts to overcome these disadvantages of ASD have led to the development of probability-based limit states design procedures such as Load and Resistance Factor Design (LRFD).

Beginning with the general load requirements in ANSI Standard A58 [Galambos et al.,

1982; Ellingwood et al., 1982], probability-based limit states design (now called Load and Resistance Factor Design or LRFD in the U.S.) has developed and has been widely used since the 1980's. In the United States, the trend toward LRFD is embodied in the ASCE 7 load standard, which has contained load combinations for LRFD since its 1982 edition; the LRFD Specification for Steel Structures [AISC, 1994] since its 1986 edition, the AASHTO LRFD Bridge Design Code [AASHTO, 1998] since its 1994 edition, and most recently the AF&PA/ASCE Standard 16-95 [AF&PA, 1996] for engineered wood construction. Probability-based limit states design codes have requirements to ensure that structures perform satisfactorily under various loads or load combinations and that structures have reliable and consistent safety levels. Code provisions which include partial safety factors (load and resistance factors), specified limit states, and load combinations have been developed to achieve these requirements. A set of partial safety factors optimizes a limit state function to achieve a target reliability level. The development of probability-based limit states design requires the following basic information [Galambos et al., 1982; Ellingwood et al., 1982]: (1) procedures for computing reliability indices; (2) limit state functions; (3) probabilistic load models; (4) probabilistic resistance models; (5) target reliability levels. Ellingwood et al. (1980) introduced a reliability-based methodology and developed a set of partial safety factors for use with American National Standard A58, and these factors are still found in LRFD specifications. Probabilistic load models are essential components in reliability analyses as well as code calibration studies which form the basis for these reliability-based code provisions. However, current probabilistic load models for environmental loadings such as snow and wind loads were developed in the late 1970's and

have remained relatively unchanged despite developments in quantifying load effects, changes in nominal load values, and the availability of additional load data.

The main objective of structural design codes and standards is to protect (life) safety by preventing structural collapse or failure during rare events in a structure's lifetime. This objective has largely been achieved for buildings in the United States subjected to natural hazards such as hurricanes and earthquakes. However, recent disasters in the United States and elsewhere around the world have highlighted the social, political, and economic ramifications of the traditional objective of codes (to prevent structural collapse during rare events). Properly built structures can stand major earthquake and hurricanes without collapse; however the consequent economic losses and social disruptions are still unacceptable. Minor damage (for example, damage to nonstructural and secondary assemblies) can amount to significant economic losses. This has led to efforts to develop performance-based design procedures in which the structural system is designed to meet multiple specific criteria under given hazard levels. The objective of performance-based design is to obtain a more reliable prediction of structural response, quantifying and controlling the damage risk to an acceptable level during the service-lifetime of the structure [Moller et al., 2001]. The advantages of performance-based design must be made clear in order for performance-based design to be an accepted alternative to present design procedures. Although performance-based seismic design has advanced for some materials and structural types, such as steel and reinforced concrete buildings and bridges, its application to light-frame wood structures remains relatively unexplored, despite the fact

that the majority of single-family residential construction in the United States is woodframe. Since light-frame wood structures have a number of advantages (including construction cost and time, aesthetics, beauty, versatility, and so on), wood is the most common construction material used in light-frame structures in the United States.

A fragility can be defined as the conditional probability of failure of a structural member or system for a given set of input variables. Structural fragility models are essential components of probabilistic safety analysis and performance-based design. The development of appropriate and usable fragility models is necessary for the development of performance-based engineering concepts for woodframe structures designed to resist natural hazards. Recent studies have developed seismic fragility curves for woodframe buildings [Ellingwood et al., 2004; Rosowsky and Kim, 2002a,b]. The focus of these studies has been on fragility assessment of woodframe structures exposed to natural hazard (earthquake). While these and other studies have begun to develop performance-based design concepts for light-frame wood structures, there are a number of unexplored areas that remain to be studied including the development of fragility curves for woodframe structures subjected to high wind loads and fragility procedures for handling multiple hazards (e.g., snow + earthquake).

The objective of structural design is to ensure structures are capable of providing reasonable levels of protection to the public against various hazards (earthquake, flood, snow, hurricane, landslide, etc.). Performance-based design ensures that a properly

designed structure satisfies specific performance objectives when structure is subjected to an event at a specific hazard level. The performance objective is therefore the coupling of a hazard level with a performance level (such as immediate occupancy or life safety). In design for natural hazards, the great source of uncertainty often arises from the hazard itself. Hazard analysis is aimed at describing, in probabilistic terms, the inherent randomness in occurrence and magnitude of the demands on the structural system. This is displayed through a hazard curve. Hazard curves can be convolved with fragility curves to evaluate failure probabilities of the structural system. This convolution process forms the basis of a probabilistic safety assessment and can be used to develop risk-based management procedures for buildings and building inventories.

1.2 Scope and Objectives

The focus of this study is on low-rise engineered woodframe structures subjected to various natural hazards (wind, snow, and earthquake). Structures having characteristics (roof slope, square footage, construction materials, etc.) typical of single-family residential construction in the U.S. are considered.

The objective of this study is to develop new contributions in performance-based design of engineered woodframe structures. Specially, fragility curves are developed for structures subjected to various natural hazards (and combinations of hazards) and new site-specific snow load models and hazard models are developed for use in probabilistic design. To accomplish these objectives, fragility curves are developed for assessing probabilistic

response of engineered woodframe structures under wind, snow and earthquake hazards. The fragility curves developed herein can be used to develop performance-based design guidelines for woodframe structures built in high hazard regions as well as to provide information on which to base structural safety or expected structural (and economic loss) assessments. Probabilistic snow load models and snow hazard curves also are developed in this study. Updated snow load models can be used in code calibration studies and in the development of next-generation partial safety factors. The snow hazard curves can be used in a number of reliability-based design and performance-based design applications including assessment of partial safety factors for limit states design, evaluation of load combinations (coincidence) factors considering multiple hazards, evaluation of failure probabilities (by convolving with fragility curves for different performance levels, and development of risk-based assessment procedures for structures (and inventories of structures) under extreme snow loading.

1.3 Organization

This dissertation is composed of four manuscripts and a series of supporting appendices. The four papers have been submitted (with the dissertation author as the lead author) to peer-reviewed journals.

The first manuscript (Chapter 2), "Fragility Assessment of Roof Sheathing Failure in High Wind Regions," has been submitted to the journal *Engineering Structures*. This paper presents a fragility methodology to assess the performance of roof sheathing subjected to

uplift (suction) pressures in high wind regions. The second manuscript (Chapter 3), “Fragility Curves for Woodframe Structures Subjected to Lateral Wind Loads,” has been submitted to the journal *Wind & Structures*. This paper presents a procedure to develop lateral displacement fragility curves for woodframe structures subjected to lateral wind loads. The third manuscript (Chapter 4), “Site-Specific Snow Load Models and Hazard Curves for Probabilistic Design,” has been submitted to the journal *Natural Hazards Review*. This paper presents procedures to update regional probabilistic snow load models for reliability analyses and to develop design snow loads and snow hazard curves for special locations (such as mountains regions and gorges) using the state of Oregon as an example. The fourth manuscript (Chapter 5), “Fragility Analysis of Woodframe Buildings Considering Combined Snow and Earthquake Loading,” has been submitted to the journal *Structural Safety*. This paper presents a procedure to evaluate appropriate snow load combination (companion action) factors for use with nominal values provided by the current design load standard [ASCE 7, 2002] when snow load is being considered in a seismic fragility analysis.

The appended information is intended to supplement the manuscripts. Appendices A to D present additional results (figure and tables) for Chapters 2 to 5, respectively.

Fragility Assessment for Roof Sheathing Failure in High Wind Regions

Kyung Ho Lee

David V. Rosowsky

For Submission to *Engineering Structures*

Elsevier Science Ltd.

The Boulevard, Langford Lane, Kidlington

Oxford, OXON, OX5 1GB, England

2. Fragility Assessment for Roof Sheathing Failure in High Wind Regions

2.1 Abstract

This paper presents a fragility assessment for roof sheathing in light-frame construction built in high wind regions. A fragility methodology is developed to assess the performance of roof sheathing subjected to uplift (suction) pressures. The majority of single-family housing in the United States is woodframe construction. A review of the performance of woodframe buildings after recent hurricanes has showed that the majority of wind damage (insured losses) was the result of a breach in the building envelope. Loss of roof sheathing and broken windows result in water penetration causing extensive interior damage and associated property and contents losses. The aim of this study was to develop a fragility model for roof sheathing uplift using available fastener test data, recently developed wind load parameter statistics, and a code-based approach for evaluating pressures. Five baseline structures considering different roof shapes, geographic locations, nail types, and enclosure conditions were investigated using simulation and system reliability concepts. Fragilities and complementary fragilities (or survivorship curves) of roof sheathing removal considering different levels of damage are developed as a function of basic wind speed (3-sec gust wind speed at 33 ft (10 m) above the ground in open terrain). The fragility models presented in this paper can be used to develop performance-based design guidelines for woodframe structures as well as tools for condition assessment and loss estimation for use with the existing building inventory.

2.2 Introduction

The majority of single-family housing in the United States is woodframe construction. Woodframe buildings are among the most vulnerable structures to high wind hazards. A review of the performance of woodframe buildings following recent hurricanes has showed that the majority of wind damage and consequent insurance losses are the result of a breach in the building envelope. Water penetration through the building envelope and broken windows causes the majority of economic losses causing extensive interior damage as well as damage to contents. Hurricane Hugo (1989) cost insurance companies US\$5.4 billion, most of which was residential damage claims. Hurricane Andrew (1992) produced insured property losses estimated at US\$17.7 billion, hurricane Iniki (1992) caused US\$1.8 billion in damage. Damage due to hurricane Opal (1995) was close to US\$2.2 billion¹. Increased population growth in hurricane-prone regions, i.e. along the Southeast and Gulf coasts of the U.S. and Hawaii, likely will result in even greater losses in the future.

The main objective of design codes and standards is to protect public (life) safety by preventing structural collapse or failure during rare events in a building's lifetime. While this objective has largely been achieved for buildings in the U.S. subjected to hurricane windstorms, economic losses and social disruption related to hurricane events are still unacceptable. This has led to current trends toward a new design philosophy (called

¹ These estimates were obtained from the *Georgia Insurance Information Service* (www.giis.org) – (December, 2003)

performance-based design) in which the structural system is designed to meet specific performance criteria under different hazard levels [Ellingwood et al., 2004].

The basic concept of performance-based design is to design a structure so that it will perform in a specified manner when subjected to various loading scenarios. Therefore, designers can design structures capable of providing reasonable levels of protection against various hazard levels. Performance-based design will require more comprehensive and quantitative probability-based procedures for managing risk and uncertainty than are found in first-generation criteria such as LRFD [Ellingwood et al., 2004]. Fragility analysis procedures roof sheathing attachment can be used for both design and assessment of woodframe structures built in high wind regions. This paper presents a fragility methodology for assessing the response of roof sheathing subject to specified demands from extreme wind loading.

2.3 LRFD and PBD

Beginning with the general load requirements in ANSI Standard A58 [Galambos et al., 1982; Ellingwood et al., 1982], probabilistic-based limit state design (now called Load and Resistance Factor Design, or LRFD, in the U.S.) has been developed and is widely used. Recently, AF&PA/ASCE Standard 16-95 for engineered wood construction adapted the LRFD design format. In LRFD engineered wood structures, the structural safety performance requirement is expressed by a set of equations (ASCE Standard 16-95),

$$\lambda\phi R' > \sum \gamma_i Q_i \quad \text{Eq. (2.1)}$$

where R' = adjusted resistance of a member, component or connection, ϕ = resistance factor that takes into account variability in short-term strength, and λ = a time-effect factor that takes into account loss of strength under long-term duration of load. On the right-hand side of Eq. (2.1), Q_i = load effect (moment, shear or axial) due to nominal load i , and γ_i = load factor that takes into account variability in load i . Nominal loads and load factors are defined in ASCE 7-02 (2002). The structural safety performance requirement expressed by Eq. (2.1) is a limit criterion beyond which structural member is judged to be unsafe or nonfunctional.

Although the LRFD design process has many advantages relative to allowable strength design (ASD), it has several shortcomings, particularly for woodframe buildings [Ellingwood et al., 2004; Rosowsky and Ellingwood, 2002].

- (1) The design and calibration process using LRFD was performed only for individual members, components or connections. It is therefore hard to predict the structural system behavior under severe natural hazards such as extreme wind events or earthquakes.
- (2) LRFD design focuses on the life safety objective. There has been little attention paid to serviceability issues, which do not impact structural safety but may have a significant social and economic impact.

(3) LRFD design cannot ensure that hazards are treated consistently.

Recent natural disasters in the U.S. and elsewhere around the world have highlighted the social, political, and economic ramifications of the traditional view of codes (to prevent structural collapse during rare events), as economic disruptions caused by structural or member failures have not been deemed acceptable by the public. Performance-based engineering is a new paradigm in which the design process for the purpose of meeting performance expectations (limit states) of the building occupants, owner, and the public. To achieve reasonable agreement between calculated and observed failure rates, properly validated system reliability analysis models are essential [Rosowsky and Ellingwood, 2002]. Seismic performance-based engineering concepts for woodframe buildings are starting to be developed [Ellingwood et al., 2004; Rosowsky and Kim, 2002]. As indicated previously, woodframe buildings are among the most vulnerable types of structures to high wind hazards. The enormous economic losses in recent hurricanes were generally the results of building envelope failure, most typically roof sheathing loss or broken windows. This paper presents a fragility methodology for assessing the response of roof sheathing subjected to specified demands from extreme wind loading.

2.4 Fragility Modeling

A fragility can be defined as the conditional probability of failure of a structural member or system for a given set of input variables [Kennedy and Ravindra, 1984]. It is expressed as:

$$P[LS] = \sum P[LS | D = x] P[D = x] \quad \text{Eq. (2.2)}$$

where D = a random demand on the system (e.g., 3-sec. gust wind speed, spectral acceleration, flood level), $P[LS | D = x]$ is the conditional probability of limit state (LS) at given demand x . The hazard is defined by the probability, $P[D = x]$. The conditional probability, $P[LS | D = x]$ is the fragility. Eq. (2.2) also can be expressed in convolution integral form if the hazard is a continuous function of demand x :

$$P[LS] = \int_0^{\infty} Fr(x) g_x(x) dx \quad \text{Eq. (2.3)}$$

where $Fr(x)$ = fragility function of demand x expressed in the form of a cumulative distribution function and $g_x(x)$ = hazard function expressed in the form of a probability density function.

The fragility of a structural system commonly is modeled using a lognormal distribution,

$$Fr(x) = \Phi \left[\frac{\ln(x) - \lambda_R}{\xi_R} \right] \quad \text{Eq. (2.4)}$$

in which $\Phi(\cdot)$ = standard normal cumulative distribution function, λ_R = logarithmic median of capacity R (in units that are dimensionally consistent with demand), and ξ_R = logarithmic standard deviation of capacity R . Hazard curves can be determined using

statistical analysis or, in the case of seismic hazard, may be obtained from agencies such as the U.S. Geological Survey. A system fragility can be obtained through a probabilistic analysis of the system. Fragilities can be used to identify a level of demand that a component or system will withstand with certain probability. Fragility curves can be used in both design and condition assessment applications [Ellingwood et al., 2004].

2.5 Fragility Model for Roof Sheathing Subjected to Wind Load

2.5.1 Description of Baseline Structures

Fragility assessments were performed for light-frame wood structures with various roof geometries (e.g., roof type, roof slope, roof height, roof truss or framing spacing, overhang), construction practices (e.g., nail type, nailing pattern), and other factors (e.g., exposure condition) subjected to wind loads. In this study, five baseline houses were considered, designated Type 1-5. These five types of single-family light-frame residential buildings were considered to be representative of much of the residential building inventory in the southeast United States. Type 1 is based on a model that has been used extensively in studies at Clemson University's Wind Load Test Facility [Rosowsky and Cheng, 1999a]. Types 2 and 3 have been considered in a recent study by the National Association of Home Builders [NAHB, 1997]. Type 1, 2, and 3 are all gable roof type buildings. Gable roofs are the most popular roof type for woodframe residential buildings in the United States. Type 4 and 5 are hip roof type buildings. Hip roofs are the second most widely used system. The five baseline structures are intended to be representative of typical single-family houses built in the U.S. Dimensions and detailed characteristics are

shown in Table 1.1. The dimensions and roof sheathing panel layouts for the Type 1 baseline structure are shown in Figure 1.1. Those for other baseline structures are shown in Appendix A.1.

2.5.2 Limit States

Roof sheathing failure due to wind load occurs when internal and external pressures acting on a panel combine to cause sufficient uplift on the panel to remove it (multiple nail withdrawal) from the roof framing. Considerable information on this failure mode is available in the literature [e.g., Rosowsky and Cheng, 1999b; Rosowsky and Schiff, 1996].

Roof sheathing uplift failure is influenced by three major parameters: resistance, wind load, and dead load. Resistance capacity generally is provided by nails, wind load refers to the uplift pressure acting on the panel, and dead load is the self-weight of roof sheathing panel (and coverings) acting in a direction opposite to the uplift pressures. The limit state function for one piece of roof sheathing uplift can be written in terms of the basic (random) variables as:

$$g(x) = R - (W - D) \quad \text{Eq. (2.5)}$$

where R = uplift resistance capacity of the nailed roof sheathing panel, W = wind load acting on the sheathing panel, and D = dead load. Sheathing panel failure can be defined as the condition where $g(x) < 0$. The wind load, and hence the failure probability, is a function of the basic wind speed (V) squared (see Eq. 2.7.a and 2.7.b). It should be noted that

dead load (D) in the Eq. (2.5) counteracts the uplift of the wind, and has a beneficial effect on roof sheathing performance. Often in light-frame structures, this dead load is relatively small and may be conservatively ignored, thereby simplifying the limit state function. In this paper, dead load is included in Eq. (2.5). System limit states were defined in this study to correspond to four different levels of damage: no damage (number of sheathing panel failures = 0), no more than one sheathing damage (number of sheathing panel failures ≤ 1), fewer than 10% of sheathing panels failed, and fewer than 25% of sheathing panels failed. Three different wind directionality cases were considered in this study: (1) all possible directions, using a directionality factor, (2) normal-to-ridge, and (3) parallel-to-ridge. The latter two cases do not require a directionality factor. These three directionality cases cover all possible wind direction scenarios for the bi-symmetric simple rectangular baseline structures considered in this study.

2.5.3 Uplift Capacity (Resistance) Statistics

The statistics assumed for uplift capacity of typical full-size roof sheathing panels of representative materials and attached using practices common are shown in Table 2.2. These statistics were obtained from previous studies including both experimental and analytical components [Rosowsky and Cheng, 1999b; Rosowsky and Schiff, 1996]. For this study, statistics were obtained for uplift capacity of individual roof sheathing panel, both 4 ft \times 8 ft (1.22 m \times 2.44 m) and 4 ft \times 4 ft (1.22 m \times 1.22 m) in size, consisting of 15/32 in. (12 mm) CDX plywood attached with smooth-shank hand-driven 8d common nails (0.131 in. (3.33 mm) diameter, 2.5 in. (63.5 mm) long) or 6d common nails (0.113 in.

(2.87 mm) diameter, 2.0 in. (50.8 mm) long), to nominal 2 in. × 4 in. (50 mm × 100 mm) Spruce-pine-fir (SPF) rafters spaced 24 inches (610 mm) on-center. The nailing schedule was 6 in. (150 mm) along the edge of the panel and 12 in. (300 mm) at interior locations [Rosowsky and Cheng, 1999b].

2.5.4 Dead Load Statistics

Dead load considered in this study is the self-weight of the roof sheathing panel. It is assumed to remain constant. The mean and COV of the dead load, which acts in a direction opposite to the wind uplift, is taken as 3.5 psf (168 N/m²) and 0.10, respectively. These values were based on estimated weights of materials and assumed values of mean-to-nominal and COV of 1.05 and 0.10, respectively [Ellingwood et al., 1980]. The dead load is assumed to be Normally distributed.

2.5.5 Wind Load Statistics

ASCE 7 (2002) defines two types of structural elements subjected to wind load: (1) main wind-force resisting systems (MWFRS), and (2) components and cladding (C&C). Different elements have different effective tributary areas as well as different wind pressure coefficients. A main wind-force resisting system is considered an assemblage of structural elements that work together to provide support and stability for the overall structure. Components and cladding elements are defined as elements of the building envelope that transfer the load to the main wind-force resisting system. Individual sheathing panels can be assumed to perform as individual components being loaded directly by the wind, with

equivalent tributary area for a critical location of a roof panel on the order of 1-2 ft² (0.093-0.186 m²), the tributary area of an individual fastener [Rosowsky and Schiff, 1996]. Wind pressures acting on the roof sheathing panels therefore were calculated using the C&C provisions in ASCE 7-02. The wind pressure acting on components and cladding for low-rise structures in ASCE 7-02 (Eq. 6-22) is determined from:

$$W = q_h [GC_p - GC_{pi}] \quad \text{Eq. (2.6)}$$

where q_h = velocity pressure evaluated at mean roof height (h), GC_p = product of gust factor and external pressure coefficient, and GC_{pi} = product of gust factor and internal pressure coefficient. The velocity pressure evaluated at height (z) in ASCE 7-02 (Eq. 6-15) is given by:

$$q_z = 0.00256K_zK_{zt}K_dV^2I \quad (\text{units: lb/ft}^2; V \text{ in mph}) \quad \text{Eq. (2.7.a)}$$

$$q_z = 0.613K_zK_{zt}K_dV^2I \quad (\text{units: N/m}^2; V \text{ in m/s}) \quad \text{Eq. (2.7.b)}$$

where q_z is equivalent to q_h at the mean roof height, K_z = the velocity pressure exposure factor, K_{zt} = the topographic factor, K_d = the wind directionality factor, V = the basic wind speed in mph (3-second gust wind speed at 33 ft (10 m) and in open terrain) (Eq. 2.7.a) and in m/s (Eq. 2.7.b), respectively, and I = the importance factor. Wind effects on low-rise buildings are characterized, for the purpose of design, as distributed static loads. The gust

pressure coefficient, GC_p , varies by panel location. For example, panels along the edge of the roof have higher external pressures than the interior panels. Nominal values of GC_p are determined for each panel using ASCE 7-02. The corresponding random variables are determined using information from ASCE 7-02 and Ellingwood and Tekie (1999). Table 2.3 summarizes the wind load parameters statistics used in this study.

2.5.6 Calculation of Probability of Failure for Individual Sheathing Panel

Before evaluating the reliability of a roof *system* comprising a collection of sheathing panels, it is necessary to calculate the probability of failure for an individual sheathing panel. The limit state function for an individual sheathing panel is given by Eq. (2.5). High wind pressures on a low-rise roof occur in the regions of flow separation at the eave, ridge, and corners at the roof. Change in external wind pressure coefficient, GC_p , results in different wind pressures at different locations on the roof. ASCE 7-02 defines three different wind zones (designated zone 1, 2 and 3) with different pressure coefficients. Effective (aggregated) nominal external pressure coefficients for individual panels can be calculated using a weighted-average method (a sum of the external wind pressures on specific zones – e.g., zone 1, 2 or 3 – multiplied by the percentage of sheathing panel area over which those pressures are assumed to act) and statistics (mean-to-nominal and COV) can be established using information provided by Ellingwood and Tekie (1999). The statistics for the product of gust factor and external pressure coefficient, GC_p , for structure Type 1 is shown in Table 2.4. An enclosed structure is assumed until first panel failure, after which the structure is assumed to be partially enclosed. (The failure of windows or

doors before first panel failure is a possibility, however this is not explicitly considered here. This could be addressed using event-tree analysis if desired.) This concept (assumption) is used in the roof sheathing system reliability calculation subsequently. ASCE 7-02 provides a wind directionality factor (0.85 for components and cladding for ordinary buildings) to account for two effects: (1) the reduced probability of maximum winds coming from any given direction, and (2) the reduced probability of the maximum pressure coefficient occurring for any given wind direction [ASCE, 2002]. It may be of interest to compare roof sheathing fragilities calculated with the directionality factor to those evaluated for a particular direction (without the directionality factor). Such a comparison can shed some light on the suitability of current directionality factors and statistics, such as those suggested by Ellingwood and Tekie (1999) for components and cladding, e.g., mean = 0.89, COV = 0.16. Roof sheathing fragilities are developed here for simple rectangular structures having both gable and hip roof types considering: (i) all possible directions with directionality factor, (ii) normal-to-ridge direction without directionality factor, and (iii) parallel-to-ridge direction without directionality factor. ASCE 7-02 provides the product of gust factor and external pressure coefficient, GC_p , considering all directions (i.e., an “envelope” of worst-case values). The “map” of pressure coefficients over the roof cannot occur simultaneously at any instant in time. (And only if the eye of a storm with rotational symmetry passes directly over the structure can the roof experience all of those pressures in a single wind event.) It is therefore necessary to understand the external pressure distributions (contours) for the normal-to-ridge and parallel-to-ridge directions, as these would be the worst-case directions. External pressures depend on roof

geometry (e.g., roof type, roof angle, plan dimensions, and overhang). Therefore, it is necessary to simplify the external pressure distribution for a particular wind direction. This was done using the work by Holmes (1994) and Xu and Reardon (1998). The statistics for GC_p for each panel were developed using the result from Ellingwood and Tekie (1999) and the nominal (weighted-average) values determined using ASCE 7-02. Table 2.4 summarizes the statistics of GC_p for the Type 1 baseline structure. The statistics of GC_p for the other baseline structures are provided in Appendix A.2.

Individual panel failure fragilities defined by Eq. (2.2) were evaluated using FORM (First-Order Reliability Method) techniques to evaluate the limit state function given by Eq. (2.5) using the statistics for wind, dead, and uplift capacity described in previous sections. In the case of structure Type 1, four individual panel types (shown on Figure 2.1) were considered: (1) full size 4 ft × 8 ft (1.22m × 2.44m) panel located along the long edge of the roof, (2) full size panel located in the corner, (3) full size panel located in the interior, and (4) half-size 4 ft × 4 ft (1.22 m × 1.22 m) panel located along the short edge. Figure 2.2 presents the fragility curves for these four individual sheathing panels in structure Type 1. For the results shown in this figure, roof sheathing is presumed to be attached using 8d common nails (0.131 in. (3.33 mm) diameter, 2.5 in. (63.5 mm) long) spaced at 6 in. (150 mm) along the edge and 12 in. (300 mm) in the interior of the panel, the structure is assumed to be located in Exposure B (suburban residential area with mostly single-family dwellings), and the all possible wind directions case is considered. Panels in these four

locations have different external pressures (see Table 2.4). The individual panel fragility curves are used in the next section to calculate the fragility for complete roof systems.

2.5.7 Calculation of Roof System Failure Probabilities

In the previous section, the probability of failure of an individual roof sheathing panel (worst-case loading) was investigated. In this section, simple system reliability concepts are utilized to construct fragility curves for limit states defined by failure of multiple roof sheathing panels. Assuming statistically independent panel failures², the CDF for system safety conditioned on wind speed can be written as:

$$F_{system}(safety|V) = F_{system}(N_f = 0|V) = \prod_{i=1}^n (1 - P_i[fail|V]) \quad \text{Eq. (2.8)}$$

where V = wind speed, N_f = number of failed panels, n = total number of panels, $P_i[fail|V]$ = failure probability of panel i given wind speed V . Eq. (2.8) can be used to calculate the fragility (conditional limit state probability) for the case of fewer than one roof sheathing panel failures as:

$$F_{system}(N_f \leq 1|V) = F_{system}(N_f = 0|V) + F_{system}(N_f = 1|V) \quad \text{Eq. (2.9)}$$

² The panel failures are, in fact, *not* statistically independent events. The pressure field acting over the roof is spatially correlated and adjacent panel capacities may be correlated as a result of sharing a common roof framing member. In a series system, however, the assumption of independence is known to be conservative and permits the closed-form expressions given by Eqns. (2.8)-(2.10).

Similarly, the fragility for the case of fewer than j roof sheathing panel failures can be written as:

$$F_{system}(N_f \leq j | V) = \sum_{i=0}^j F_{system}(N_f = i | V) \quad \text{Eq. (2.10)}$$

Since the baseline houses each have at least 30 roof sheathing panels which must be included when considering the case of all wind directions, and at least 10 roof sheathing panels when considering any one wind direction, Eq. (2.10) can become cumbersome. Numerical simulation can be used to simplify the analysis. The failure of an individual panel was calculated using the simple closed-form procedure described in the previous section. Then using Eq. (2.10), the system failure probability for each given system limit state at a given wind speed was calculated. This procedure was repeated for wind speeds ranging from 50 mph (22 m/sec) to 200 mph (89 m/sec). The following two assumptions were made in the system analysis:

- (1) Roof sheathing failures are assumed to be statistically independent.
- (2) The internal pressure condition is assumed to be an “enclosed” before the failure of the first roof sheathing panel, and “partially enclosed” after the first panel fails.

2.6 Results

The complementary fragilities (or survivorship curves) for roof sheathing failure can be

plotted as complementary lognormal cumulative distributions:

$$\hat{S}(x) = 1 - Fr(x) = 1 - \Phi \left[\frac{\ln(x) - \lambda_R}{\xi_R} \right] \quad \text{Eq. (2.11)}$$

in which $\Phi(\cdot)$ = standard normal cumulative distribution function, λ_R = logarithmic median of capacity R (in units that are dimensionally consistent with demand), and ξ_R = logarithmic standard deviation of capacity R (approximately equal to the coefficient of variation, V_R , when $V_R < 0.3$). Figure 2.3 shows that the complementary lognormal cumulative distribution provides a good fit to the calculated roof sheathing survivorship curves. The complementary fragility curves in Figure 2.3 were developed for the Type 2 baseline structure using 8d common nails (0.131 inch (3.33 mm) diameter, 2.5 inch (63.5 mm) long) spaced at 6 in. (150 mm) along the panel edge and 12 in. (300 mm) in the panel field, and located in Exposure C (open terrain). The survivorship (complementary fragility) can be viewed most simply as the limit state non-exceedance probability for a given wind speed (3-second gust wind speed at 33 ft. (10 m) above the ground in Exposure C). Table 2.5 summarizes the best-fit lognormal parameters for the roof sheathing complementary fragilities determined for the different baseline structures, exposure conditions, nail types, and system limit states.

Figures 2.4 – 2.8 present selected roof system survivorship curves considering sheathing panel failure (removal). Figure 2.4 presents a comparison of $\hat{S}(x)$ curves for the different

wind direction cases. (The “all directions” case includes the wind directionality factor.) Figure 2.5 shows a comparison of $\hat{S}(x)$ curves for the different system limit states, again considering all possible wind directions. The results in Figures 2.4 and 2.5 are based on an analysis of baseline structure Type 1 (located in Exposure B) with sheathing attached using 6d common nails (0.113 in. (2.87 mm) diameter, 2.0 in. (50.8 mm) long). Roof sheathing survivorships vary with roof shape and slope, exposure condition, and nail size/schedule. Figure 2.6 shows a comparison of $\hat{S}(x)$ curves for two different nail sizes, (building Type 3 located in Exposure B). The effect of nail size on system failure probability is seen to be quite large. For example, considering building Type 3 located in Exposure B (Figure 2.6), the probability of no panel failures when using 8d nails is about 75% when the basic wind speed is 100 mph. The corresponding safety (no damage) probability when using 6d nails is negligible. These complementary fragilities illustrate the significant reduction in capacity when sheathing panels are attached using the smaller (6d) nail. Figure 2.7 presents a comparison of $\hat{S}(x)$ curves for different exposure conditions. Finally, Figure 2.8 presents a comparison of $\hat{S}(x)$ curves for the five different baseline structures. It may not be reasonable to compare these curves directly since the structures have different roof configurations, panel layouts, etc. However, to the extent the structures are comparable, the effect of overhangs can be seen clearly. Complementary fragilities for the roofs with overhangs (Type 2, 3, and 5) are lower than those for roofs without overhangs. The roof system survivorship curves for the other baseline structures considering different exposure conditions, nail types, wind direction profiles, and system limit states may be found in Appendix A.3. In most cases, the $\hat{S}(x)$ curves considering all possible wind directions are

lower than those for the directional cases (normal-to-ridge and parallel-to-ridge). This might suggest that current directionality factors for components and cladding are conservative.

2.7 Summary and Conclusions

This paper presented selected results of a study to develop roof sheathing fragility and complementary fragility (survivorship) curves for low-rise woodframe structures built in high wind regions. Five simple baseline woodframe structures, representative of residential construction in the southeast United States, were considered. Roof sheathing survivorship curves were developed for each baseline structure considering four different damage limit states (percent sheathing removal) as well as different considering wind directionality profiles, nail types, and exposure conditions. The complementary fragilities were found to be well fit by a complementary lognormal cumulative distribution. Selected results were presented in this paper, while more complete results may be found in Appendix A.3.

The fragility methodology described herein can be used to develop performance-based design guidelines for woodframe structures in high wind regions as well as to provide information on which to base structural safety or expected loss (structural, economic) assessments. Fragilities (or complements of survivorships) such as those presented here also can be convolved with appropriate wind speed hazard (demand) functions to evaluate failure probabilities for the different damage levels. The fragility methodology in this study can be used to predict roof sheathing performance, improve the reliability of roof systems

designed to resist high wind loads and (when coupled with a loss model) predict economic loss due to roof sheathing failure and quantify the role of building envelope integrity. In order for fragility curves such as those developed in this study to reach their fullest potential as design and/or assessment tools, they will need to be properly validated using post-disaster damage survey data.

2.8 References

AF&PA (1996), *Load and Resistance Factor Design (LRFD) Manual for Engineered Wood Construction*, American Forest and Paper Association, Washington, DC.

ASCE (2002), *Minimum Design Loads for Buildings and Other Structures, Standard ASCE 7-02*. Structural Engineering Institute of the American Society of Civil Engineers, Reston, VA.

Cook, N.J. (1985), *The Designer's Guide to Wind Loading of Building Structures – Part 2 Static Structures*, Butterworths, Borough Green, Sevenoaks, Kent TN15 8PH, England.

Ellingwood, B.R., Galambos, T.V., MacGregor, J.G. and Cornell, C.A. (1980), *Development of a Probability Based Load Criterion for American National Standard A58*. Special Publication 577, U.S. Department of Commerce, National Bureau of Standards, Washington, DC.

Ellingwood, B.R., MacGregor, T.V., Galambos, T.V., and Cornell, C.A. (1982), "Probability Based Load Criteria: Load Factors and Load Combinations," *Journal of Structural Division*, ASCE, 108(5):978-997.

Ellingwood, B.R. and Tekie, P.B. (1999), "Wind load statistics for probability-based structural design," *Journal of Structural Engineering*, ASCE, 125(4):453-463.

Ellingwood, B.R., Rosowsky, D.V., Li, Y. and Kim, J.H. (2004), "Fragility assessment of light-frame construction subjected to wind and earthquake hazards," *Journal of Structural Engineering*, ASCE. (in press)

Galambos, T.V., Ellingwood, B.R., Macgregor, J.G. and Cornell, C.A. (1982), "Probability-based load criteria: Assessment of current design practice," *Journal of Structural Division*, ASCE, 108(5):959-977.

Holmes, J.D. (1994), "Wind pressures on tropical housing," *Journal of Wind Engineering and Industrial Aerodynamics*, 53:105-123.

Kennedy R.P. and Ravindra, M.K. (1984), "Seismic fragilities for nuclear power plant studies," *Nuclear Engineering and Design*, 79(1):47-68.

NAHB (1997), *Housing Affordability through Design Efficiency Program*. NAHB Research Center. Inc., Upper Marlboro, MD.

Rosowsky, D.V. and Schiff, S.D. (1996), "Probabilistic modeling of roof sheathing uplift capacity," *Proceedings: ASCE Specialty Conference on Probabilistic Mechanics and Structural Reliability*, Worcester, MA, pp. 334-337.

Rosowsky, D.V. and Cheng, N. (1999a), "Reliability of light-frame roofs in high-wind regions. I: Wind loads," *Journal of Structural Engineering*, ASCE, 125(7):725-733.

Rosowsky, D.V. and Cheng, N. (1999b), "Reliability of light-frame roofs in high-wind regions. II: Reliability analysis," *Journal of Structural Engineering*, ASCE, 125(7):734-739.

Rosowsky, D.V. and Ellingwood, B.R. (2002), "Performance-based engineering of wood frame housing: Fragility analysis methodology," *Journal of Structural Engineering*, ASCE, 128(1):32-38.

Rosowsky, D.V. and Kim, J.H. (2002), *Reliability Studies*, CUREE Publication No. W-10, Consortium of Universities for Research in Earthquake Engineering, Richmond, CA.

Xu, Y.L. and Reardon, G.F. (1998), "Variations wind pressure on hip roofs with roof pitch," *Journal of Wind Engineering and Industrial Aerodynamics*, 73:267-284.

Table 2.1 - Dimensions and characteristics of baseline houses

properties	Type 1	Type 2	Type 3	Type 4	Type 5
Plan dimension	22.6 ft × 40 ft (6.9m × 12.2m)	28.0 ft × 40 ft (8.5m × 12.2m)	28.0 ft × 40 ft (8.5m × 12.2m)	28.0 ft × 40 ft (8.5m × 12.2m)	30 ft × 38 ft (9.1m × 11.6m)
No. of stories	1	1	2	1	1
Roof type	Gable	Gable	Gable	Hip	Hip
Roof slope	4:12 (18.4°)	6:12 (26.6°)	8:12 (33.7°)	4:12 (18.4°)	6:12 (26.6°)
Roof framing spacing	24 inch (61 cm)	24 inch (61 cm)	24 inch (61 cm)	24 inch (61 cm)	24 inch (61 cm)
Overhang	none	12 inch (30.5 cm)	12 inch (30.5 cm)	none	12 inch (30.5 cm)

Table 2.2 – Summary of resistance statistics

Nail type/spacing	Panel size	Mean	COV	CDF	References:
8d nail ⁽¹⁾ 6 in. / 12 in. (15.2 cm / 30.5 cm)	4 ft × 8 ft (1.22 m × 2.44m)	57.7 psf (2.76 KN/m ²)	0.20	Normal	Rosowsky and Cheng, 1999b; Rosowsky and Schiff, 1996
	4 ft × 4 ft (1.22 m × 1.22 m)	73.3 psf (3.51 KN/m ²)	0.20	Normal	
6d nail ⁽²⁾ 6 in. / 12 in. (15.2 cm / 30.5 cm)	4 ft × 8 ft (1.22 m × 2.44 m)	25.0 psf (1.20 KN/m ²)	0.15	Normal	
	4 ft × 4 ft (1.22 m × 1.22 m)	32.0 psf (1.53 KN/m ²)	0.15	Normal	

(1) 0.131 inch (3.33 mm) diameter, 2.5 inch (63.5 mm) long

(2) 0.113 inch (2.87 mm) diameter, 2.0 inch (50.8 mm) long

Table 2.3 – Summary of wind load parameters statistics

parameters	category	nominal	mean	COV	CDF	
K_z	Exp B	0 ft - 30 ft (0 m – 9.1 m)	0.70	0.71*	0.19*	Normal
	Exp C	0 ft - 15 ft (0 m – 4.6 m)	0.85	0.82*	0.14*	Normal
		16 ft - 20 ft (4.9 m – 6.1 m)	0.90	0.84	0.14	
	Exp D	0 ft - 15 ft (0 m – 4.6 m)	1.03	0.99*	0.14*	Normal
16 ft - 20 ft (4.9 m – 6.1 m)		1.08	1.04*	0.14*		
K_d	components and cladding	0.85	0.89	0.16	Normal	
GC_{pi}	enclosed	0.18	0.15*	0.33*	Normal	
	partially enclosed	0.55	0.46*	0.33*		
GC_p	see Table 2.4 and Appendix A.2				Normal	
K_{zt}	deterministic (1.0)					
I	deterministic (1.0)					

* modified from Ellingwood and Tekie (1999).

Table 2.4 - Summary of GC_p statistics for Structure Type 1

nominal GC_p (ASCE 7-02)			Type 1 (roof slope = 18.4°)											
Zone 3	Zone 2	Zone 1												
-2.6	-1.7	-0.9												
			<table border="1"> <thead> <tr> <th colspan="3">GCp values at each panel</th> </tr> <tr> <th>all directions</th> <th>normal -to-ridge</th> <th>parallel-to-ridge</th> </tr> </thead> <tbody> <tr> <td> </td> <td> </td> <td> </td> </tr> </tbody> </table>			GCp values at each panel			all directions	normal -to-ridge	parallel-to-ridge			
GCp values at each panel														
all directions	normal -to-ridge	parallel-to-ridge												
nominal*	mean**	COV	number of panels											
			all directions	normal -to-ridge direction	parallel-to-ridge direction									
a	-1.861	-1.768	0.12	8	0	4								
b	-1.532	-1.455	0.12	12	10	2								
c	-1.500	-1.425	0.12	4	0	2								
d	-0.900	-0.855	0.12	8	16	10								
				32	26	18								

* calculated using weighted-average method

** calculated using mean-to-nominal value provided by Ellingwood and Tekie (1999)

Table 2.5 – Lognormal parameters for roof sheathing fragilities

Baseline Structure	Exposure condition	Nail type and spacing	Damage level (3,4,5,6)	Wind direction					
				all directions		normal-to-ridge direction		parallel-to-ridge direction	
				λ	ξ	λ	ξ	λ	ξ
Structure Type 1	Exp B	6d nail ⁽¹⁾ 6 in. / 12 in. (15.2 cm / 30.5 cm)	level 1	4.353	0.0686	4.411	0.0670	4.372	0.0766
			level 2	4.383	0.0674	4.421	0.0586	4.401	0.0685
			level 3	4.410	0.0519	4.453	0.0439	4.459	0.0524
			level 4	4.492	0.0376	4.554	0.0376	4.608	0.0435
		8d nail ⁽²⁾ 6 in. / 12 in. (15.2 cm / 30.5 cm)	level 1	4.680	0.0898	4.743	0.0935	4.718	0.0961
			level 2	4.734	0.0806	4.768	0.0726	4.762	0.0825
			level 3	4.770	0.0580	4.811	0.0517	4.826	0.0590
			level 4	4.862	0.0417	4.920	0.0414	4.983	0.0491
	Exp C	6d nail ⁽¹⁾ 6 in. / 12 in. (15.2 cm / 30.5 cm)	level 1	4.296	0.0675	4.356	0.0636	4.317	0.0754
			level 2	4.324	0.0633	4.366	0.0539	4.340	0.0626
			level 3	4.349	0.0493	4.393	0.0407	4.392	0.0477
			level 4	4.425	0.0348	4.484	0.0344	4.538	0.0396
		8d nail ⁽²⁾ 6 in. / 12 in. (15.2 cm / 30.5 cm)	level 1	4.623	0.0911	4.683	0.0878	4.659	0.0934
			level 2	4.673	0.0783	4.709	0.0690	4.699	0.0778
			level 3	4.708	0.0551	4.750	0.0488	4.759	0.0558
			level 4	4.795	0.0396	4.855	0.0394	4.911	0.0458
	Exp D	6d nail ⁽¹⁾ 6 in. / 12 in. (15.2 cm / 30.5 cm)	level 1	4.205	0.0702	4.264	0.0647	4.221	0.0726
			level 2	4.229	0.0634	4.272	0.0550	4.245	0.0622
			level 3	4.256	0.0457	4.298	0.0405	4.298	0.0476
			level 4	4.331	0.0353	4.391	0.0345	4.444	0.0396
		8d nail ⁽²⁾ 6 in. / 12 in. (15.2 cm / 30.5 cm)	level 1	4.530	0.0872	4.594	0.0888	4.563	0.0947
			level 2	4.578	0.0784	4.615	0.0705	4.605	0.0764
			level 3	4.613	0.0555	4.656	0.0491	4.665	0.0550
			level 4	4.701	0.0396	4.761	0.0393	4.817	0.0460
Structure Type 2	Exp B	6d nail ⁽¹⁾ 6 in. / 12 in. (15.2 cm / 30.5 cm)	level 1	4.236	0.0753	4.312	0.0727	4.257	0.0833
			level 2	4.296	0.0786	4.348	0.0667	4.319	0.0834
			level 3	4.339	0.0563	4.404	0.0465	4.425	0.0531
			level 4	4.446	0.0351	4.583	0.0436	4.627	0.0438
		8d nail ⁽²⁾ 6 in. / 12 in. (15.2 cm / 30.5 cm)	level 1	4.568	0.0938	4.648	0.0890	4.608	0.1010
			level 2	4.655	0.0939	4.704	0.0819	4.692	0.0964
			level 3	4.709	0.0596	4.773	0.0531	4.797	0.0595
			level 4	4.818	0.0384	4.958	0.0477	5.005	0.0487
	Exp C	6d nail ⁽¹⁾ 6 in. / 12 in. (15.2 cm / 30.5 cm)	level 1	4.181	0.0695	4.260	0.0652	4.199	0.0744
			level 2	4.230	0.0737	4.288	0.0625	4.253	0.0739
			level 3	4.276	0.0446	4.338	0.0419	4.355	0.0480
			level 4	4.377	0.0328	4.509	0.0400	4.554	0.0397
		8d nail ⁽²⁾ 6 in. / 12 in. (15.2 cm / 30.5 cm)	level 1	4.506	0.0906	4.592	0.0892	4.546	0.0947
			level 2	4.590	0.0885	4.643	0.0776	4.623	0.0884
			level 3	4.643	0.0556	4.707	0.0490	4.726	0.0544
			level 4	4.749	0.0363	4.883	0.0443	4.931	0.0448

Table 2.5 – Lognormal parameters for roof sheathing fragilities (continued)

Baseline Structure	Exposure condition	Nail type and spacing	Damage level	Wind direction					
				all directions		normal-to-ridge direction		parallel-to-ridge direction	
				λ	ξ	λ	ξ	λ	ξ
Structure Type 3	Exp B	6d nail ⁽¹⁾ 6 in. / 12 in. (15.2 cm / 30.5 cm)	level 1	4.337	0.0661	4.350	0.0735	4.388	0.0797
			level 2	4.418	0.0871	4.372	0.0644	4.443	0.0856
			level 3	4.443	0.0663	4.441	0.0438	4.506	0.0536
			level 4	4.511	0.0357	4.590	0.0391	4.648	0.0415
		8d nail ⁽²⁾ 6 in. / 12 in. (15.2 cm / 30.5 cm)	level 1	4.665	0.0905	4.687	0.0953	4.732	0.0981
			level 2	4.778	0.1012	4.730	0.0792	4.810	0.1011
			level 3	4.810	0.0728	4.807	0.0503	4.878	0.0633
			level 4	4.883	0.0395	4.968	0.0433	5.029	0.0461
	Exp C	6d nail ⁽¹⁾ 6 in. / 12 in. (15.2 cm / 30.5 cm)	level 1	4.279	0.0649	4.293	0.0698	4.332	0.0708
			level 2	4.357	0.0807	4.313	0.0592	4.375	0.0737
			level 3	4.381	0.0629	4.377	0.0400	4.436	0.0446
			level 4	4.444	0.0355	4.518	0.0347	4.573	0.0366
		8d nail ⁽²⁾ 6 in. / 12 in. (15.2 cm / 30.5 cm)	level 1	4.596	0.0898	4.630	0.0951	4.674	0.0968
			level 2	4.702	0.0967	4.668	0.0748	4.742	0.0915
			level 3	4.731	0.0733	4.741	0.0474	4.807	0.0554
			level 4	4.805	0.0377	4.895	0.0398	4.954	0.0414
Structure Type 4	Exp B	6d nail ⁽¹⁾ 6 in. / 12 in. (15.2 cm / 30.5 cm)	level 1	4.746	0.0920	4.760	0.0860	4.795	0.0929
			level 2	4.816	0.0872	4.861	0.1005	4.987	0.1461
			level 3	4.839	0.0660	4.880	0.0850	4.998	0.1371
			level 4	4.906	0.0420	4.948	0.0497	5.051	0.0997
	Exp C	8d nail ⁽²⁾ 6 in. / 12 in. (15.2 cm / 30.5 cm)	level 1	4.690	0.0934	4.704	0.0853	4.738	0.0912
			level 2	4.754	0.0833	4.796	0.0941	4.909	0.1288
			level 3	4.777	0.0661	4.816	0.0747	4.917	0.1208
			level 4	4.840	0.0399	4.875	0.0448	4.971	0.0790
Structure Type 5	Exp B	6d nail ⁽¹⁾ 6 in. / 12 in. (15.2 cm / 30.5 cm)	level 1	4.575	0.0940	4.591	0.0939	4.603	0.0937
			level 2	4.665	0.0944	4.691	0.1039	4.695	0.1009
			level 3	4.710	0.0651	4.753	0.0652	4.764	0.0611
			level 4	4.802	0.0405	4.916	0.0518	4.915	0.0482
	Exp C	8d nail ⁽²⁾ 6 in. / 12 in. (15.2 cm / 30.5 cm)	level 1	4.518	0.0844	4.531	0.0892	4.546	0.0943
			level 2	4.601	0.0898	4.623	0.0952	4.627	0.0921
			level 3	4.647	0.0572	4.681	0.0600	4.693	0.0558
			level 4	4.734	0.0380	4.838	0.0479	4.839	0.0445

(1) 0.113 inch (2.87 mm) diameter, 2.0 inch (50.8 mm) long

(2) 0.131 inch (3.33 mm) diameter, 2.5 inch (63.5 mm) long

(3) damage level 1 – no sheathing failures

(4) damage level 2 – no more than one sheathing panel failure

(5) damage level 3 – fewer than 10% of sheathing panels failed

(6) damage level 4 – fewer than 25% of sheathing panels failed

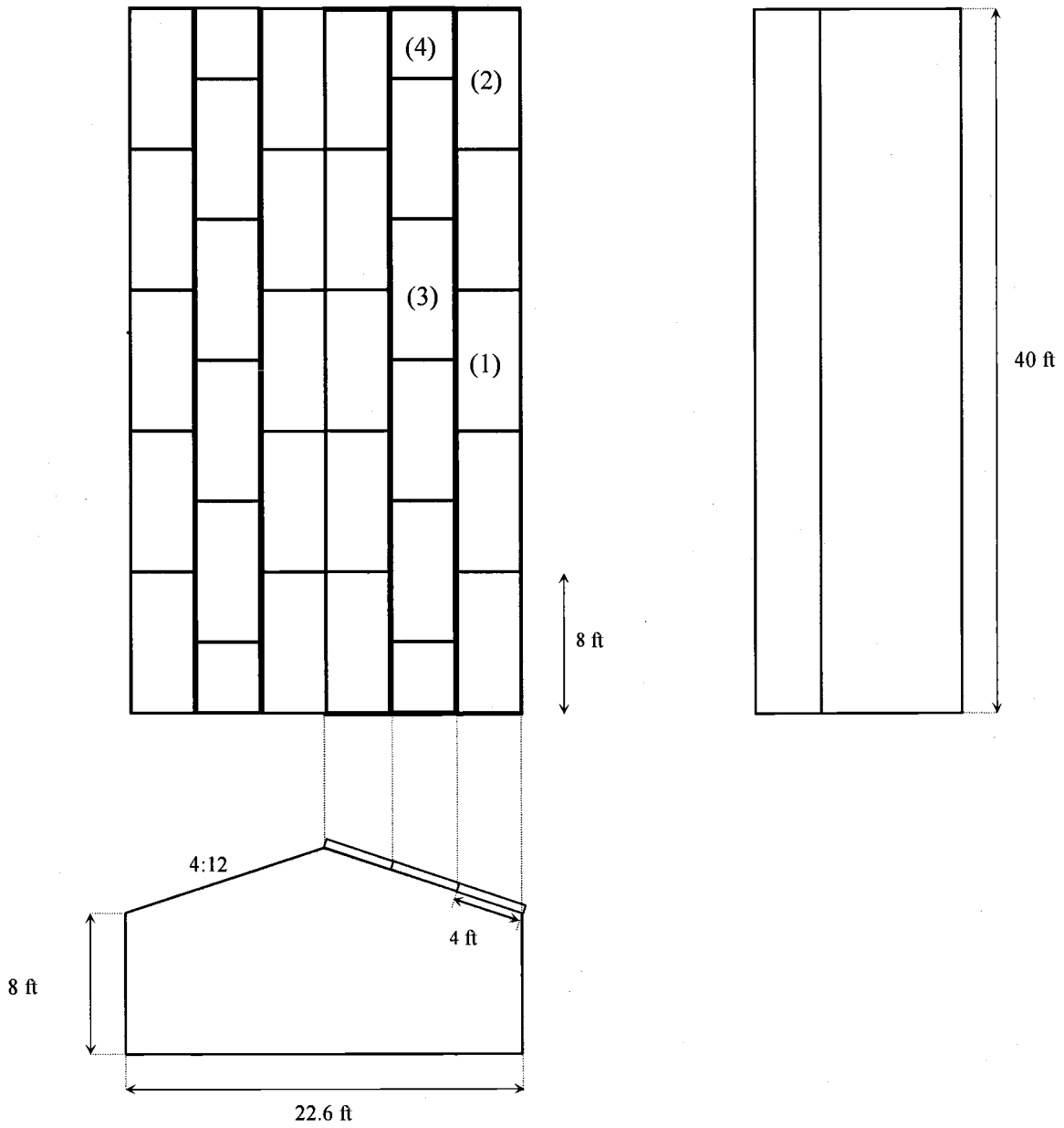


Figure 2.1 – Dimensions and panel layout showing 4 panel locations, Structure Type 1

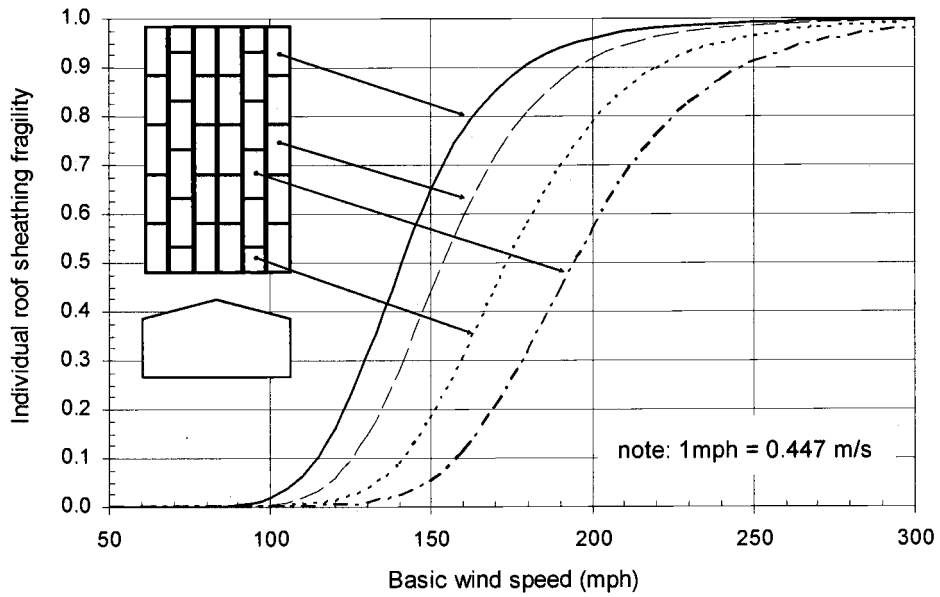


Figure 2.2 - Fragilities for individual roof sheathing failure
(Structure Type 1 / Exposure B / 8d nail – 6 in./12 in. spacing)

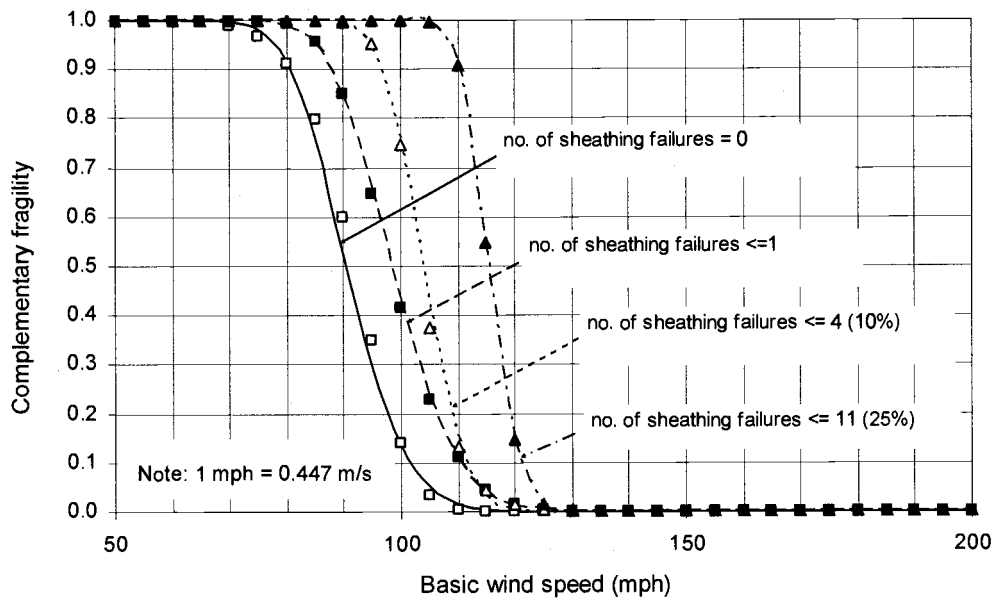


Figure 2.3 – Lognormal fitted roof system complementary fragilities
(Structure Type 2 / Exposure C / 8d nail – 6 in./12 in. spacing)

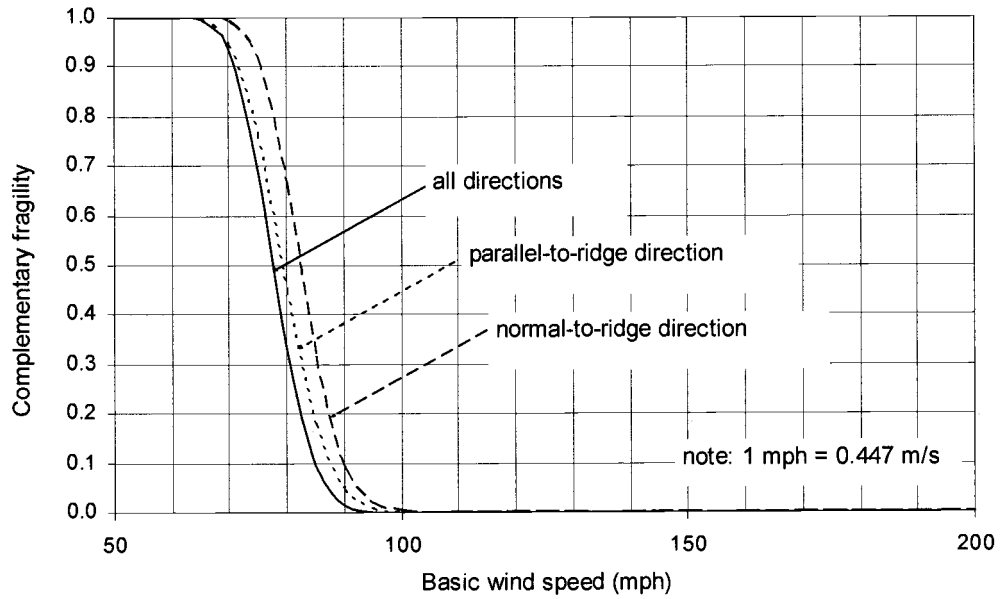


Figure 2.4 – Comparison of roof system survivorship curves for different wind directions
 (Structure Type 1 / Exposure B / 6d nail – 6 in./12 in. spacing)
 [damage level: no sheathing failure]

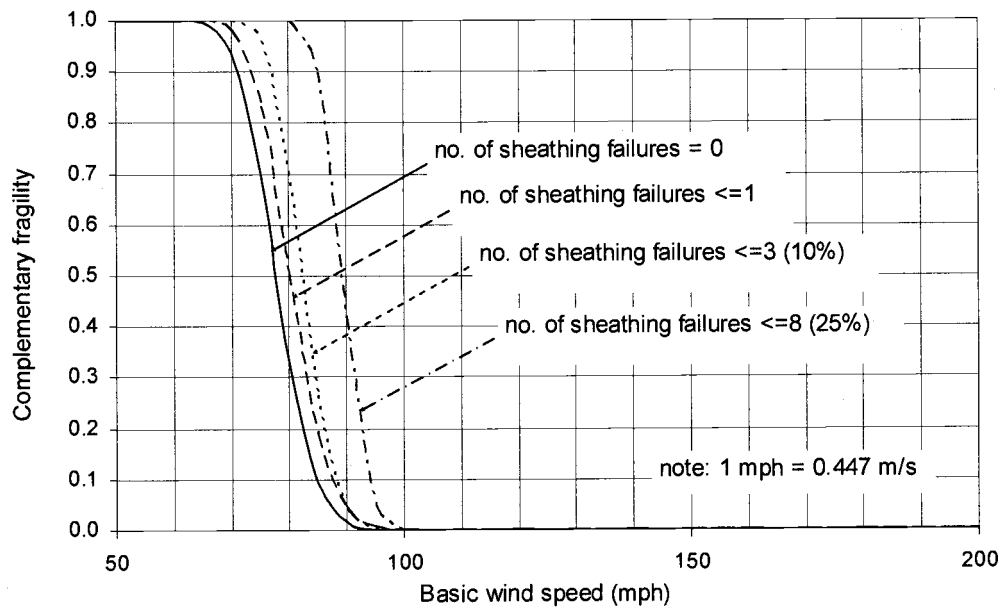


Figure 2.5 – Comparison of roof system survivorship curves for different damage levels
 (Structure Type 1 / Exposure B / 6d nail – 6 in./12 in. spacing)
 [all possible wind directions]

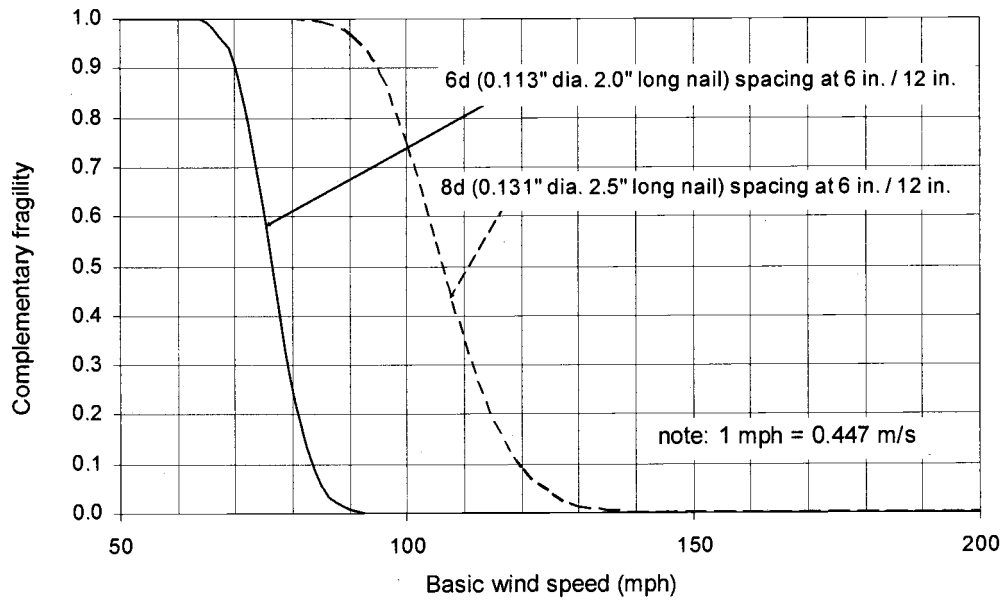


Figure 2.6 – Comparison of roof system survivorship curves for different nail types
 (Structure Type 3 / Exposure B / all possible wind directions)
 [damage level: no sheathing failures]

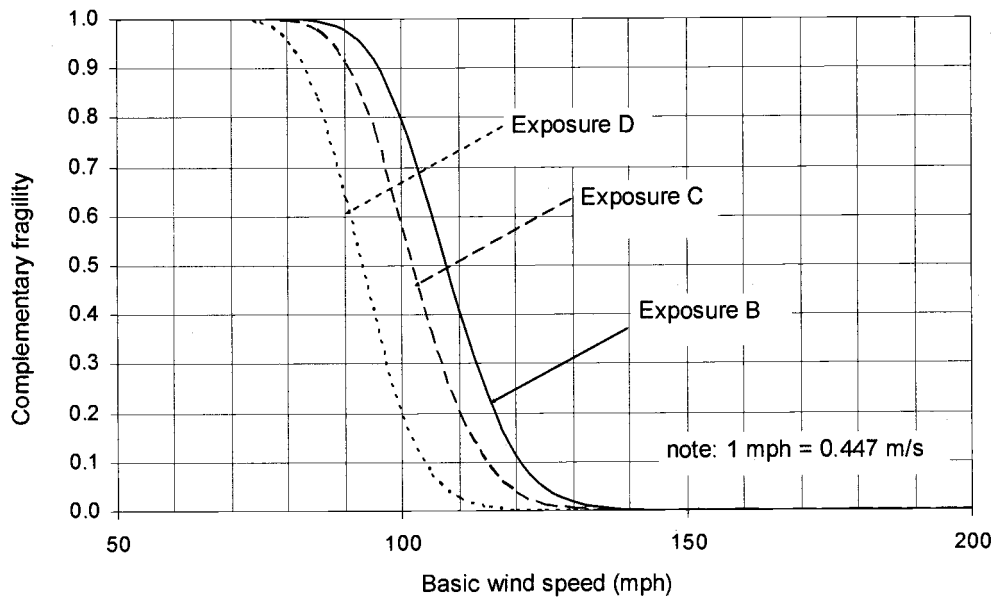


Figure 2.7 – Comparison of roof system survivorship curves for different exposures
 (Structure Type 1 / 8d nail – 6 in./12 in. spacing / all possible wind directions)
 [damage level: no sheathing failures]

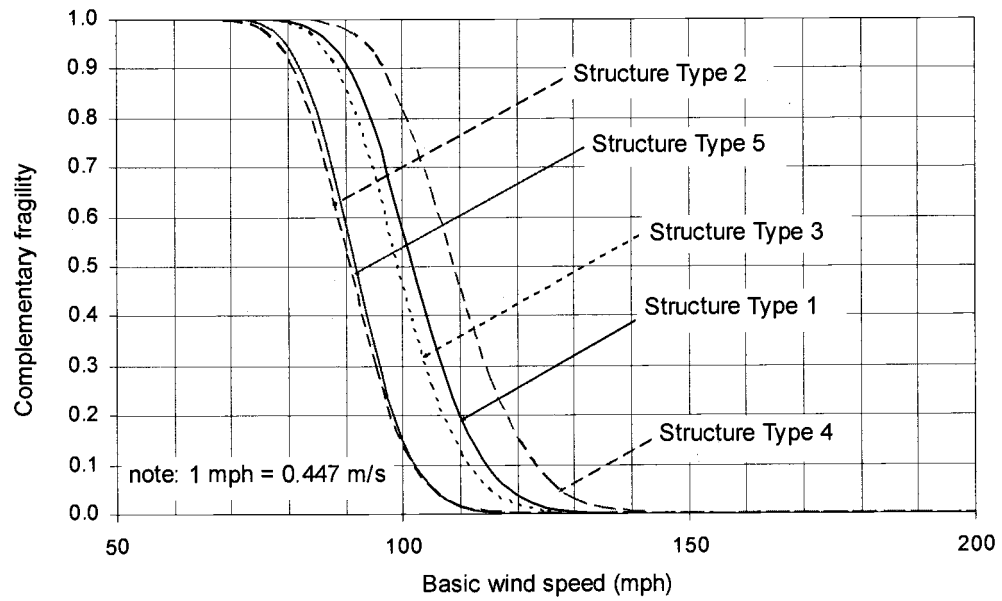


Figure 2.8 – Comparison of roof system survivorship curves for different baseline structures
(Exposure C / 8d nail – 6 in./12 in. spacing / all possible wind directions)
[damage level: no sheathing failures]

Fragility Curves for Woodframe Structures Subjected for Lateral Wind Loads

Kyung Ho Lee

David V. Rosowsky

For Submission to *Wind & Structures*

Techno-Press

P.O. Box 33, Yusong,

Daejon 305-600, Korea

3. Fragility Curves for Woodframe Structures Subjected to Lateral Wind Loads

3.1 Abstract

This paper describes a procedure to develop fragility curves for woodframe structures subjected to lateral wind loads. The fragilities are cast in terms of horizontal displacement criteria (maximum drift at the top of the shearwalls). The procedure is illustrated through the development of fragility curves for one and two-story residential woodframe buildings in high wind regions. The structures were analyzed using a monotonic pushover analysis to develop the relationship between displacement and base shear. The base shear values were then transformed to equivalent nominal wind speeds using information on the geometry of the baseline buildings and the wind load equations (and associated parameters) in ASCE 7-02. Displacement vs. equivalent nominal wind speed curves were used to determine the critical wind direction, and Monte Carlo simulation was used along with wind load parameter statistics provided by Ellingwood and Tekie (1999) to construct displacement vs. wind speed curves. Wind speeds corresponding to a presumed limit displacement were used to construct fragility curves. Since the fragilities were fit well using a lognormal CDF and had similar logarithmic standard deviations (ξ), a quick analysis to develop approximate fragilities is possible, and this also is illustrated. Finally, a compound fragility curve, defined as a weighted combination of individual fragilities, is developed.

3.2 Introduction

The primary objective of structural design codes and standards is to protect (life) safety by preventing structural collapse or failure during rare events in a building's lifetime. While this objective has largely been achieved for buildings in the U.S. subjected to hurricane wind storms, economic losses and social disruption related to hurricane event are still unacceptable [Ellingwood et al., 2004]. Recent disasters in the U.S. and elsewhere around the world have highlighted the social, political, and economic ramifications of the traditional view of codes (to prevent structural collapse during rare events), as economic disruptions caused by structural failures have not been deemed acceptable by the public. This has led to efforts to develop performance-based design procedures in which the structural system is designed to meet multiple specific criteria under given hazard levels. Performance-based engineering is a new paradigm in which the design process is structured to meet performance expectations (limit states) of the building occupants, owner, and the public. Although performance-based seismic design has advanced for some materials and structural types, such as steel and reinforced concrete buildings and bridges, its application to light-frame wood structures remains relatively unexplored. Performance-based seismic engineering concepts for woodframe buildings are starting to be developed [Ellingwood et al., 2004; Rosowsky and Kim, 2002a and 2002b]. The focus of that work has been on fragility assessments for woodframe structures exposed to seismic hazards using displacement-based criteria.

Many residential low-rise structures are located along the hurricane-prone coastlines of the

United States. Most of these are light-frame wood structures. A review of the performance of woodframe buildings after recent hurricanes – Hugo (1989), Andrew (1992), Iniki (1992), and Opal (1995) – has shown that the majority of damage is due to wind and water. Recent studies have developed fragility curves for roof sheathing uplift in low-rise wood structures [Lee and Rosowsky, 2004; Ellingwood et al., 2004]. However, lateral displacement from wind pressures acting on the walls and roofs in woodframe structures also can result in structural damage, loss of fenestration, and water ingress into the building. In this study, fragility curves are developed for displacement criteria (maximum shearwall drift) considering lateral wind loads. Like the previous studies which focused on roof sheathing, the hazard is still the wind (speed), however the relevant load effect is the sum of the lateral forces acting on the structure rather than (localized) uplift forces. This paper presents a procedure for constructing fragility curves to assess the response of wood shearwalls subjected to lateral wind load. This was accomplished using monotonic pushover analysis of three baseline structures, Monte Carlo simulation, and statistical fitting techniques. The application of fragility curves to the evaluation of a portfolio of structures is illustrated through the construction of a compound fragility curve.

3.3 Structural Analysis

Three baseline woodframe structures were considered. The structures, which have characteristics (roof slope, square footage, construction material, etc.) typical of single-family residential construction in the U.S., are designated TYPE-I, TYPE-II, and TYPE-III in this paper. The basic construction characteristics of these structures were taken (with

some modifications) from other sources [NAHB, 1997; Kim, 2003]. Detailed wall characteristics for the TYPE-I and TYPE-II structures were assumed for this study, while those for the TYPE-III structure were able to be taken directly from Kim (2003). Table 3.1 summarizes the dimensions and construction details for the three baseline structures. It should be noted that the contributions of nonstructural finish materials (e.g., gypsum wall board, stucco) and partition walls are not considered in this study. Figures 3.1(a) - (c) show the detailed shearwall configurations for the TYPE-I, TYPE-II, and TYPE-III structure, respectively.

Monotonic pushover analysis was conducted to develop curves relating base shear to displacement at the top of the shearwall. Two programs, originally developed as part of the CUREE-Caltech Woodframe Project, were used. The program CASHEW [Folz and Filtrault, 2000, 2001] was used to evaluate the dynamic response of individual woodframe shearwalls, and the results were then used as input to a subsequent program to analyze complete woodframe structures. CASHEW is a numerical model capable of predicting the load-displacement response of wood shearwalls under quasi-static cyclic loading. With information on shearwall geometry, material properties, and the hysteretic behavior of the individual fasteners, CASHEW can be used to calculate the parameters of an equivalent single degree-of-freedom (SDOF) oscillator for an isolated shearwall. The equivalent SDOF model can be then used for either monotonic or cyclic analysis of the shearwall, or to evaluate shearwall response under an actual or synthetic ground motion record. The SDOF oscillator also can become input information into the program SAWS [Folz and

Filatroul, 2003] which is used to analyze complete woodframe structures. In the SAWS program, the light-frame structure is composed of two primary components: rigid horizontal diaphragms and nonlinear lateral load-resisting shearwall elements. In the modeling of the structure, it is assumed that both the floor and roof elements have sufficiently high in-plane stiffness to be considered rigid elements. This is a reasonable assumption for typically constructed diaphragms with a planar aspect ratio on the order of 2:1, as supported by experimental results from full-scale diaphragm tests [Phillips et al., 1993]. The actual three-dimensional building is degenerated into a two-dimensional planar model using zero-height shearwall elements connected between the diaphragm and the foundation. In this study, the distribution of the lateral load over the height of a structure is assumed to be uniform, a reasonable assumption for low-rise buildings. The SAWS program assigns nodal loads which are applied to the center of mass at each floor level. Figure 3.2 shows examples of pushover curves (one for each load direction) for the TYPE-III structure.

3.4 Wind Loads

Once the displacement vs. base shear curve (Figure 3.2) is determined, the next step is to convert base shears to equivalent nominal wind speeds in order to determine the critical (weakest) direction for the structure. ASCE (2002) provides different external pressure coefficients (GC_{pf}) for different building surfaces (Figure 6-10 in ASCE 7-02). Therefore, base shears are determined by summing the wind pressures multiplied by their respective projected areas. The procedure for then converting base shear to equivalent wind speed is

described in this section.

ASCE 7-02 (2002) defines two types of structural elements subjected to wind load: (1) main wind-force resisting systems (MWFRS), and (2) components and cladding (C&C). Different elements have different effective tributary areas as well as different wind pressure coefficients. A main wind-force resisting system (MWFRS) is considered an assemblage of structural elements that work together to provide support and stability for the overall structure. Components and cladding (C&C) elements are defined as elements of the building envelope that transfer the load to the main wind-force resisting system. Shearwalls and horizontal diaphragms can be considered main wind-force resisting systems. Therefore, lateral wind pressures acting on the wall and roof in this study were calculated using the MWFRS provisions in ASCE 7-02. The wind pressure acting on a main wind-force resisting system for low-rise structures in ASCE (2002) (Eq. 6-18) can be determined from:

$$W = q_h [(GC_{pf}) - (GC_{pi})] \quad \text{Eq. (3.1)}$$

where q_h = velocity pressure evaluated at mean roof height (h), GC_{pf} = product of gust factor and external pressure coefficient, and GC_{pi} = product of gust factor and internal pressure coefficient. The velocity pressure evaluated at height z in ASCE 7-02 (Eq. 6-15) is given by:

$$q_z = 0.00256K_zK_{zt}K_dV^2I \quad \text{Eq. (3.2)}$$

where q_z is velocity pressure (equivalent to q_h) at the mean roof height in units of lb/ft². K_z = the velocity pressure exposure coefficient, K_{zt} = the topographic factor, K_d = the wind directionality factor, V = the basic wind speed (3-second gust wind speed at 33 ft (10 m) in open terrain) in mph, and I = the importance factor. Wind effects on low-rise buildings are characterized for the purpose of design as distributed static loads. The external pressure coefficient, GC_{pf} , varies by wind direction and wall and roof surfaces. The wind pressure can be determined from Eqns. (3.1) and (3.2) as:

$$W = 0.00256K_zK_{zt}K_dV^2I[(GC_{pf}) - (GC_{pi})] \quad \text{Eq. (3.3)}$$

where, W is a wind pressure in lb/ft². The internal pressure effect in Eq. (3.3) is ignored since it is assumed that pressure effects on internal walls are symmetric about the center line of the building with the opposing wall having equal magnitudes of force but opposite direction. Therefore, Eq. (3.3) can be simplified as:

$$W = 0.00256K_zK_{zt}K_dV^2I(GC_{pf}) \quad \text{Eq. (3.4)}$$

External pressure coefficient, GC_{pf} , depends on location on the building surface (see Figure 6-10 in ASCE 7-02). Therefore, Eq. (3.4) can be presented as a summation of each wind pressures acting on various locations as:

$$W = \sum_{i=1}^n W_{(i)} = \sum_{i=1}^n 0.00256 K_z K_{zt} K_d V^2 I (GC_{pf}^{(i)}) \quad \text{Eq. (3.5)}$$

where $GC_{pf}^{(i)}$ = external pressure coefficient at location i . In the case of low-rise structures, V , K_z , K_{zt} , K_d and I do not depend on the specific location i . The total base shear for a structure can be expressed as the summation of wind pressures multiplied by the corresponding projected areas.

$$\begin{aligned} B &= \sum_{i=1}^n [W_{(i)} \times A_{(i)}] = \sum_{i=1}^n [0.00256 K_z K_{zt} K_d V^2 I (GC_{pf}^{(i)}) \times A_{(i)}] \\ &= 0.00256 K_z K_{zt} K_d V^2 I \sum_{i=1}^n [(GC_{pf}^{(i)}) \times A_{(i)}] \end{aligned} \quad \text{Eq. (3.6)}$$

where B = base shear (lbs), $W_{(i)}$ = wind pressure acting on surface i (psf), and $A_{(i)}$ = projected area (ft²) of surface i . The equivalent wind speed corresponding to this value of base shear can then be obtained as:

$$V = \left(\frac{B}{0.00256 K_z K_{zt} K_d I \sum_{i=1}^n [GC_{pf}^{(i)} \times A_{(i)}]} \right)^{\frac{1}{2}} \quad \text{Eq. (3.7)}$$

In Eq. (3.7), equivalent wind speed V is given in units of mph, base shear B in lbs, and

area $A_{(i)}$ in square feet. Note that wind pressures acting on the roof surfaces were resolved into horizontal and vertical components, and that both horizontal pressures on the roof and external pressures on the front and back walls were considered in determining the net lateral load on the structure.

3.5 Lateral Wind Fragilities

Using pushover curves (displacement vs. base shear), the relation between base shear and wind speed given by Eq. (3.7), and the nominal wind load parameters in Table 3.2, displacement vs. equivalent nominal wind speed curves were obtained. Figure 3.3 shows the displacements vs. wind speed curves for shearwalls in the different wind directions for the TYPE-III building assuming Exposure C. (Appendix B.1 shows the displacement vs. equivalent nominal wind speed curves for the other baseline buildings assuming Exposure C.) As shown in Figure 3.3, the North and South walls in all three baseline structures performed the worst, and therefore the critical direction of wind loading was the East-West direction. For the one-story baseline buildings, displacement was calculated at the top of the shearwall. For the two-story baseline building, the critical displacement was taken as the largest of: (1) drift at the top of the first story; (2) interstory drift; and (3) drift at the top of the second story (roof diaphragm level), and the appropriate heights were used to evaluate drift ratios per FEMA 356. In general, the drifts at the top of the structure governed. Therefore, displacement at the top of the second story (roof diaphragm level) relative to the ground (i.e., full building height) was considered when evaluating drift

performance. Two displacement limit states were considered, namely drift ratios (ratios of lateral displacement to wall height) of 1% and 2%. These are the drift limits suggested by FEMA 356 for woodframe shearwalls corresponding to the IO (immediate occupancy) and LS (life safety) performance levels, respectively. Figure 3.3 was developed using nominal wind load parameters provided by ASCE 7-02 [ASCE, 2002]. Figure 3.4 shows curves developed using Monte Carlo simulation and the wind load statistics in Table 3.2. The fragility of a structural system can modeled using a lognormal distribution,

$$Fr(x) = \Phi \left[\frac{\ln(x) - \lambda_R}{\xi_R} \right] \quad \text{Eq. (3.8)}$$

in which $\Phi[\bullet]$ = standard normal cumulative distribution function, λ_R = logarithmic median of capacity R , and ξ_R = logarithmic standard deviation of capacity R . Using the wind speeds at each displacement limit, lateral wind load fragilities (conditional probabilities of failure) were developed and fit using a lognormal distribution as shown in Figure 3.5. Figures 3.4 and 3.5 were developed for the TYPE-III structure assuming Exposure C and including the wind directionality factor as a random variable (mean=0.86, COV=0.125). ASCE 7-02 provides a wind directionality factor of 0.85 (for MWFRS in ordinary buildings) to account for two effects: (1) the reduced probability of maximum winds coming from any given direction, and (2) the reduced probability of the maximum pressure coefficient occurring for any given wind direction [ASCE, 2002]. Since only the worst wind direction case is considered in this study, it may not be necessary to consider a

wind directionality effect. Thus, two types of fragilities were developed in this study: one that includes the wind directionality effect (directionality factor modeled as a random variable) and one that does not (no directionality factor). Figure 3.6 shows a comparison of fragilities with and without consideration of wind directionality. Table 3.3 presents a complete set of lognormal parameters for the fragility curves considering all cases. Appendix B.2 shows selected results for the lateral wind fragility curves using the simulation technique.

Since the variation in the dispersion parameter (ξ) in Table 3.3 is small, the lateral wind load fragilities can be obtained directly and more easily if we determine the wind speed corresponding to the median fragility, $Fr(x) = 0.5$. The wind speed corresponding to the median fragility can be determined using Eq. (3.7), the median values of wind load statistics in Table 3.2, and the base shear corresponding to the drift limit (from the deterministic pushover analysis). Using Eq. (3.7) and the median values of wind load parameters in Eq. (3.7), the median wind speeds at the 1% and 2% drift limits were determined to be 175 mph (78.2 m/s) and 194 mph (86.7 m/s), respectively. The mean of the logarithmic standard deviation ξ (for the case including the wind directionality factor) in Table 3.3 is 0.11. Therefore, quick estimations of the lognormal fragility parameters would be $\lambda = \ln(175) = 5.16$ and $\xi = 0.11$ for the 1% drift limit, and $\lambda = \ln(194) = 5.27$ and $\xi = 0.11$ for the 2% drift limit. Using these parameters, one obtains estimates of the fragility curves without the need for simulation or statistical fitting techniques. Appendix B.3 presents a complete set of lognormal parameters for the fragility curves considering all

cases for use in this quick analysis. Figure 3.7 shows that fragilities constructed using the simplified analysis are very close to those developed using simulation.

3.6 Compound Fragility

Fragility curves also have application to pre-disaster vulnerability assessment as well as post-disaster condition assessment. Some of these potential applications have been discussed elsewhere [Rosowsky and Ellingwood, 2002]. It may be possible, for example, to use fragility curves such as those developed in this paper, to evaluate a single aggregate fragility that applies to a building inventory (portfolio), rather than a single structure. The implications to disaster planners as well as the insurance industry are obvious. Consider a portfolio of structures that can be divided into n classes of buildings (types, ages, materials, condition, etc.) where the relative percentage of class i is given by a weighting term w_i . A *compound fragility* $Fr^{(C)}(x)$ (for the portfolio of structures) can be computed as:

$$Fr^{(C)}(x) = \sum_{i=1}^n w_i Fr^{(i)}(x) \quad \text{Eq. (3.9)}$$

where w_i = weight for structure type i , and $Fr^{(i)}(x)$ = individual fragility for structure type i .

Assuming all of the individual fragilities can be described by a lognormal distribution, Eq.

(3.9) can be written:

$$Fr^{(C)}(x) = \sum_{i=1}^n w_i \Phi\left(\frac{\ln(x) - \lambda_{R,i}}{\xi_{R,i}}\right) \quad \text{Eq. (3.10)}$$

where $\Phi(\cdot)$ = standard normal CDF, $\lambda_{R,i}$ = logarithmic median of capacity R of structure i , and $\xi_{R,i}$ = logarithmic standard deviation of capacity R of structure i . Figure 3.8 shows the compound fragility (considering the 1% drift limit) computed using Eq. (3.10) for a portfolio of structures consisting of 50% TYPE-I buildings, 30% TYPE-II buildings, and 20% TYPE-III buildings. All structures are assumed to be located in Exposure C. The individual structure fragilities, constructed using the simplified procedure, also are shown in Figure 3.8.

3.7 Summary and Conclusions

This study developed fragility curves for low-rise woodframe structures subjected to lateral wind loads. To accomplish this, three baseline structures were analyzed using a monotonic pushover analysis procedure that resulted in displacement vs. base shear curves. The base shears were then transformed to equivalent nominal wind speeds using configuration information of the baseline buildings and the wind load equations in ASCE 7 (2002). The displacement vs. equivalent nominal wind speed curves were used to determine the critical wind direction. Monte Carlo simulation was used along with statistics for wind load parameters to construct displacement vs. wind speed curves, and wind speeds corresponding to different displacement limits were then plotted to form fragility curves. The lateral wind fragility curves were well fit by a lognormal CDF. Since the range of

lognormal dispersion parameter ξ was small, approximate fragility curves also were able to be developed using the median value of wind speed at each drift limit and the average value of ξ . This approach does not require numerical simulation or statistical fitting techniques. Finally, a procedure was described for constructing a compound fragility which could be used to evaluate expected performance of an inventory of buildings.

The fragility methodology described herein can be used to develop performance-based design guidelines for woodframe structures in high wind regions as well as provide information on which to base structural safety and expected structural or economic loss assessments. Fragilities such as those presented here also can be convolved with wind hazard curves to evaluate probabilities of failure (in this case, excessive lateral drift) considering different performance levels.

3.8 References

ASCE (2002), *Minimum Design Loads for Buildings and Other Structures, Standard ASCE 7-02*. Structural Engineering Institute of the American Society of Civil Engineers, Reston, VA.

Durham, J.P. (1998), "Seismic Response of Wood Shearwalls with Oversized Oriented Strand Board Panels," MAsC Thesis, University of British Columbia, Vancouver, Canada.

Ellingwood, B.R. and Tekie, P.B. (1999), "Wind load statistics for probability-based structural design," *Journal of Structural Engineering*, ASCE, 125(4):453-463.

Ellingwood, B.R., Rosowsky, D.V., Li, Y. and Kim, J.H. (2004), "Fragility assessment of light-frame construction subjected to wind and earthquake hazards," *ASCE Journal of Structural Engineering*, ASCE. (in press)

FEMA (2000a), *Prestandard and Commentary for the Seismic Rehabilitation of Buildings*, Federal Emergency Management Agency, Washington, DC.

FEMA (2000b), *Global Topics Report on the Prestandard and Commentary for the Seismic Rehabilitation of Buildings*, Federal Emergency Management Agency, Washington, DC.

Folz, B. and Filiatrault, A. (2000), *CASHEW- Version 1.0: A Computer Program for Cyclic Analysis of Wood Shear Walls*, CUREE Publication No. W-08, Consortium of Universities for Research in Earthquake Engineering, Richmond, CA.

Folz, B. and Filiatrault, A. (2001), "Cyclic Analysis of Wood Shear Walls," *Journal of Structural Engineering*, ASCE, 127(4):433-441.

Folz, B. and Filiatrault, A. (2003), *SAWS – A Computer Program for Seismic Analysis of Woodframe Structures*, CUREE Publication No. W-21, Consortium of Universities for Research in Earthquake Engineering, Richmond, CA.

Kim, J.H. (2003), "Performance-Based Seismic Design of Light-Frame Shearwalls," Ph.D. dissertation, Department of Civil, Construction, and Environmental Engineering, Oregon State University, Corvallis, OR.

Lee, K.H. and Rosowsky, D.V. (2004), "Fragility Curves for Roof Sheathing Failure in High Wind Regions." (submitted to *Engineering Structures*)

NAHB (1997), *Housing Affordability through Design Efficiency Program*. NAHB Research Center. Inc., Upper Marlboro, MD.

Rosowsky, D.V and Ellingwood, B.R. (2002), "Performance-Based Engineering of Wood Frame Housing: a Fragility Analysis Methodology," *ASCE Journal of Structural Engineering*, 128(1):32-38.

Rosowsky, D.V. and Kim, J.H. (2002a), *Reliability Studies*, CUREE Publication No. W-10, Consortium of Universities for Research in Earthquake Engineering, Richmond, CA.

Rosowsky, D.V. and Kim, J.H. (2002b), "Performance-Based Seismic Design of Wood Shearwalls," *Proceedings: World Conference on Timber Engineering (WCTE 2002)*, Selangor, Malaysia.

Philips, Y.L., Itani, R.Y. and McLean, D.L. (1993) "Lateral Load Sharing by Diaphragms in Wood-Frame Buildings," *Journal of Structural Engineering*, ASCE, 119(5):1556-1571.

Table 3.1 - Dimensions and construction details for baseline structures

		TYPE-I	TYPE-II	TYPE-III
Plan dimension		28 ft × 40 ft (8.5 m × 12.2 m)	28 ft × 40 ft (8.5 m × 12.2 m)	20 ft × 32 ft (6.1 m × 9.8 m)
No. of stories		1	2	1
Wall	height	8 ft (2.44 m)	16 ft (4.88 m)	8 ft (2.44 m)
	stud spacing	16 in o.c. (40.6 cm)	16 in o.c. (40.6 cm)	24 in o.c. (61 cm)
	stud size	2 in. × 4 in. ⁽³⁾ (50 mm × 100 mm)	2 in. × 4 in. ⁽³⁾ (50 mm × 100 mm)	2 in. × 4 in. ⁽³⁾ (50 mm × 100 mm)
	sheathing panel	OSB 3/8 in. (9.5mm)	OSB 3/8 in. (9.5mm)	OSB 3/8 in. (9.5mm)
	nail type	8d box nail ⁽¹⁾	8d box nail ⁽¹⁾	Durham spiral nail ⁽²⁾
	nail schedule [edge/field]	6 in. / 12 in. (150 mm / 300 mm)	6 in. / 12 in. (150 mm / 300 mm)	6 in. / 12 in. (150 mm / 300 mm)
	hold-down	assumed to be designed and installed properly		
Roof	type	Gable	Gable	Gable
	slope	6:12 (26.6°)	8:12 (33.7°)	4:12 (18.4°)
	overhang	12 inch (30.5 cm)	12 inch (30.5 cm)	12 inch (30.5 cm)

(1) 2 ½ in. (63.5mm) long × 0.113 in. (2.87 mm) diameter

(2) 2 in. (150 mm) long × 0.105 in. (2.67 mm) diameter

(3) the top-plate and end studs are double members while the sole-plate and interior studs are single members.

Table 3.2 – Statistics for wind load parameters
(based on work by Ellingwood and Tekie, 1999)

Wind load parameters		categories	nominal	Mean-to-nominal (mean)	COV	CDF
Velocity pressure	K_z	Exp B	0.70	1.01 (0.71)	0.19	Normal
		Exp C	0.85	0.96 (0.82)	0.14	
		Exp D	1.03	0.96 (0.99)	0.14	
Directionality	K_d	MWFRS	0.85	1.01 (0.86)	0.125	Normal
Topographic	K_{zt}	-	deterministic (= 1.0)			
Importance	I	-	deterministic (= 1.0)			
External pressure	GC_{pf}	zones 1,2,3,4	(1)	0.86	0.18	Normal
		zones 1E,2E,3E,4E	(1)	0.80	0.18	Normal

(1) from Figure 6-10 in ASCE 7-02

Table 3.3 – Lognormal parameters for lateral wind fragilities determined by simulation

drift limit	structure	exposure	with directionality factor		without directionality factor	
			λ	ξ	λ	ξ
1%	TYPE-I	B	5.43	0.12	5.35	0.11
		C	5.35	0.10	5.28	0.08
		D	5.25	0.11	5.18	0.08
	TYPE-II ⁽¹⁾	B	5.14	0.12	5.16	0.11
		C	5.06	0.10	5.08	0.08
		D	4.97	0.10	4.99	0.08
	TYPE-III	B	5.25	0.13	5.16	0.12
		C	5.17	0.10	5.10	0.09
		D	5.08	0.12	5.00	0.09
2%	TYPE-I	B	5.52	0.12	5.45	0.11
		C	5.45	0.10	5.37	0.08
		D	5.36	0.11	5.27	0.09
	TYPE-III	B	5.36	0.13	5.29	0.12
		C	5.28	0.10	5.21	0.09
		D	5.19	0.11	5.12	0.09

(1) Note: the TYPE-II structure failed before the 2% drift limit was reached.

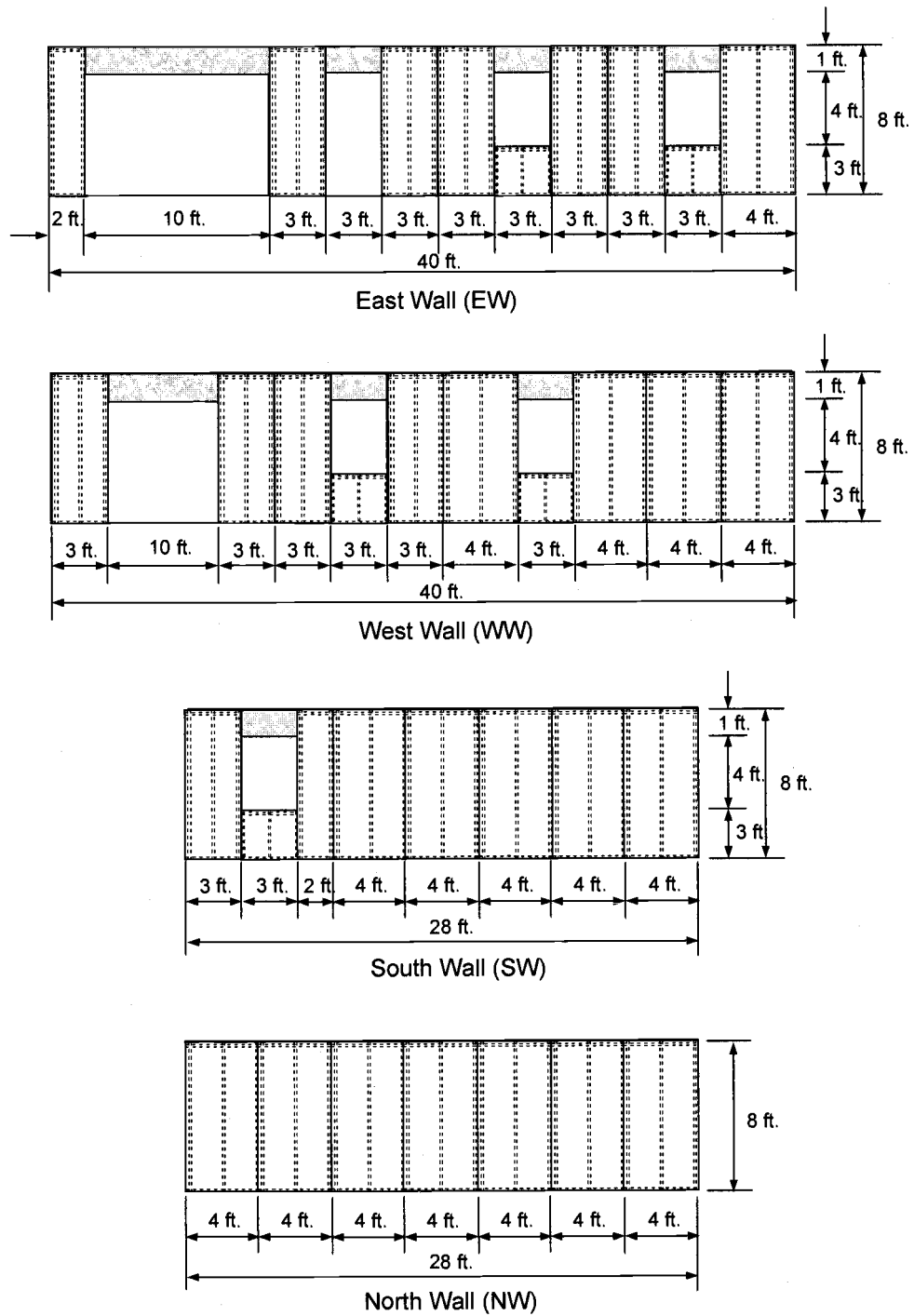
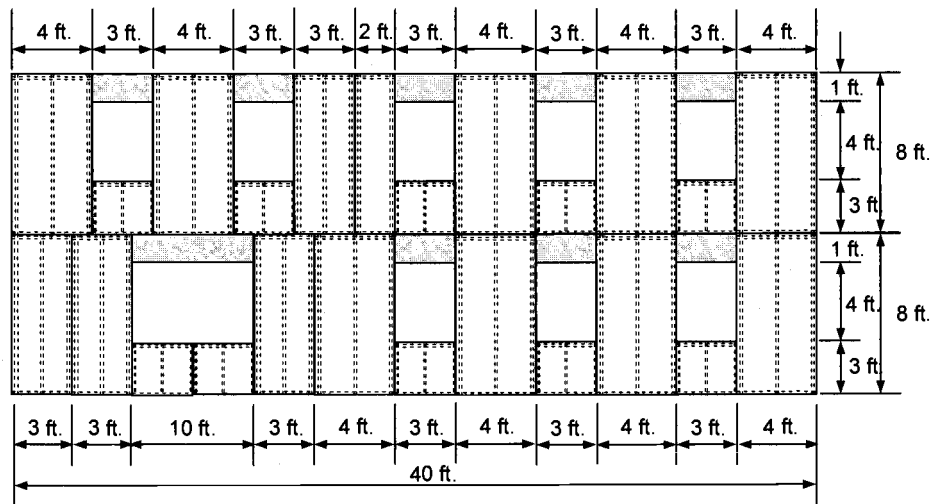
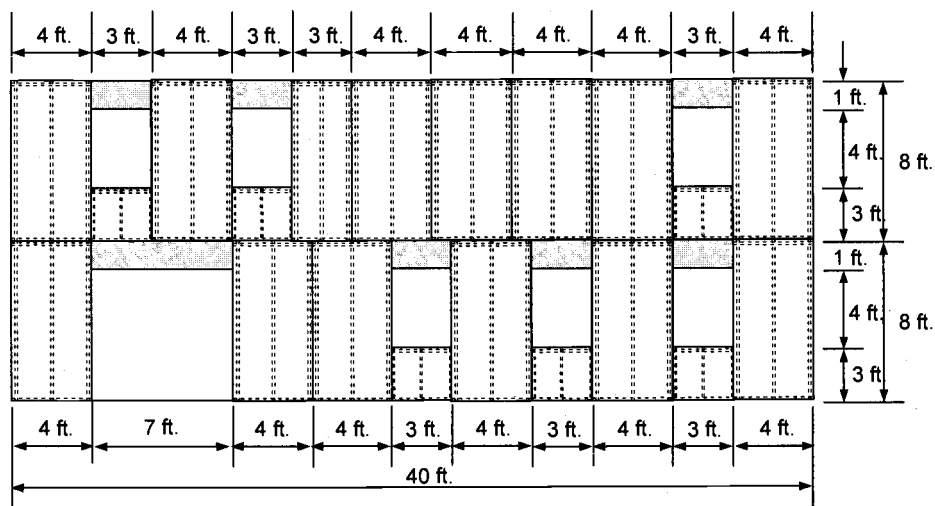


Figure 3.1(a) – Detailed wall configurations for Type-I house model



East Wall (EW)



West Wall (WW)

Figure 3.1(b) – Detailed wall configurations for Type-II house model

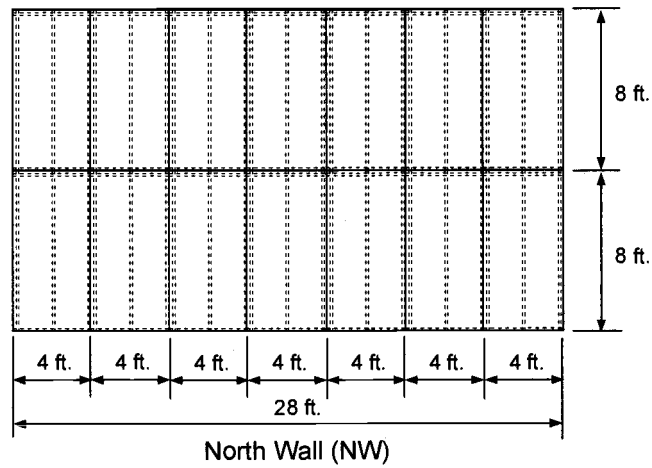
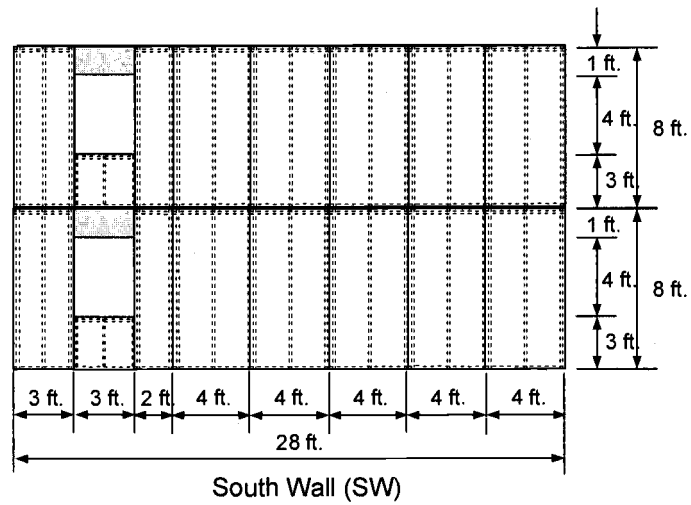


Figure 3.1(b) – Detailed wall configurations for Type-II house model (continued)

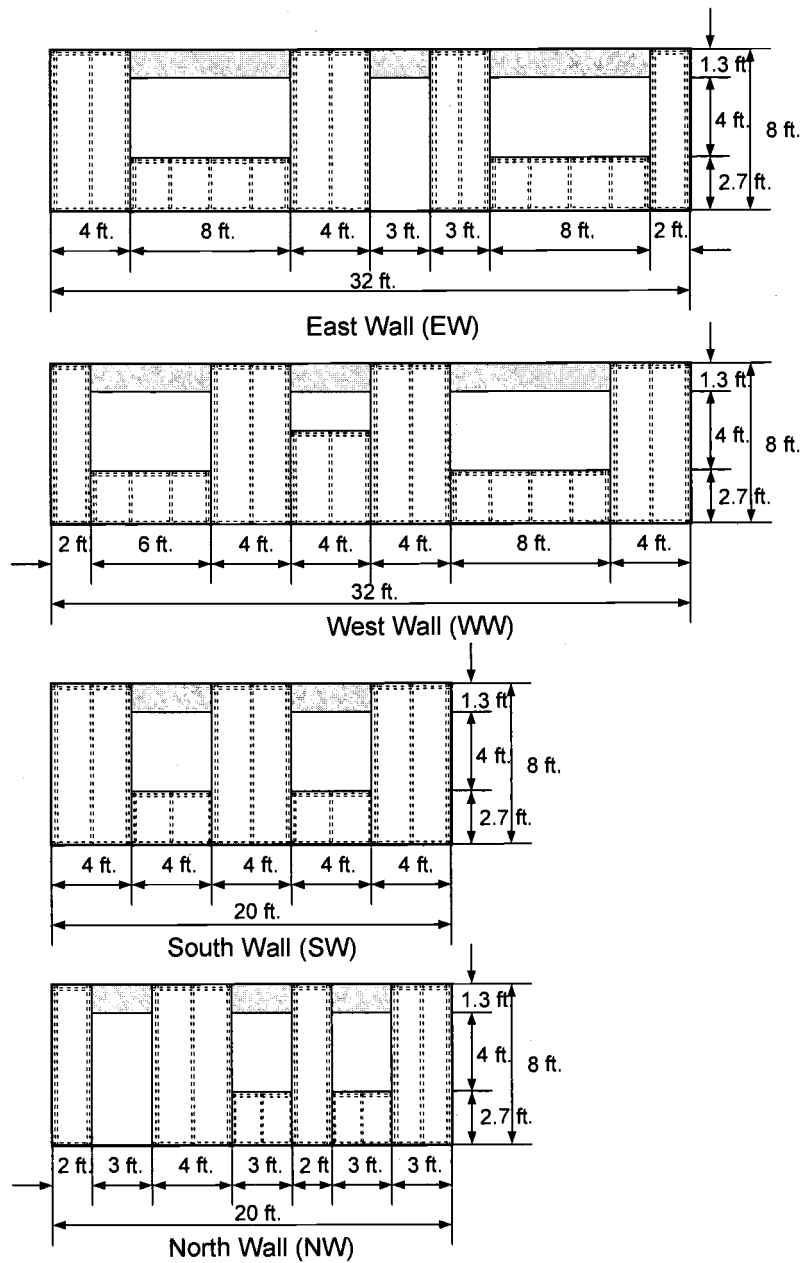


Figure 3.1(c) – Detailed wall configurations for Type-III house model

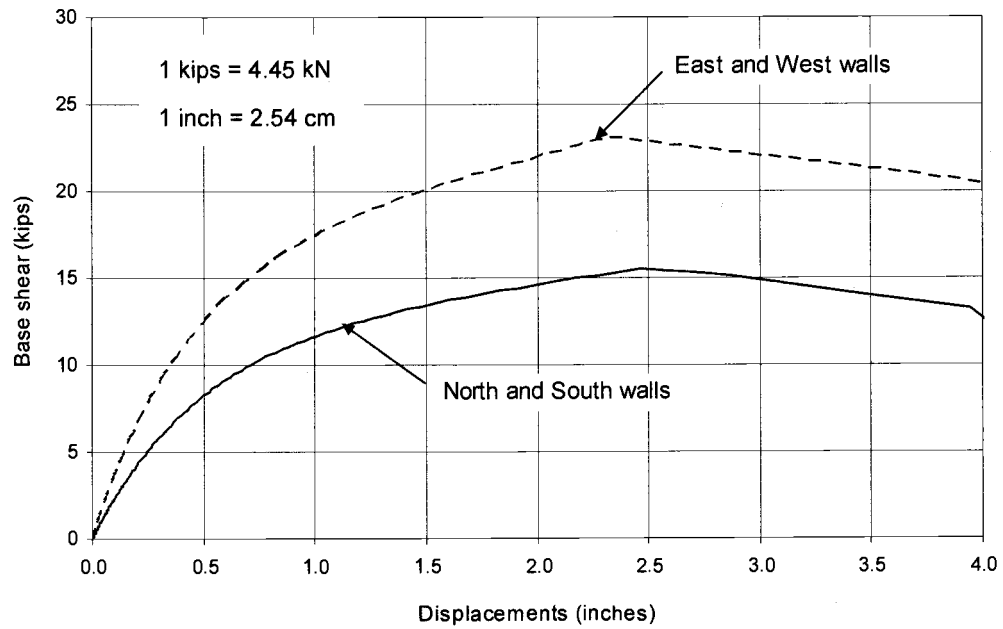


Figure 3.2 – Pushover curves for Type-III building considering two different load directions

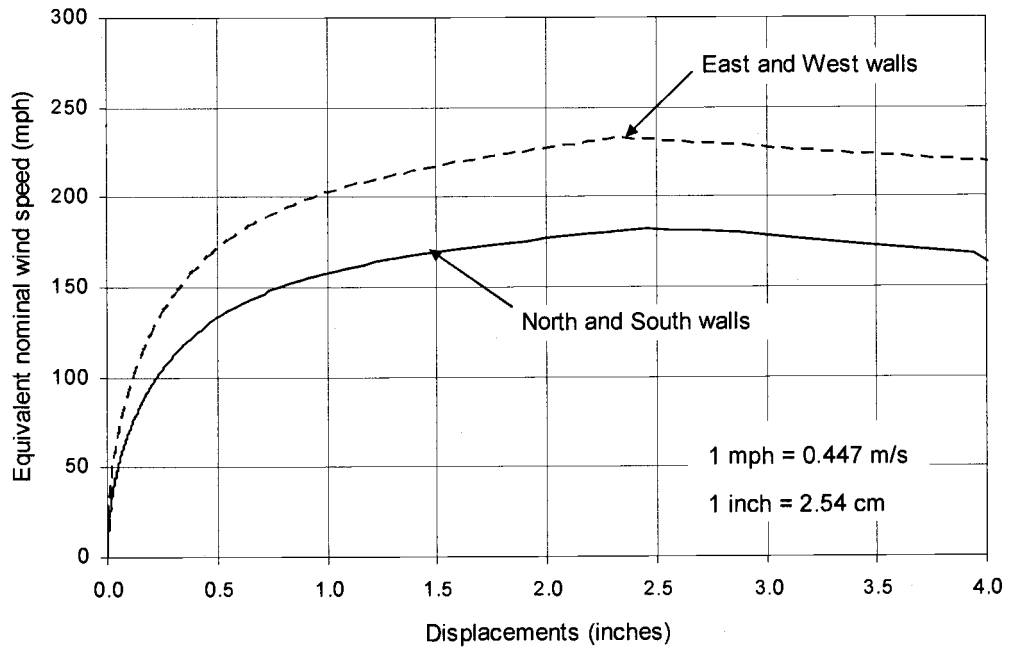


Figure 3.3 – Equivalent wind speed pushover curves for Type-III building considering two different wind directions

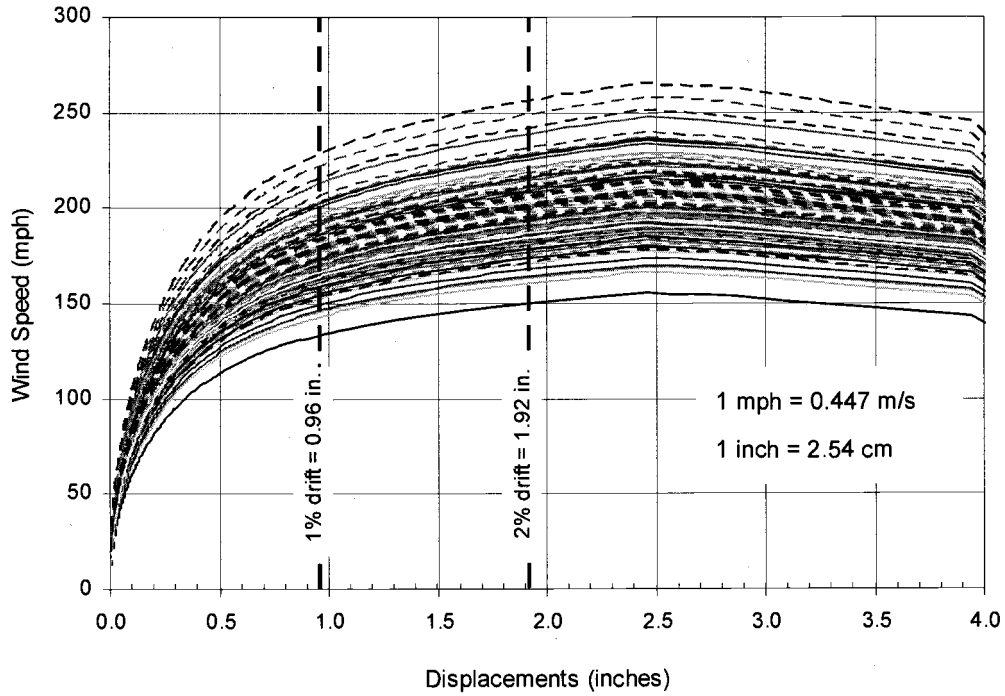


Figure 3.4 – Equivalent wind speed pushover curves considering random wind load [Type-III building, Exposure C, with directionality factor]

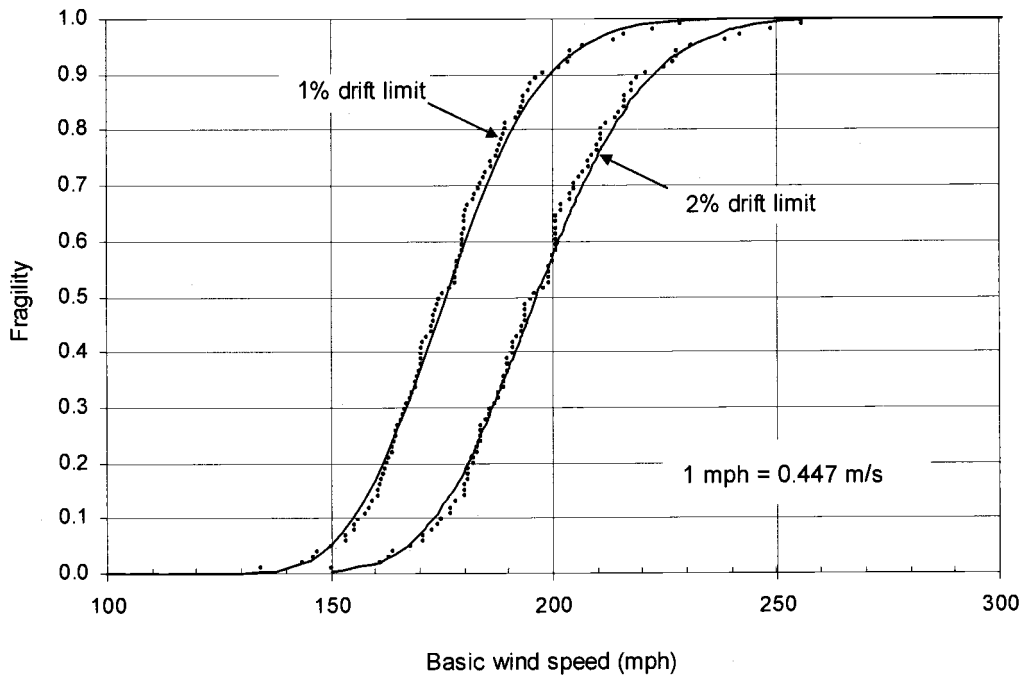


Figure 3.5 – Lognormal-fitted fragility curves for different displacement limits [TYPE-III building, Exposure C, with directionality factor]

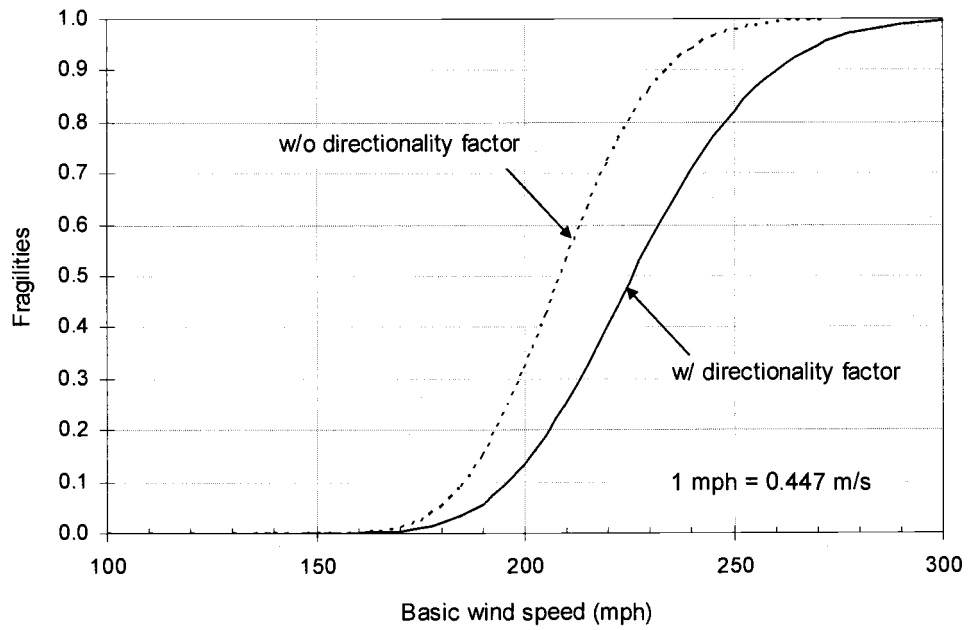


Figure 3.6 – Fragility comparison with and without wind directionality factor
 [TYPE-I building, 1% drift limit, Exposure B]

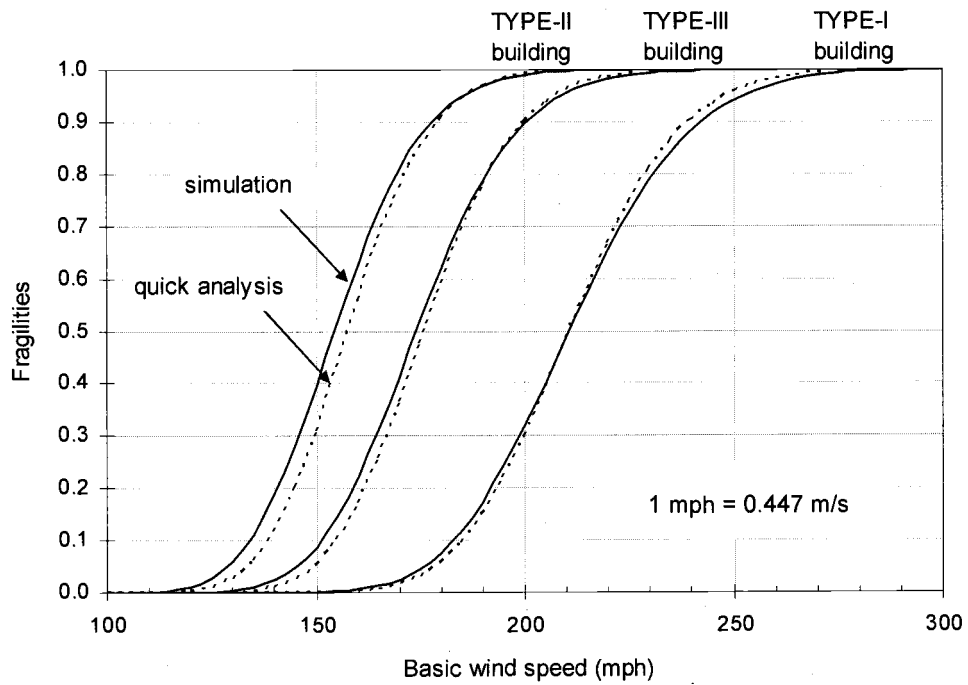


Figure 3.7 – Comparison of fragilities using the simulation and the quick analysis
 [1% drift limit, Exposure C, with directionality factor]

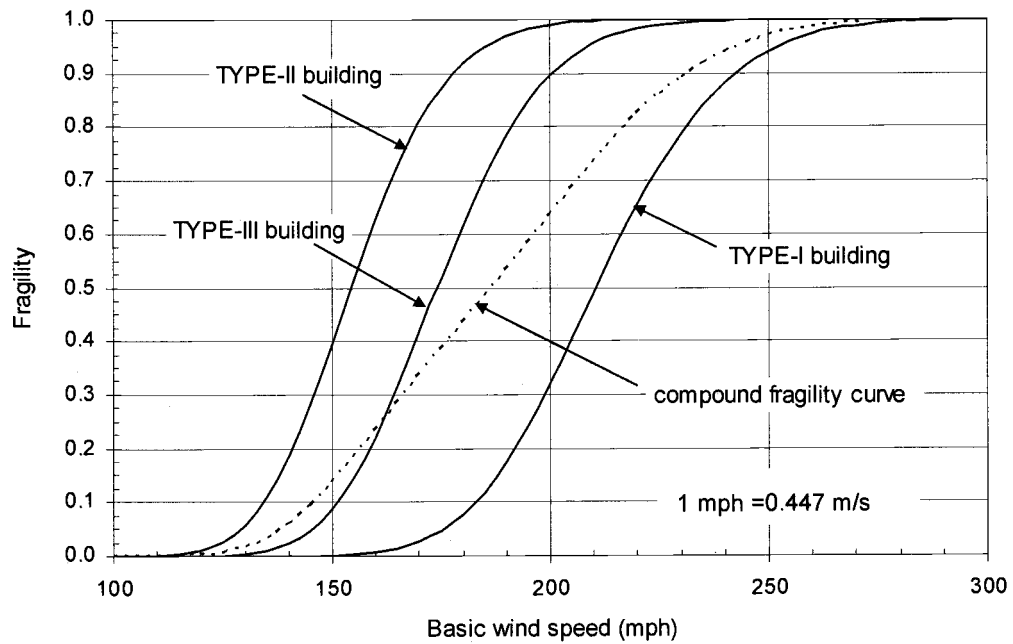


Figure 3.8 – Example of compound fragility curve
 [1% drift limit, Exposure C, with directionality factor]
 [Example for TYPE-I (50%), TYPE-II (30%), and TYPE III (20%)]

Site-Specific Snow Load Models and Hazard Curves for Probabilistic Design

Kyung Ho Lee

David V. Rosowsky

For Submission to *Natural Hazards Review*

ASCE (American Society of Civil Engineers)

1801 Alexander Bell Drive

Reston, VA 20191-4400, USA

4. Site-Specific Snow Load Models and Hazard Curves for Probabilistic Design

4.1 Abstract

This paper describes a study to develop site-specific probabilistic snow load models for use in reliability analyses of structures in the United States. Annual maximum snow water-equivalent depth data measured at 93 first-order weather stations was obtained from the National Climatic Data Center [NCDC, 2002]. These were then converted to annual maximum ground snow loads and statistics at each site were obtained using graphical fitting techniques. The 50-year maximum roof snow load values (in ratio to code-specified nominal values) were then evaluated site-by-site using the statistics for annual maximum ground snow, extreme value theory, Monte Carlo simulation, statistics for ground-to-roof conversion factors, and the nominal ground snow load values in ASCE 7 (2002). Finally, the 84 sites in the continental U.S. (excluding 9 sites in Alaska) were grouped on the basis of the 5% exclusion values of actual-to-nominal 50-year maximum roof snow load. Aggregated statistics for 50-year roof snow load in three geographic regions (designated Northeast, Midwest/Mid-Atlantic, and Northern Midwest/Mountain West) were determined. The roof snow load models developed in this study can be used in code calibration studies and development of next-generation partial safety factors. Snow load models such as those developed herein are developed using data from weather stations typically located at airport or military base locations. Therefore, they are not applicable to special locations such as mountainous regions or gorges. ASCE 7 (2002) suggests that design snow loads in

such cases should be based on local snow information with consideration given to the orientation, elevation, and records available at each location. Using the state of Oregon as an example, this study also develops county-scale design ground snow load curves and then post-processes this information into snow hazard curves. Both the design ground snow load curves and the snow hazard curves are presented as functions of elevation for each county area (defined as areas having similar ground snow load versus elevation relationships). To evaluate structural performance of a building subjected to snow load in a performance-based framework, snow hazard curves can be convolved with fragility curves for the building. This study demonstrates one approach for developing snow hazard curves for special regions (mountain areas and gorges) for use in such performance-based design applications.

4.2 Introduction

The weight of snow on a roof can be a significant structural load to be considered when designing structures in mountainous regions of the western U.S. or other high-snow regions. Winter storms, bringing snow, ice, and rain, cause several roof collapses each year. These collapses account for millions of dollars in property damage and interruption of production and operation [ZSC, 2003].

Probability-based structural design concepts have evolved considerably over the past two decades, leading to the most recent probability-based limit states design codes such as LRFD. Limit states design codes have requirements to ensure that structures perform

satisfactorily under various load effects and load combinations, and that structures have reliable and consistent safety levels. Probabilistic load models are essential components in reliability analyses which form the basis for these code provisions. The current LRFD load factors [ASCE, 2002] are based on probabilistic snow load models developed in the late 1970's. These models have remained unchanged despite developments in quantifying snow load effects [O'Rourke and Stiefel, 1983; Bennett, 1989], nominal ground snow load values [ASCE, 2002], and the availability of additional load data [NCDC, 2002].

Standards such as ASCE 7 (2002) and the IBC (2003) provide design ground snow load maps for use in structural design. However, most mountain areas, including many locations in the Northwest U.S., are designated as regions for which site-specific case studies are required. The Structural Engineers Association of Oregon (SEAO) published a design snow guide for the state, released first in 1971 and revised in 1978 [SEAO, 1978]. However, more than 25 years of additional snow data are available and statistical techniques have evolved considerably since that guide was developed. This study demonstrates one approach for developing snow hazard curves (using the state of Oregon as a case study) for these special regions, having both mountains and gorges. Specially, snow load design curves having different MRI (mean recurrence interval) values and ground snow hazard curves are developed on the basis of "county areas" (geographic groupings which have similar load versus elevation relationships). For use in performance-based design, the design snow curves for each county area were then converted to ground snow load hazard curves for different elevations.

This study therefore had two main objectives:

- 1) Update site-specific probabilistic snow load models for the continental U.S. (for reliability analysis and code calibration studies) using more than 25 years of additional snow data, an improved understanding of snow load effects, and improved simulation and statistical fitting techniques.
- 2) Construct design ground snow load models (for reliability-based design) and ground snow hazard curves (for performance-based design) for the state of Oregon.

4.3 Probabilistic Snow Load Model

4.3.1 Background

For design purposes, roof snow load often is calculated on the basis of information on the ground snow cover. Roof snow loads can be derived using ground snow data and field surveys on ground and roof snow covers which have provided information on ground-to-roof snow conversion as a function of roof exposure, geometry, and thermal characteristics. In work that formed the basis for the LRFD provisions in ASCE 7, Ellingwood et al. (1980) assumed the snow load acting on a roof could be determined as:

$$S = C_s q \quad \text{Eq. (4.1)}$$

where S = roof snow load, q = ground snow load, and C_s = conversion factor for ground snow load to roof snow load. The conversion factor C_s depends on roof exposure,

geometry and thermal conditions. Ellingwood et al. (1980) assumed that C_s followed a Normal distribution with a mean of 0.50 and a COV of 0.23. Analysis of snow water-equivalent depth data by Tobiasson and Redfield (1980) indicated that the annual maximum ground snow loads followed a lognormal distribution with parameters that vary by site. Using the snow water-equivalent depth data, Ellingwood et al. (1980) estimated annual maximum ground snow load statistics for eight sites in the northeastern part of the United States and developed 50-year maximum ground snow statistics for these sites using extreme value theory. The CDF of the 50-year ground snow load was then converted to a CDF of 50-year roof snow load with knowledge of statistics of the parameter C_s . Monte Carlo simulation was then used to generate realizations of the 50-year maximum roof snow load and an Extreme Type II distribution was fit to the 90th percentile value and above of the distribution. A single, aggregated set of parameters for the actual-to-nominal roof snow load (S/S_n , with nominal value S_n taken from the 1972 ANSI A58.1 Standard) was then developed considering the eight sites. The ratio of S/S_n (aggregated for the eight sites) was found to have an Extreme Type II distribution with parameters $u = 0.72$ and $k = 5.82$. The corresponding values of mean-to-nominal and COV were 0.82 and 0.26, respectively.

Current snow load statistics used for code calibration and other reliability studies were developed on the basis of analyses performed in the 1970's. Since then, more than 25 years of additional snow data have become available, new information on converting ground-to-roof snow loads has been developed [O'Rourke and Stiefel, 1983; Bennett, 1988], and improvements have been made in statistical fitting/estimation techniques. Current roof

snow load statistics also are based on aggregate statistics from a small number of sites in the northeastern U.S. Therefore, it seems right time to update probabilistic snow load model for reliability analyses.

4.3.2 Ground Snow Load Data

Snow water-equivalent depth data and snow depth data are available from the NCDC (2002). Since snow density varies by time of year and geographic location, it is difficult to convert snow depth to snow load using a simple factor. Therefore, the snow water-equivalent depth is converted directly to ground snow load as follows:

$$P_g = \left(\frac{62.4}{12} \right) d_w \quad \text{Eq. (4.2)}$$

where P_g = ground snow load in lb/ft^2 , d_w = snow water-equivalent depth in inches. A total of 93 sites in high snow regions in the U.S. (including 9 sites in Alaska) were selected in this study. These are first-order weather stations which are typically located at airports or military bases. The average number of years of records was about 40. Figure 4.1 shows the distribution of the 84 continental U.S. sites used to develop the probabilistic snow load models. Annual maximum snow water-equivalent depth data for the sites was obtained from the NCDC (2002).

4.3.3 Conversion Factors for Roof Snow Load

ASCE 7 (2002) provides the following equation to convert from ground snow to roof snow:

$$P_{f,n} = 0.7C_e C_t I P_{g,n} \quad \text{Eq. (4.3)}$$

where $P_{f,n}$ = nominal flat-slope roof snow, C_e = exposure factor, C_t = thermal factor, I = importance factor ($I = 1$ for ordinary building), and $P_{g,n}$ = nominal ground snow load. Bennett (1988) suggested the following relationship between ground snow load and roof snow load based on the examination of numerous sites:

$$P_f = 0.47C'_e C'_t \varepsilon P_g \quad \text{Eq. (4.4)}$$

where P_f = flat roof snow load, C'_e = exposure factor, C'_t = thermal factor (values for C'_e and C'_t were provided in ANSI A58.1, 1982), ε = error term (random variable) which accounts for scatter in the conversion factor data unrelated to exposure and thermal terms [O'Rourke and Stiefel, 1983], and P_g = ground snow load. Dividing Eq. (4.4) by Eq. (4.3) results in:

$$\frac{P_f}{P_{f,n}} = \left(\frac{0.47}{0.7} \right) \left(\frac{C'_e}{C_e} \right) \left(\frac{C'_t}{C_t} \right) \varepsilon \left(\frac{P_g}{P_{g,n}} \right) = 0.67 \varepsilon \left(\frac{P_g}{P_{g,n}} \right) \quad \text{Eq. (4.5)}$$

Since the exposure factor C'_e and thermal factor C'_t in ANSI A58.1 (1982) are not significantly different from those in ASCE 7 (2002), the ratios C'_e/C_e and C'_t/C_t are assumed to be unity in Eq. (4.5). ASCE 7 (2002) accounts for roof slope factor with the following:

$$P_{s,n} = C_s P_{f,n} \quad \text{Eq. (4.6)}$$

where $P_{s,n}$ = nominal slope roof snow load, $P_{f,n}$ = nominal flat roof snow load, C_s = roof slope factor. Since Eq. (4.4) does not have a factor to account for roof slope, the conversion factor suggested by Ellingwood and O'Rourke (1985) is used here. Thus,

$$P_s = \hat{C}_s P_f \quad \text{Eq. (4.7)}$$

where P_s = sloped roof snow load, P_f = flat roof snow load, and \hat{C}_s = roof slope conversion factor given by Ellingwood and O'Rourke (1985) as follows:

$$\hat{C}_s = 1 - \frac{(\theta - 25)}{35} \quad \text{for } \theta > 25^\circ \quad \text{Eq. (4.8a)}$$

$$\hat{C}_s = 1 \quad \text{for } \theta \leq 25^\circ \quad \text{Eq. (4.8b)}$$

where θ = roof angle in degree. Eqns. (4.5) - (4.7) can be re-arranged to form the following equation:

$$\frac{P_s}{P_{s,n}} = 0.67 \varepsilon \left(\frac{\hat{C}_s}{C_s} \right) \left(\frac{P_g}{P_{g,n}} \right) = C \left(\frac{P_g}{P_{g,n}} \right) \quad \text{Eq. (4.9)}$$

O'Rourke and Stiefel (1983) determined that ε may be assumed to follow a lognormal distribution with $\lambda_\varepsilon = 0.0$ and $\zeta_\varepsilon = 0.42$ (corresponding to a mean of 1.09 and a coefficient of variation of 0.44). The roof slope factor \hat{C}_s / C_s is 1.0 for structures having a roof angle less than 25° . For structures having a 33° roof angle, this factor decreases to 0.86 (see Figure 7-2a in ASCE 7-02). In this study, structures having roof angles less than 25° were considered (conservative). Thus, the mean conversion factor C in Eq. (4.9) is calculated as $(0.67)(1.09)(1.0) = 0.73$ with a COV of 0.44 (corresponding lognormal parameters $\lambda_C = -0.40$ and $\zeta_C = 0.42$).

4.3.4 Updated Snow Load Models

Annual maximum snow water-equivalent depth data were converted to annual maximum ground snow loads using Eq. (4.2). Graphical fitting techniques were used to evaluate the best-fit distribution and parameters for the annual maximum ground snow loads. For 80% of the sites, the annual maximum ground snow load was best-fit by a lognormal distribution; the other 20% of the sites were best-fit by an Extreme Type I distribution. In all cases, the best fit was determined over the entire range of values. Table 4.1 shows the statistics for annual maximum ground snow load for the 93 sites. Figure 4.2 shows an example of a lognormal distribution fit to the annual maximum ground snow load data at

Rapid City, SD. Assuming the annual maximum ground snow loads are statistically independent and identically distributed, the CDF of the 50-year maximum ground snow load can be derived from the CDF of the annual maximum ground snow load as:

$$F_{S_{50}}(s) = [F_S(s)]^{50} \quad \text{Eq. (4.10)}$$

where S = annual maximum ground snow load and S_{50} = 50-year maximum ground snow load. If the annual maximum ground snow is assumed to follow a Lognormal distribution (80% of the sites follow lognormal distribution for annual maximum ground snow) and the annual maxima are statistically independent, the CDF of 50-year maximum ground snow S_{50} can be written as:

$$F_{S_{50}}(s) = [F_S(s)]^{50} = \left[\Phi \left(\frac{\ln(s) - \lambda_s}{\xi_s} \right) \right]^{50} \quad \text{Eq. (4.11)}$$

where λ_s and ξ_s are lognormal distribution parameters for the annual maximum snow loads. A similar expression can be written for the CDF of S_{50} when S follows an Extreme Type I distribution. Values of the 50-year maximum ground snow load can then be generated using Monte Carlo simulation. Statistics for actual-to-nominal 50-year maximum roof snow load can be determined using the nominal ground snow load values in ASCE 7 (2002), the simulated values of 50-year maximum ground snow load, and statistics for ground-to-roof snow load conversion (Eq. 4.9). The resulting distribution for the simulated

values of 50-year maximum actual-to-nominal roof snow load is not well-fit over its entire range by any single distribution. Instead, a lognormal distribution (which was found to provide the best overall fit) was fit to the 50-year maximum roof snow load above the 90th-percentile value. This upper-tail region is the critical region for probabilistic load models. Figure 4.3 shows an example of fitting a lognormal distribution to the actual-to-nominal 50-year maximum roof snow load (statistics shown in Table 4.2) at Rapid City, SD. Since the mean-to-nominal ratio varies widely (see Table 4.2), a single aggregated mean-to-nominal value for all sites has little value. Therefore, high snow regions were grouped on the basis of 95th-percentile values of actual-to-nominal 50-year maximum roof snow load. Of course, any number of different groupings may be possible, however for illustration, three groupings in the continental U.S. were considered. These regions, shown in Figure 4.4, are (1) Northeast, (2) Midwest/Mid-Atlantic, and (3) Northern Midwest/Mountain West. Aggregated statistics for each region are shown in Table 4.3. The statistics differ from those developed by Ellingwood et al. (1980) (mean-to-nominal = 0.82, and COV = 0.26) due to (1) differences in the conversion factor statistics, (2) differences in the nominal ground snow loads (ASCE 7, 2002 and ANSI A58.1, 1972), and (3) differences in site locations and number of sites considered.

4.4 Oregon Snow Hazard Curves

4.4.1 Background

Snow load provisions in ASCE 7 (2002) were developed using concurrent records of the ground snow depth and ground snow load (from snow water-equivalent depth) at 204 first-

order weather stations for periods averaging 33 years in length going up through the winter of 1992. A mathematical relationship was developed between the 2% depths and the 2% loads³. The nonlinear best-fit relationship between these extreme values was used to estimate the 2% ground snow loads at about 9200 other locations at which only snow depths were measured. These loads, as well as the extreme-value loads developed directly from snow load measurement at the 204 locations, were used to construct the maps. However, large areas of the Rocky Mountain West and Northwest regions (Montana, Idaho, Oregon, Washington, and Northern California) are designated as special “case study” regions for design snow load. The Structural Engineers Association of Oregon [SEAO, 1978] provides information on design ground snow loads for the state of Oregon. Most recently revised in 1978, the document presents design ground snow loads (33-year MRI values) versus elevation. This design load guideline document was developed on the basis of maximum recorded weights of snow on the ground as determined from measurements made by the Soil Conservative Service, Oregon State University, and the State Engineer of Oregon. Design snow loads for 23 county areas (groupings) were developed from monthly maximum measurements taken during the snow season from 1940 to 1969. All maximum values were then compared to the results of a Log Pearson Type 3 frequency analysis at the 3% level (equivalent to a return-period of 33 years). The site-specific 33-MRI snow loads in each county area were plotted versus the site elevation, and linear or exponential regression lines were fit. While useful for inferring design values for strength design, this

³ These terms are used in the ASCE 7 commentary and refer to the 2% (upper) exclusion values or 98th- percentile values, i.e., 50-year mean recurrence interval (MRI) values.

Oregon design snow load guide is not suitable for performance-based design as it only considers a single hazard level. Since the design guideline was first developed, more than 30 years of additional data have become available and remote-sensed weather stations have collected daily snow water-equivalent depth data throughout the Western United States. Thus, there is considerable new information on which to base updated design snow guidelines.

4.4.2 Ground Snow Load Data for Oregon

Snow water-equivalent depth data for the Western U.S. can be downloaded from the NRCS (National Resources Conservation Service) website⁴. NRCS provides real-time snow and climate data using automated remote sensing collected at sites in the mountainous regions of the western United States since 1980. This SNOTEL network of remote-sensed weather stations collect snow water-equivalent depth, snow depth, precipitation, temperature and other climatic elements in daily, monthly and yearly intervals. This information is used for forecasting and management of water supplies. NRCS also provides snow water-equivalent depth data collected from weather stations in mountain areas prior to 1980. The annual maximum snow water-equivalent depth data used in this study were obtained from 250 NRCS stations in Oregon (average period of record = 42 years) and 3 NCDC weather stations in Oregon (average period of record = 27 years).

⁴ ftp://ftp.wcc.nrcs.usda.gov/data/snow/snow_course/ - (March, 2003)

4.4.3 Development of Design Ground Snow Load

Snow load in mountainous regions can be both site and elevation-specific. Since large areas of Oregon are mountainous, it is necessary to divide the state into regions having similar trends or relationships between ground snow load and elevation. The Structural Engineers Association of Oregon, [SEAO, 1978] divided the state into 23 regions (county areas) on the basis of such snow characteristics. The present study uses the same regions as SEAO (1978) with some modifications: country areas G-19, 20, 21, and 22 were combined into P-01 and P-02. Figure 4.5 shows the NRCS and NCDC weather station sites and county area definitions used in the development of the Oregon design snow curves. Most NRCS weather stations are located in the Cascades Mountains, the range running along the western part of the state, or in the mountainous region in the northeast of part of the state.

The second objective of this study was to develop site-specific design snow load curves as functions of elevation considering different mean recurrence intervals (MRI's). Design curves were developed for each county area shown on Figure 4.5. Selected results are shown in this paper, however a complete sets of these curves are shown in Appendix C.1. Annual maximum ground snow loads for the 253 NRCS and NCDC stations, many of which are located in mountainous areas and gorges, were used. Statistical analysis and graphical fitting techniques were used to determine the best-fit distribution and parameters at each site. Site and elevation-specific ground snow loads having different annual exceedance probabilities (ranging from 0.1% to 50%) were then determined and design curves were constructed as functions of elevation for each county area using regression

analysis. Figure 4.6 shows the design snow load curves county area G-18 developed using this procedure.

County area G-18 has nine NRCS stations located at elevations ranging 4800 ft - 7900 ft (1463 m - 2408 m). The annual maximum ground snow loads for the stations in county area G-18 were found to follow an Extreme Type I (ET-I) distribution. Using a Type I distribution and the corresponding parameters, the values of ground snow load corresponding to different annual exceedance probabilities can be determined and these can be plotted versus elevation. Regression lines then can be determined for each annual exceedance probability level. In the case of area G-18, exponential curves provided the best-fit (with least square regression values greater than 0.95). Other groups had either linear or exponential regression curves (Appendix C.1).

4.4.4 Oregon Snow Hazard Curves

The design snow load curves developed in the previous section (snow load vs. elevation) for different annual exceedance probabilities can be useful for structural design. However, in order to be used in a hazard analysis, information presented in the design curves must be recast in the form of ground snow load hazard curves. Ground snow hazard curves can be used for performance-based design of structures subjected to snow loads, or combinations of loads including snow. Failure probabilities also can be calculated by convolving the ground snow hazard curves with fragility curves (e.g., for roof capacity, lateral deflections, etc.) which include ground-to-roof conversions.

A probabilistic model for snow hazard can be presented as a relationship between annual exceedance probability and ground snow load. This can be described by a complementary cumulative distribution function (CCDF), $G_x(x)$. Depending on the location/elevation, Oregon snow hazard curves may be best-fit by a lognormal, Extreme Type I, or exponential CCDF. These can be written as follows:

$$G_x(x) = 1 - \Phi\left(\frac{\ln(x) - \lambda}{\xi}\right) \quad (\text{lognormal}) \quad \text{Eq. 4.12(a)}$$

$$G_x(x) = 1 - \exp[-\exp[-k(x - u)]] \quad (\text{ET-I}) \quad \text{Eq. 4.12(b)}$$

$$G_x(x) = \exp(-vx) \quad (\text{exponential}) \quad \text{Eq. 4.12(c)}$$

In Eq. 4.12(a), $\Phi[\bullet]$ = standard normal cumulative distribution function, λ = logarithmic median, and ξ = logarithmic standard deviation (approximately equal to the coefficient of variation, V , when $V < 0.3$). In Eq. 4.12(b), u and k are ET-I scale and shape parameters, respectively. In Eq. 4.12(c), v = parameter for the exponential distribution. Parameters for the annual ground snow load hazard were determined from the annual maximum ground snow load statistics and best-fit distribution. Figure 4.7 presents the ground snow hazard curves for county area G-18. In this case, the ET-I distribution provided the best-fit at all elevations. Annual ground snow load hazard curves for the other areas shown in Figure 4.7 may be found in Appendix C.2, however Table 4.4 presents a summary of the hazard

functions and parameters for all county areas and elevations.

4.5 Summary and Conclusions

This paper reports on a study having two main objectives: (1) to develop improved (updated) snow load models for reliability analysis, and (2) to develop site/elevation-specific design snow load curves and corresponding snow hazard curves using the state of Oregon as an example. To accomplish the first objective, snow water-equivalent depth data were collected from NCDC first-order weather stations and best-fit distributions for annual maximum ground snow load were determined. Statistics for actual-to-nominal 50-year maximum roof snow loads were then determined using the nominal ground snow load values in ASCE 7 (2002), statistics for ground-to-roof snow load conversion, extreme value theory, Monte Carlo simulation, and graphical fitting techniques. The lognormal distribution was found to provide the best fit above the 90th-percentile values of actual-to-nominal 50-year maximum roof snow load for the sites considered. The continental U.S. was then divided into three regions based on comparable 95th-percentile values of actual-to-nominal 50-year roof snow load. Finally, aggregated statistics for actual-to-nominal 50-year maximum roof snow load for three regions were calculated. The Northeast region has a mean-to-nominal 50-year maximum roof snow load of 0.61 and COV of 0.53, the Midwest/Mid-Atlantic region has a mean-to-nominal 50-year maximum roof snow load of 0.84 and COV of 0.60, and the Northern Midwest/Mountain West has a mean-to-nominal 50-year maximum roof snow load of 0.80 and COV of 0.58. The aggregated statistics for these three regions, or the site-specific snow load statistics developed as part of this study

can be used for code calibration studies and development of next-generation partial safety factors.

To accomplish the second objective in this study, water-equivalent depth data for Oregon snow was collected from the NRCS and the NCDC, and statistics for annual maximum ground snow load at each site were determined. The state of Oregon was divided into 21 county areas, each having similar ground snow load versus elevation relationships. Best-fit distributions and parameters were then determined for the annual maximum ground snow load. Site and elevation-specific ground snow loads having different annual exceedance probabilities (ranging from 0.1% to 50%) were then determined and design curves were constructed as functions of elevation for each county area using regression analysis. These design snow curves can form the basis of design guidelines for Oregon snow load and can also be converted to ground snow load hazard curves. A procedure for constructing snow hazard curves for special regions (mountain and gorge regions) at different elevations also was presented in this paper. Such hazard curves can be used in a number of reliability-based design and performance-based design applications including assessment of partial safety factors for limit states design, evaluation of load combination (coincidence) factors considering multiple hazards, evaluation of failure probabilities (by convolving with fragility curves) for different performance levels, and development of risk-based assessment procedures for structures (and inventories of structures) under extreme snow loading.

4.6 References

ANSI A58.1 (1972), *Building Code Requirements for Minimum Design Loads in Buildings and Other Structures*, American National Standards Institute, New York, NY.

ANSI A58.1 (1982), *Minimum Design Loads for Buildings and Other Structures*, American National Standards Institute, New York, NY.

ASCE (2002), *Minimum Design Loads for Buildings and Other Structures*, Standard ASCE 7-02, Structural Engineering Institute of the American Society of Civil Engineers, Reston, VA.

Bennett, R.M. (1988), "Snow load factors for LRFD," *Journal of Structural Engineering*, ASCE, 114(10):2371-2383.

Ellingwood, B.R., Galambos, T.V., MacGregor, J.G. and Cornell, C.A. (1980), *Development of a Probability Based load Criterion for American National Standard A58*. Special Publication 577, U.S. Department of Commerce, National Bureau of Standards, Washington, DC.

Ellingwood, B.R. and Redfield, R. (1983), "Ground snow loads for structural design," *Journal of Structural Engineering*, ASCE, 109(4):950-964.

Ellingwood, B.R. and O'Rourke, M.J. (1985), "Probabilistic models of snow loads on structures," *Structural Safety*, 2:291-299.

Ellingwood, B.R. and Tekie, P.B. (2001), "Fragility analysis of concrete gravity dams," *Journal of Infrastructure Systems*, ASCE 7(2):41-48.

Galambos, T.V., Ellingwood, B.R., Macgregor, J.G. and Cornell, C.A. (1982), "Probability-based load criteria: Assessment of current design practice," *Journal of Structural Division*, ASCE, 108(5):959-977.

IBC (2003), *International Building Code*, International Code Council, Falls Church, VA.

NCDC (2002) – National Climatic Data Center – NCDC Climate Data Online,
<http://cdo.ncdc.noaa.gov/pls/plclimprod/poemain.accessrouter> - (July, 2002)

O'Rourke, M.J. and Stiefel, U. (1983), "Roof snow loads for structural design," *Journal of Structural Engineering*, ASCE, 109(7):1527-1537.

SEAO (1978), "Snow Load Analysis for Oregon," Structural Engineers Association of Oregon, State of Oregon, Department of Commerce, Building Codes Division, Salem, OR.

Tobiasson, W. and Redfield, R. (1980), "Snow load for the United States, Parts I and II," U.S. Army Cold Regions Research and Laboratory Report, Hanover, NH.

ZSC (2003), *Risk Topics – Snow loading roof collapse*, Zurich Service Corporation, Schaumburg, IL.

Table 4.1 - Statistics for annual maximum ground snow load

Site	State	WBAN ⁽¹⁾	Yrs. of record	Mean (psf ⁽²⁾)	COV	Best-fit distribution parameters		
						distribution	parameter 1 λ (LN) or u (ET-I)	parameter 2 ξ (LN) or k (ET-I)
Anchorage	AK	26451	47	15.3	0.65	LN	2.53	0.66
Barrow	AK	27502	37	9.8	0.62	LN	2.07	0.67
Bethel	AK	26615	45	12.2	0.66	LN	2.29	0.68
Cold Bay	AK	25624	38	10.5	0.96	LN	2	0.84
Fair Banks	AK	26411	48	23.5	0.52	LN	3.04	0.47
Homer	AK	25507	27	12.9	0.89	LN	2.25	0.79
Juneau	AK	25309	32	15.5	0.79	LN	2.48	0.73
Kodiak	AK	25501	39	8.6	1.12	LN	1.87	0.73
Kotzebue	AK	26616	36	17.9	0.77	LN	2.7	0.62
McGrath	AK	26510	47	27	0.51	ET-I	20.84	0.09
Talkeetna	AK	26528	25	32.7	0.45	LN	3.38	0.49
Yakutat	AK	25339	50	53.7	0.54	LN	3.81	0.65
Denver	CO	23062	44	5.7	0.71	LN	1.55	0.61
Bridgeport	CT	94702	44	6.2	0.75	LN	1.56	0.74
Hartford	CT	14740	42	10.1	0.7	ET-I	6.94	0.18
Washington	DC	13743	38	6.1	0.82	LN	1.48	0.86
Des Moines	IA	14933	45	7.2	0.7	LN	1.75	0.7
Dubuque	IA	94908	45	10.7	0.8	LN	2.11	0.71
Sioux City	IA	14943	44	7.9	0.85	LN	1.74	0.81
Waterloo	IA	94910	38	9.1	0.63	ET-I	6.47	0.22
Boise	ID	24131	42	3.3	0.71	LN	0.94	0.72
Pocatello	ID	24156	49	4.3	0.9	LN	1.22	0.66
Chicago	IL	94846	38	6.4	0.7	LN	1.7	0.56
Moline	IL	14923	44	6.6	0.69	LN	1.7	0.6
Peoria	IL	14842	45	5	0.82	LN	1.4	0.65
Rockford	IL	94822	38	6.7	0.73	LN	1.74	0.58
Springfield	IL	93822	42	6.1	0.81	LN	1.5	0.81
Evansville	IN	93817	38	4	0.72	LN	1.16	0.7
Fort Wayne	IN	14827	50	5.9	0.8	LN	1.53	0.71
Indianapolis	IN	93819	47	5.7	0.81	LN	1.49	0.7
Wichita	KS	3928	41	3.7	0.75	LN	1.01	0.81
Covington / Cincinnati	KY	93814	43	4.4	1.01	LN	1.2	0.71
Boston	MA	14739	45	10	0.67	ET-I	6.95	0.19
Worcester	MA	94746	37	13.6	0.56	ET-I	10.18	0.17
Baltimore	MD	93721	40	5.8	0.86	LN	1.45	0.82
Caribou	ME	14607	46	38.1	0.46	ET-I	30.21	0.07
Portland	ME	14764	43	19.7	0.6	ET-I	14.41	0.11
Alpena	MI	94849	38	17.9	0.43	ET-I	14.4	0.17
Detroit	MI	94847	41	7.9	0.79	LN	1.79	0.74
Grand Rapids	MI	94860	49	11.9	0.78	LN	2.23	0.72
Houghton Lake	MI	94814	32	14.1	0.6	ET-I	10.31	0.15
Lansing	MI	14836	39	10.5	0.67	LN	2.15	0.66

Table 4.1 - Statistics for annual maximum ground snow load (continued)

Site	State	WBAN ⁽¹⁾	Yrs. of record	Mean (psf ⁽²⁾)	COV	Best-fit distribution parameters		
						distribution	parameter 1 λ (LN) or u (ET-I)	parameter 2 ξ (LN) or k (ET-I)
Sault Ste. Marie	MI	14847	45	31.6	0.45	ET-I	25.16	0.09
Duluth	MN	14913	47	25.8	0.45	ET-I	20.49	0.11
International Falls	MN	14918	45	17.8	0.47	ET-I	14.06	0.15
Minneapolis -St. Paul	MN	14922	45	12.4	0.68	LN	2.26	0.76
Rochester	MN	14925	44	11.8	0.61	ET-I	8.55	0.18
Billings	MT	24033	45	6.2	0.67	LN	1.67	0.52
Glasgow	MT	94008	47	5.4	0.72	LN	1.46	0.70
Great Falls	MT	24143	45	6.3	0.63	LN	1.69	0.55
Helena	MT	24144	43	6.5	0.69	LN	1.67	0.67
Missoula	MT	24153	49	7.3	0.72	LN	1.75	0.69
Bismarck	ND	24011	49	7.3	0.86	LN	1.68	0.78
Fargo	ND	14914	44	10.4	0.75	LN	2.00	0.93
Norfolk	NE	14941	46	6.9	0.90	LN	1.62	0.77
Omaha	NE	14942	26	6.5	0.78	LN	1.58	0.70
Scottsbluff	NE	24028	46	4.2	0.55	ET-I	3.17	0.55
Concord	NH	14745	48	18.0	0.58	ET-I	13.28	0.12
Atlantic City	NJ	93730	34	4.6	1.11	LN	1.13	0.86
Newark	NJ	14734	44	5.2	0.93	LN	1.23	1.00
Reno	NV	23185	39	3.4	0.97	LN	0.88	0.81
Albany	NY	14735	48	10.2	0.55	LN	2.18	0.56
New York	NY	94789	28	5.6	0.82	LN	1.40	0.85
Rochester	NY	14768	50	13.5	0.66	LN	2.40	0.66
Akron	OH	14895	49	5.4	0.58	LN	1.54	0.56
Cleveland	OH	14820	50	7.3	0.71	LN	1.78	0.63
Columbus	OH	14821	46	5.2	1.19	LN	1.28	0.80
Mansfield	OH	14891	37	7.0	1.09	LN	1.54	0.85
Toledo	OH	94830	41	4.2	0.76	LN	1.26	0.57
Pendleton	OR	24155	41	3.8	0.63	LN	1.13	0.69
Portland	OR	24229	17	2.9	0.81	LN	0.85	0.64
Salem	OR	24232	21	2.8	0.52	LN	0.89	0.60
Allentown	PA	14737	45	8.1	1.01	LN	1.80	0.75
Philadelphia	PA	13739	45	4.7	0.72	LN	1.29	0.74
Pittsburgh	PA	94823	48	7.3	0.85	LN	1.70	0.75
Providence	RI	14765	43	7.7	0.70	LN	1.80	0.73
Aberdeen	SD	14929	35	9.1	0.79	LN	1.87	0.88
Rapid City	SD	24090	44	5.0	0.74	LN	1.37	0.69
Sioux Falls	SD	14944	50	10.7	0.87	LN	2.02	0.88
Burlington	VT	14742	48	14.3	0.66	LN	2.47	0.63

Table 4.1 - Statistics for annual maximum ground snow load (continued)

Site	State	WBAN ⁽¹⁾	Yrs. of record	Mean (psf ⁽²⁾)	COV	Best-fit distribution parameters		
						distribution	parameter 1 λ (LN) or u (ET-I)	parameter 2 ξ (LN) or k (ET-I)
Olympia	WA	24227	27	5.5	0.93	LN	1.38	0.83
Seattle	WA	24233	27	4.9	0.82	LN	1.26	0.88
Yakima	WA	24243	40	6.7	0.79	LN	1.61	0.83
Green Bay	WI	14898	49	10.5	0.65	LN	2.15	0.67
La Crosse	WI	14920	16	7.4	0.89	LN	1.63	0.88
Madison	WI	14837	44	9.2	0.80	LN	1.91	0.82
Milwaukee	WI	14839	44	9.3	0.74	LN	2.00	0.70
Beckley	WV	3872	36	8.1	0.75	LN	1.84	0.73
Charleston	WV	13866	42	4.4	0.98	LN	1.09	0.91
Huntington	WV	03860	33	5.0	0.82	LN	1.26	0.90
Casper	WY	24089	45	4.0	0.56	LN	1.26	0.50
Cheyenne	WY	24018	48	6.4	0.86	LN	1.58	0.77
Sheridan	WY	24029	45	6.5	0.71	LN	1.67	0.62

(1) WBAN: A five-digit station identifier used at NCDC for digital data storage and general station identification purposes

(2) 1 psf = 47.88 N/m²

Table 4.2 – Statistics for 50-year maximum roof snow load

Site	ST	wban	Nominal ground snow (psf ⁽¹⁾)	50-year maximum roof snow load					
				(Lognormal distribution)					
				λ	ξ	Mean-to- nominal	COV	90% value	95% value
Anchorage	AK	26451	50	-0.38	0.49	0.77	0.52	1.29	1.50
Barrow	AK	27502	25	-0.26	0.53	0.89	0.57	1.52	1.85
Bethel	AK	26615	40	-0.47	0.54	0.72	0.58	1.26	1.51
Cold Bay	AK	25624	25	0.55	0.84	2.46	1.00	5.23	7.05
Fair Banks	AK	26411	60	-0.42	0.51	0.75	0.54	1.27	1.53
Homer	AK	25507	40	-0.17	0.61	1.02	0.67	1.82	2.28
Juneau	AK	25309	60	-0.47	0.56	0.73	0.61	1.25	1.59
Kodiak	AK	25501	30	-0.14	0.69	1.10	0.78	2.06	2.69
Kotzebue	AK	26616	60	-0.32	0.57	0.85	0.61	1.51	1.85
McGrath	AK	26510	70	-0.45	0.47	0.71	0.49	1.16	1.37
Talkeetna	AK	26528	120	-0.82	0.49	0.50	0.52	0.83	0.99
Yakutat	AK	25339	150	-0.48	0.45	0.68	0.47	1.11	1.31
Denver	CO	23062	20	-0.44	0.54	0.75	0.58	1.29	1.55
Bridgeport	CT	94702	30	-0.70	0.52	0.57	0.56	0.97	1.17
Hartford	CT	14740	30	-0.36	0.46	0.78	0.48	1.24	1.47
Washington	DC	13743	25	-0.52	0.59	0.71	0.65	1.26	1.56
Des Moines	IA	14933	25	-0.39	0.48	0.76	0.51	1.25	1.50
Dubuque	IA	94908	30	-0.11	0.55	1.04	0.59	1.81	2.30
Sioux City	IA	14943	30	-0.40	0.56	0.78	0.61	1.39	1.69
Waterloo	IA	94910	30	-0.51	0.47	0.67	0.49	1.09	1.31
Boise	ID	24131	10	-0.34	0.53	0.82	0.57	1.42	1.72
Pocatello	ID	24156	15	-0.15	0.53	0.99	0.57	1.70	2.07
Chicago	IL	94846	25	-0.58	0.55	0.65	0.60	1.13	1.38
Moline	IL	14923	25	-0.47	0.50	0.71	0.54	1.18	1.43
Peoria	IL	14842	20	-0.48	0.58	0.73	0.63	1.29	1.56
Rockford	IL	94822	25	-0.42	0.51	0.75	0.55	1.28	1.53
Springfield	IL	93822	20	-0.28	0.55	0.87	0.59	1.51	1.87
Evansville	IN	93817	15	-0.47	0.51	0.72	0.55	1.18	1.45
Fort Wayne	IN	14827	20	-0.32	0.57	0.86	0.62	1.50	1.85
Indianapolis	IN	93819	20	-0.38	0.57	0.81	0.62	1.39	1.71
Wichita	KS	3928	15	-0.51	0.54	0.69	0.59	1.19	1.46
Covington /Cincinnati	KY	93814	20	-0.40	0.60	0.80	0.65	1.43	1.80
Boston	MA	14739	40	-0.71	0.48	0.55	0.51	0.92	1.09
Worcester	MA	94746	40	-0.45	0.45	0.70	0.47	1.14	1.33
Baltimore	MD	93721	25	-0.46	0.59	0.75	0.64	1.35	1.66
Caribou	ME	14607	100	-0.49	0.45	0.68	0.47	1.09	1.27
Portland	ME	14764	60	-0.49	0.46	0.68	0.49	1.11	1.31

Table 4.2 – Statistics for 50-year maximum roof snow load (continued)

Site	ST	wban	Nominal ground snow (psf ⁽¹⁾)	50-year maximum roof snow load					
				(Lognormal distribution)					
				λ	ξ	Mean-to- nominal	COV	90% value	95% value
Alpena	MI	94849	50	-0.57	0.44	0.63	0.46	0.98	1.16
Detroit	MI	94847	20	-0.01	0.54	1.15	0.58	1.97	2.43
Grand Rapids	MI	94860	35	-0.12	0.50	1.01	0.54	1.72	2.00
Houghton Lake	MI	94814	50	-0.68	0.48	0.57	0.51	0.94	1.12
Lansing	MI	14836	25	-0.11	0.53	1.03	0.57	1.78	2.13
Sault Ste. Marie	MI	14847	80	-0.49	0.48	0.68	0.51	1.14	1.34
Duluth	MN	14913	60	-0.39	0.47	0.75	0.50	1.26	1.46
International Falls	MN	14918	50	-0.59	0.46	0.62	0.48	1.00	1.19
Minneapolis -St. Paul	MN	14922	50	-0.60	0.52	0.63	0.56	1.07	1.30
Rochester	MN	14925	50	-0.85	0.47	0.48	0.50	0.78	0.92
Billings	MT	24033	20	-0.41	0.51	0.76	0.55	1.26	1.55
Glasgow	MT	94008	30	-0.89	0.54	0.48	0.59	0.81	1.00
Great Falls	MT	24143	20	-0.49	0.54	0.71	0.58	1.23	1.49
Helena	MT	24144	20	-0.28	0.54	0.87	0.58	1.50	1.85
Missoula	MT	24153	20	-0.21	0.57	0.96	0.62	1.68	2.08
Bismarck	ND	24011	40	-0.70	0.56	0.58	0.61	1.02	1.25
Fargo	ND	14914	50	-0.74	0.44	0.52	0.47	0.83	0.98
Norfolk	NE	14941	25	-0.28	0.60	0.91	0.66	1.66	2.04
Omaha	NE	14942	25	-0.53	0.56	0.69	0.61	1.19	1.48
Scottsbluff	NE	24028	15	-0.70	0.48	0.56	0.51	0.92	1.09
Concord	NH	14745	70	-0.79	0.50	0.51	0.53	0.86	1.03
Atlantic City	NJ	93730	20	-0.27	0.60	0.91	0.65	1.67	2.05
Newark	NJ	14734	20	-0.36	0.61	0.84	0.61	1.56	1.87
Reno	NV	23185	15	-0.47	0.63	0.77	0.70	1.39	1.75
Albany	NY	14735	40	-0.74	0.48	0.54	0.51	0.87	1.05
New York	NY	94789	30	-0.80	0.58	0.53	0.63	0.95	1.16
Rochester	NY	14768	40	-0.31	0.50	0.83	0.54	1.39	1.65
Akron	OH	14895	20	-0.65	0.49	0.59	0.52	0.98	1.17
Cleveland	OH	14820	20	-0.21	0.54	0.94	0.59	1.61	2.01
Columbus	OH	14821	20	-0.20	0.71	1.05	0.81	2.08	2.65
Mansfield	OH	14891	20	-0.10	0.60	1.32	0.66	1.97	2.45
Toledo	OH	94830	20	-0.70	0.56	0.58	0.60	1.01	1.24
Pendleton	OR	24155	20	-1.00	0.55	0.43	0.60	0.75	0.90
Portland	OR	24229	10	-0.36	0.59	0.84	0.65	1.47	1.88
Salem	OR	24232	10	-0.67	0.47	0.57	0.50	0.93	1.11
Allentown	PA	14737	25	-0.02	0.57	1.15	0.62	2.03	2.54
Philadelphia	PA	13739	20	-0.65	0.53	0.60	0.57	1.01	1.25

Table 4.2 – Statistics for 50-year maximum roof snow load (continued)

Site	ST	wban	Nominal ground snow (psf ⁽¹⁾)	50-year maximum roof snow load					
				(Lognormal distribution)					
				λ	ξ	Mean-to-nominal	COV	90% value	95% value
Pittsburgh	PA	94823	25	-0.32	0.57	0.86	0.62	1.53	1.85
Providence	RI	14765	50	-0.98	0.47	0.42	0.50	0.69	0.83
Aberdeen	SD	14929	50	-0.79	0.55	0.53	0.59	0.91	1.15
Rapid City	SD	24090	25	-0.81	0.57	0.52	0.62	0.93	1.13
Sioux Falls	SD	14944	40	-0.25	0.54	0.90	0.58	1.55	1.95
Burlington	VT	14742	50	-0.52	0.53	0.69	0.57	1.18	1.42
Olympia	WA	24227	15	0.07	0.58	1.27	0.63	2.21	2.80
Seattle	WA	24233	20	-0.48	0.55	0.72	0.60	1.26	1.53
Yakima	WA	24243	15	0.11	0.54	1.28	0.58	2.21	2.73
Green Bay	WI	14898	40	-0.57	0.53	0.65	0.57	1.12	1.33
La Crosse	WI	14920	40	-0.67	0.58	0.61	0.63	1.09	1.32
Madison	WI	14837	30	-0.28	0.57	0.89	0.62	1.58	1.94
Milwaukee	WI	14839	30	-0.27	0.52	0.87	0.56	1.49	1.79
Beckley	WV	3872	20	-0.07	0.55	1.09	0.60	1.88	2.30
Charleston	WV	13866	20	-0.42	0.59	0.78	0.64	1.40	1.73
Huntington	WV	03860	20	-0.48	0.56	0.73	0.61	1.26	1.56
Casper	WY	24089	25	-1.18	0.49	0.34	0.52	0.58	0.69
Cheyenne	WY	24018	20	-0.17	0.58	1.00	0.63	1.79	2.17
Sheridan	WY	24029	20	-0.33	0.55	0.84	0.59	1.45	1.80

(1) 1 psf = 47.88 N/m²

Table 4.3 – Composite statistics for 50-year maximum actual-to-nominal roof snow loads by geographic groupings

Northeast (26 sites)				Midwest / Mid-Atlantic (37 sites)				Northern Midwest/ Mountain West (18 sites)			
mean-to-nominal			COV	mean-to-nominal			COV	mean-to-nominal			COV
avg.	min.	max.		avg.	min.	max.		avg.	min.	max.	
0.61	0.42	0.83	0.53	0.84	0.58	1.32	0.60	0.80	0.34	1.28	0.58

Table 4.4 – Distribution and parameters for Oregon snow hazard

Group	Elevation ⁽¹⁾	Distribution	Parameter 1	Parameter 2
G-01	0 ft	Lognormal	$\lambda = 0.98$	$\xi = 0.715$
	1000 ft	Lognormal	$\lambda = 1.79$	$\xi = 0.694$
	2000 ft	Lognormal	$\lambda = 2.61$	$\xi = 0.672$
	3000 ft	Lognormal	$\lambda = 3.42$	$\xi = 0.650$
	4000 ft	Lognormal	$\lambda = 4.23$	$\xi = 0.628$
G-02	0 ft	Lognormal	$\lambda = 1.19$	$\xi = 0.667$
	1000 ft	Lognormal	$\lambda = 2.15$	$\xi = 0.608$
	2000 ft	Lognormal	$\lambda = 3.11$	$\xi = 0.549$
	3000 ft	Lognormal	$\lambda = 4.07$	$\xi = 0.490$
	4000 ft	Lognormal	$\lambda = 5.03$	$\xi = 0.431$
	5000 ft	Lognormal	$\lambda = 5.98$	$\xi = 0.372$
G-03	500 ft	Lognormal	$\lambda = 1.02$	$\xi = 0.876$
	2000 ft	Lognormal	$\lambda = 3.27$	$\xi = 0.720$
	3000 ft	Lognormal	$\lambda = 4.38$	$\xi = 0.501$
	4000 ft	Lognormal	$\lambda = 4.89$	$\xi = 0.437$
G-04 (north)	0 ft	Exponential	$\nu = 0.120$	
	1000 ft	Exponential	$\nu = 0.067$	
	2000 ft	Exponential	$\nu = 0.040$	
	3000 ft	ET-I	$u = 38.29$	$k = 0.029$
	4000 ft	ET-I	$u = 81.80$	$k = 0.018$
	5000 ft	ET-I	$u = 180.50$	$k = 0.012$
G-04 (south)	0 ft	Exponential	$\nu = 0.750$	
	1000 ft	Exponential	$\nu = 0.305$	
	2000 ft	Exponential	$\nu = 0.125$	
	3000 ft	ET-I	$u = 12.51$	$k = 0.066$
	4000 ft	ET-I	$u = 43.60$	$k = 0.031$
	5000 ft	ET-I	$u = 137.37$	$k = 0.015$
G-05	0 ft	Exponential	$\nu = 0.526$	
	1000 ft	Exponential	$\nu = 0.248$	
	2000 ft	Exponential	$\nu = 0.119$	
	3000 ft	Exponential	$\nu = 0.059$	
	4000 ft	ET-I	$u = 28.69$	$k = 0.041$
	5000 ft	ET-I	$u = 79.39$	$k = 0.025$
	6000 ft	ET-I	$u = 236.20$	$k = 0.017$

Table 4.4 – Distribution and parameters for Oregon snow hazard (continued)

Group	Elevation	Distribution	Parameter 1	Parameter 2
G-06	1000 ft	Lognormal	$\lambda = 1.27$	$\xi = 0.899$
	2000 ft	Lognormal	$\lambda = 2.00$	$\xi = 0.806$
	3000 ft	Lognormal	$\lambda = 2.73$	$\xi = 0.713$
	4000 ft	Lognormal	$\lambda = 3.46$	$\xi = 0.620$
	5000 ft	Lognormal	$\lambda = 4.19$	$\xi = 0.527$
	6000 ft	Lognormal	$\lambda = 4.92$	$\xi = 0.435$
G-07	1000 ft	Exponential	$\nu = 0.362$	
	2000 ft	Exponential	$\nu = 0.182$	
	3000 ft	Exponential	$\mu = 0.082$	
	4000 ft	ET-I	$u = 17.16$	$k = 0.067$
	5000 ft	ET-I	$u = 44.47$	$k = 0.039$
	6000 ft	ET-I	$u = 109.43$	$k = 0.024$
G-08	4000 ft	Exponential	$\nu = 0.157$	
	4500 ft	Lognormal	$\lambda = 3.76$	$\xi = 0.457$
	5000 ft	Lognormal	$\lambda = 4.40$	$\xi = 0.419$
	5500 ft	Lognormal	$\lambda = 4.79$	$\xi = 0.405$
	6000 ft	Lognormal	$\lambda = 5.07$	$\xi = 0.397$
G-09	4000 ft	Exponential	$\nu = 0.161$	
	4500 ft	Lognormal	$\lambda = 2.93$	$\xi = 0.525$
	5000 ft	Lognormal	$\lambda = 4.49$	$\xi = 0.390$
	5500 ft	Lognormal	$\lambda = 5.08$	$\xi = 0.370$
	6000 ft	Lognormal	$\lambda = 5.44$	$\xi = 0.362$
G-10	2000 ft	Exponential	$\nu = 0.124$	
	3000 ft	Exponential	$\nu = 0.058$	
	4000 ft	ET-I	$u = 27.63$	$k = 0.048$
	5000 ft	ET-I	$u = 67.79$	$k = 0.028$
	6000 ft	ET-I	$u = 178.17$	$k = 0.018$
G-11 (Rain Shadow)	1000 ft	ET-I	$u = 12.52$	$k = 0.078$
	2000 ft	ET-I	$u = 20.96$	$k = 0.057$
	3000 ft	ET-I	$u = 35.20$	$k = 0.043$
	4000 ft	ET-I	$u = 59.58$	$k = 0.032$
	5000 ft	ET-I	$u = 102.44$	$k = 0.025$
	6000 ft	ET-I	$u = 181.30$	$k = 0.020$
G-11 (Hood River County)	1000 ft	ET-I	$u = 23.00$	$k = 0.064$
	2000 ft	ET-I	$u = 40.98$	$k = 0.039$
	3000 ft	ET-I	$u = 73.52$	$k = 0.024$
	4000 ft	ET-I	$u = 133.17$	$k = 0.015$
	5000 ft	ET-I	$u = 244.78$	$k = 0.010$
	6000 ft	ET-I	$u = 459.90$	$k = 0.006$

Table 4.4 – Distribution and parameters for Oregon snow hazard (continued)

Group	Elevation	Distribution	Parameter 1	Parameter 2
G-12	1000 ft	Exponential	$\nu = 0.070$	
	2000 ft	ET-I	$u = 15.81$	$k = 0.065$
	3000 ft	ET-I	$u = 26.08$	$k = 0.047$
	4000 ft	ET-I	$u = 45.63$	$k = 0.036$
G-13	1000 ft	Lognormal	$\lambda = 0.59$	$\xi = 0.750$
	2000 ft	Lognormal	$\lambda = 1.38$	$\xi = 0.678$
	3000 ft	Lognormal	$\lambda = 2.71$	$\xi = 0.606$
	4000 ft	Lognormal	$\lambda = 2.96$	$\xi = 0.534$
	5000 ft	Lognormal	$\lambda = 3.76$	$\xi = 0.462$
	6000 ft	Lognormal	$\lambda = 4.55$	$\xi = 0.390$
G-14	2000 ft	Exponential	$\nu = 0.400$	
	3000 ft	Exponential	$\nu = 0.160$	
	4000 ft	ET-I	$u = 10.27$	$k = 0.123$
	5000 ft	ET-I	$u = 28.17$	$k = 0.072$
	6000 ft	ET-I	$u = 81.70$	$k = 0.048$
G-15	4000 ft	Exponential	$\nu = 0.108$	
	4500 ft	ET-I	$u = 13.26$	$k = 0.098$
	5000 ft	ET-I	$u = 21.56$	$k = 0.080$
	5500 ft	ET-I	$u = 30.30$	$k = 0.067$
	6000 ft	ET-I	$u = 39.04$	$k = 0.066$
G-16	4000 ft	ET-I	$u = 19.13$	$k = 0.069$
	5000 ft	ET-I	$u = 25.80$	$k = 0.060$
	6000 ft	ET-I	$u = 35.03$	$k = 0.053$
	7000 ft	ET-I	$u = 48.09$	$k = 0.047$
G-17	4000 ft	ET-I	$u = 5.46$	$k = 0.558$
	5000 ft	ET-I	$u = 8.96$	$k = 0.258$
	6000 ft	ET-I	$u = 14.73$	$k = 0.122$
	7000 ft	ET-I	$u = 24.22$	$k = 0.058$
	8000 ft	ET-I	$u = 39.74$	$k = 0.028$
G-18	4000 ft	ET-I	$u = 7.98$	$k = 0.174$
	5000 ft	ET-I	$u = 16.01$	$k = 0.098$
	6000 ft	ET-I	$u = 32.21$	$k = 0.055$
	7000 ft	ET-I	$u = 65.07$	$k = 0.031$
	8000 ft	ET-I	$u = 132.11$	$k = 0.018$

Table 4.4 – Distribution and parameters for Oregon snow hazard (continued)

Group	Elevation	Distribution	Parameter 1	Parameter 2
P-01	2000 ft	Lognormal	$\lambda = 1.23$	$\xi = 0.693$
	3000 ft	Lognormal	$\lambda = 2.01$	$\xi = 0.604$
	4000 ft	Lognormal	$\lambda = 2.80$	$\xi = 0.516$
	5000 ft	Lognormal	$\lambda = 3.58$	$\xi = 0.427$
	6000 ft	Lognormal	$\lambda = 4.36$	$\xi = 0.339$
	7000 ft	Lognormal	$\lambda = 5.15$	$\xi = 0.250$
P-02	2000 ft	ET-I	$u = 43.61$	$k = 0.049$
	3000 ft	ET-I	$u = 55.47$	$k = 0.043$
	4000 ft	ET-I	$u = 70.65$	$k = 0.038$
	5000 ft	ET-I	$u = 90.12$	$k = 0.033$
	6000 ft	ET-I	$u = 115.19$	$k = 0.029$
	7000 ft	ET-I	$u = 147.54$	$k = 0.026$
G-23	2000 ft	Lognormal	$\lambda = 1.79$	$\xi = 0.698$
	3000 ft	Lognormal	$\lambda = 2.09$	$\xi = 0.669$
	4000 ft	Lognormal	$\lambda = 2.39$	$\xi = 0.640$
	5000 ft	Lognormal	$\lambda = 2.69$	$\xi = 0.611$
	6000 ft	Lognormal	$\lambda = 2.99$	$\xi = 0.581$
	7000 ft	Lognormal	$\lambda = 3.29$	$\xi = 0.552$

(1) 1ft = 0.305 m

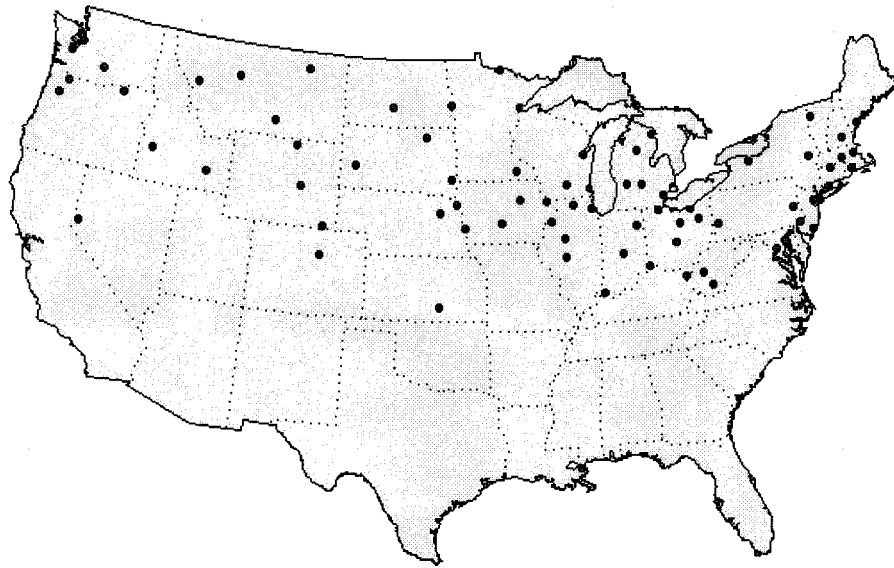


Figure 4.1 – 84 sites in the continental United States used to develop probabilistic snow load model

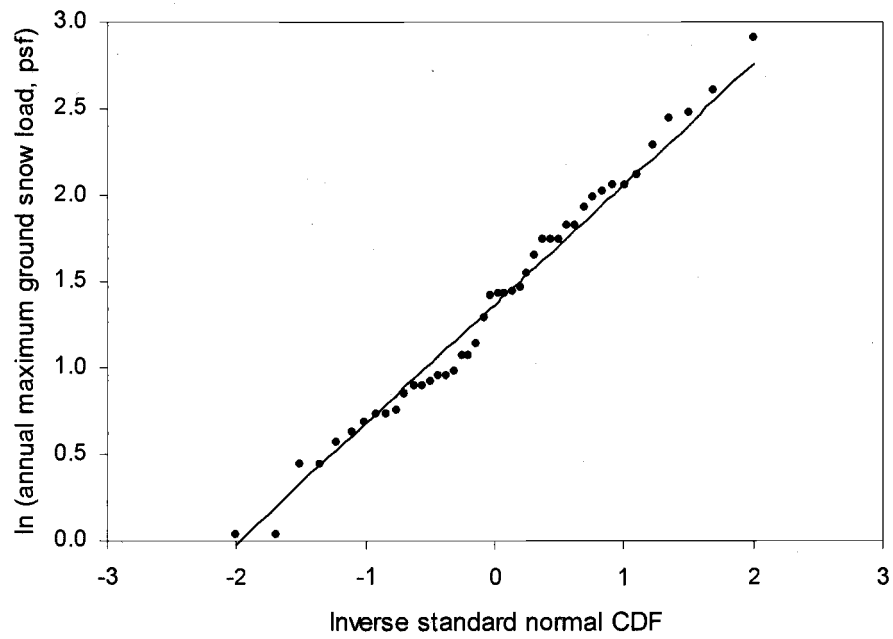


Figure 4.2 - Lognormal probability paper showing fit of annual maximum ground snow load (Rapid City, SD)

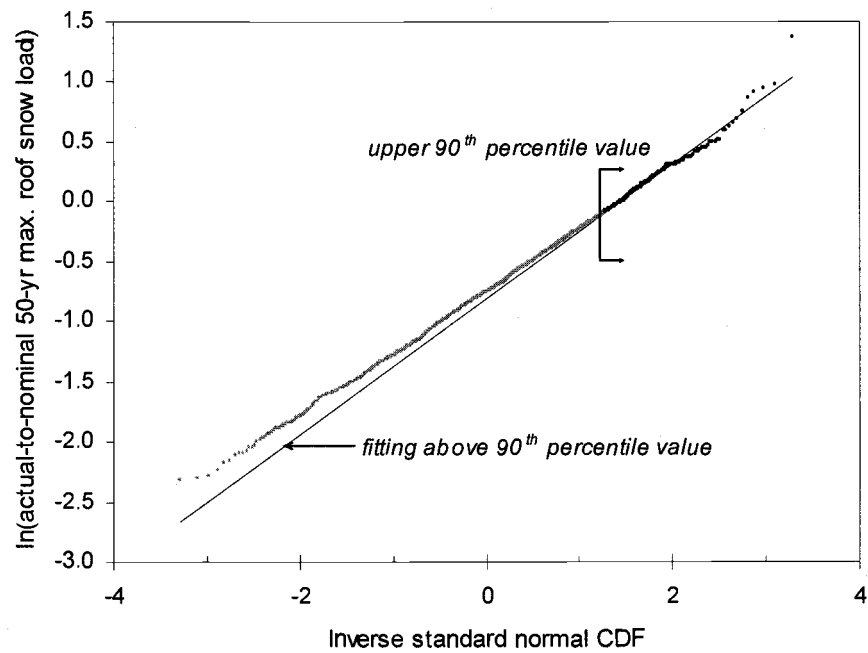


Figure 4.3 - Lognormal probability paper showing fit of actual-to-nominal 50-year maximum roof snow load (Rapid City, SD)

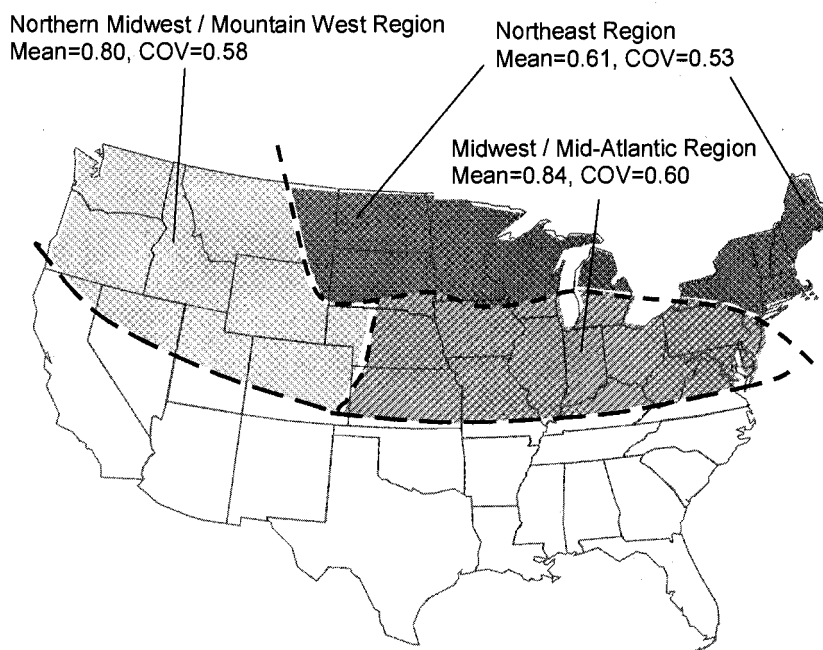


Figure 4.4 – Composite statistics for actual-to-nominal 50-year maximum roof snow loads for different regions

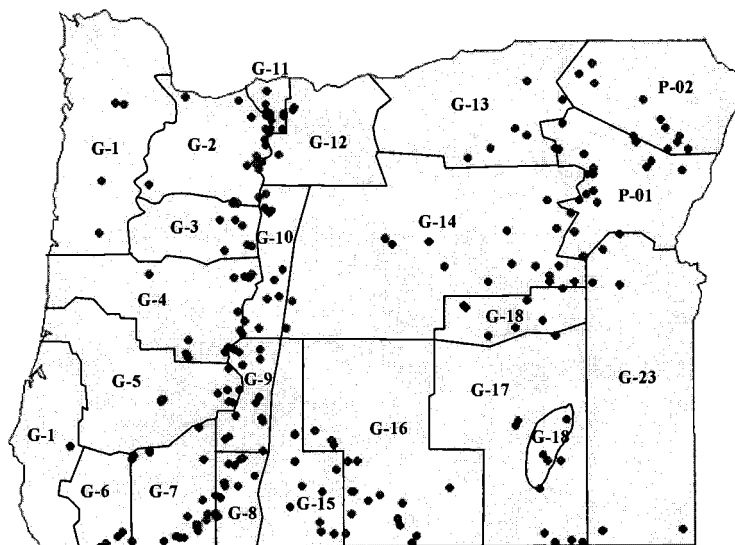


Figure 4.5 – NRCS and NCDC weather stations and county areas for Oregon snow loads

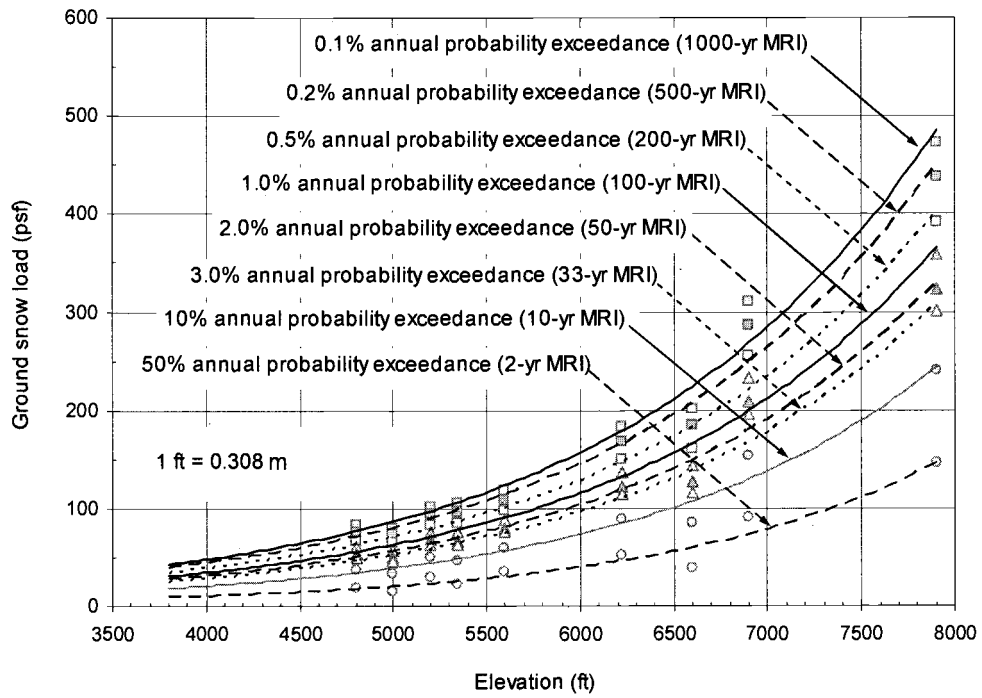


Figure 4.6 – Design ground snow load curves for G-18

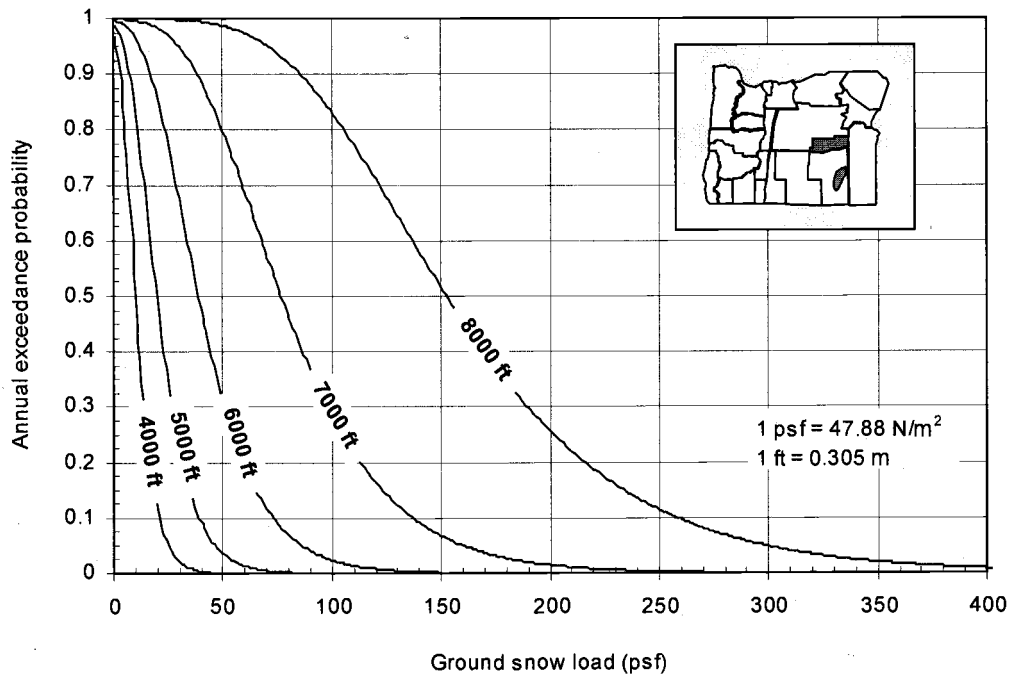


Figure 4.7 – Ground snow hazard curves for G-18 (shaded regions shown on inset map)

Fragility Analysis of Woodframe Buildings Considering Combined
Snow and Earthquake Loading

Kyung Ho Lee

David V. Rosowsky

For Submission to *Structural Safety*

Elsevier Science Bv

P.O. box 211, Amsterdam,

1000AE, Netherlands

5. Fragility Analysis of Woodframe Buildings Considering Combined Snow and Earthquake Loading

5.1 Abstract

This paper describes a study to evaluate appropriate snow load combination factors (companion action factors) for use with nominal values provided by the current design load standard for structural design in the United States [ASCE, 2002] when snow load is being considered in a seismic fragility analysis. The procedure is illustrated through the development of seismic fragility curves for one and two-story woodframe structures in three locations (Memphis TN, Carbondale, IL, and Boston, MA) having both moderate snow and seismic hazards. The fragilities are cast in terms of displacement criteria (maximum shearwall drift) with the snow load serving to add seismic weight to the structure. The structures are analyzed using a nonlinear dynamic time-history analysis procedure. The seismic hazard is defined using USGS (United States Geological Survey) seismic hazard maps and uncertainty in the seismic hazard at each location is characterized by a suite of ordinary ground motion records. The ground snow hazard is defined through an analysis of data from first-order weather stations at the sites considered. Through a series of multi-hazard convolutions, parametric studies, and the construction of fragility curves, relationships between design reference periods (T_{ref}) and snow load factor ($\gamma_{s,d}$) for use in constructing displacement-based seismic fragilities and calculating failure probabilities (by convolving with appropriate seismic hazard functions) are established. Practical implications for fragility analysis considering multiple hazards and performance-

based design of woodframe structures also are discussed.

5.2 Introduction

The load combinations used in structural design as specified in the ASCE 7 load standard were determined based on probabilistic load combination analysis [Ellingwood et al., 1980; Galambos et al., 1982]. In the latest edition of ASCE 7 [ASCE, 2002], the load combination including seismic effects is:

$$1.2D + 1.0E + 0.5L + 0.2S \quad \text{Eq. (5.1)}$$

where, D , E , L and S are nominal dead, earthquake, live, and snow loads, respectively. Ellingwood and Rosowsky (1996) conducted a study to re-evaluate the snow load factor for combinations involving earthquake and snow load since the load combination equation provided by NEHRP (1992) differed from those in the 1993 and 1995 editions of ASCE 7. NEHRP (1992) suggested a snow load factor of 0.7 rather than 0.2 when snow is taken in combination with earthquake. The relevant load combination in the 1993 and 1995 versions of ASCE 7 is the same as Eq. (5.1). Ellingwood and Rosowsky (1996) used probabilistic load modeling techniques to develop appropriate snow load combination factors based on an ultimate strength limit state. They found that approximately 20% of the nominal snow load should be used in combination with the nominal earthquake load when considering ultimate strength and a 50-year reference period. Higher companion action factors on snow load did not appear to be warranted based on probabilistic event

combination analysis, even where snow is present for significant periods during the winter. O'Rourke and Speck, Jr. (1992) also estimated the appropriate roof snow load to be used in earthquake design calculations based on the ultimate strength limit state. Their analysis suggested the approximate roof snow load for seismic calculations was 20% of the 50-year mean recurrence interval ground snow load. Based on the findings of these studies, no change to the companion action factor (0.2) was suggested for the next version of ASCE 7.

Performance-based design has gained interest in recent years among structural engineers and researchers. Recent disasters in the U.S. and elsewhere around the world have highlighted the social, political, and economic ramifications of the traditional view of codes (to prevent structural collapse during rare events), as economic disruptions caused by structural failures have not been deemed acceptable by the public. Performance-based engineering is a new paradigm in which the design process is structured to meet performance expectations (limit states) of the building occupants, owner, and the public. Although performance-based seismic design has advanced for some materials and structural types, such as steel and reinforced concrete buildings and bridges, its application to light-frame wood structures remains relatively unexplored. Seismic performance-based engineering concepts for woodframe buildings are starting to be developed [Ellingwood et al., 2004; Rosowsky and Kim, 2002a and 2002b]. The focus has been on fragility assessments for woodframe structures exposed to natural hazard (earthquake) using displacement-based criteria. Rosowsky and Kim (2002 a,b) developed a framework for performance-based seismic design of woodframe shearwalls. One challenge for

performance-based design of wood structures is evaluating appropriate levels of roof snow load. Since dead loads are typically small for these types of structures, roof snow load may represent a significant portion of the total effective seismic mass. This additional seismic mass can significantly affect the performance of light-frame structures under seismic loading. Since the snow load factor for combining earthquake and snow loads specified in ASCE 7 was developed on an ultimate strength basis, this load factor (companion action factor) may not be appropriate for use in performance-based design. The objective of this study is to develop appropriate snow load combination factors (companion action factors) for use in a seismic fragility analysis. To do this, a multi-hazard convolution technique which considers a fragility surface and two hazard curves was developed.

5.3 Sites Considered

Snow load combination factors for used in displacement-based seismic fragility analysis were developed considering two baseline structures (representative one and two-story woodframe buildings) in three geographic locations: Memphis, TN; Carbondale, IL; and Boston, MA. These sites were selected as moderate snow and seismic zones in the U.S. Seismic and ground snow hazards for these three sites were developed specifically at the Memphis International Airport, the Carbondale sewage plant, and Boston's Logan International Airport. Detailed site information is shown in Table 5.1.

5.4 Baseline Structures

Two baseline woodframe structures are considered. The first (designated Type A) is a one-

story single-family residential structure. The structure has plan dimensions of 32 ft × 20 ft (9.8 m × 6.1 m) and has openings for doors and windows. The shearwalls in the structure are built using 3/8 in. (9.5 mm) OSB attached to the framing using 0.105 in. (2.67 mm) diameter by 2 in. (150mm) long spiral nails [Durham, 1998]. In most cases, a 6 in. / 12 in. (150 mm / 300 mm) fastener schedule (6 in. (150 mm) along the edge of the panel and 12 in. (300 mm) at interior locations of the panel) was used. The top-plate and end studs are double members while the sole-plate and the interior studs are single members. The framing members are nominal 2 in. × 4 in. (50 mm × 100 mm), spaced (in most cases) at 24 in. (600 mm) on-center. Properly designed and installed hold-downs are assumed to be present. The contributions of nonstructural finish materials (e.g., gypsum wallboard, stucco) are not considered. The contributions of the partition walls to the seismic capacity are not considered, however the partition walls are included in the dead load calculation. The seismic weight of the building, calculated considering the roof and the upper half of the walls, was found to be 15 kips (66.7 kN). The plan and section views for the Type A structure are shown in Figure 5.1(a). The shearwalls in this baseline structure are shown in Figure 5.1(b).

The second baseline structure (designated Type B) is a two-story single-family residential structure, based on a model from the CUREE Caltech Woodframe Project [Fischer et al., 2001]. The structure has plan dimensions of 20 ft × 16 ft (6.1 m × 4.9 m) and has openings for various doors and windows. The shearwalls in the structure are built using 3/8 in. (9.5 mm) OSB attached to the framing using 0.113 in. (2.87 mm) diameter by 2.5 in.

(63.5 mm) long 8d box nails. In general, a 6 in. / 12 in. (150 mm / 300 mm) (edge / field) nailing schedule was used. A denser 3 in. / 12 in. (75 mm / 300 mm) nailing schedule was used for the shearwalls on either sides of the garage door opening. Hold-downs are assumed to be properly designed and installed. The contributions of nonstructural finish materials (e.g., gypsum wallboard, stucco) are not considered. As with the first baseline structure, the partition walls are only included in the dead load calculation. The seismic weight of this building was calculated as 13.9 kips (61.8 kN) at the second floor diaphragm and 10.7 kips (47.6 kN) at the roof diaphragm. Plan and section view of this baseline structure is shown in Appendix D.1. More information about this structure is provided elsewhere [Fischer et al., 2001].

5.5 Limit State Probability Calculation by Convolution Integrals

Snow load combination (companion action) factors are developed in this study through a comparison of failure probabilities obtained by convolving seismic fragilities (with assumed deterministic snow load) with a seismic hazard curve, with those obtained through a convolution of a fragility surface and two hazard curves (snow and earthquake). If a structure is exposed to a single hazard, a failure probability can be calculated by convolving a fragility (conditional limit state probability function) with a hazard function. However, in the case of two hazards which may occur simultaneously, a different technique is needed to calculate limit state probabilities. Such is the case with two additive load effects such as seismic and snow loads. The next section describes the calculation of limit state probabilities considering a single hazard. This section that follows present a

description of the technique developed to consider two hazards.

5.5.1 Limit State Probability Calculation Considering One Hazard

The limit state (LS) probability for a structure exposed to a single hazard can be expressed in terms of discrete random variables as follows:

$$P_f = \sum_{x=0}^{\infty} P[LS | X = x] P[X = x] = \sum_{x=0}^{\infty} P[R < X | X = x] P[X = x] \quad \text{Eq. (5.2)}$$

in which the limit state is the condition in which the resistance (or capacity) R is less than the load effect (or demand) X . The conditional probability $P[LS | X = x]$ is the probability of reaching the limit state (LS) at a given demand level, $X = x$. The term $P[X = x]$ is the marginal hazard probability. Eq. (5.2) can be expressed in terms of continuous random variables as:

$$P_f = \int_{x=0}^{x=\infty} F_r(x) g_x(x) dx \quad \text{Eq. (5.3)}$$

where $F_r(x)$ = fragility function in the form of a cumulative distribution function (CDF), and $g_x(x)$ = hazard function in the form of a probability density function (PDF). In probabilistic terms, the fragility defines the capability of an engineered system to withstand a particular level of demand. Eq. (5.3) also can be expressed as:

$$P_f = \int_{x=0}^{x=\infty} f_r(x) G_x(x) dx \quad \text{Eq. (5.4)}$$

where $f_r(x)$ = fragility function in the form of a probability density function (PDF), and $G_x(x)$ = hazard function in the form of a complementary cumulative distribution function (CCDF). In either form, the fragility curve and hazard curve must be expressed in terms of a dimensionally consistent demand variable (e.g., wind speed, spectral acceleration, flood height, ground snow load). The convolution integral in Eq. (5.3) is illustrated in Figure 5.2. Probabilistic safety assessment combines the probabilistic definitions of hazard (demand) and fragility (capacity), and leads to the calculation of a limit state probability. In Eqns. (5.3) and (5.4), the fragility (system response) is fully uncoupled from the hazard (demand) in the limit state analysis. Thus, assuming statistical independence between years, the annual failure probability (obtained by convolving the fragility with the annual hazard curve) can be transformed into an N -year failure probability using extreme value theory shown in Eq. (5.5).

$$p_f^{(N)} = 1 - (1 - p_f^{(1)})^N \quad \text{Eq. (5.5)}$$

where $p_f^{(N)}$ = probability of failure in N years, and $p_f^{(1)}$ = annual failure probability. This N -year failure probability ($p_f^{(N)}$) calculated using Eq. (5.5) is equal to the N -year failure probability obtained from a convolution of the fragility and the N -year reference period hazard since the fragility and hazard are fully uncoupled.

5.5.2 Limit State Probability Calculation Considering Two Hazards

In the previous section, the calculation of a limit state probability by convolving a fragility with a single hazard was illustrated. However, in the case of a structure subjected to two hazards having additive load effects (e.g., seismic + snow), the convolution concept must be expanded. This two-hazard form is shown in Eq. (5.6).

$$P_f = \sum_{x=0}^{\infty} \sum_{y=0}^{\infty} P[LS | (X = x \cap Y = y)] P[X = x \cap Y = y] \quad \text{Eq. (5.6)}$$

where the limit state (LS) is the condition in which the resistance or capacity (R) is less than the load effect or demand (X and Y) due to the two hazards. The conditional probability $P[LS | (X = x \cap Y = y)]$ is the probability that the limit state (LS) is reached at given levels of demands x and y acting simultaneously. The joint probability $P[X = x \cap Y = y]$ is the probability that demand levels x and y occur at the same time. If the two hazard events X and Y are statistically independent (as would be reasonably assumed for the case of snow and earthquake), Eq. (5.6) can be written:

$$P_f = \sum_{x=0}^{\infty} \sum_{y=0}^{\infty} P[R < X + Y | (X = x \cap Y = y)] P[X = x] P[Y = y] \quad \text{Eq. (5.7)}$$

where $P[R < X + Y | (X = x \cap Y = y)]$ is the conditional limit state probability at given demand levels x and y , and $P[X = x]$ and $P[Y = y]$ are the marginal hazard probabilities of X and Y , respectively. Eq. (5.7) can be expressed in terms of continuous random

variables as:

$$P_f = \int_{x=0}^{\infty} \int_{y=0}^{\infty} F_r(x, y) g_x(x) g_y(y) dy dx \quad \text{Eq. (5.8)}$$

where $F_r(x, y)$ is a *fragility surface* expressed as a joint distribution function in terms of demands X and Y , and $g_x(x)$ and $g_y(y)$ are the hazard functions for X and Y . Note that the hazard functions in Eq. (5.8) are expressed as PDF's. The bivariate convolution integral in Eq. (5.8) is illustrated in Figure 5.3. In the case of one hazard (X), the fragility curve can be expressed in terms of demand X in two dimensions (e.g., seismic fragility without consideration of roof snow load is located in the x - z plane.). However, in the case of two hazards (X and Y), the fragility must be expressed in terms of demands X and Y as a three-dimensional surface. To solve for the failure probability, Eq. (5.8) is reduced to:

$$P_f = \int_{x=0}^{\infty} g_x(x) \int_{y=0}^{\infty} F_r(x, y) g_y(y) dy dx = \int_{x=0}^{\infty} F_r^{(y)}(x) g_x(x) dx \quad \text{Eq. (5.9)}$$

where $F_r^{(y)}(x)$ = fragility curve obtained by convolving the fragility surface $F_r(x, y)$ with the marginal hazard function $g_y(y)$. Alternatively, Eq. (5.8) also can be reduced to:

$$P_f = \int_{y=0}^{\infty} g_y(y) \int_{x=0}^{\infty} F_r(x, y) g_x(x) dx dy = \int_{y=0}^{\infty} F_r^{(x)}(y) g_y(y) dy \quad \text{Eq. (5.10)}$$

where $F_r^{(x)}(y)$ = fragility curve obtained by convolving the fragility surface $F_r(x, y)$ with

the marginal hazard function $g_x(x)$. Eqns. (5.9) and (5.10) are equivalent and result in the same probability of failure. The probability of failure in a certain reference period can be estimated using Eq. (5.9) or Eq. (5.10) only when the hazard curves correspond to the same period. In other words, a 50-yr probability of failure can be obtained when $g_x(x)$ and $g_y(y)$ represent 50-yr reference period hazard curves. It should be noted that the fragility curve $F_r^{(Y)}(x)$ and the marginal hazard curve $g_x(x)$ in Eq. (5.9) are not fully uncoupled since the fragility $F_r^{(Y)}(x)$ includes the effects of hazard Y (considering a certain reference period). Therefore, extreme value theory in Eq. (5.5) can not be applied to the case of multiple hazards as formulated in Eqns. (5.6)-(5.10). Eqns. (5.8) and (5.9) were used to calculate the failure probabilities for shearwalls under combined snow and earthquake loading with failure defined as the maximum lateral shearwall displacement (in given reference period) exceeding a drift limit. These failure probabilities were then compared with those obtained considering one hazard only (earthquake) and different levels of (deterministic) snow load in order to determine appropriate snow load companion action factors for use in a seismic fragility analysis. This is described in the following sections.

5.6 Probabilistic Description of Hazards

5.6.1 Seismic Hazards

A probabilistic model of seismic hazard, $G_x(x)$, typically expresses the annual exceedence probability of ground motion parameter x , generally defined as spectral acceleration at the fundamental period of the structure. The other parameters that characterize ground motion, such as frequency content, magnitude/intensity of earthquake, duration of excitation,

epicenter distance, site rock/soil condition, geographical location and earthquake mechanism are subsumed in the fragility analysis [Ellingwood and Tekie, 2001]. The seismic hazard curve can be described approximately by an Extreme Type II (ET-II) distribution [Cornell, 1968]. The seismic hazard expressed in the form of a complementary cumulative distribution function (CCDF) of ET-II form is given by:

$$G_X(x) = 1 - \exp\left[-\left(\frac{u}{x}\right)^k\right] \quad \text{Eq. (5.11)}$$

in which u and k are the ET-II scale and shape parameters, respectively. Parameter k determines the slope of the hazard curve and is related to the coefficient of variation in parameter X . Table 5.2 presents the ET-II parameters for the three sites considered in this study and for different reference periods. The parameters were computed based on data provided by the U.S. Geological Survey (USGS). Spectral acceleration data for the 0.2-second fundamental period was used in this study. The USGS provides spectral accelerations for 10% in 50 years (10/50) and 2% in 50 years (2/50). ET-II distribution parameters for 50 years reference period which make the CCDF meet these two points (a couple of spectral accelerations and exceedance probabilities in 50 years) were calculated. Exceedance probabilities in different periods for the spectral acceleration values can also be obtained using extreme value theory. In the same way, ET-II distribution parameters for the reference period can be calculated. A complementary cumulative distribution (CCDF) form of the hazard curve also can be expressed in the form of an ET-II probability density

function (PDF) as:

$$g_x(x) = \frac{k}{x} \left(\frac{u}{x} \right)^k e^{-\left(\frac{u}{x} \right)^k} \quad \text{Eq. (5.12)}$$

Note that hazard curves in this PDF form are referred to as *marginal hazard curves* in this paper. Figure 5.4 presents seismic hazard curves for one site (Carbondale, IL) considering three different reference periods. This figure was developed using Eq. (5.12) and the ET-II parameters in Table 5.2. Hazard curves such as those shown in Figure 5.4 were used in the multi-hazard convolution described later.

5.6.2 Snow Hazards

Snow hazard curves were developed for the three sites in this study using probabilistic analysis of ground snow load data. Water-equivalent depth data and snow depth data are both available from the National Climatic Data Center [NCDC, 2004]. Since snow density is time-varying and also varies by geographic location, it is difficult to convert snow depth to snow load directly. It was therefore decided to directly convert the water-equivalent depth to ground snow load. Statistics for annual maximum ground snow load can then be estimated using a probability paper or any other technique. Since water-equivalent depth data is not available for Carbondale, IL, snow data for Evansville, IN and St. Louis, MO were used to evaluate ground snow load statistics for that location. Specially, the snow load statistics for Carbondale, IL were taken as the average of the statistics for Evansville and St.

Louis. These two sites are the nearest locations having water-equivalent depth data and are equidistant from Carbondale, IL. Table 5.3 shows the annual ground snow load statistics for the three sites. The ground snow load for the two Midwestern sites (Carbondale and Memphis) is best fit by a lognormal distribution, while the ground snow load for Boston, MA is best fit by an Extreme Type I (ET-I) distribution. A probabilistic model for snow hazard presents a relation between annual exceedence probability and ground snow. The ground snow hazard curve therefore can be described by a complementary cumulative lognormal or ET-I distribution as follows:

$$G_x(x) = 1 - \Phi\left[\frac{\ln(x) - \lambda}{\xi}\right] \quad (\text{Lognormal}) \quad \text{Eq. (5.13.a)}$$

$$G_x(x) = 1 - \exp[-\exp(-k(x - u))] \quad (\text{ET-I}) \quad \text{Eq. (5.13.b)}$$

In Eq. (5.13.a), $\Phi[\bullet]$ = standard normal cumulative distribution function, λ = logarithmic median, and ξ = logarithmic standard deviation (approximately equal to the coefficient of variation, V , when $V < 0.3$). In Eq. (5.13.b), u and k are ET-I scale and shape parameters, respectively. Table 5.4 shows the parameters for ground snow load at the three sites for different reference periods. Parameters for the annual ground snow load hazard were determined from the annual extreme ground snow statistics and assumed distribution. Using extreme value theory, hazard curves for other reference periods were obtained and

corresponding distribution parameters were obtained through a graphical parameter estimation technique. The hazard curve also can be expressed in the form of a probability density function (PDF) as:

$$g_x(x) = \frac{1}{\sqrt{2\pi}\xi x} \exp\left[-\frac{1}{2}\left(\frac{\ln(x) - \lambda}{\xi}\right)^2\right] \quad (\text{Lognormal}) \quad \text{Eq. (5.14.a)}$$

$$g_x(x) = k \exp[-k(x-u) - e^{-k(x-u)}] \quad (\text{ET-I}) \quad \text{Eq. (5.14.b)}$$

Figure 5.5 shows the marginal ground snow hazard curves in this form for Carbondale, IL. Hazard curves such as those in Figure 5.5 were used in the multi-hazard convolutions described later.

Conversion factors for converting ground snow load to roof snow load were obtained from the current load standard. ASCE 7 [ASCE, 2002] provides the following conversion factor:

$$p_s = 0.7C_s C_e C_t I p_g \quad \text{Eq. (5.15)}$$

where p_s = roof snow load, p_g = ground snow load, C_s = roof slope factor, C_e = exposure factor, C_t = thermal factor, and I = importance factor (taken as 1.0). In this study, roofs are assumed to be warm and have slopes less than 30° ($C_s = 1$); the baseline structures are assumed to be located in exposure C with a partially exposed roof ($C_e = 1$),

and are normally heated (see Table 7-3 in ASCE 7-02) ($C_e = 1$). All parameters in Eq. (5.15) were treated as deterministic.

5.7 Structural Analysis

Nonlinear dynamic time-history analyses were performed on the baseline structures using a suite of scaled ordinary ground motion (OGM) records to characterize the seismic hazard. The results were used to develop seismic fragility surfaces including snow load effects. The program CASHEW [Folz and Filiatrault, 2000, 2001] was used to evaluate the dynamic response of the shearwalls in the structures. CASHEW is a numerical model capable of predicting the load-displacement response of wood shearwalls under quasi-static cyclic loading. With information on shearwall geometry, material properties, and the hysteretic behavior of the individual fasteners, CASHEW can be used to calibrate the parameters of an equivalent SDOF oscillator (modified Stewart hysteretic model) for each shearwall. The seismic response of a complete structure can be predicted using the program SAWS [Folz and Filiatrault, 2003]. This program assumes the light-frame structure is composed of two primary components: rigid horizontal diaphragms and nonlinear lateral load resisting shearwall elements with parameters provided by the SDOF oscillator developed for each shearwall using CASHEW. The program assumes that both the floor and roof elements have sufficiently high in-plane stiffness to be considered rigid elements. This is a reasonable assumption for typical diaphragms with a planar aspect ratio on the order of 2:1, as supported by experimental results from full-scale diaphragm tests [Philips et al., 1993]. The actual three-dimensional building is degenerated into a two-dimensional

planar model using zero-height shearwall elements connected between the diaphragm and the foundation. All diaphragms in the building model are assumed to have infinite in-plane stiffness. The ground motions used for Boston, MA in this study were obtained from Somerville et al. (1997). The suite of twenty ordinary ground motion records is assumed to be representative of the 10% in 50 years (10/50) hazard level for Boston, MA. The ground motions for Carbondale, IL and Memphis, TN were obtained from the Mid-America Earthquake Center⁵. The two suites of ten ordinary ground motion records also are assumed to be representative of the 10/50 hazard level. Each record was scaled such that its mean 5% damped spectral value matched the design response spectrum (constructed using the procedure in the NEHRP Guidelines [FEMA, 2000 a,b] and assuming seismic zone 2 and soil type D (stiff soil) for the sites, and a 1% damping ratio for the structures) over the period range defining the plateau region. Note that the period range of the plateau region, typically about 0.1 sec to 0.6 sec, covers most light-frame wood structures. The plateau of the design response spectrum was increased from 0.1g to 4.0g (in increments of 0.1g) and the records were rescaled to each level. The results from each subsequent analysis were then used to define one point on a fragility curve. Three displacement limit states were considered, namely drift ratios (ratios of lateral displacement to wall height) of 1%, 2%, and 3%. These are the drift limits suggested by FEMA 356 for woodframe shearwalls corresponding to the IO (immediate occupancy), LS (life safety), and CP (collapse prevention) performance levels, respectively. The North and South walls in both the Type A

⁵ see: <http://mae.ce.uiuc.edu/newsite/research/rr-1/gmotions/> - (February, 2004)

(one-story) and Type B (two-story) structures performed worse because of the many openings and the relatively small number of fasteners. Therefore, the seismic loading was applied in an East – West (weakest) direction in the analysis of both structures. For the Type A structure (one-story building), displacement was measured at the top of the shearwall. For the Type B structure (two-story building), the critical displacement was taken as the largest of: (1) drift at top of first story; (2) interstory drift; and (3) drift at top of second story (roof level), and the appropriate heights were used to evaluate drift limits per FEMA 356. In general, the drift ratios at the top of the structure governed. Therefore, the displacement at the top of the second story (roof level) relative to the ground (i.e., full building height) was considered when evaluating drift performance.

5.8 Seismic Fragility Surface

A fragility curve is a conditional limit state probability expressed in terms of a single demand quantity (e.g., spectral acceleration, flood height, wind speed, ground snow). In the case of a system subjected to *two* hazards (as is the case with earthquake and snow load in this study), an alternative formulation must be sought such that the fragility is expressed in terms of the two demands (hazards). In some ways, this violates the axiom of a fragility analysis in which the fragility and the hazard must be uncoupled. This results in some limitations, for example the use of extreme value theory to extend the results to other reference periods, as discussed previously.

The seismic fragilities including the combination of roof snow load (additional seismic

weight) were developed in three-dimensions where the x -axis = spectral acceleration, the y -axis = ground snow load, and the z -axis = fragility (see Figure 5.3). Seismic fragility curves considering different deterministic roof snow loads also were developed. Figure 5.6 shows an example of seismic fragility curves $F_r(x)$ which is well-fit by a Lognormal CDF. This example was developed for the case of the one-story building (Type A structure) in Boston, MA with a ground snow load of 10 psf and considering a 1% drift limit. In all cases (three locations, two baseline structures, three drift limits), the fragilities were well-fit by a Lognormal distribution. Figure 5.7 presents one example of a suite of seismic fragilities considering different roof snow load effects. The fragilities in Figure 5.7 were developed for the one-story building (Type A structure) in Carbondale, IL considering a 1% drift limit. Referring back to Figure 5.3, the fragility curves in Figure 5.7 would be projections onto one (e.g., x - z) plane. The fragilities $F_r(x)$ in Figure 5.7 can be recast into a form showing ground snow load vs. seismic fragility for discrete spectral accelerations as shown in Figure 5.8. Here, the fragilities $F_r(y)$ represent projections onto the *other* (e.g., y - z) plane in Figure 5.3. Fragilities of the form $F_r(y)$ are convolved with the 1-year, 5-yr, 10-yr, 25-yr, 50-yr, and 100-yr snow hazards in the next section to determine appropriate snow load combination (companion action) factors.

5.9 Evaluation of Snow Load Combination (companion action) Factors

Projection of fragility surfaces onto the x - z and y - z planes were developed in the previous section. In this section, fragilities are convolved with snow hazards for different reference periods ranging from one year to 100 years. The fragilities, $F_r^{(Y=1yr)}(x)$ in Eq. (5.9), are

determined by convolving the fragility surface $F_r(x, y)$ with the annual snow hazard curve in the form of a PDF (see Figure 5.5). Figure 5.9 shows a comparison of $F_r^{(Y=1yr)}(x)$ with the fragility curves $F_r(x)$ convolved with the different values of (deterministic) ground snow load. In this case, $F_r^{(Y=1yr)}(x)$ (the fragility surface convolved with the marginal annual snow hazard curve) is very close to the fragility $F_r(x)$ when the ground snow is equal to 5 psf. If these two fragilities are convolved with the marginal annual seismic hazard curve $g_X(x)$, the limit state probabilities are calculated as 3.63×10^{-4} and 3.62×10^{-4} , respectively, i.e., nearly identical. Thus, in this case, the appropriate snow load for use in the seismic fragility analysis would be about 5 psf (239.4 N/m²). Since this site (Carbondale, IL) has a code-specified nominal value of ground snow load of 20 psf (957.6 N/m²), the snow load combination factor for one-year reference period would be about 0.25. Comparisons of $F_r^{(Y=1yr)}(x)$ and $F_r^{(Y=50yr)}(x)$ with the fragility curve $F_r(x)$ in for Boston, MA are shown in Appendix D.2. Figure 5.10 shows the resulting fragilities $F_r^{(Y)}(x)$ when convolved with the snow hazards having reference periods ranging from one to 100 years. Again, the vertical axis $F_r^{(Y)}(x)$ is the fragility obtained through a convolution of the fragility surface $F_r(x, y)$ and the snow hazard curve $g_Y(y)$.

Table 5.5 shows the limit state probabilities obtained through the multi-convolution procedure described previously for the one-story structure (Type A) in Carbondale, IL considering a 1% drift limit. Through comparisons of the limit state probabilities ($P_{f(S+E)}$) obtained using the multi-hazard convolution procedure with those obtained using the

seismic hazard convolution only ($p_{f(E)}$), appropriate values of snow load can be obtained (interpolating between values of deterministic snow loads as needed). These are shown in Table 5.6. To evaluate snow load combination (companion action) factors for use with current design snow load values, the results in Table 5.6 must be presented as ratios to the nominal ground snow loads in ASCE 7-02 [ASCE, 2002]. These factors are plotted as a function of reference period in Figure 5.11. The results in Figure 5.11 suggest that the snow load combination factors (for a given reference period), are not sensitive to geographic location, structure type, or drift limit. Figure 5.12 shows median and 95th-percentile values (assuming a Normal distribution) of the snow companion action factor, again as a function of reference period.

5.10 Summary and Conclusions

Snow load on light-frame structures can represent a significant increase in effective seismic weight when the structure is subjected to seismic loading. The objective of this study was to evaluate appropriate snow load combination (companion action) factors for use with nominal ground snow load values provided by ASCE 7 (2002) when the snow load is being considered (as additional seismic weight) in a seismic fragility analysis. To accomplish this, a technique for handling two (independent) hazards in a fragility analysis was developed. The fragilities are cast in terms of displacement criteria with the snow load serving to add seismic weight to the structures. The seismic hazard is defined using USGS seismic hazard maps and uncertainty in the seismic hazard at a given location is characterized by a suite of

10-20 ordinary ground motion records. The ground snow load hazard is defined through an analysis of water-equivalent depth data obtained from the NCDC. Two baseline woodframe structures were analyzed using a non-linear dynamic time-history analysis procedure. Seismic fragility surfaces having spectral acceleration on the x -axis, ground snow loads on the y -axis, and seismic fragility on the z -axis were developed using the results of the dynamic time-history analysis, post-processed to evaluate limit state failure probabilities considering different drift limits. It was then shown how the fragility surface could be convolved sequentially with the two marginal hazard curves (snow and seismic) to evaluate failure probabilities. This was done for reference periods up to 100 years. Next, these failure probabilities were compared to those obtained by convolving seismic fragilities developed using deterministic values of snow loads with seismic hazard curves. This comparison allowed the estimation of appropriate values of snow load for use in the seismic fragility analysis. Finally, snow load combination (companion action) factors were determined as the ratio of these snow load values to the nominal snow loads in ASCE 7 (2002).

The snow load companion action factors were not sensitive to geographic location, type of structure, or choice of drift limit. They are, however, sensitive to choice of reference period. The median value of snow load combination factors ranged from 0.22 for a one-year reference period to 0.87 for a 100-year reference period. As a comparison, Ellingwood and Rosowsky (1996) suggested a companion action factor of 0.2 on snow load when combined with earthquake load in ultimate strength design (50-year reference period). The

corresponding median companion action factor (50-year reference period) obtained in this study was about 0.75, suggesting the effect of roof snow load in combination with earthquake load may be more significant for displacement-based limit states. It is also important to note that this study considered regions having both moderate snow and seismic hazards. The companion action factors developed in this study can be used to specify appropriate values of snow load to be used when performing a displacement-based seismic fragility analysis.

5.11 References

ASCE (2002), *Minimum Design Loads for Buildings and Other Structures, Standard ASCE 7-02*. Structural Engineering Institute of the American Society of Civil Engineers, Reston, VA.

Cornell, C.A. (1968), "Engineering seismic risk analysis," *Bulletin of the Seismological Society of America*, 58(5):1583-1606.

Durham, J.P. (1998), "Seismic Response of Wood Shearwalls with Oversized Oriented Strand Board Panels," MASC Thesis, University of British Columbia, Vancouver, Canada.

Ellingwood, B.R., Galambos, T.V., MacGregor, J.G. and Cornell, C.A. (1980), *Development of a Probability Based Load Criterion for American National Standard A58*. Special Publication 577, U.S. Department of Commerce, National Bureau of Standards, Washington, DC.

Ellingwood, B.R. and Rosowsky, D.V. (1996), "Combining snow and earthquake loads for limit states design," *Journal of Structural Engineering*, ASCE, 122(11):1364-1368.

Ellingwood, B.R. and Tekie, P.B. (2001), "Fragility analysis of concrete gravity dams," *Journal of Infrastructure Systems*, ASCE, 7(2):41-48.

Ellingwood, B.R., Rosowsky, D.V., Li, Y. and Kim, J.H. (2004), "Fragility assessment of light-frame construction subjected to wind and earthquake hazards," *Journal of Structural Engineering*, ASCE. (in press)

FEMA (2000a), *Prestandard and Commentary for the Seismic Rehabilitation of Buildings*, Federal Emergency Management Agency, Washington, DC.

FEMA (2000b), *Global Topics Report on the Prestandard and Commentary for the Seismic Rehabilitation of Buildings*, Federal Emergency Management Agency, Washington, DC.

Fischer, D., Filiatrault, A., Folz, B., Uang, C-M. and Seible, F. (2001), *Shake Table Tests of a Two-Story Woodframe House*, CUREE Publication No. W-06, Consortium of Universities for Research in Earthquake Engineering, Richmond, CA.

Folz, B. and Filiatrault, A. (2000), *CASHEW- Version 1.0: A Computer Program for Cyclic Analysis of Wood Shear Walls*, CUREE Publication No. W-08, Consortium of Universities for Research in Earthquake Engineering, Richmond, CA.

Folz, B. and Filiatrault, A. (2001), "Cyclic Analysis of Wood Shear Walls," *Journal of Structural Engineering*, ASCE, 127(4):433-441.

Folz, B. and Filiatrault, A. (2003), *SAWS – A Computer Program for Seismic Analysis of Woodframe Structures*, CUREE Publication No. W-21, Consortium of Universities for Research in Earthquake Engineering, Richmond, CA.

Galambos, T.V., Ellingwood, B.R., MacGregor, J.G. and Cornell, C.A. (1982), "Probability based load criteria: assessment of current design practice." *Journal of Structural Division*, ASCE, 108(5):959-977.

NCDC (2004) – National Climatic Data Center – NCDC Climate Data Online, <http://cdo.ncdc.noaa.gov/CDO/dataproduct> - (February, 2004)

NEHRP (1992), *NEHRP recommended provisions for seismic resistant design of buildings. FEMA Rep. No. 222*, Federal Emergency Management Agency (FEMA), Washington, DC.

O'Rourke, M.J. and Speck, Jr., R.S. (1992), "Roof-Snow Load for Seismic – Design Calculations," *Journal of Structural Engineering*, ASCE, 118(9):2338-2350.

Philips, Y.L., Itani, R.Y. and McLean, D.L. (1993) "Lateral Load Sharing by Diaphragms in Wood-Frame Buildings," *Journal of Structural Engineering*, ASCE, 119(5):1556-1571.

Rosowsky, D.V. (2002), "Reliability-Based Seismic Design of Wood Shear Walls," *Journal of Structural Engineering*, ASCE, 128(11):1439-1453.

Rosowsky, D.V. and Kim, J.H. (2002a), *Reliability Studies*, CUREE Publication No. W-10, Consortium of Universities for Research in Earthquake Engineering, Richmond, CA.

Rosowsky, D.V. and Kim, J.H. (2002b), "Performance-Based Seismic Design of Wood Shearwalls," *Proceedings: World Conference on Timber Engineering (WCTE 2002)*, Selangor, Malaysia.

Rosowsky, D.V. and Kim, J.H. (2003), "A Probabilistic Framework for Performance-Based Design of Wood Shearwalls," *Proceedings: 9th International Conference on Applications of Statistics and Probability in Civil Engineering (ICASP9)*, San Francisco, CA.

Somerville, P., Smith., Punyamurthula, S. and Sun, J. (1997), *Development of Ground Motion Time Histories for Phase 2 of the FEMA/SAC Steel Project*, Report No. SAC/BD-97/04, SAC Joint Venture, Sacramento, CA.

USGS (2004) – United States Geology Service – Seismic Hazard Map,
<http://eqhazmaps.usgs.gov/> - (February, 2004)

Table 5.1- Site information

site	zip code	location	WBAN ⁽¹⁾	latitude	longitude
Memphis, TN	38116	Memphis Int'l AP	13893	35.05	-89.98
Carbondale, IL ⁽²⁾	62901	Carbondale sewage plant	111265 ⁽³⁾	37.73	-89.17
Boston, MA	02128	Boston Logan Int'l AP	14739	42.37	-71.02
Evansville, IN ⁽⁴⁾	47725	Evansville Regional AP	93817	38.05	-87.52
St. Louis, MO ⁽⁴⁾	63134	St. Louis Int'l AP	13994	38.75	-90.37

(1) a five-digit station identifier used by NCDC for digital data storage

(2) water-equivalent depth data is not available for this site

(3) corporation ID

(4) sites used to interpolate snow load statistics for Carbondale, IL

Table 5.2 – Seismic hazard parameters

reference period (yrs)	Boston, MA		Memphis, TN		Carbondale, IL	
	ET-II parameters		ET-II parameters		ET-II parameters	
	<i>u</i>	<i>k</i>	<i>u</i>	<i>k</i>	<i>u</i>	<i>k</i>
1	0.0012	1.423	0.0029	1.313	0.0064	1.518
5	0.0036	1.426	0.0101	1.316	0.0187	1.521
10	0.0059	1.430	0.0172	1.319	0.0298	1.524
25	0.0116	1.441	0.0355	1.329	0.0558	1.536
50	0.0195	1.460	0.0624	1.347	0.0908	1.557
100	0.0335	1.501	0.1123	1.385	0.1510	1.601

Table 5.3 – Statistics for annual maximum ground snow load

site	year of record	mean (psf)	COV	CDF	scale parameter	shape parameter
Memphis, TN	19	3.38	1.17	LN	$\lambda = 0.75$	$\xi = 0.93$
Carbondale, IL	no data	4.81 ⁽¹⁾	0.81 ⁽¹⁾	LN	$\lambda = 1.32$ ⁽²⁾	$\xi = 0.71$ ⁽²⁾
Boston, MA	45	9.96	0.67	ET-I	$u = 6.95$	$k = 0.19$
Evansville, IN	38	4.04	0.72	LN	$\lambda = 1.16$	$\xi = 0.70$
St. Louis, MO	39	5.72	0.91	LN	$\lambda = 1.47$	$\xi = 0.72$

Note: 1 psf = 47.88 N/m²

(1) mean and COV calculated from LN parameters

(2) average of LN parameters for St. Louis and Evansville

Table 5.4 – Ground snow hazard parameters

reference period (yrs)	Boston, MA		Memphis, TN		Carbondale, IL	
	ET-I parameters		LN parameters		LN parameters	
	u	k	λ	ξ	λ	ξ
1	6.95	0.19	0.75	0.93	1.32	0.71
5	15.6	0.19	1.60	0.81	1.96	0.62
10	18.2	0.19	1.95	0.72	2.23	0.56
25	24.1	0.19	2.32	0.70	2.43	0.55
50	28.0	0.19	2.70	0.58	2.72	0.48
100	31.0	0.19	2.91	0.56	2.93	0.44

Table 5.5 – Comparison of limit states probabilities

(Type A building, Carbondale, IL, 1% drift limit)

Reference Period (yrs)		1	5	10	25	50	100	
result of multi-hazard convolution, $P_{f(S+E)}$		3.63E-04	1.96E-03	4.07E-03	1.05E-02	2.22E-02	4.69E-02	
result of seismic hazard convolution only, $P_{f(E)}$	deterministic snow load	0 psf	3.26E-04	1.64E-03	3.27E-03	8.19E-03	1.63E-02	3.25E-02
		5 psf	3.62E-04	1.82E-03	3.64E-03	9.10E-03	1.82E-02	3.63E-02
		10 psf	3.98E-04	2.00E-03	4.00E-03	1.00E-02	2.00E-02	4.00E-02
		20 psf	4.79E-04	2.40E-03	4.81E-03	1.21E-02	2.41E-02	4.81E-02

Note: 1 psf = 47.88 N/m²

Table 5.6 – Snow loads (in psf) for EQ+S

site	baseline structure	drift limit	reference period (years)					
			1	5	10	25	50	100
Carbondale, IL ⁽¹⁾	Type A	1%	5.1	8.9	10.9	12.7	15.4	18.2
		2%	5.0	10.2	11.8	13.8	15.6	18.4
Memphis, TN ⁽²⁾	Type A	2%	1.9	3.6	4.5	6.3	6.9	8.1
		3%	2.4	3.6	4.3	6.2	6.8	8.8
Boston, MA ⁽³⁾	Type A	1%	7.6	21.1	23.1	27.5	30.9	37.1
		2%	9.8	18.3	20.7	27.0	30.9	33.9
	Type B	1%	7.6	17.4	19.1	29.3	32.4	34.7
		2%	8.2	17.7	19.5	26.2	29.7	33.3

Note: 1 psf = 47.88 N/m²

(1) nominal snow load in ASCE 7-02 = 20 psf

(2) nominal snow load in ASCE 7-02 = 10 psf

(3) nominal snow load in ASCE 7-02 = 40 psf

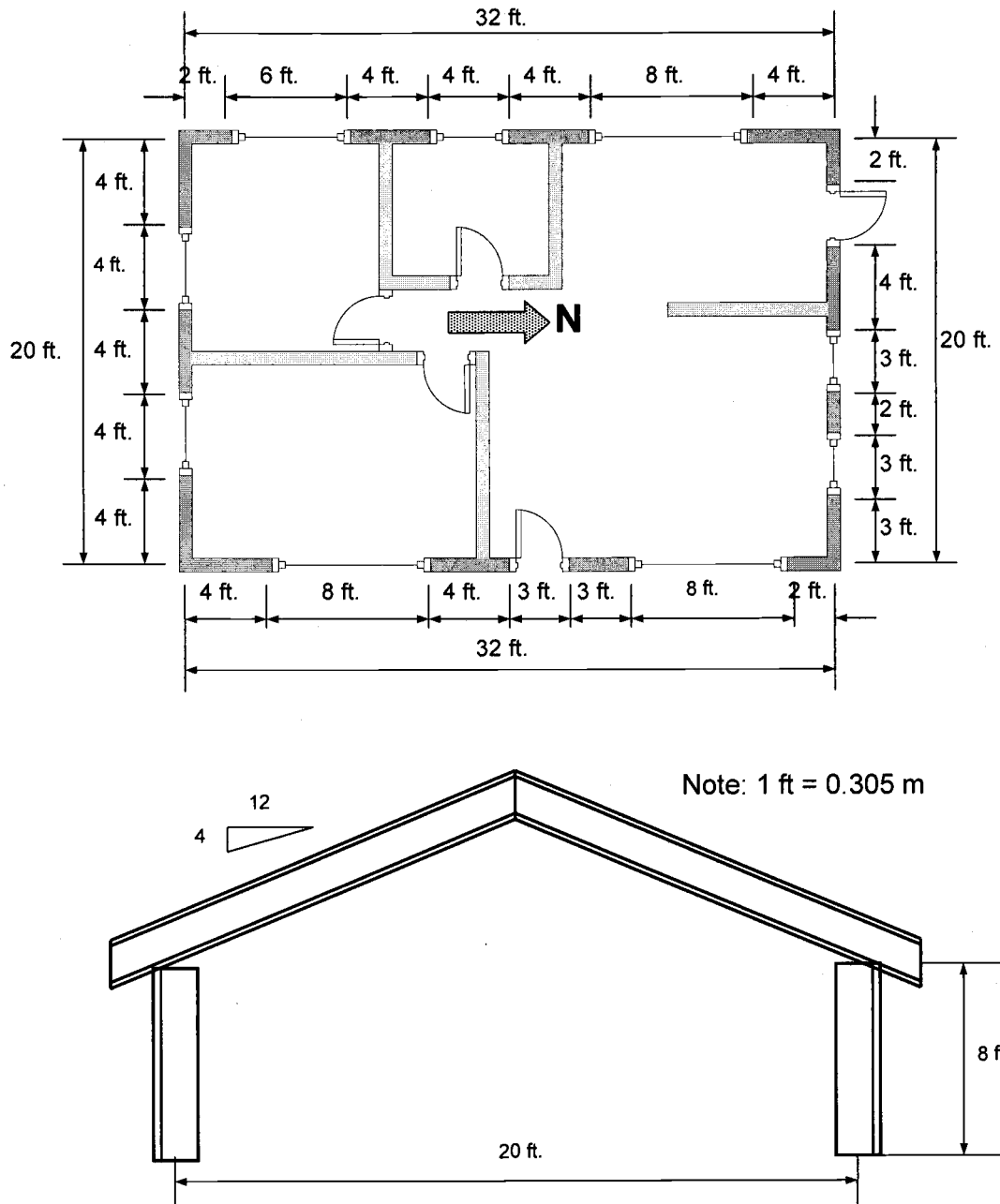


Figure 5.1(a) - Plan and section views for Type A structure

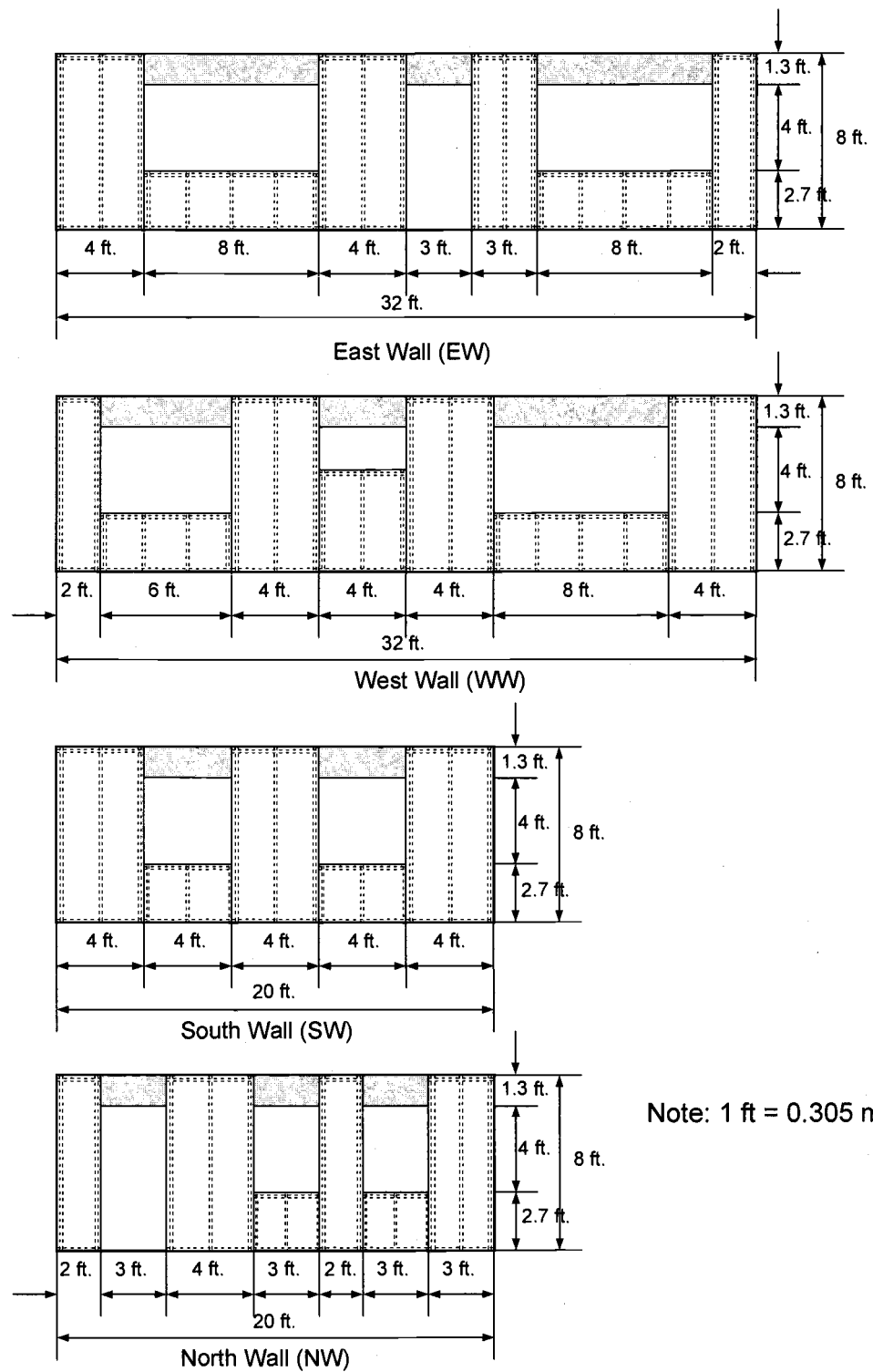


Figure 5.1(b) - Detailed shearwall configurations for Type A structure

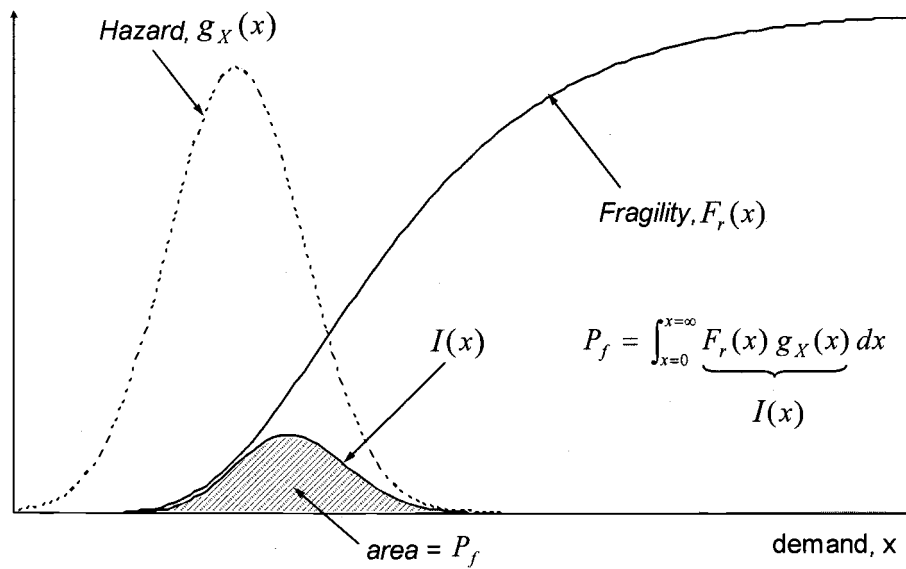


Figure 5.2 – Determination of limit state probability (single hazard)

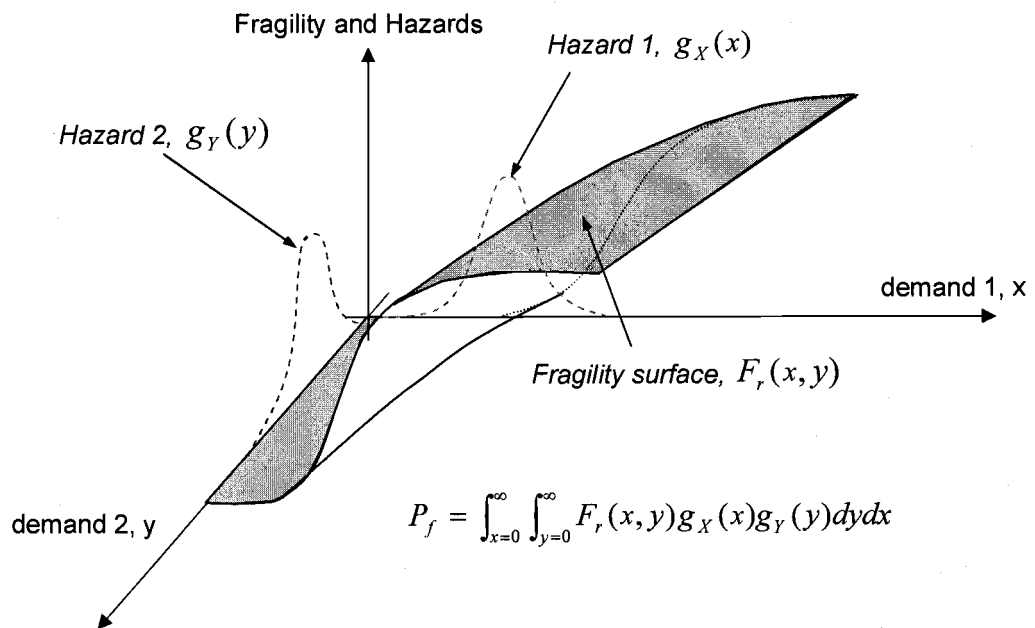


Figure 5.3 – Determination of limit state probability (two hazards)

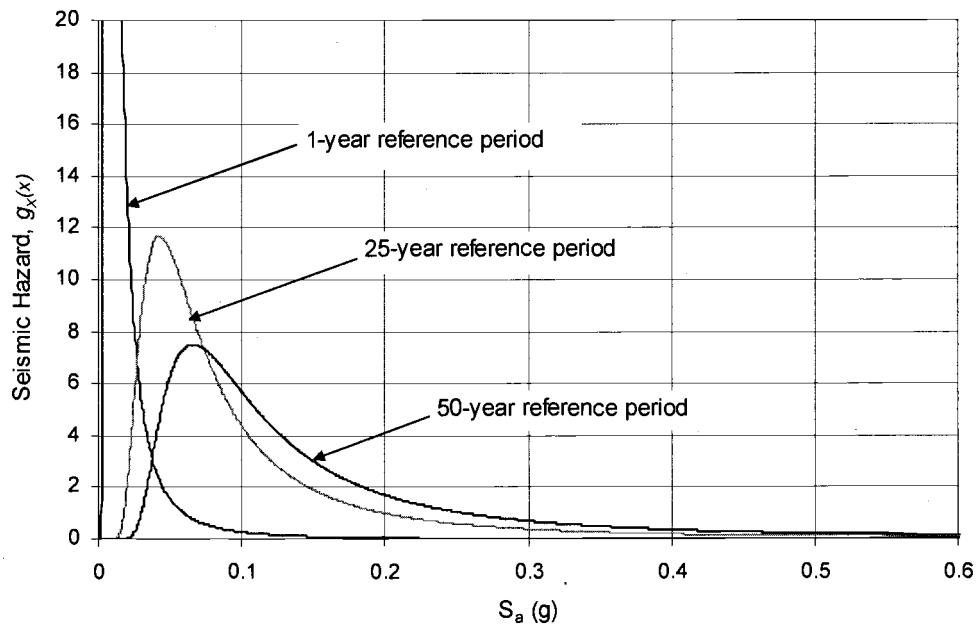


Figure 5.4 – Marginal seismic hazard curves for different reference periods (Carbondale, IL)

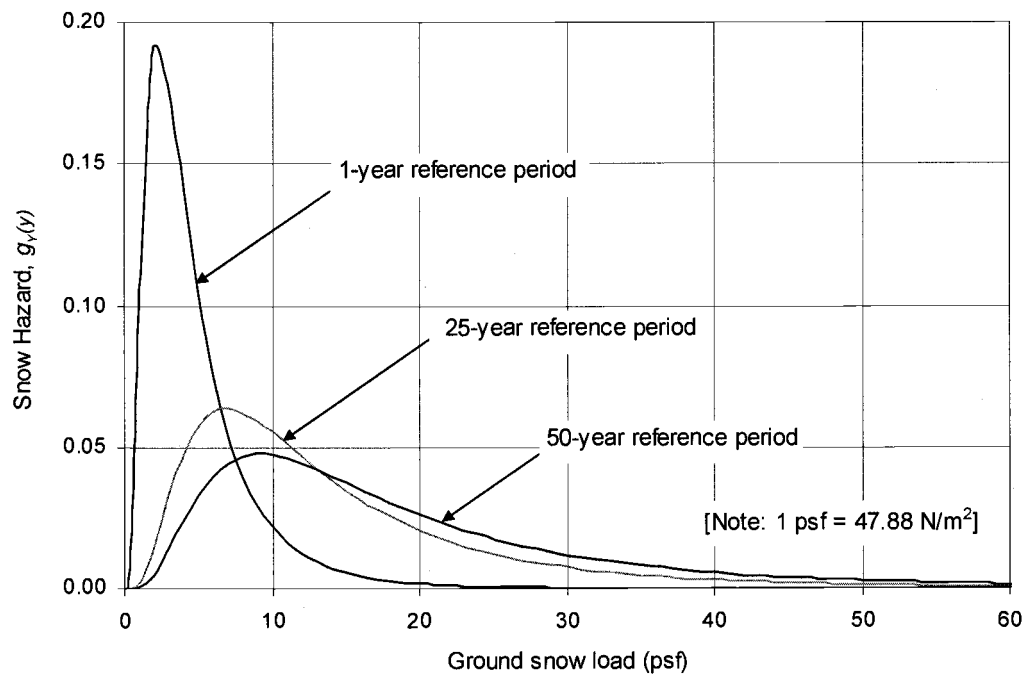


Figure 5.5 – Marginal ground snow hazard curves for different reference periods (Carbondale, IL)

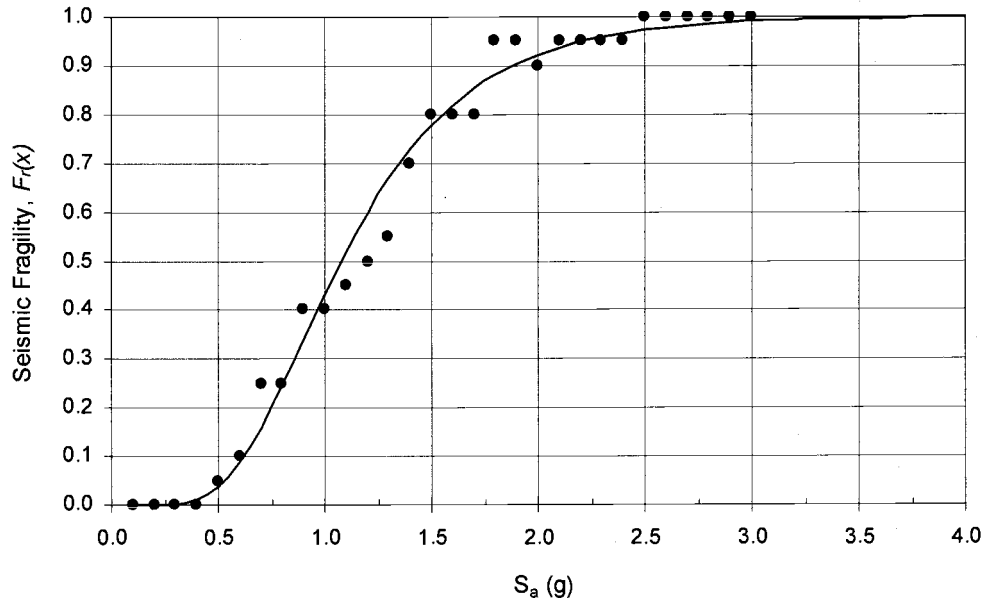


Figure 5.6 – Lognormal seismic fragility

[Type A building / Boston, MA / 1% drift limit / 10 psf (478.8 N/m²) ground snow]

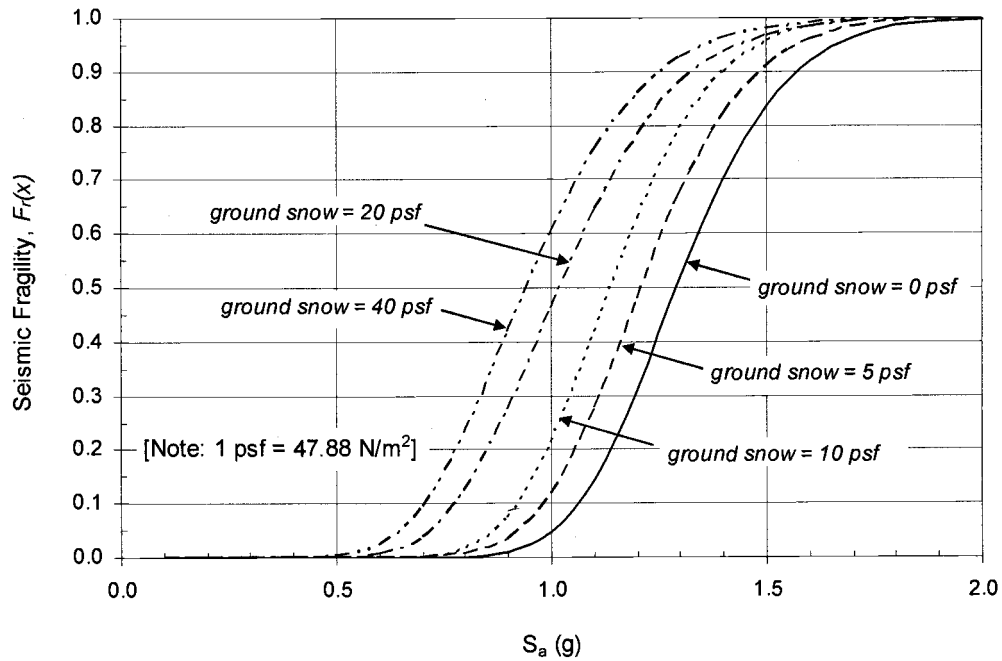


Figure 5.7 – Seismic fragilities considering various deterministic ground snow loads

[Type A building / Carbondale, IL / 1% drift limit]

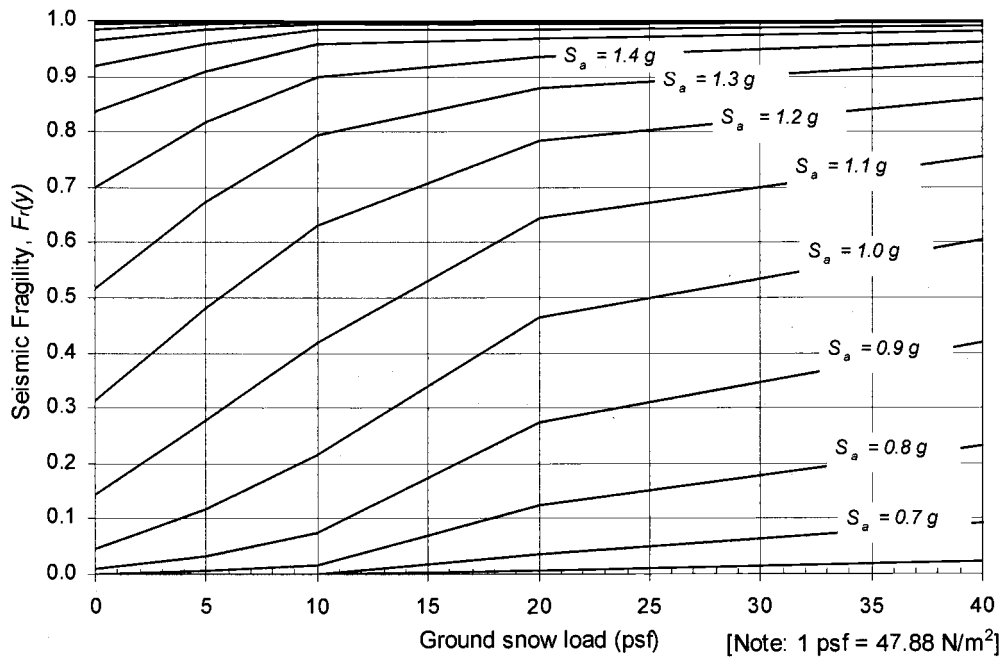


Figure 5.8 – Alternate presentation: Seismic fragility vs. ground snow load
 [Type A building / Carbondale, IL / 1% drift limit]

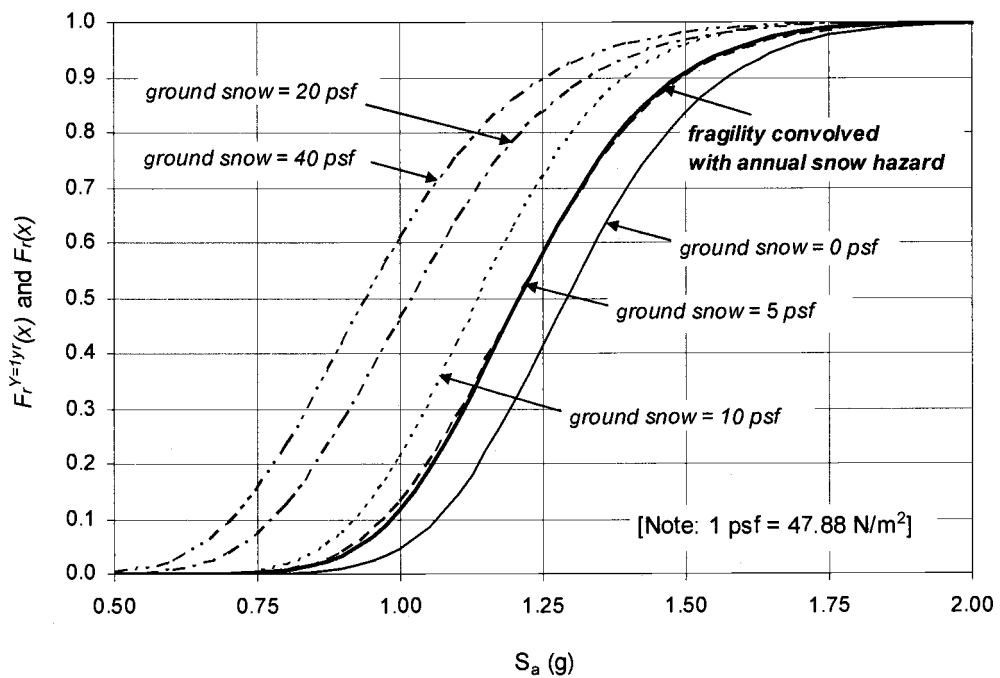


Figure 5.9 – Comparison of $F_r^{Y=1yr}(x)$ with $F_r(x)$
 [Type A building / Carbondale, IL / 1% drift limit]

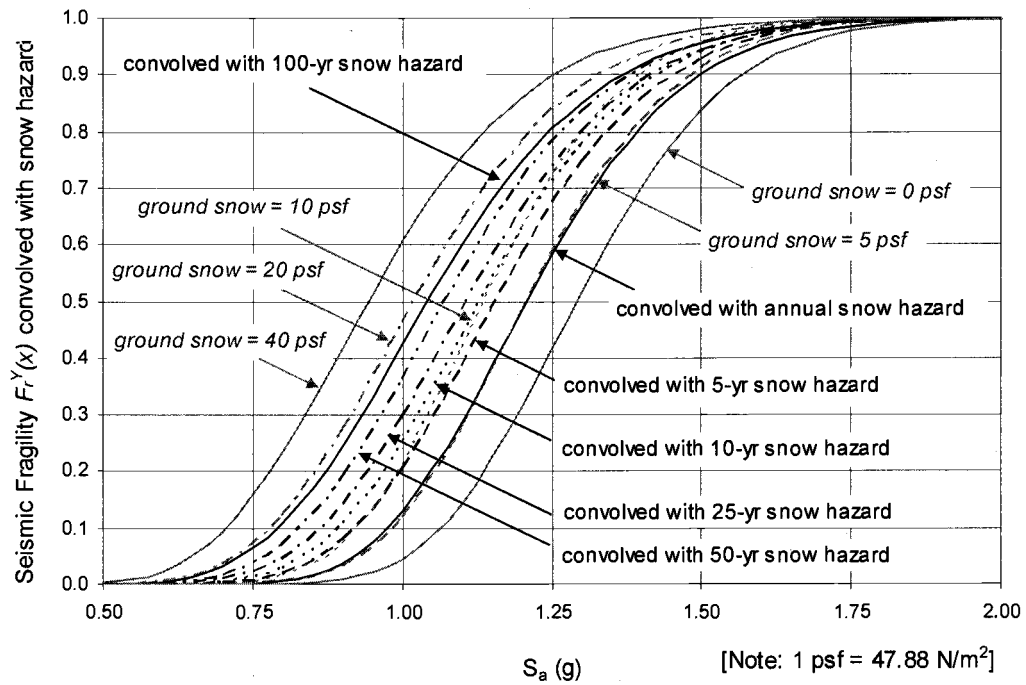


Figure 5.10 – Seismic fragilities convolved with snow hazards
[Carbondale, IL / Type A building / 1% drift limit]

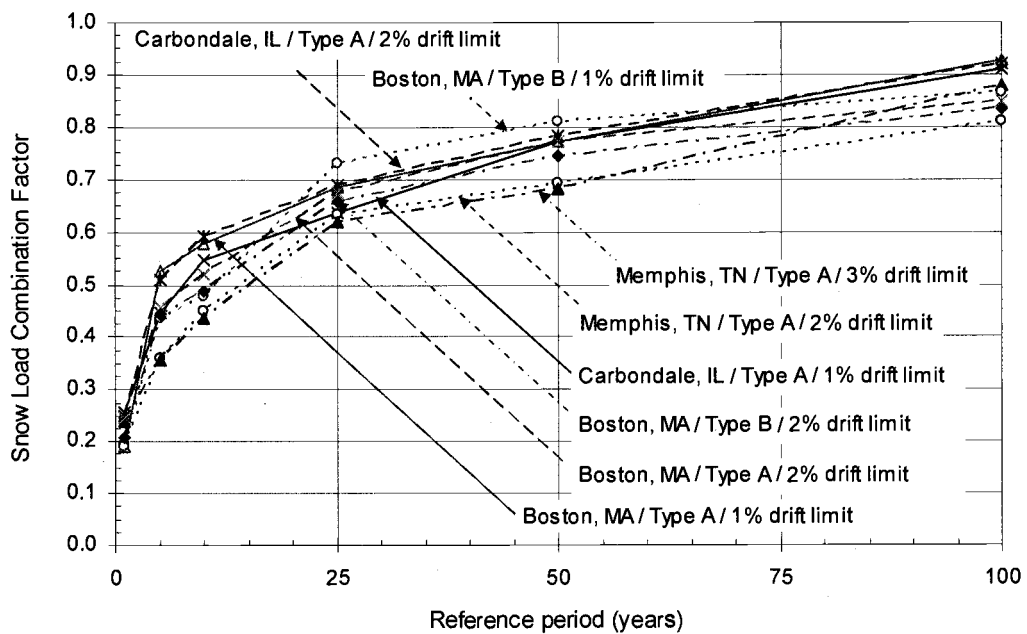


Figure 5.11 – Snow load combination factors for determining additional seismic weight to use in seismic fragility analysis

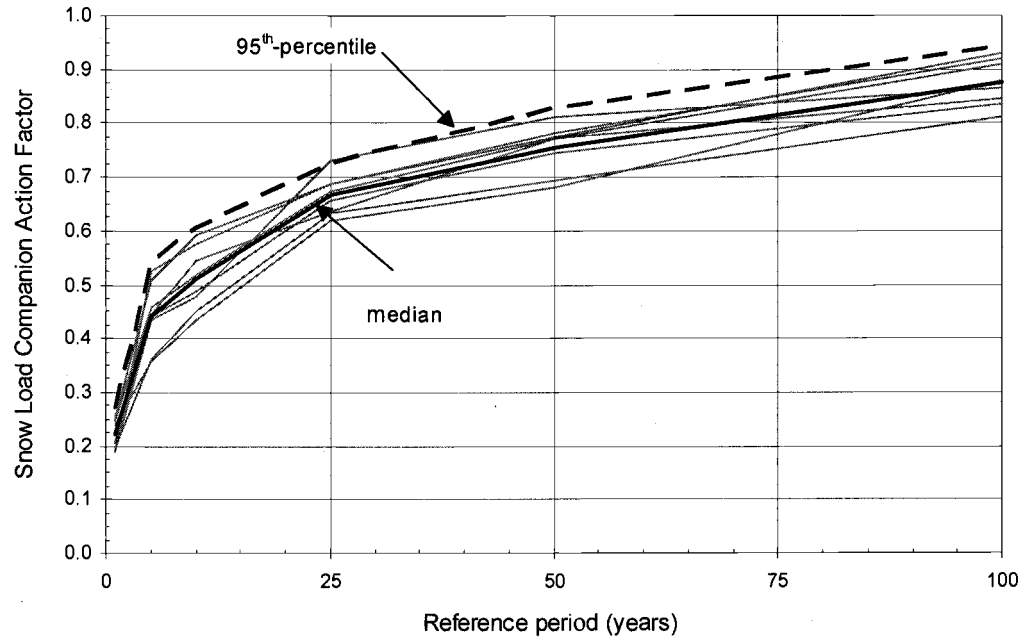


Figure 5.12 – Summary of snow load combination factors for determining additional seismic weight to use in seismic fragility analysis

6. Conclusions and Recommendations

Structural design codes have evolved continuously since the first modern codes were established in the 19th century in order to ensure safer and more economical structures. The allowable stress design format has been widely used since the late 19th century. During the past two decades, probability-based limit states design concepts have evolved and are increasingly being used for various material and structural types. Limit states design, such as LRFD in the U.S., has requirements to ensure that structures perform satisfactorily under various loads and load combinations and that properly designed structures have reliable and consistent safety levels. Performance-based design concepts recently have gained interest among designers and researchers as alternatives to traditional (strength) design procedures. Performance-based engineering procedures require reliable predictions of structural response in order to quantify and limit damage to acceptable levels during the service-life of the structure.

The objective of this study was to develop new contributions in performance-based design of engineered woodframe structures. Specially, fragility curves were developed for structures subjected to various natural hazards (and combinations of hazards) and new site-specific snow load models and hazard models were developed for use in probabilistic design. To accomplish these objectives, fragility curves were developed for assessing probabilistic response of engineered woodframe structures under wind, snow and

earthquake hazards. The fragility curves developed herein can be used to develop performance-based design guidelines for woodframe structures built in high hazard regions as well as to provide information on which to base structural safety or expected structural (and economic loss) assessments. Probabilistic snow load models and snow hazard curves also were developed in this study. Updated snow load models can be used in code calibration studies and in the development of next-generation partial safety factors. The snow hazard curves can be used in a number of reliability-based design and performance-based design applications including assessment of partial safety factors for limit states design, evaluation of load combinations (coincidence) factors considering multiple hazards, evaluation of failure probabilities (by convolving with fragility curves for different performance levels, and development of risk-based assessment procedures for structures (and inventories of structures) under extreme snow loading.

6.1 Conclusions

The following conclusions were drawn from this research:

1. The fragility methodologies (Chapters 2 and 3) described in this study can be used to develop performance-based design guidelines for woodframe structures in high wind regions as well as to provide information on which to base structural safety or expected loss (structural, economic) assessments.
2. The fragility methodologies (Chapters 2 and 3) can be used to predict structural system performance designed to resist high wind loads and (when coupled with a loss model) predict economic loss due to roof sheathing failure (Chapter 2).

3. The aggregated statistics for snow loads or site-specific snow load statistics (Chapter 4) can be used for code calibration studies and development of next-generation partial safety factors in LRFD.
4. The compound fragility concept (Chapter 3) can be used to construct a single aggregated fragility that applies to a building inventory, rather than single structure.
5. The design ground snow loads for Oregon can form the basis of design guidelines for Oregon snow loads and also can be converted to ground snow hazard curves.
6. Snow hazard curves (for special regions such as mountains and gorges) at different elevations (Chapter 4) can be used in a number of reliability-based design and performance-based design applications including assessment of partial safety factors for limit states design. These also can be used in evaluation of load failure probability (by convolving with fragility curves) for different performance levels, and development of risk-based assessment procedures for structures under extreme snow loading.
7. The snow load companion factors developed in Chapter 5 are not sensitive to geographic location, type of structures, or choice of drift limit. However, they are sensitive to choice of reference period. This study found that the median value of snow load combination factors ranged from 0.22 for one-year period to 0.75 for a 50-year reference period.
8. The companion action factors (Chapter 5) developed in this study can be used to specify appropriate values for snow load to be used when performing a displacement-based seismic fragility analysis.

6.2 Recommendations

The following might be suggested as topics for future study:

1. In order for fragility curves such as those developed in this study to reach their fullest potential as design or assessment tools, they will need to be properly validated using a combination of laboratory test results and post-disaster damage survey data.
2. Site-specific probabilistic wind load models (for both inland and coastal sites) can be developed similarly to the snow load models in this study. Such models will be necessary for code calibration studies and the development of next-generation partial safety factors for LRFD.
3. The baseline structures considered in this study are relatively simple. Fragility assessments for more complicated structures are necessary to allow for more realistic damage assessment of building inventories.
4. The companion action factors for combined snow and earthquake loads were developed based on moderate snow / moderate earthquake regions (Mid-America and Northeast regions). Factors also can be developed for high snow / high earthquake regions (Alaska) or moderate snow / high earthquake regions (Northern California).

The companion action factors developed herein were determined using convolution techniques. When such techniques are not possible, it may also be possible to evaluate these factors using event-based simulation technique.

Bibliography

AASHTO (1998), *AASHTO LRFD Bridge Design Specifications*, American Association of State Highway and Transportation Officials, Washington, DC.

AF&PA (1996), *Load and Resistance Factor Design (LRFD) Manual for Engineered Wood Construction*, American Forest and Paper Association, Washington, DC.

AISC (1994), *Manual of Steel Construction, Load and Resistance Factor Design*, American Institute of Steel Construction, Chicago, IL.

ANSI A58.1 (1972), *Building Code Requirements for Minimum Design Loads in Buildings and Other Structures*, American National Standards Institute, New York, NY.

ANSI A58.1 (1982), *Minimum Design Loads for Buildings and Other Structures*, American National Standards Institute, New York, NY.

ASCE (2002), *Minimum Design Loads for Buildings and Other Structures*, Standard ASCE 7-02, Structural Engineering Institute of the American Society of Civil Engineers, Reston, VA.

Bennett, R.M. (1988), "Snow load factors for LRFD," *Journal of Structural Engineering*, ASCE, 114(10):2371-2383.

Cook, N.J. (1985), *The Designer's Guide to Wind Loading of Building Structures – Part 2 Static Structures*, Butterworths, Borough Green, Sevenoaks, Kent TN15 8PH, England.

Cornell, C.A. (1968), "Engineering seismic risk analysis," *Bulletin of the Seismological Society of America*, 58(5):1583-1606.

Durham, J.P. (1998), "Seismic Response of Wood Shearwalls with Oversized Oriented Strand Board Panels," MASC Thesis, University of British Columbia, Vancouver, Canada.

Ellingwood, B.R., Galambos, T.V., MacGregor, J.G. and Cornell, C.A. (1980), *Development of a Probability Based Load Criterion for American National Standard A58*. Special Publication 577, U.S. Department of Commerce, National Bureau of Standards, Washington, DC.

Ellingwood, B.R., MacGregor, T.V., Galambos, T.V., and Cornell, C.A. (1982), "Probability Based Load Criteria: Load Factors and Load Combinations," *Journal of Structural Division*, ASCE, 108(5):978-997.

Ellingwood, B.R. and Redfield, R. (1983), "Ground snow loads for structural design," *Journal of Structural Engineering*, ASCE, 109(4):950-964.

Ellingwood, B.R. and O'Rourke, M.J. (1985), "Probabilistic models of snow loads on structures," *Structural Safety*, 2:291-299.

Ellingwood, B.R. and Rosowsky, D.V. (1996), "Combining snow and earthquake loads for limit states design," *Journal of Structural Engineering*, ASCE, 122(11):1364-1368.

Ellingwood, B.R. and Tekie, P.B. (1999), "Wind load statistics for probability-based structural design," *Journal of Structural Engineering*, ASCE, 125(4):453-463.

Ellingwood, B.R. and Tekie, P.B. (2001), "Fragility analysis of concrete gravity dams," *Journal of Infrastructure Systems*, ASCE, 7(2):41-48.

Ellingwood, B.R., Rosowsky, D.V., Li, Y. and Kim, J.H. (2004), "Fragility assessment of light-frame construction subjected to wind and earthquake hazards," *Journal of Structural Engineering*, ASCE. (in press)

FEMA (2000a), *Prestandard and Commentary for the Seismic Rehabilitation of Buildings*, Federal Emergency Management Agency, Washington, DC.

FEMA (2000b), *Global Topics Report on the Prestandard and Commentary for the Seismic Rehabilitation of Buildings*, Federal Emergency Management Agency, Washington, DC.

Fischer, D., Filiatrault, A., Folz, B., Uang, C-M. and Seible, F. (2001), *Shake Table Tests of a Two-Story Woodframe House*, CUREE Publication No. W-06, Consortium of Universities for Research in Earthquake Engineering, Richmond, CA.

Folz, B. and Filiatrault, A. (2000), *CASHEW- Version 1.0: A Computer Program for Cyclic Analysis of Wood Shear Walls*, CUREE Publication No. W-08, Consortium of Universities for Research in Earthquake Engineering, Richmond, CA.

Folz, B. and Filiatrault, A. (2001), "Cyclic Analysis of Wood Shear Walls," *Journal of Structural Engineering*, ASCE, 127(4):433-441.

Folz, B. and Filiatrault, A. (2003), *SAWS – A Computer Program for Seismic Analysis of Woodframe Structures*, CUREE Publication No. W-21, Consortium of Universities for Research in Earthquake Engineering, Richmond, CA.

Galambos, T.V., Ellingwood, B.R., MacGregor, J.G. and Cornell, C.A. (1982), "Probability based load criteria: assessment of current design practice." *Journal of Structural Division*, ASCE, 108(5):959-977.

Holmes, J.D. (1994), "Wind pressures on tropical housing," *Journal of Wind Engineering and Industrial Aerodynamics*, 53:105-123.

IBC (2003), *International Building Code*, International Code Council, Falls Church, VA.

Kennedy R.P. and Ravindra, M.K. (1984), "Seismic fragilities for nuclear power plant studies," *Nuclear Engineering and Design*, 79(1):47-68.

Kim, J.H. (2003), "Performance-Based Seismic Design of Light-Frame Shearwalls," Ph.D. dissertation, Department of Civil, Construction, and Environmental Engineering, Oregon

State University, Corvallis, OR.

Lee, K.H. and Rosowsky, D.V. (2004), "Fragility Curves for Roof Sheathing Failure in High Wind Regions." (submitted to *Engineering Structures*)

Moller, O., Foshi, R.O. and Rubinstein, M. (2001), "Reinforced Concrete Structures under Seismic Excitation: Reliability and Performance Based Design," *Proceedings: 8th International Conference on Structural Safety and Reliability (ICOSSAR '01)*, Newport Beach, CA.

NAHB (1997), *Housing Affordability through Design Efficiency Program*. NAHB Research Center. Inc., Upper Marlboro, MD.

NCDC (2002) – National Climatic Data Center – NCDC Climate Data Online, <http://cdo.ncdc.noaa.gov/pls/plclimprod/poemain.accessrouter> - (July, 2002)

NCDC (2004) – National Climatic Data Center – NCDC Climate Data Online, <http://cdo.ncdc.noaa.gov/CDO/dataproduct> - (February, 2004)

NEHRP (1992), *NEHRP recommended provisions for seismic resistant design of buildings. FEMA Rep. No. 222*, Federal Emergency Management Agency (FEMA), Washington, DC.

O'Rourke, M.J. and Stiefel, U. (1983), "Roof snow loads for structural design," *Journal of Structural Engineering*, ASCE, 109(7):1527-1537.

O'Rourke, M.J. and Speck, Jr., R.S. (1992), "Roof-Snow Load for Seismic – Design Calculations," *Journal of Structural Engineering*, ASCE, 118(9):2338-2350.

Philips, Y.L., Itani, R.Y. and McLean, D.L. (1993) "Lateral Load Sharing by Diaphragms in Wood-Frame Buildings," *Journal of Structural Engineering*, ASCE, 119(5):1556-1571.

Rosowsky, D.V. and Schiff, S.D. (1996), "Probabilistic modeling of roof sheathing uplift capacity," *Proceedings: ASCE Specialty Conference on Probabilistic Mechanics and Structural Reliability*, Worcester, MA, pp. 334-337.

Rosowsky, D.V. and Cheng, N. (1999a), "Reliability of light-frame roofs in high-wind regions. I: Wind loads," *Journal of Structural Engineering*, ASCE, 125(7):725-733.

Rosowsky, D.V. and Cheng, N. (1999b), "Reliability of light-frame roofs in high-wind regions. II: Reliability analysis," *Journal of Structural Engineering*, ASCE, 125(7):734-739.

Rosowsky, D.V. and Kim, J.H. (2002a), *Reliability Studies*, CUREE Publication No. W-10, Consortium of Universities for Research in Earthquake Engineering, Richmond, CA.

Rosowsky, D.V. and Kim, J.H. (2002b), "Performance-Based Seismic Design of Wood Shearwalls," *Proceedings: World Conference on Timber Engineering (WCTE 2002)*, Selangor, Malaysia.

Rosowsky, D.V. (2002), "Reliability-Based Seismic Design of Wood Shear Walls," *Journal of Structural Engineering*, ASCE, 128(11):1439-1453.

Rosowsky, D.V. and Ellingwood, B.R. (2002), "Performance-Based Engineering of Wood Frame Housing: a Fragility Analysis Methodology," *Journal of Structural Engineering*, ASCE, 128(1):32-38.

Rosowsky, D.V. and Kim, J.H. (2003), "A Probabilistic Framework for Performance-Based Design of Wood Shearwalls," *Proceedings: 9th International Conference on Applications of Statistics and Probability in Civil Engineering (ICASP9)*, San Francisco, CA.

SEAO (1978), "Snow Load Analysis for Oregon," Structural Engineers Association of Oregon, State of Oregon, Department of Commerce, Building Codes Division, Salem, OR.

Somerville, P., Smith., Punyamurthula, S. and Sun, J. (1997), *Development of Ground Motion Time Histories for Phase 2 of the FEMA/SAC Steel Project*, Report No. SAC/BD-97/04, SAC Joint Venture, Sacramento, CA.

Tobiasson, W. and Redfield, R. (1980), "Snow load for the United States, Parts I and II," U.S. Army Cold Regions Research and Laboratory Report, Hanover, NH.

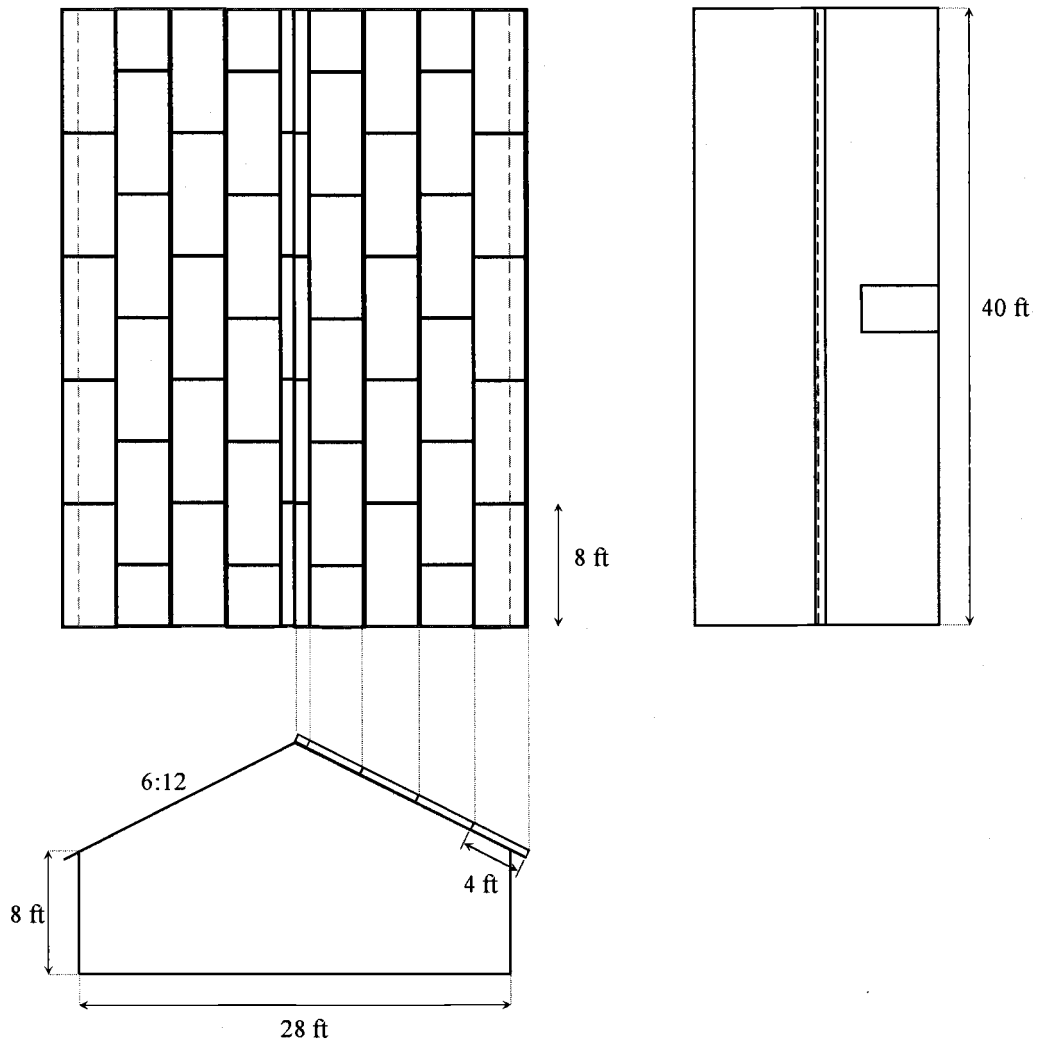
USGS (2004) – United States Geology Service – Seismic Hazard Map, <http://eqhazmaps.usgs.gov/> - (February, 2004)

Xu, Y.L. and Reardon, G.F. (1998), "Variations wind pressure on hip roofs with roof pitch," *Journal of Wind Engineering and Industrial Aerodynamics*, 73:267-284.

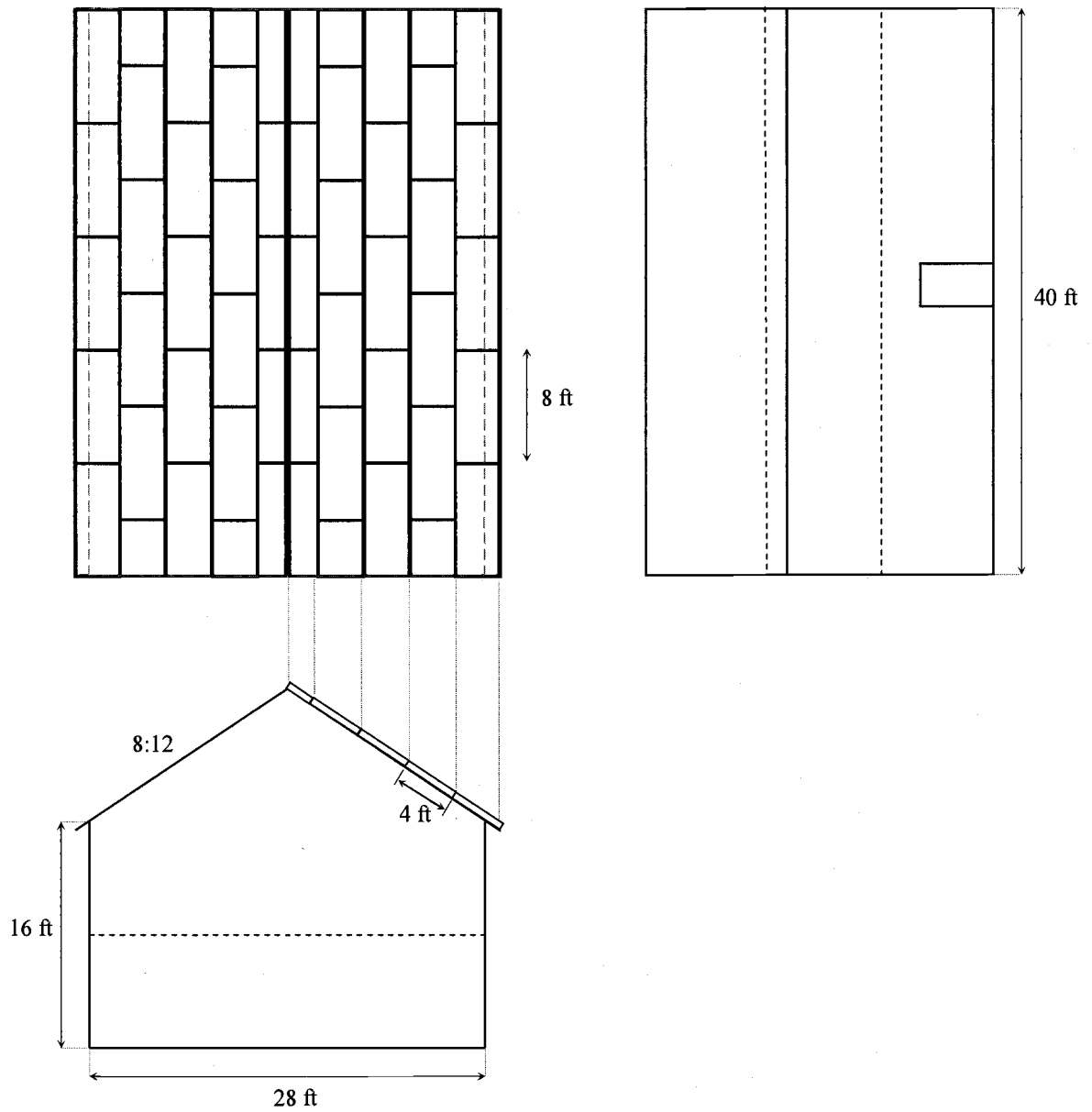
ZSC (2003), *Risk Topics – Snow loading roof collapse*, Zurich Service Corporation, Schaumburg, IL.

Appendices

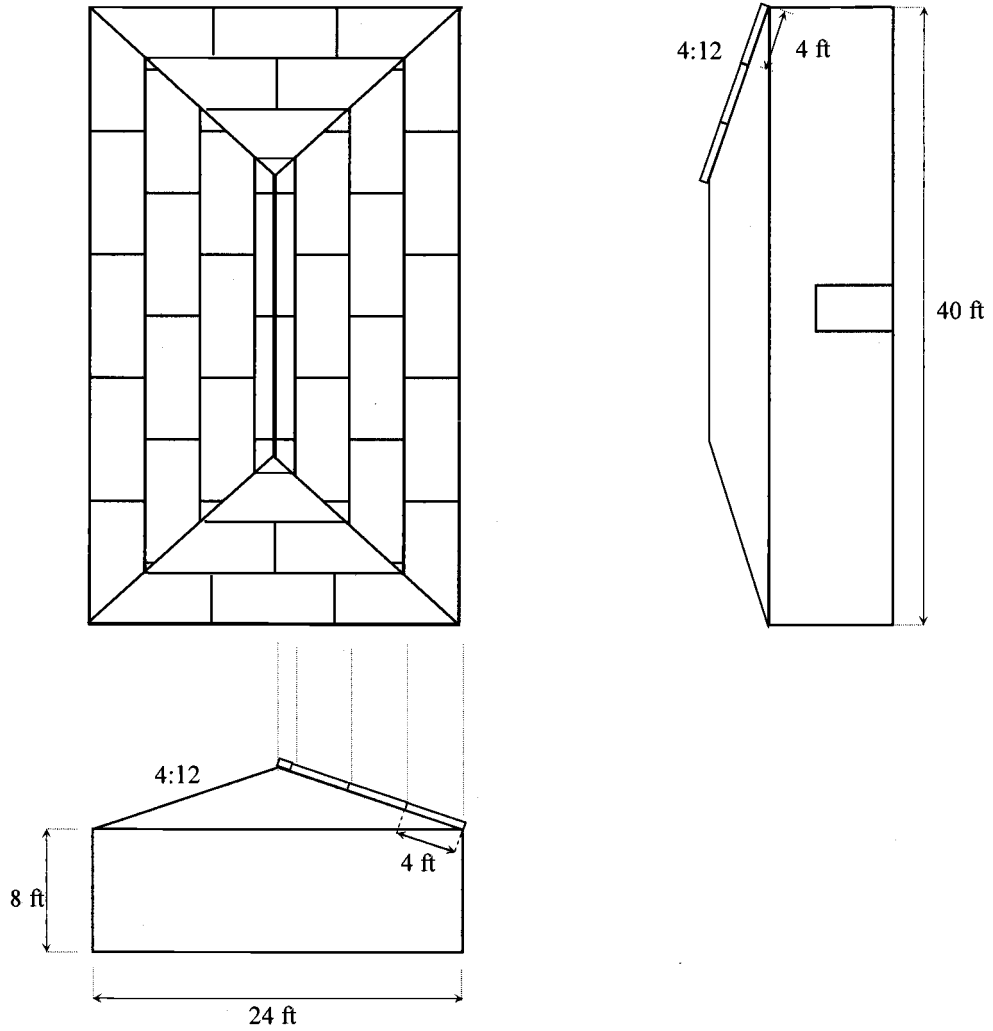
Appendix A.1 – Dimension and panel layouts for other baseline structures



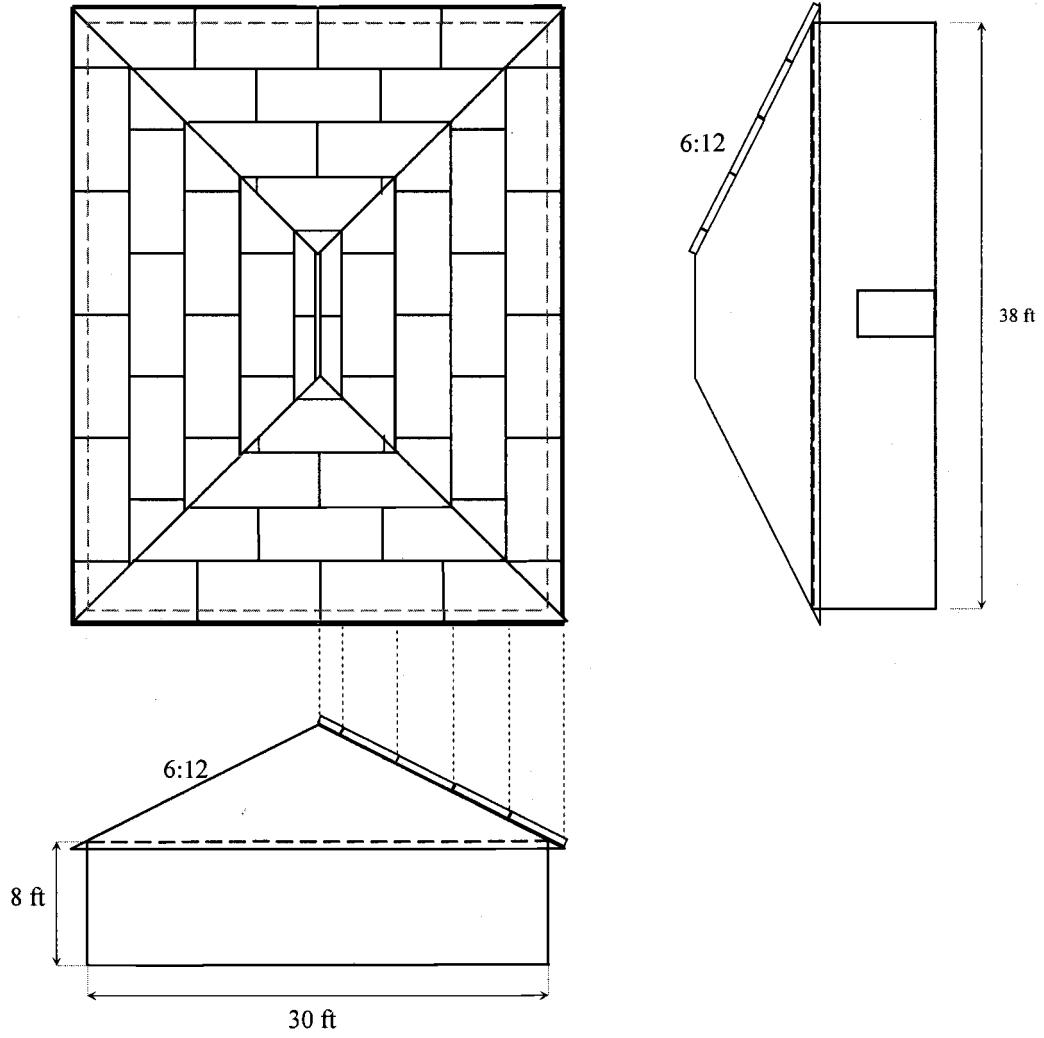
A.1(a) – Dimensions and panel layouts, Structure Type 2



A.1(b) – Dimensions and panel layouts, Structure Type 3



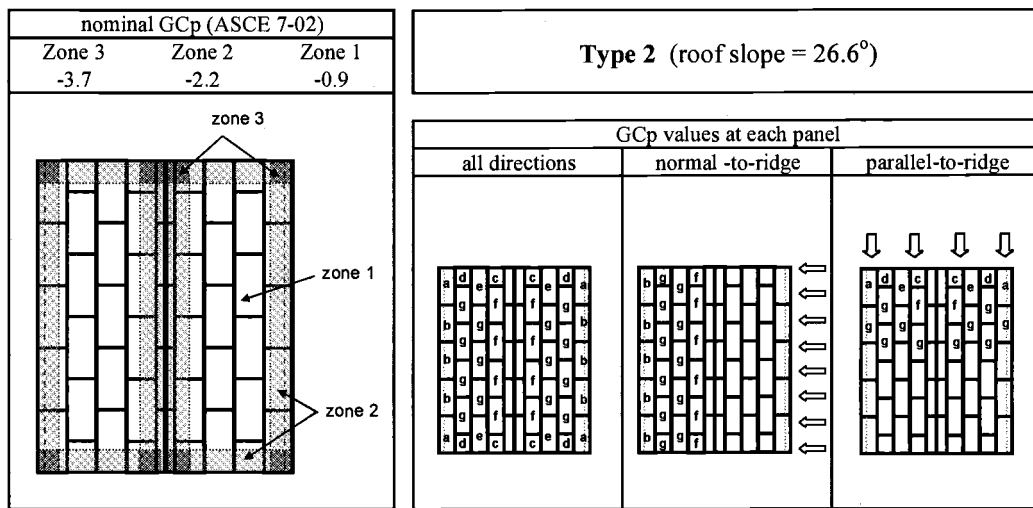
A.1(c) – Dimensions and panel layouts, Structure Type 4.



A.1(d) – Dimensions and panel layouts, Structure Type 5

Appendix A.2 – Summary of GC_p statistics for other baseline structures

A.2(a) – Summary of GC_p statistics for Structure Type 2

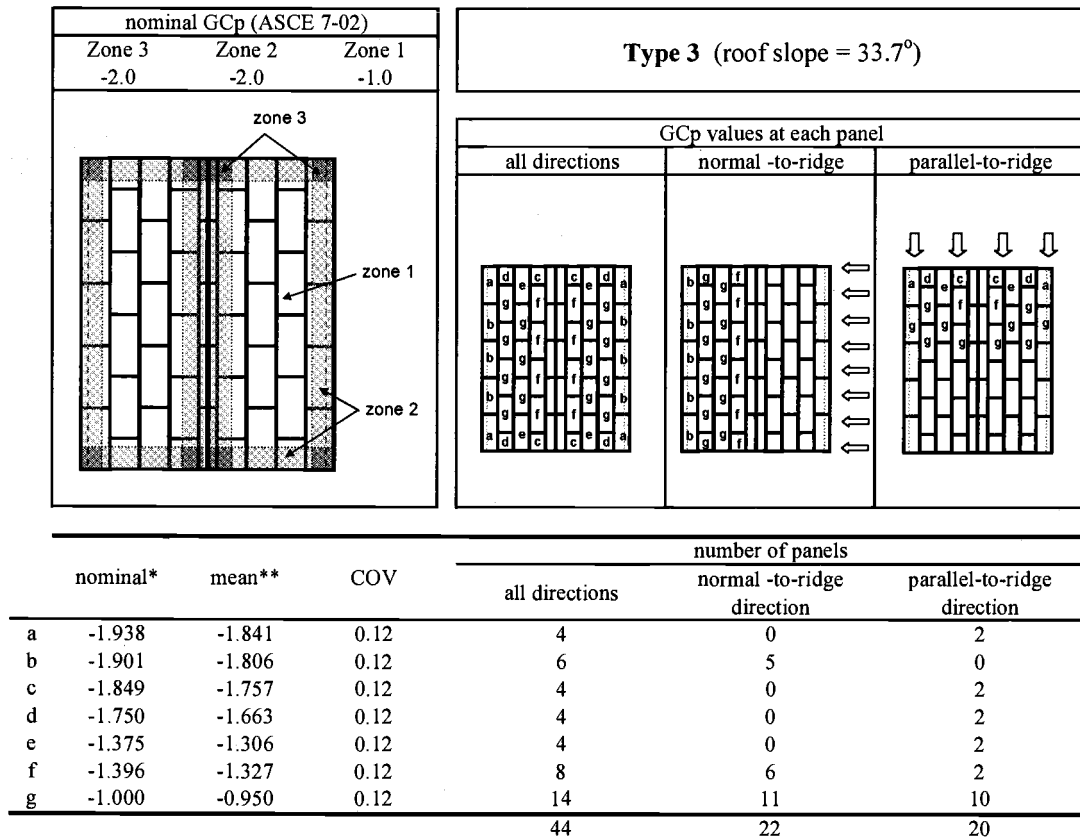


	nominal*	mean**	COV	number of panels		
				all directions	normal -to-ridge direction	parallel-to-ridge direction
a	-2.540	-2.413	0.12	4	0	2
b	-1.989	-1.890	0.12	6	5	0
c	-2.811	-2.670	0.12	4	0	2
d	-1.875	-1.781	0.12	4	0	2
e	-1.388	-1.318	0.12	4	0	2
f	-1.739	-1.652	0.12	8	6	2
g	-0.900	-0.855	0.12	14	11	10
				44	22	20

* calculated using weighted-average method

** calculated using mean-to-nominal value provided by Ellingwood and Tekie (1999)

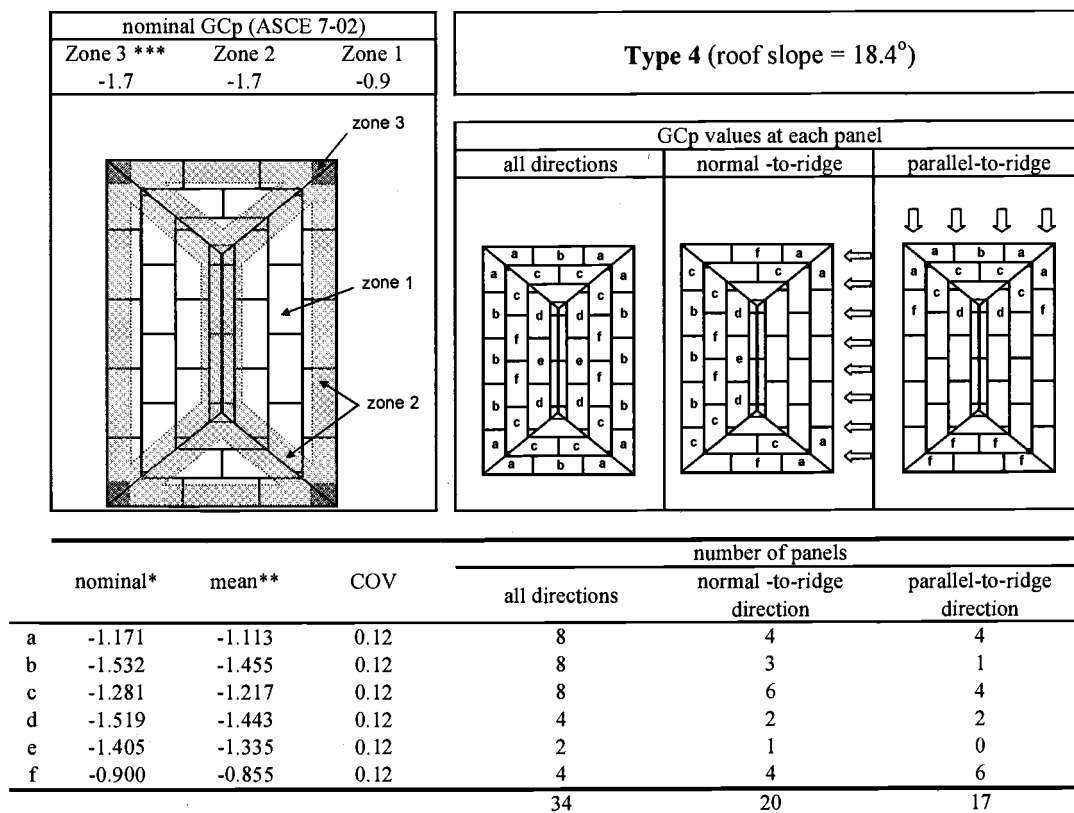
A.2(b) – Summary of GC_p statistics for Structure Type 3



* calculated using weighted-average method

** calculated using mean-to-nominal value provided by Ellingwood and Tekie (1999)

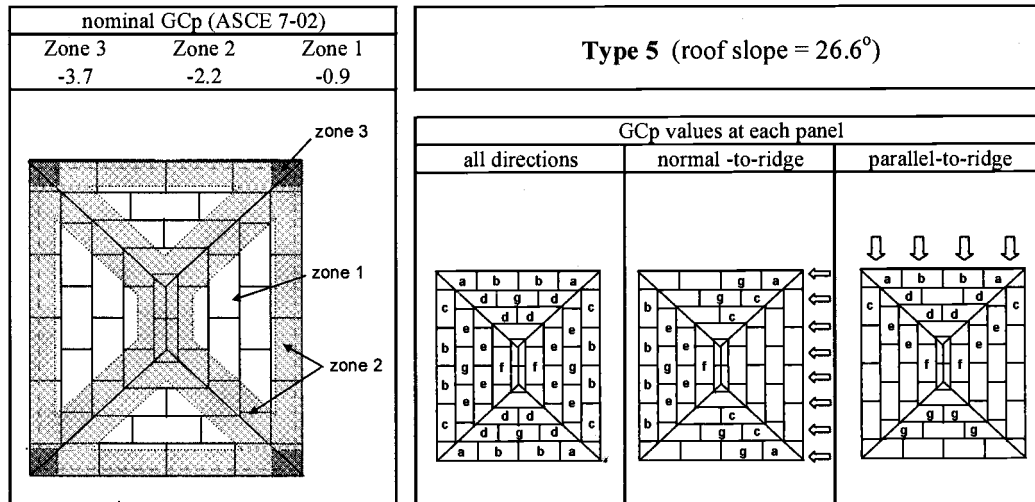
A.2(c) – Summary of GC_p statistics for Structure Type 4



* calculated using weighted-average method

** calculated using mean-to-nominal value provided by Ellingwood and Tekie (1999)

A.2(d) – Summary of GC_p statistics for Structure Type 5

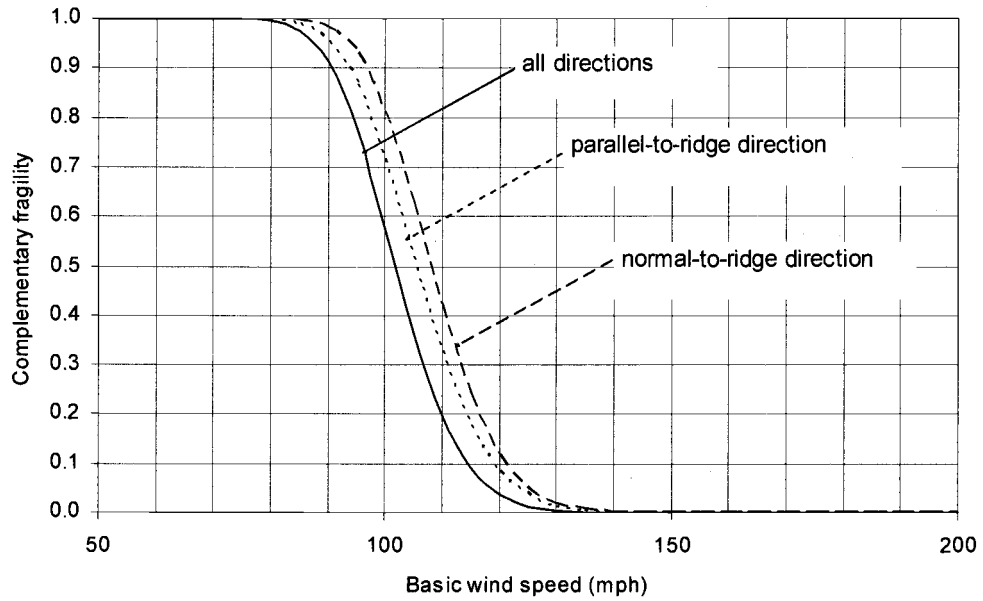


	nominal*	mean**	COV	number of panels		
				all directions	normal -to-ridge direction	parallel-to-ridge direction
a	-2.470	-2.347	0.12	4	2	2
b	-1.989	-1.890	0.12	8	4	2
c	-2.095	-1.990	0.12	4	4	2
d	-1.769	-1.681	0.12	8	0	4
e	-1.104	-1.049	0.12	8	4	4
f	-1.379	-1.310	0.12	2	1	2
g	-0.900	-0.855	0.12	4	4	4
				38	19	20

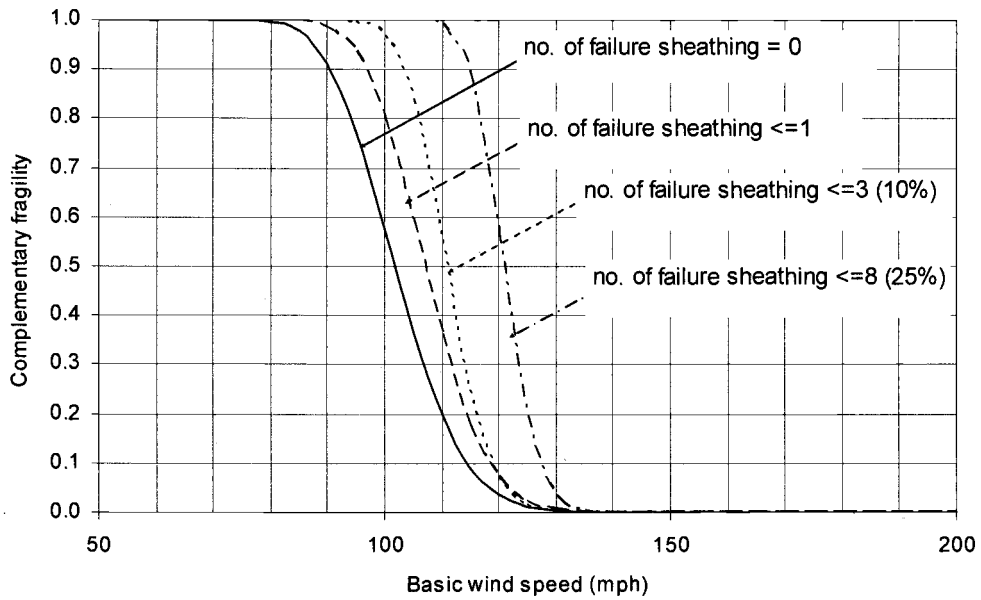
* calculated using weighted-average method

** calculated using mean-to-nominal value provided by Ellingwood and Tekie (1999)

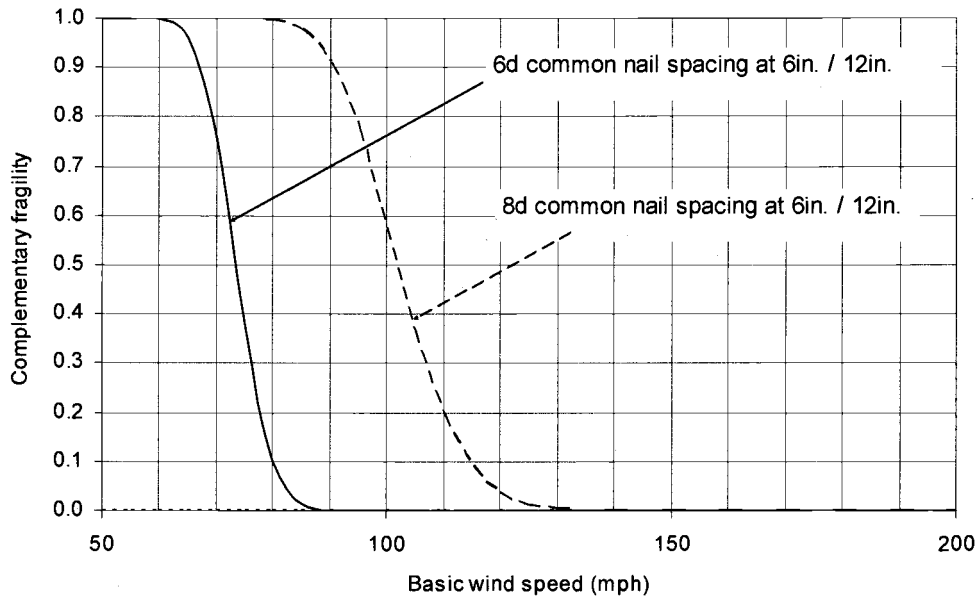
Appendix A.3 – Complementary fragility curves for other baseline structures



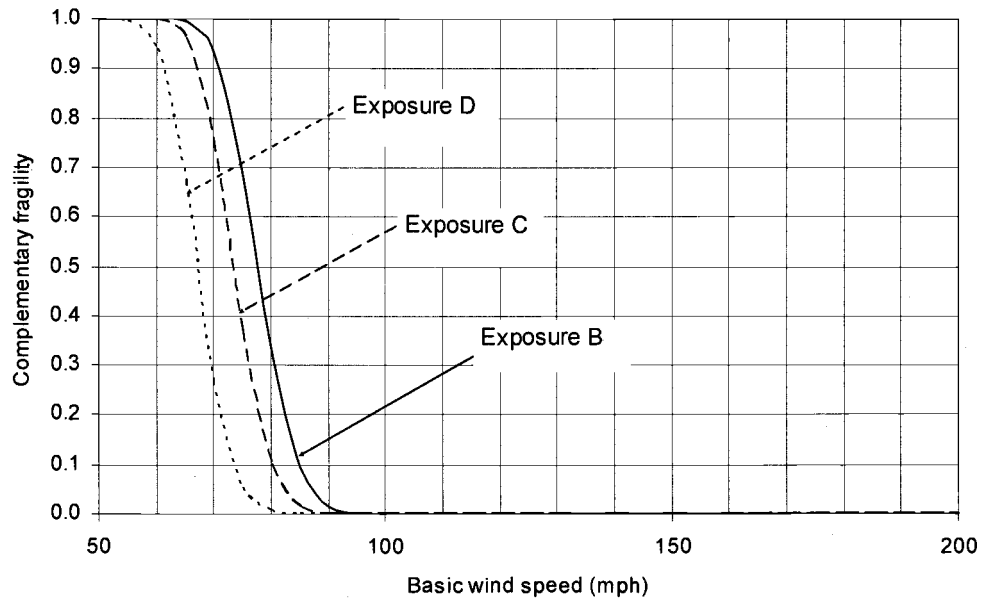
A.3.1(a) – Comparison of roof sheathing survivorship curves for different wind directions
 Structure Type 1 / Exposure C / 8d nail -6 in./12in. spacing
 [damage level: no sheathing failure]



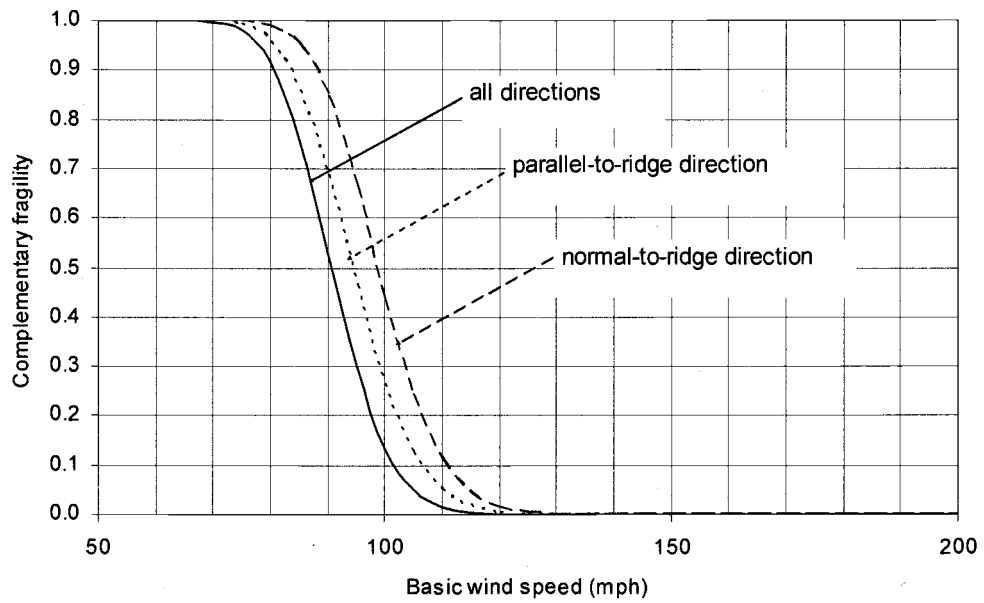
A.3.1(b) – Comparison of roof sheathing survivorship curves for different damage level
 Structure Type 1 / Exposure C / 8d nail -6 in./12in. spacing
 [damage level: no sheathing failure]



A.3.1(c) – Comparison of roof sheathing survivorship curves for different nail types
 Structure Type 1 / Exposure C / all possible wind directions
 [damage level: no sheathing failure]



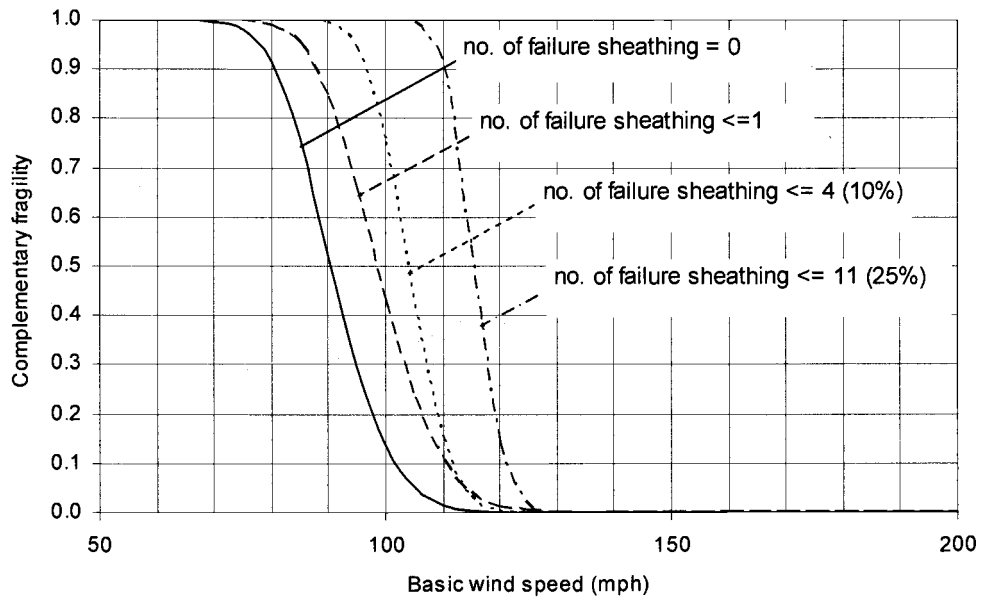
A.3.1(d) – Comparison of roof sheathing survivorship curves for different exposures
 Structure Type 1 / 6d nail – 6in./12in. spacing / all possible wind directions
 [damage level: no sheathing failure]



A.3.2(a) – Comparison of roof sheathing survivorship curves for different wind directions

Structure Type 2 / Exposure C / 8d nail – 6 in./12in. spacing

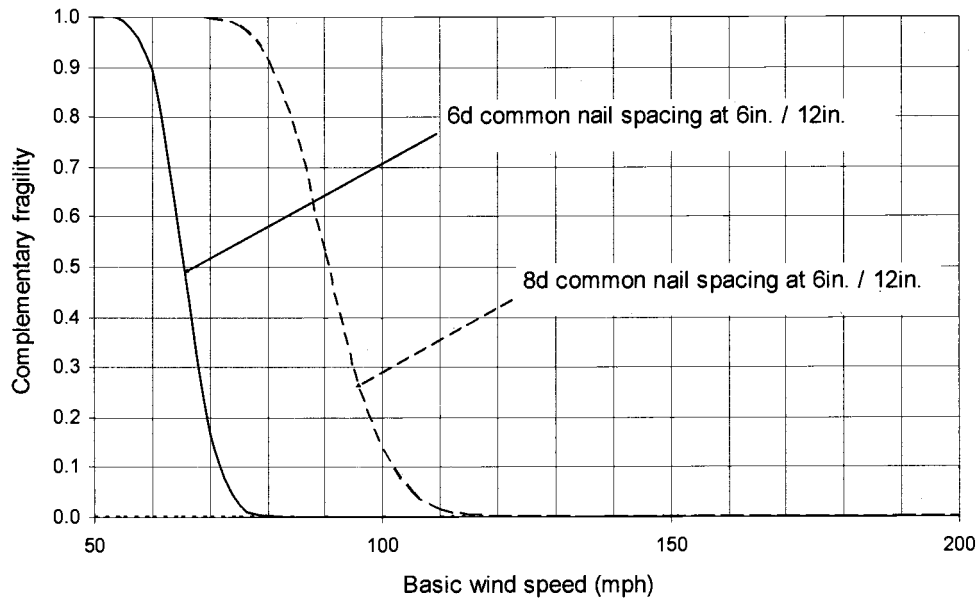
[damage level: no sheathing failure]



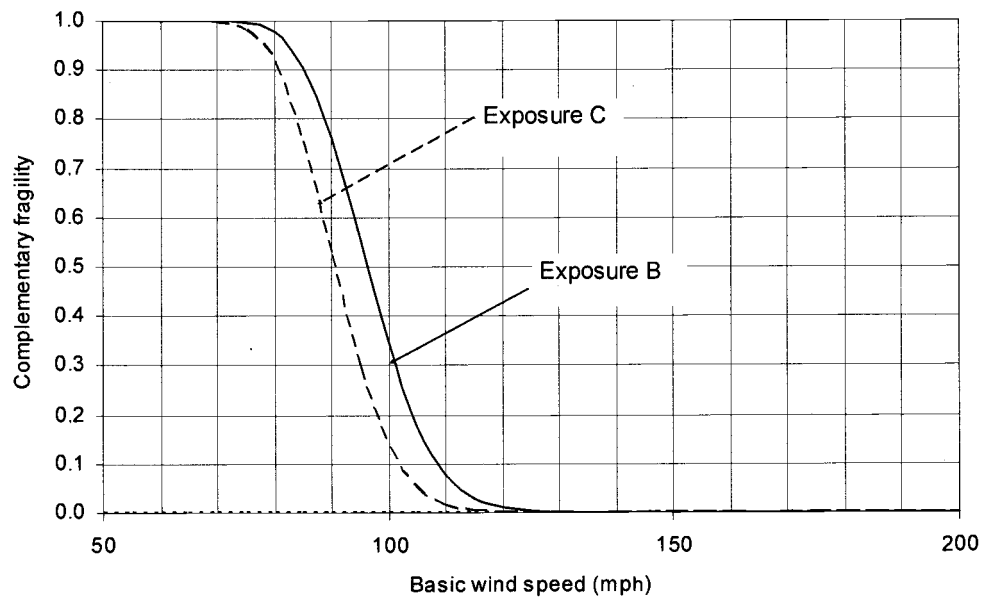
A.3.2(b) – Comparison of roof sheathing survivorship curves for different damage level

Structure Type 2 / Exposure C / 8d nail – 6 in./12in. spacing

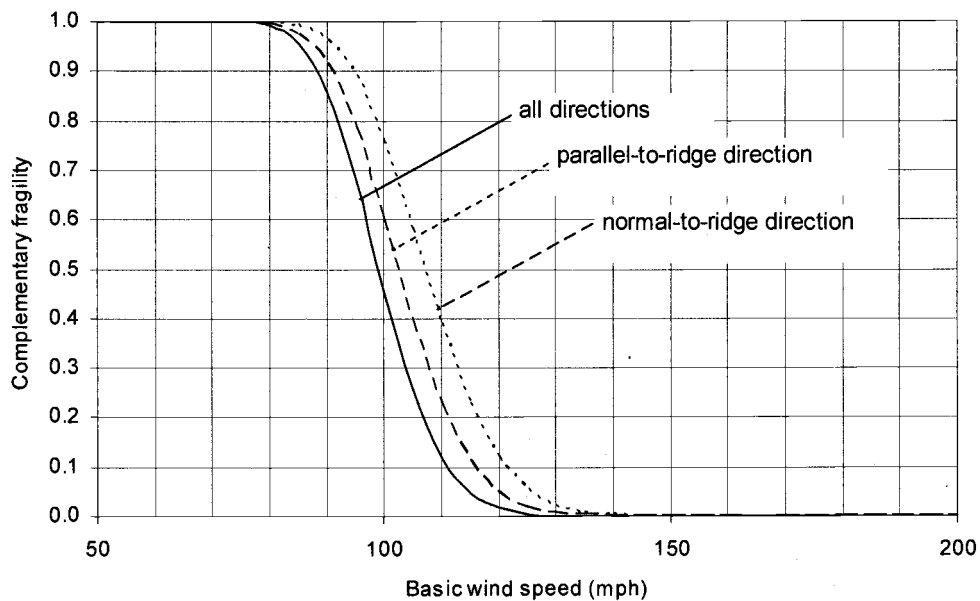
[damage level: no sheathing failure]



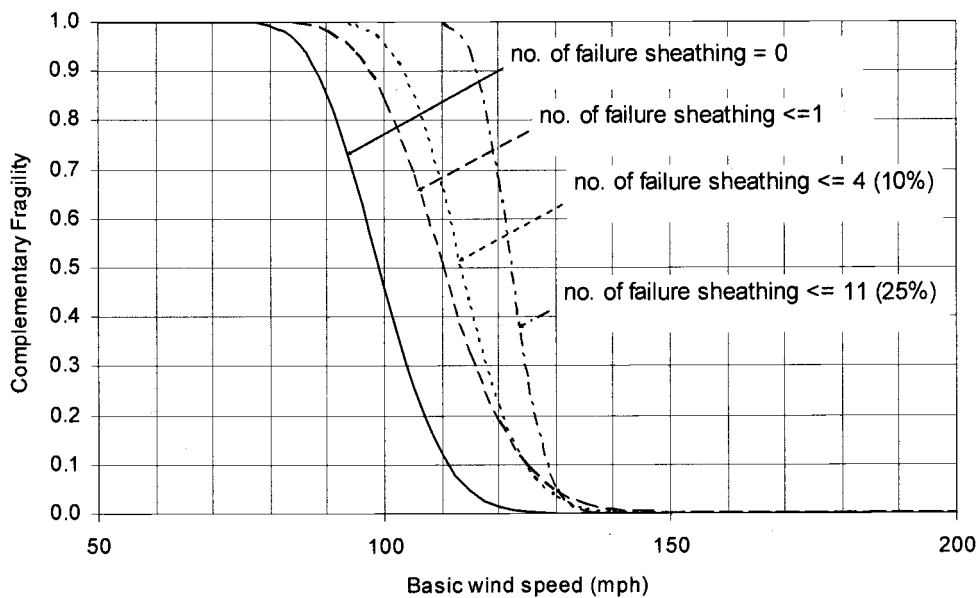
A.3.2(c) – Comparison of roof sheathing survivorship curves for different nail types
 Structure Type 2 / Exposure C / all possible wind directions
 [damage level: no sheathing failure]



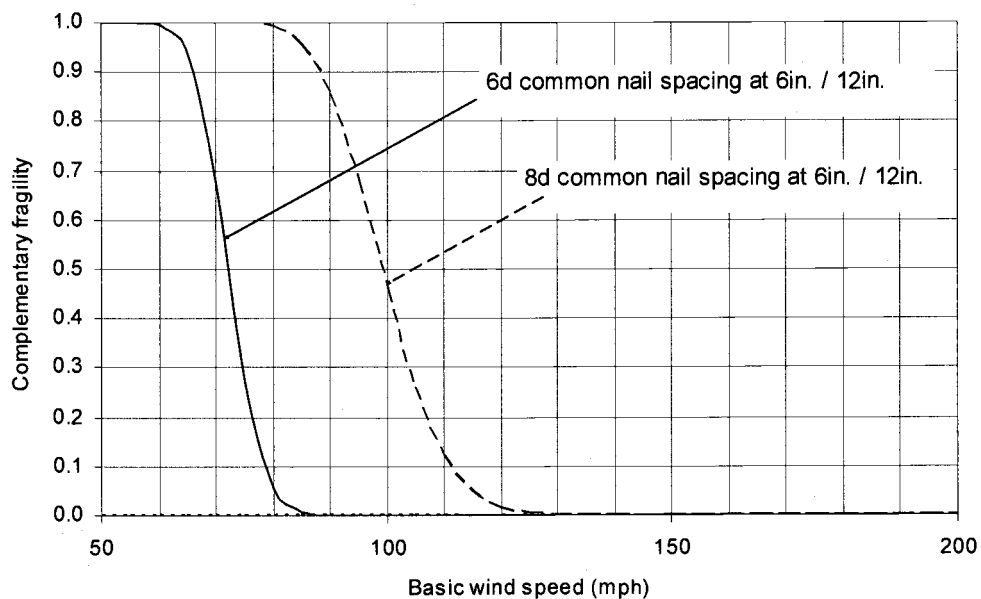
A.3.2(d) – Comparison of roof sheathing survivorship curves for different exposures
 Structure Type 2 / 8d nail – 6in./12in. spacing / all possible wind directions
 [damage level: no sheathing failure]



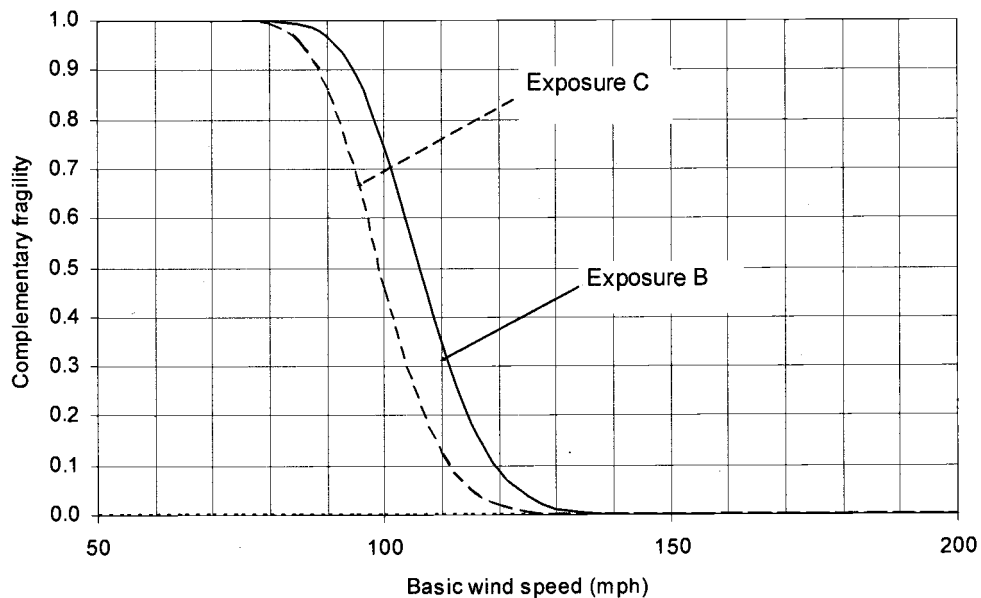
A.3.3(a) – Comparison of roof sheathing survivorship curves for different wind directions
 Structure Type 3 / Exposure C / 8d nail – 6 in./12in. spacing
 [damage level: no sheathing failure]



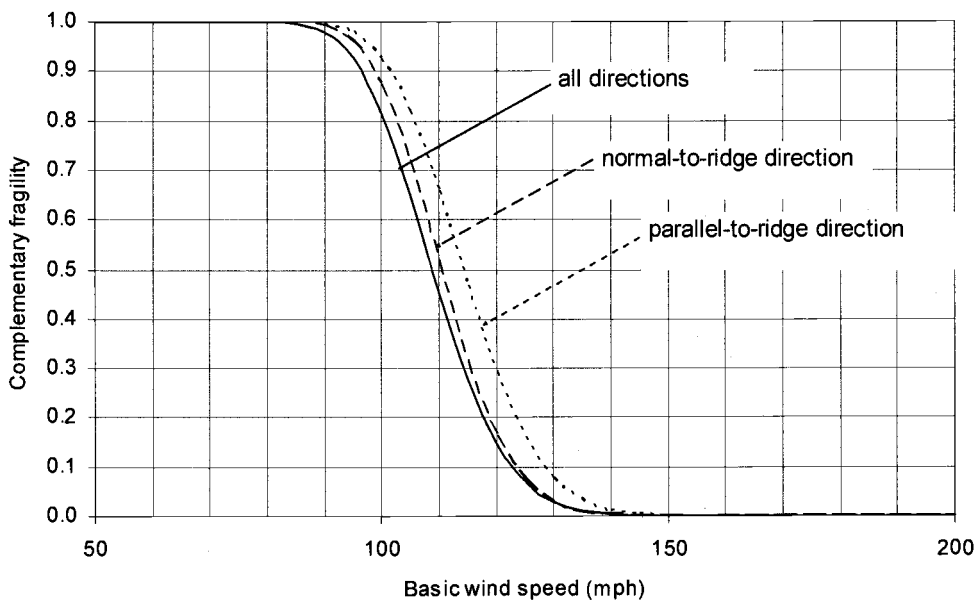
A.3.3(b) – Comparison of roof sheathing survivorship curves for different damage level
 Structure Type 3 / Exposure C / 8d nail – 6 in./12in. spacing
 [damage level: no sheathing failure]



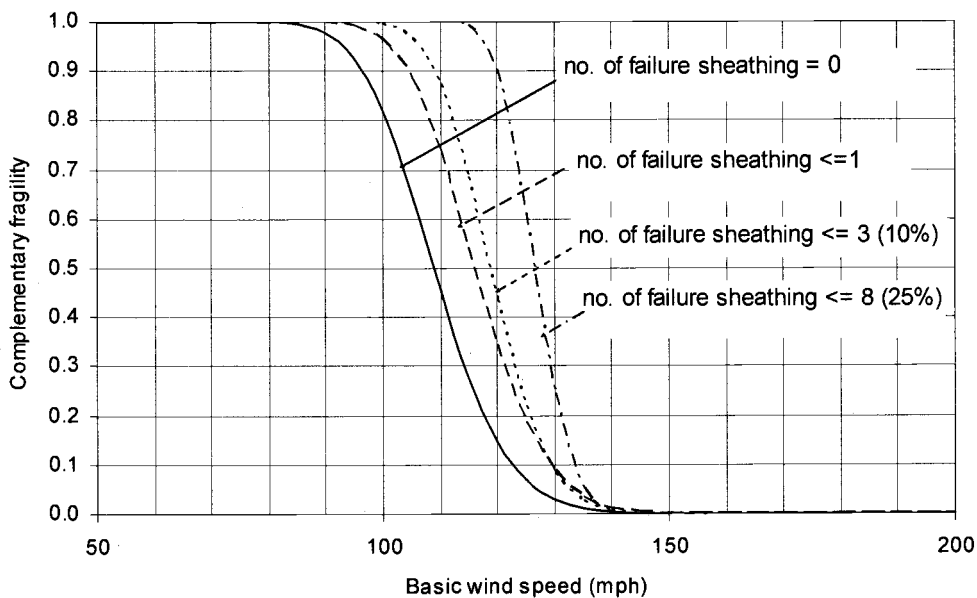
A.3.3(c) – Comparison of roof sheathing survivorship curves for different nail types
 Structure Type 3 / Exposure C / all possible wind directions
 [damage level: no sheathing failure]



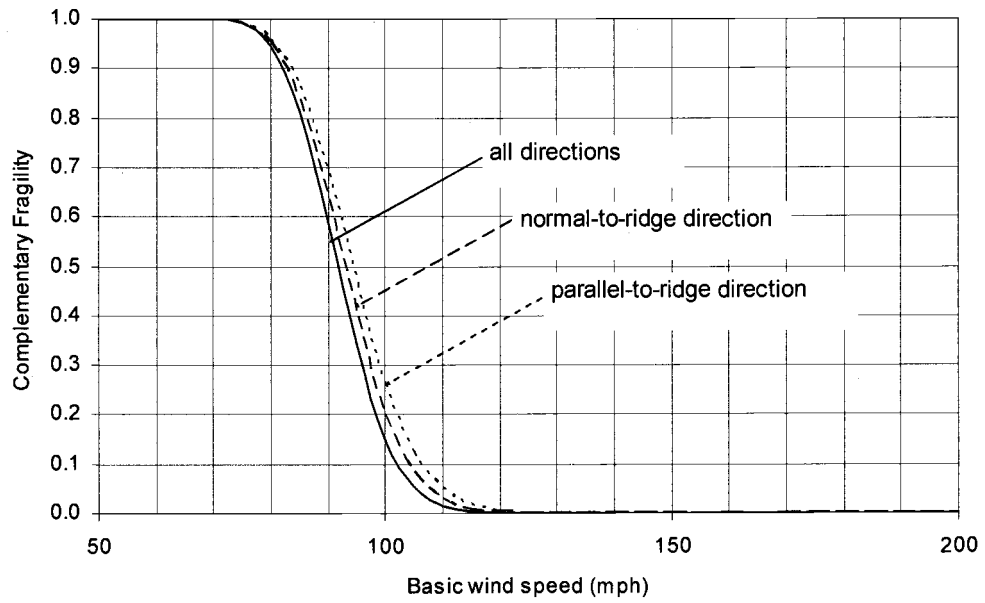
A.3.3(d) – Comparison of roof sheathing survivorship curves for different exposures
 Structure Type 3 / 8d nail – 6in./12in. spacing / all possible wind directions
 [damage level: no sheathing failure]



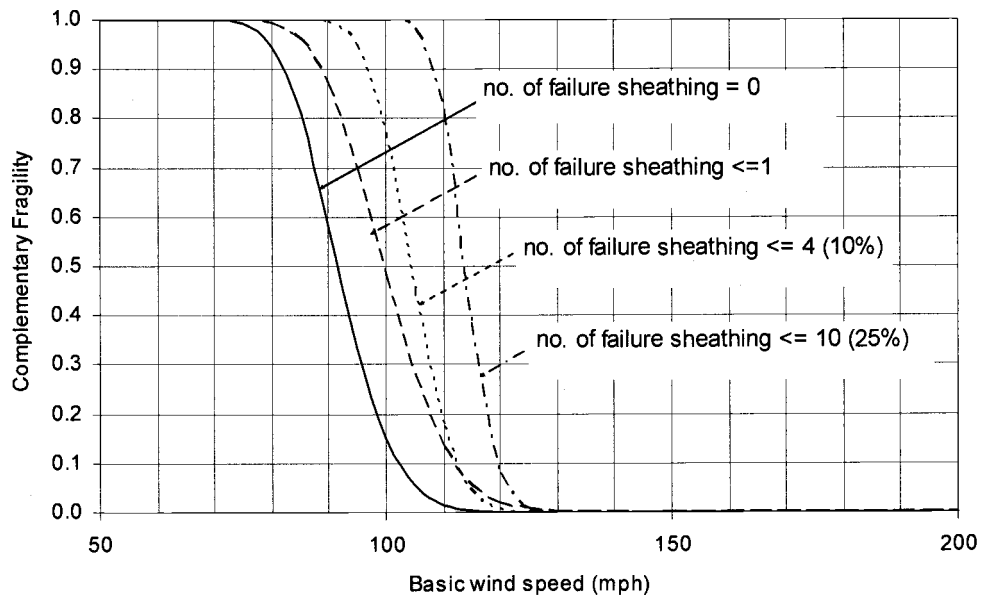
A.3.4(a) – Comparison of roof sheathing survivorship curves for different wind directions
 Structure Type 4 / Exposure C / 8d nail – 6 in./12in. spacing
 [damage level: no sheathing failure]



A.3.4(b) – Comparison of roof sheathing survivorship curves for different damage level
 Structure Type 4 / Exposure C / 8d nail – 6 in./12in. spacing
 [damage level: no sheathing failure]

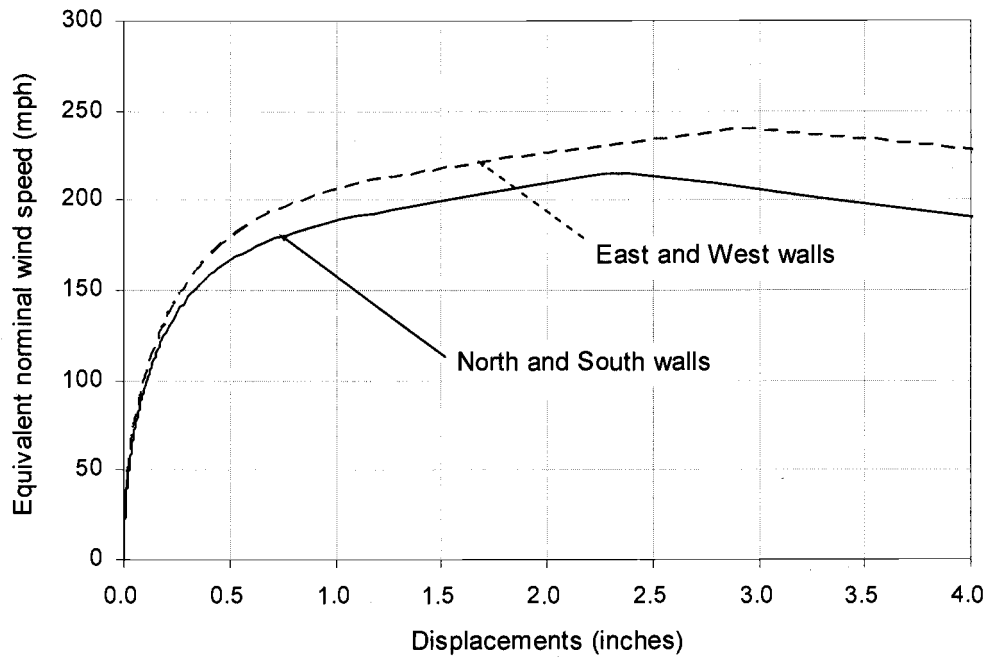


A.3.5(a) – Comparison of roof sheathing survivorship curves for different wind directions
 Structure Type 5 / Exposure C / 8d nail – 6 in./12in. spacing
 [damage level: no sheathing failure]

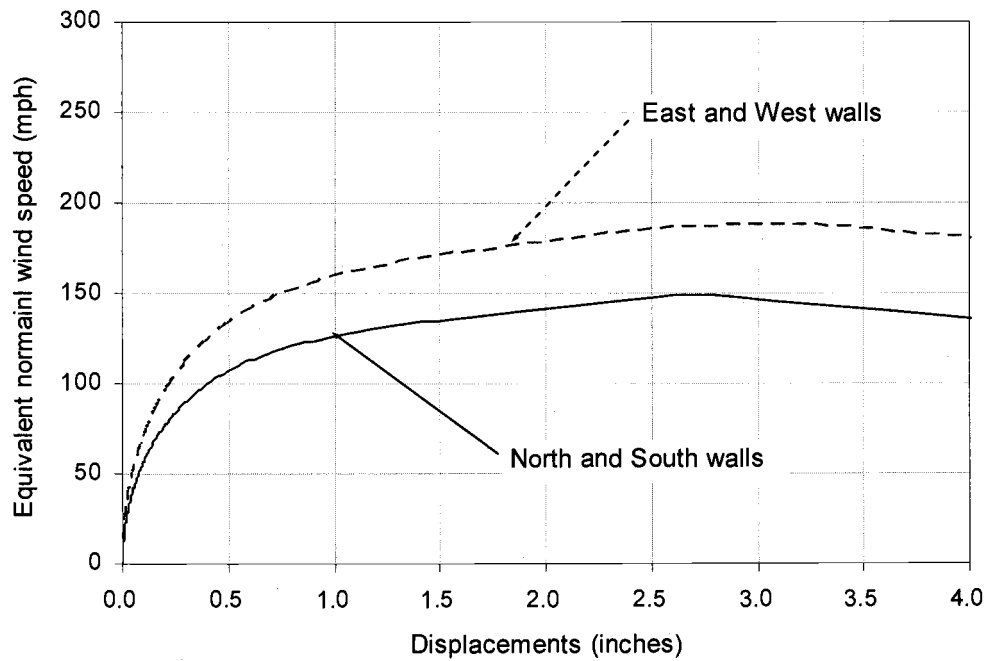


A.3.5(b) – Comparison of roof sheathing survivorship curves for different damage level
 Structure Type 5 / Exposure C / 8d nail – 6 in./12in. spacing
 [damage level: no sheathing failure]

**Appendix B.1 – Equivalent wind speed pushover curves for other buildings
considering two different load directions**

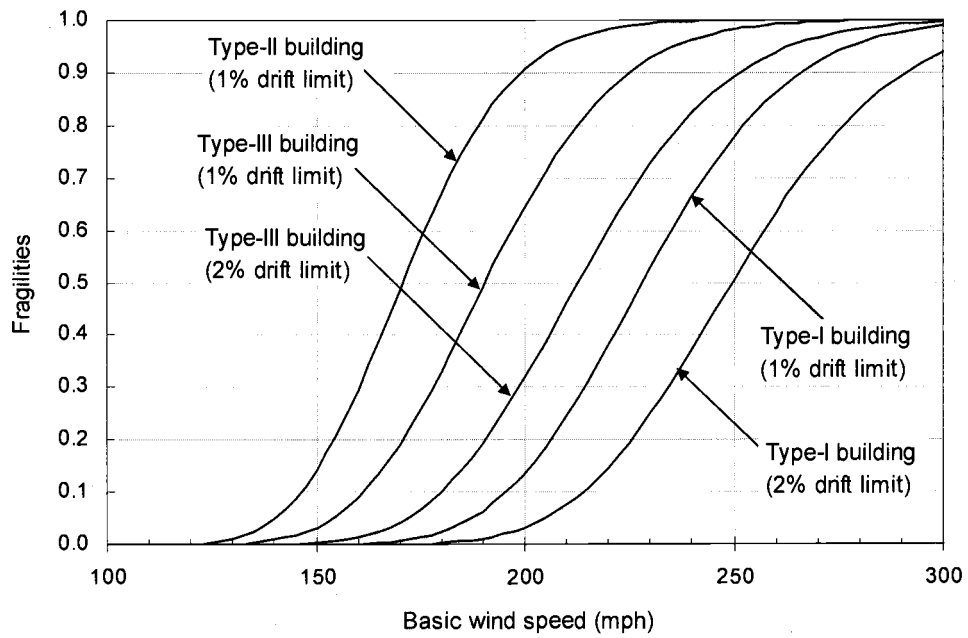


B.1(a) – Equivalent wind speed pushover curves for Type-I building considering two different load directions

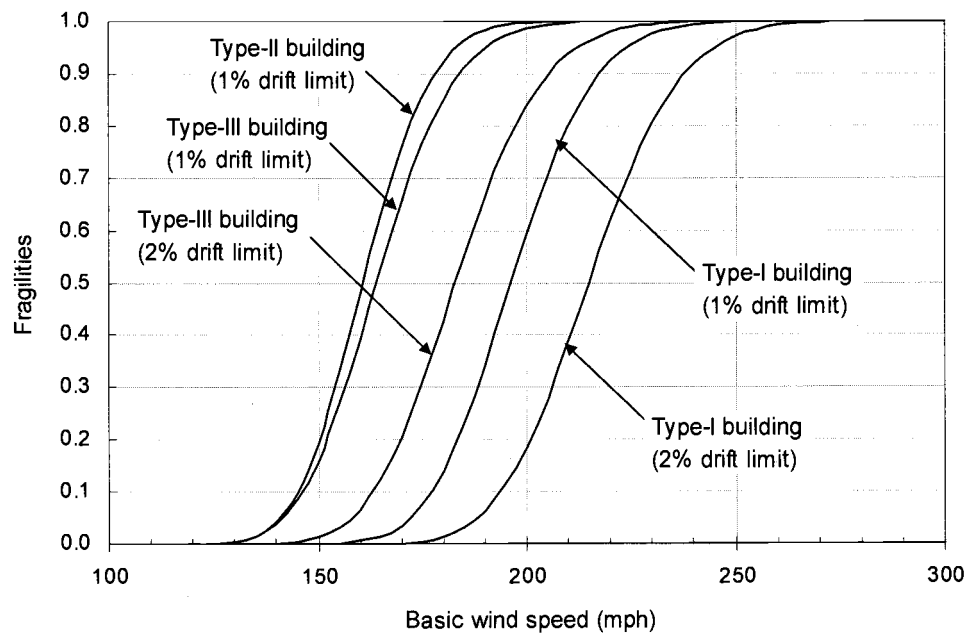


B.1(b) – Equivalent wind speed pushover curves for Type-II building considering two different load directions

Appendix B.2 – Lateral wind fragilities



B.2(a) – Lateral wind fragility using the simulation
[Exposure B, with directionality factor]



B.2(b) – Lateral wind fragility using the simulation
[Exposure C, without directionality factor]

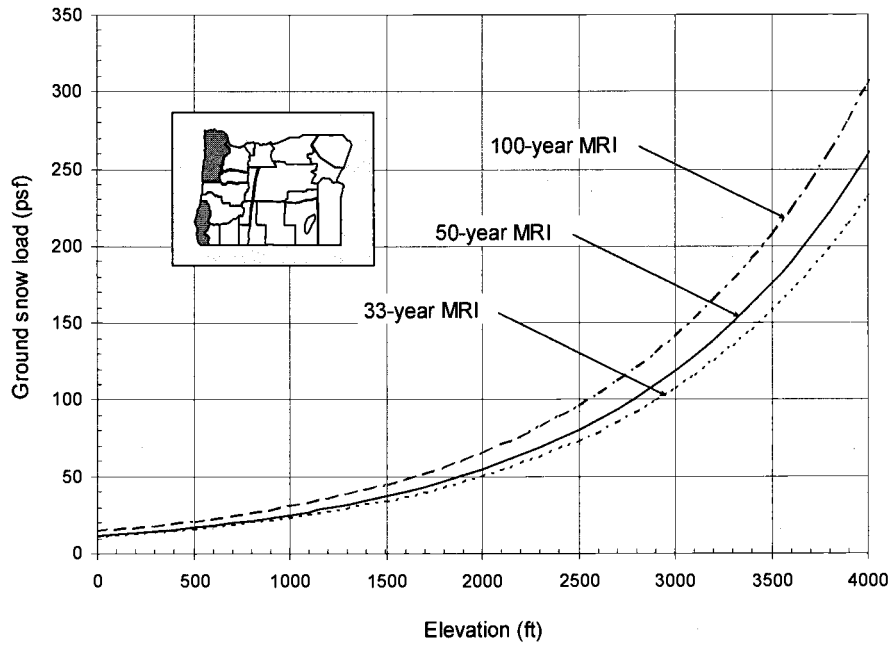
**Appendix B.3 – Lognormal parameters for lateral wind fragilities determined
by quick analysis**

B.3 – Lognormal parameters for lateral wind fragilities determined by quick analysis

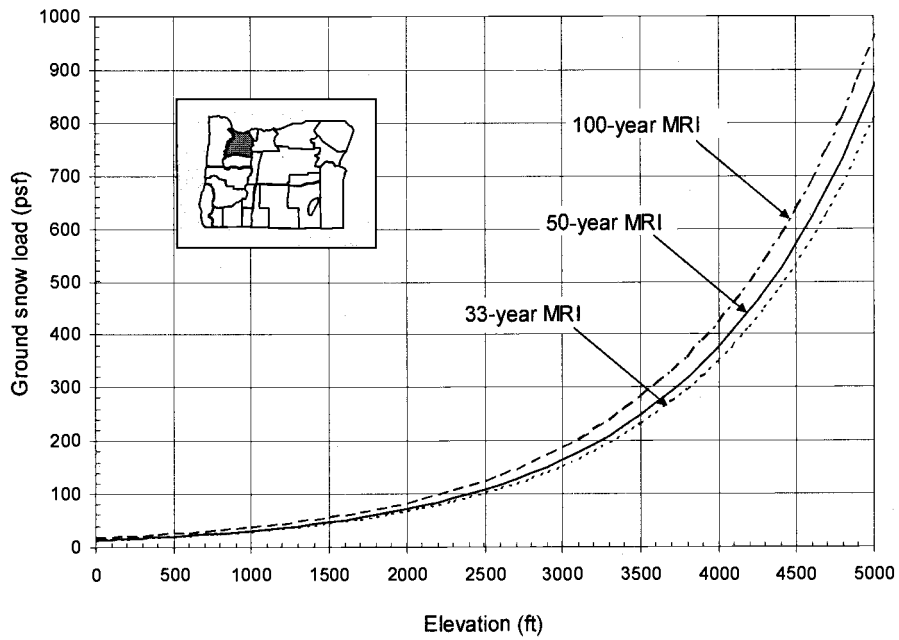
drift limits	structure	exposure	with the directionality factor			without the directionality factor		
			wind speed ⁽²⁾	λ ⁽³⁾	ξ ⁽⁴⁾	wind speed ⁽²⁾	λ ⁽³⁾	ξ ⁽⁴⁾
1%	TYPE-I	B	225	5.42	0.11	208	5.34	0.09
		C	210	5.35	0.11	193	5.26	0.09
		D	188	5.24	0.11	176	5.17	0.09
	TYPE-II ⁽¹⁾	B	168	5.12	0.11	173	5.15	0.09
		C	155	5.04	0.11	160	5.08	0.09
		D	142	4.96	0.11	147	4.99	0.09
	Type-III	B	186	5.23	0.11	175	5.16	0.09
		C	175	5.16	0.11	163	5.09	0.09
		D	157	5.06	0.11	149	5.00	0.09
2%	TYPE-I	B	247	5.51	0.11	230	5.44	0.09
		C	231	5.44	0.11	214	5.37	0.09
		D	211	5.35	0.11	194	5.27	0.09
	Type-III	B	210	5.35	0.11	195	5.27	0.09
		C	194	5.27	0.11	181	5.20	0.09
		D	177	5.18	0.11	165	5.11	0.09

- (1) TYPE-II was failed before 2% drift limit (3.84 in.)
(2) Obtained using median values of wind load statistics
(3) $\ln[\text{wind speed}^{(2)}]$
(4) average of ξ s in Table 3

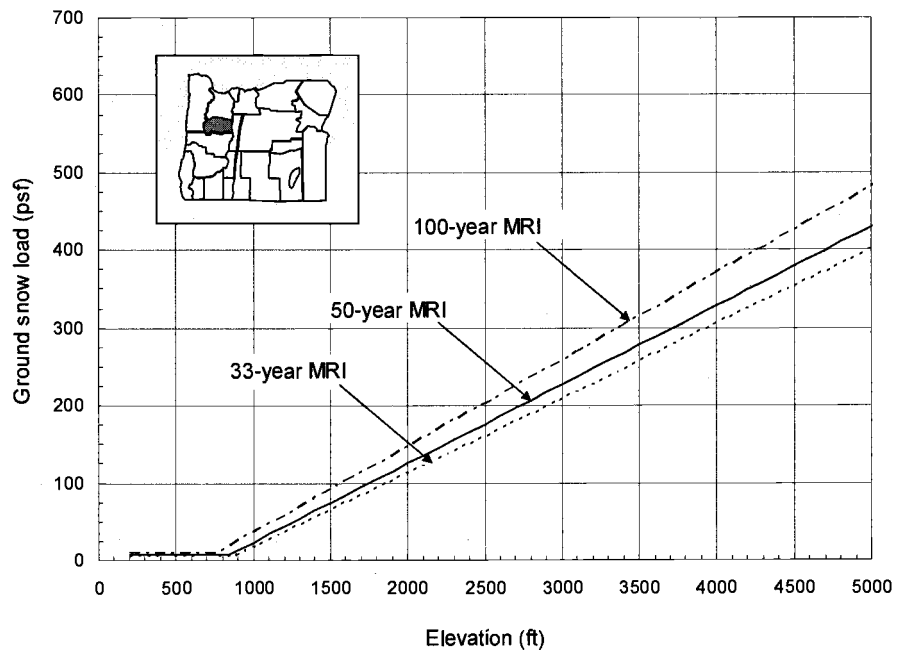
Appendix C.1 – Complete results for design ground snow load curves for Oregon



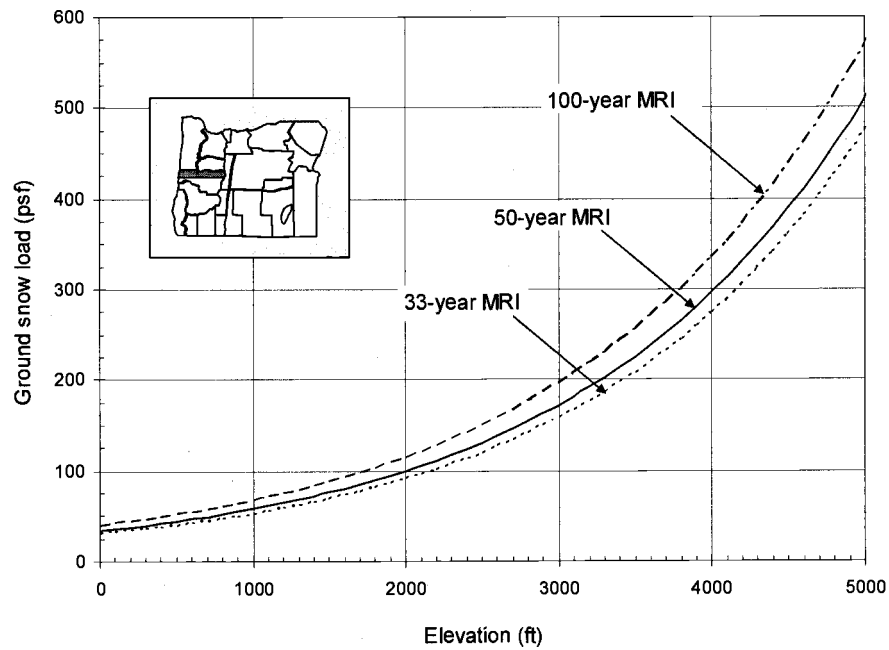
C.1(a) – Design ground snow load curves for G-01



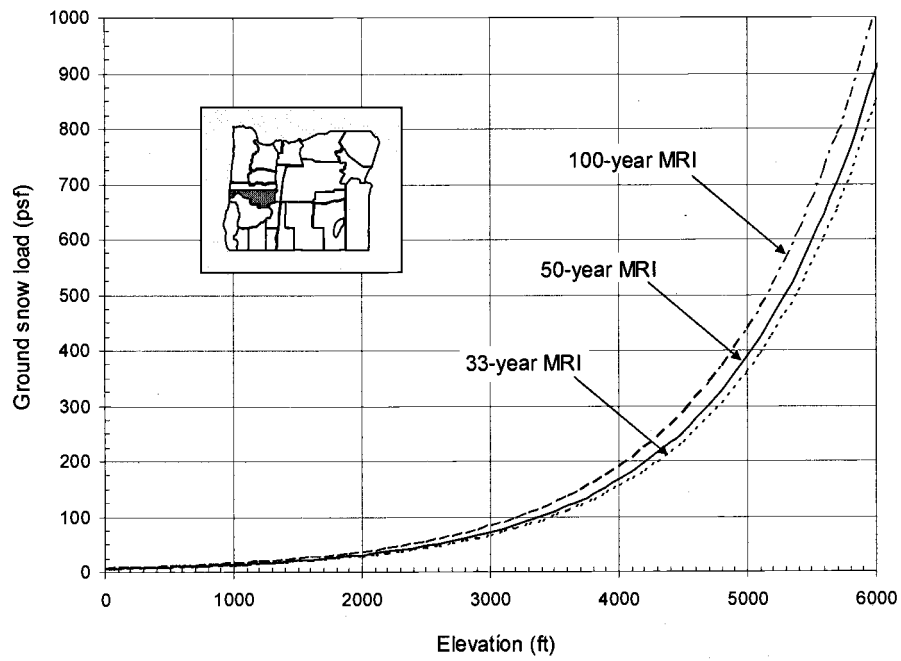
C.1(b) – Design ground snow load curves for G-02



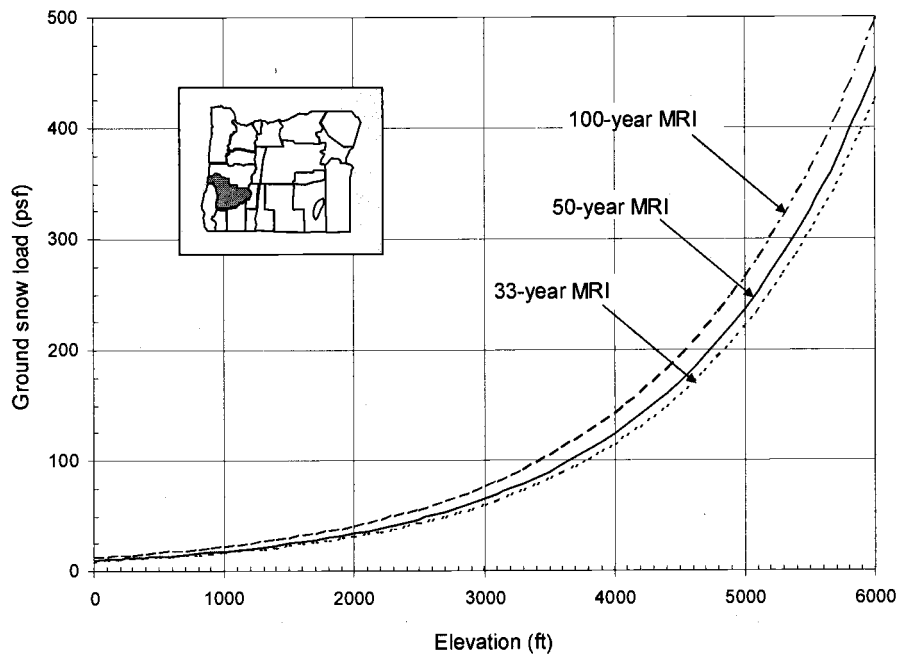
C.1(c) – Design ground snow load curves for G-03



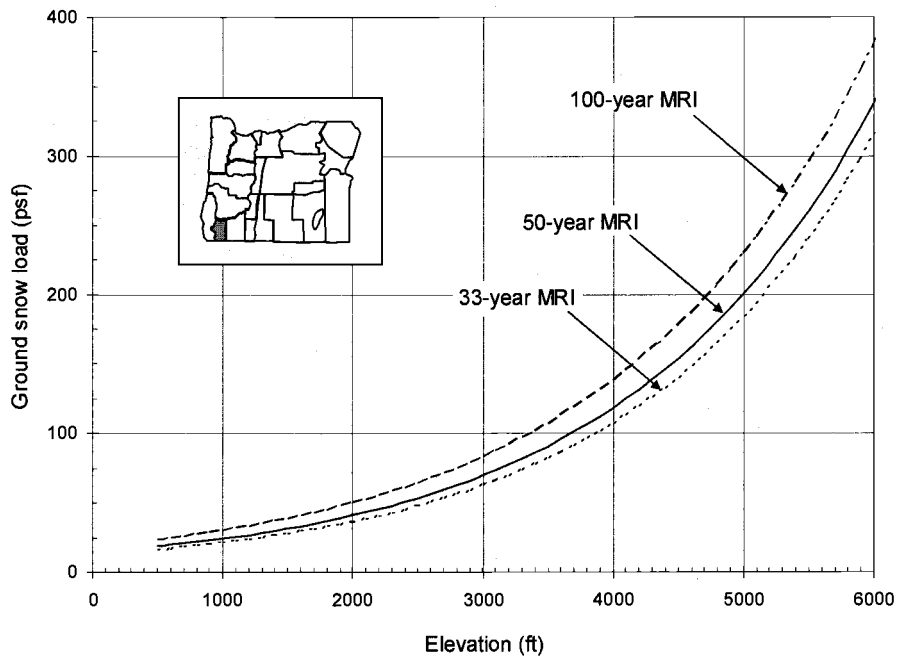
C.1(d) – Design ground snow load curves for G-04 (North)



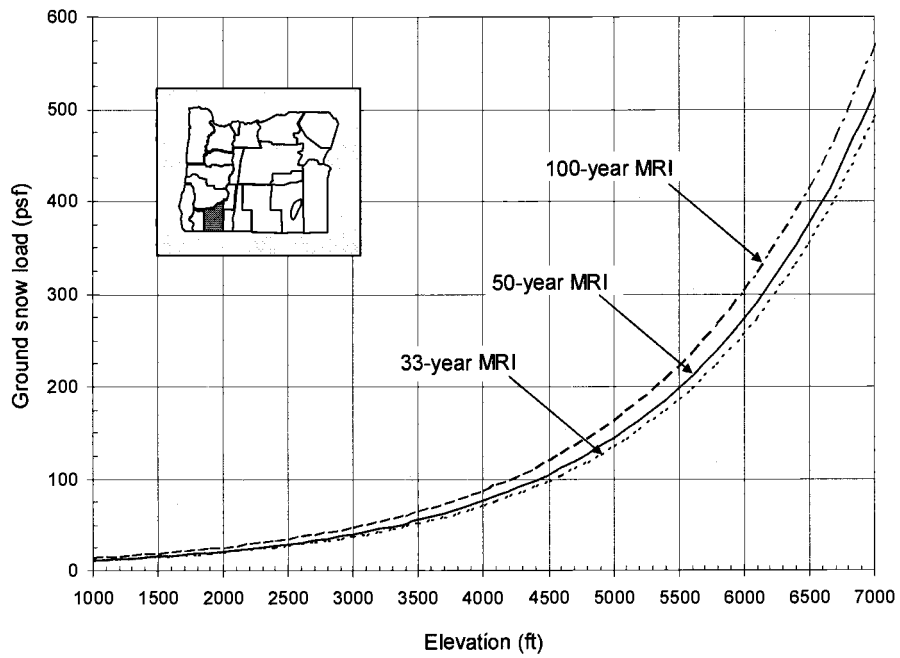
C.1(e) – Design ground snow load curves for G-04 (South)



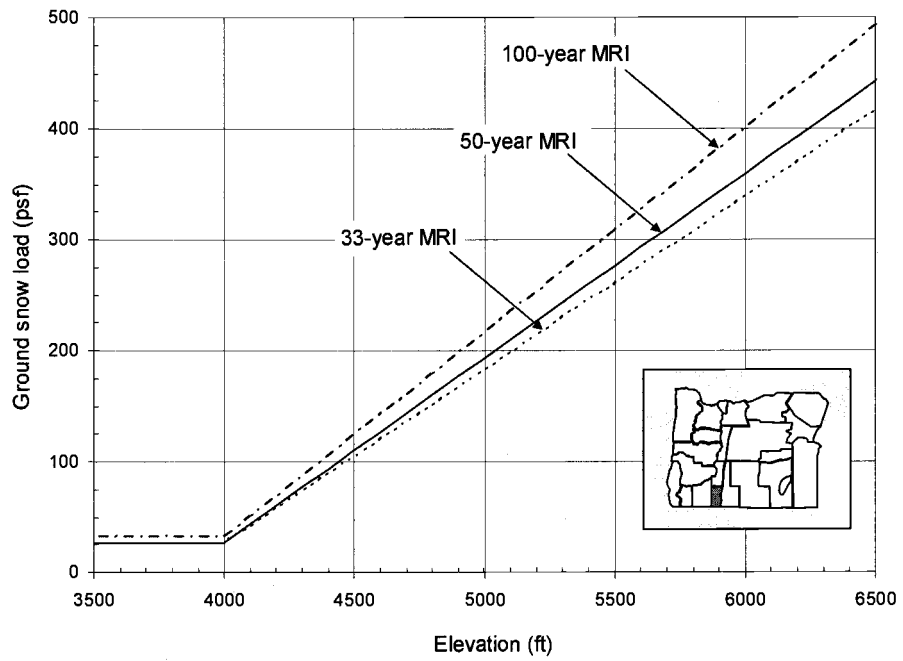
C.1(f) – Design ground snow load curves for G-05



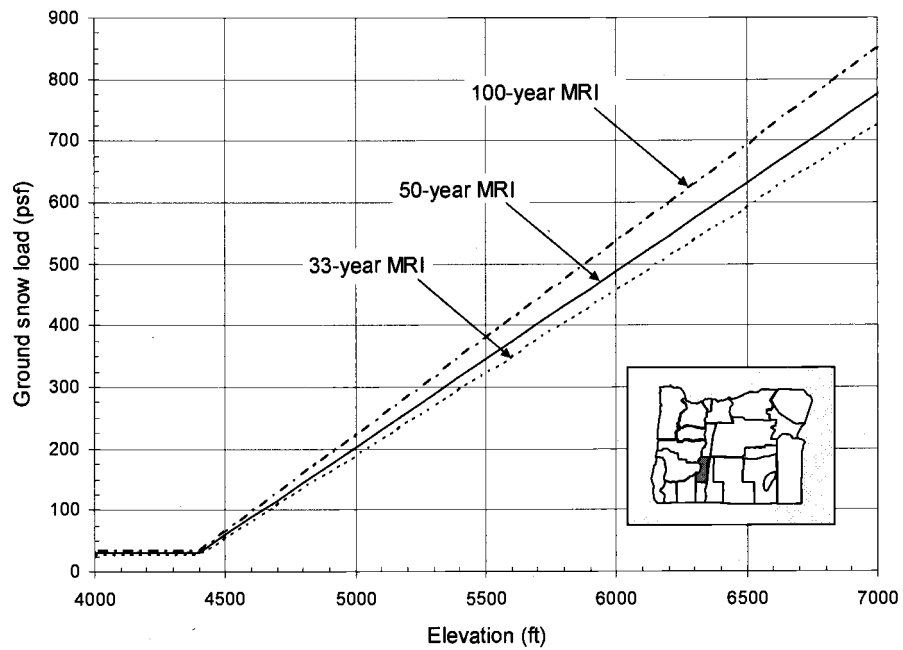
C.1(g) – Design ground snow load curves for G-06



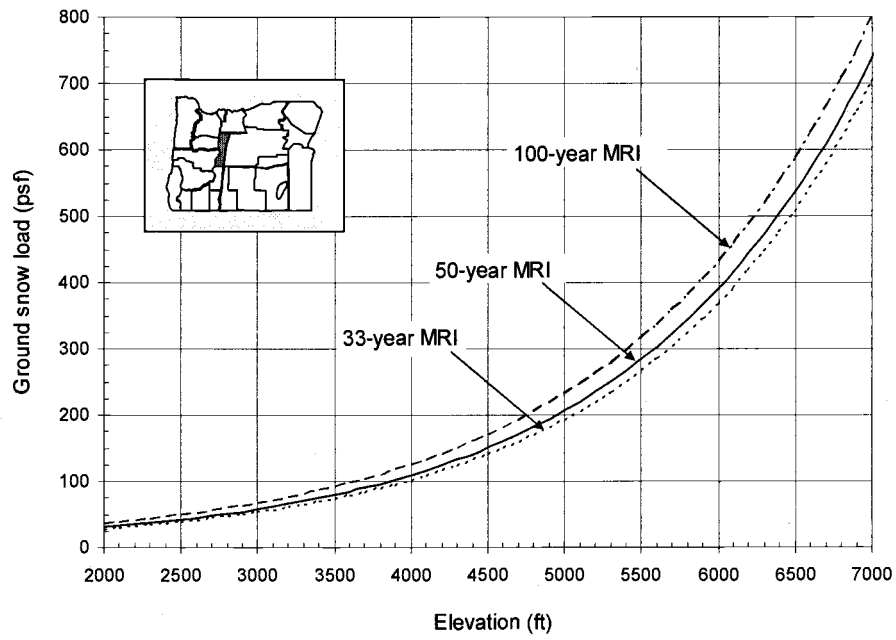
C.1(h) – Design ground snow load curves for G-07



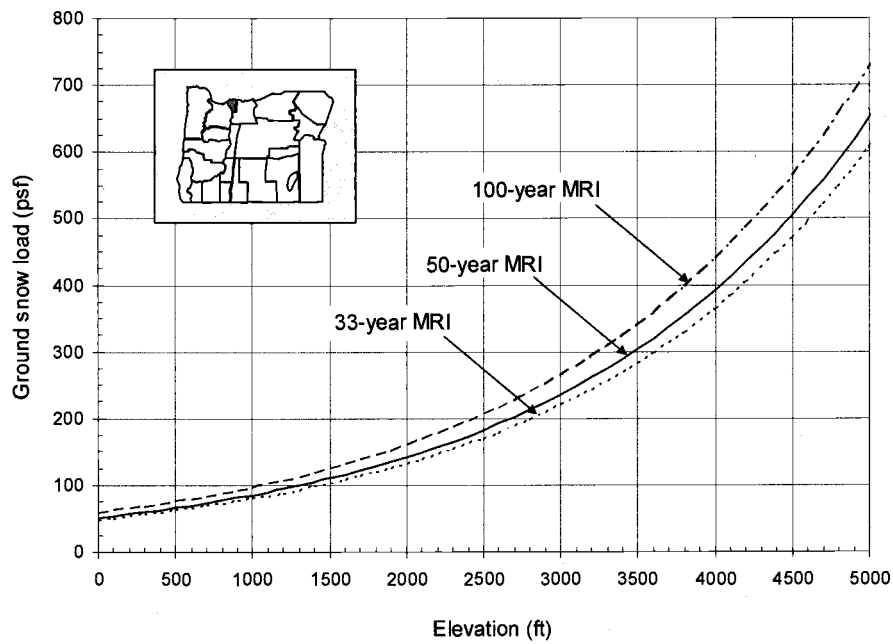
C.1(i) – Design ground snow load curves for G-08



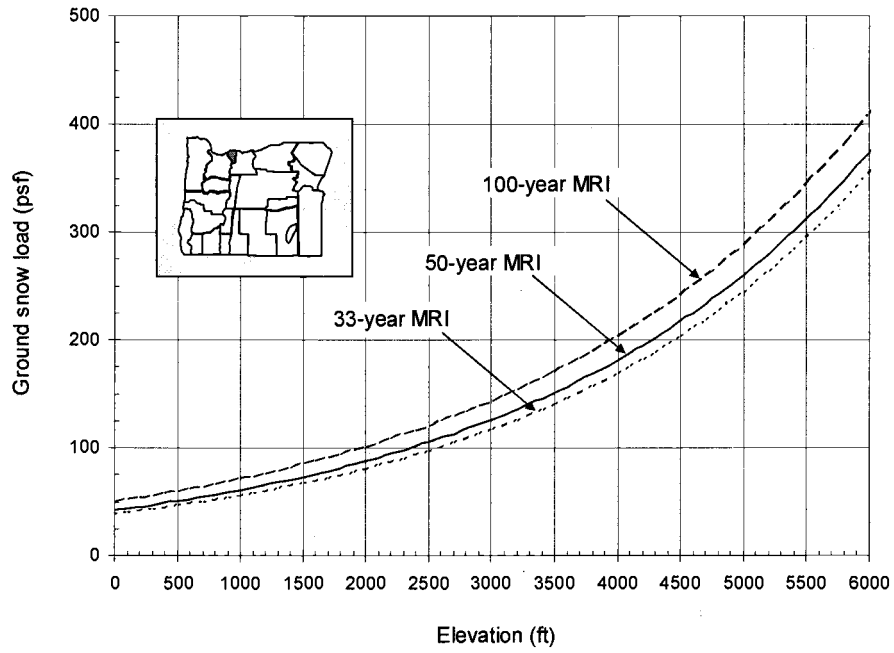
C.1(j) – Design ground snow load curves for G-09



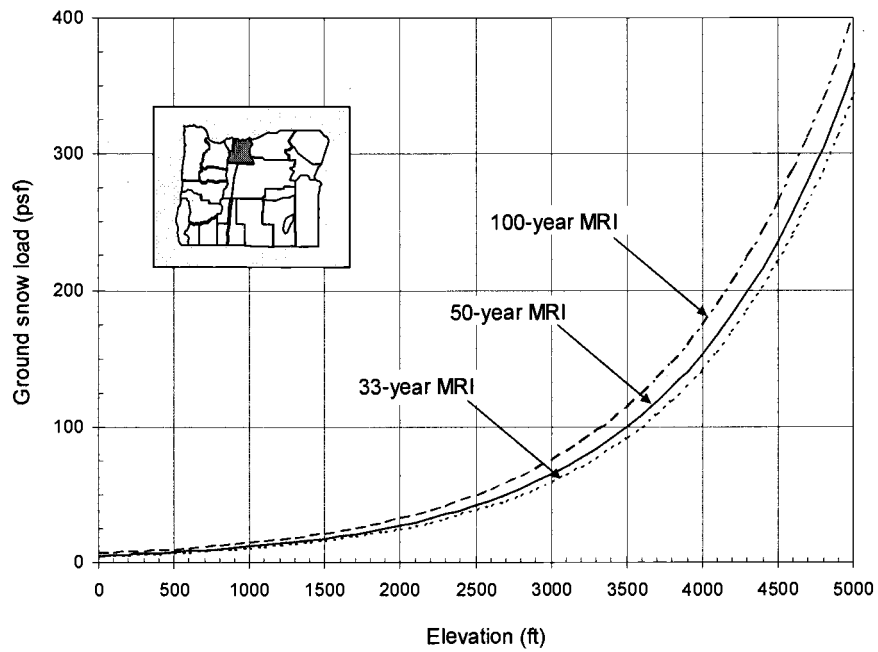
C.1(k) – Design ground snow load curves for G-10



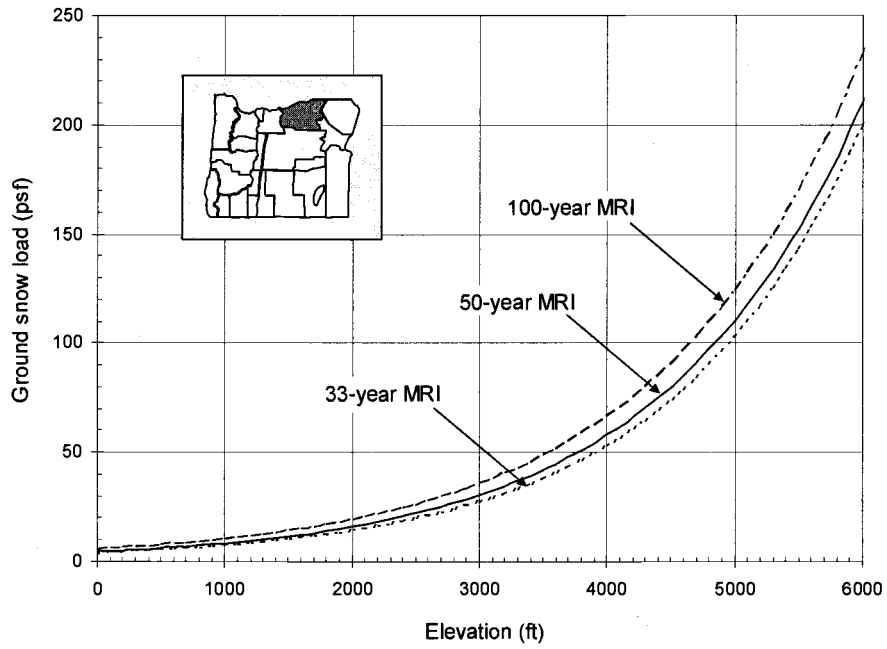
C.1(l) – Design ground snow load curves for G-11 (Hood River County)



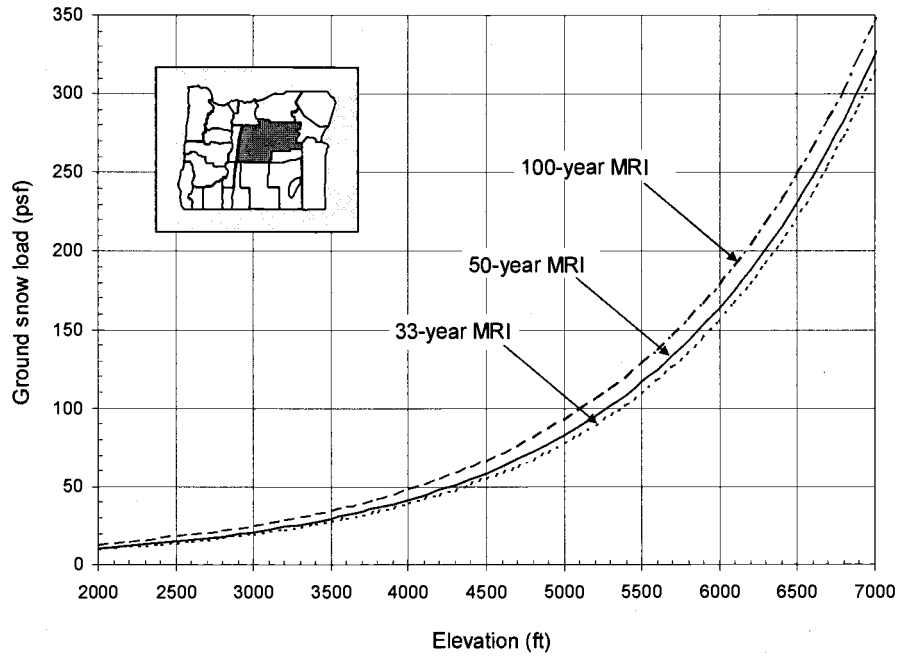
C.1(m) – Design ground snow load curves for G-11
(Rain Shadow - Northeast side of Mt. Hood only)



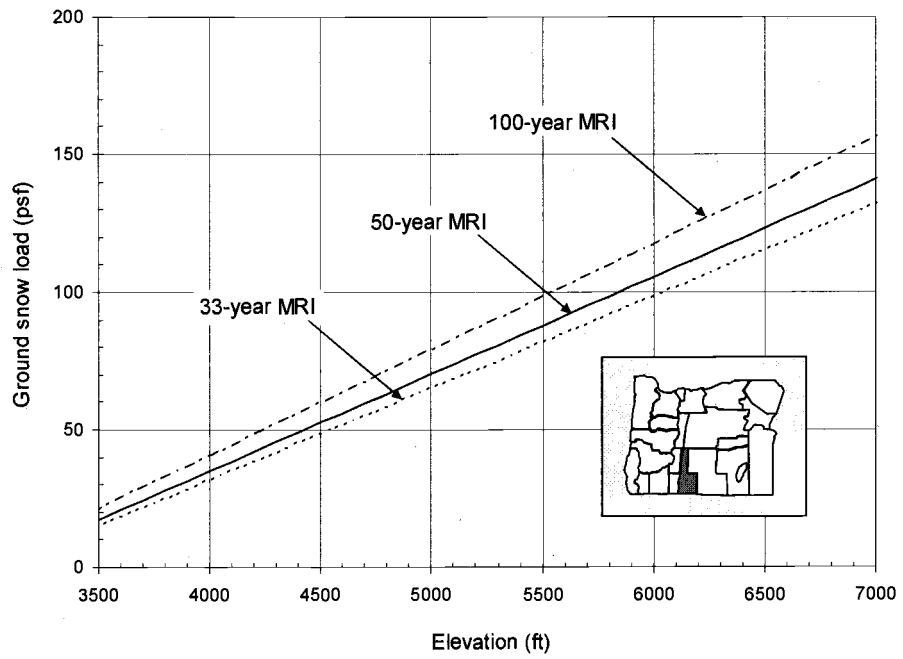
C.1(n) – Design ground snow load curves for G-12



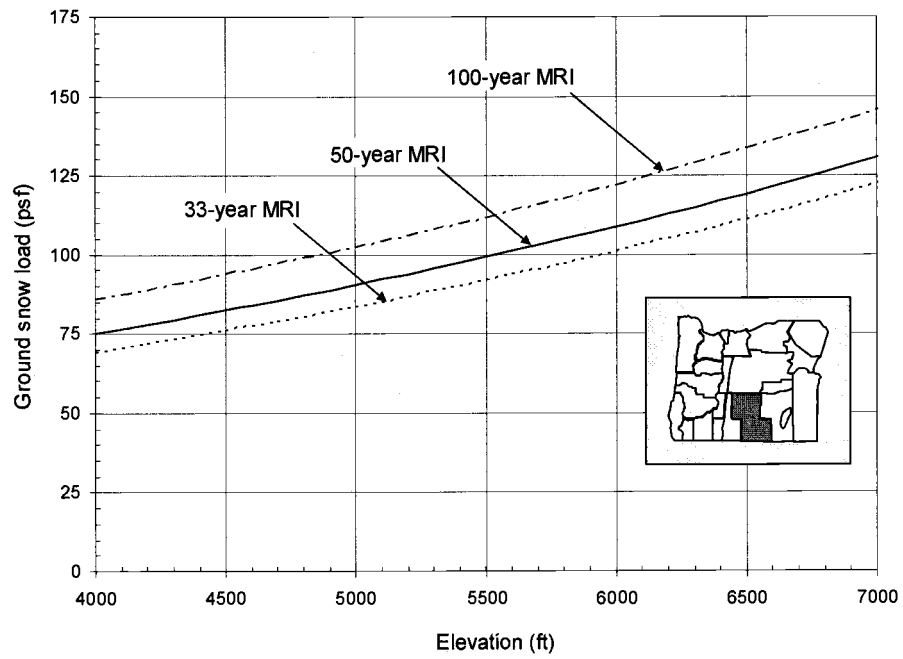
C.1(o) – Design ground snow load curves for G-13



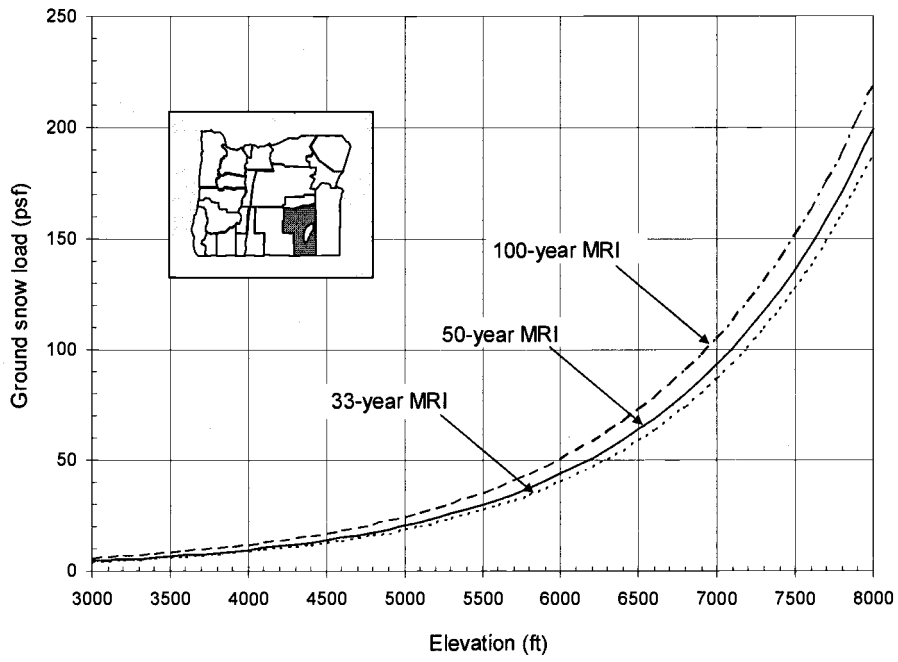
C.1(p) – Design ground snow load curves for G-14



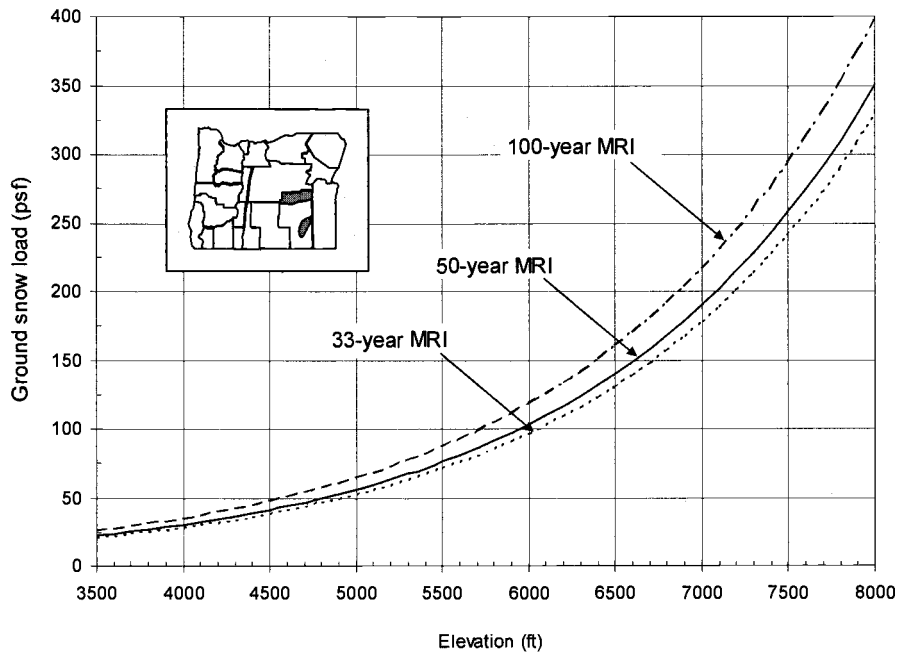
C.1(q) – Design ground snow load curves for G-15



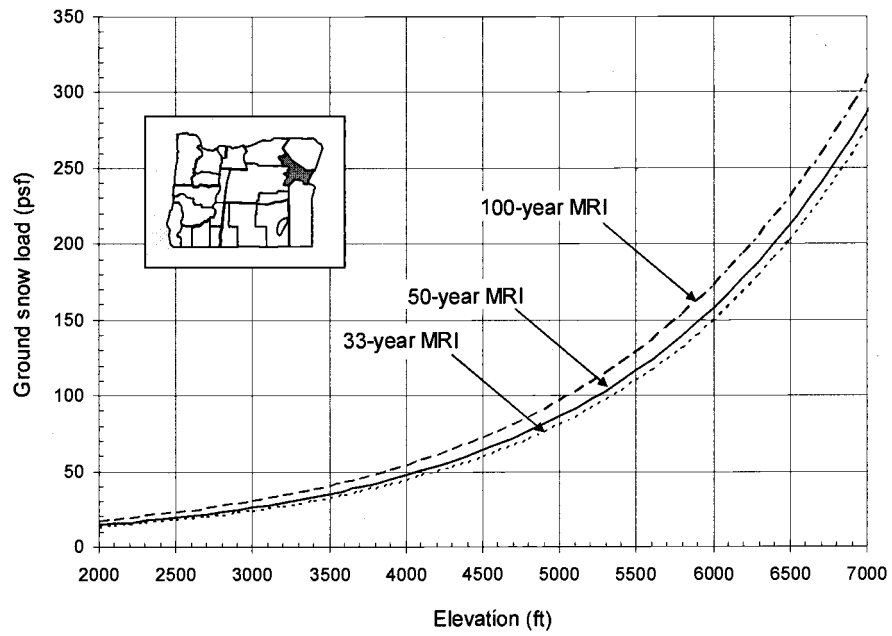
C.1(r) – Design ground snow load curves for G-16



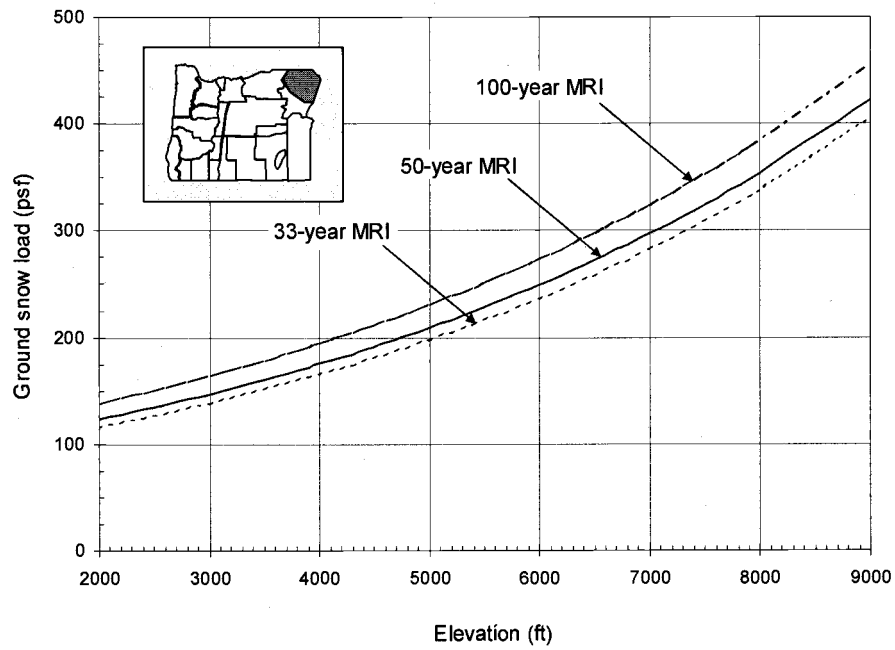
C.1(s) – Design ground snow load curves for G-17



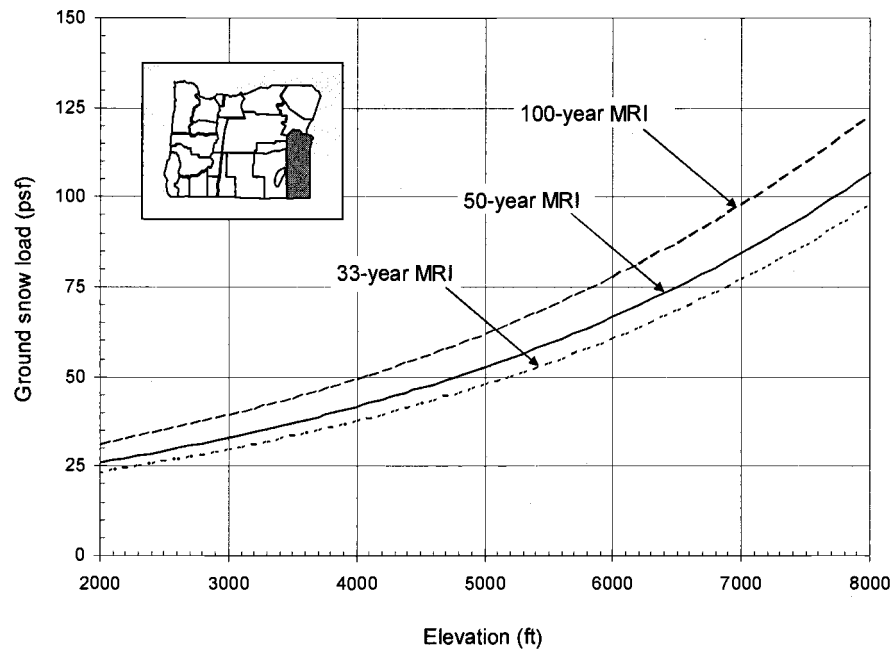
C.1(t) – Design ground snow load curves for G-18



C.1(u) – Design ground snow load curves for P-01

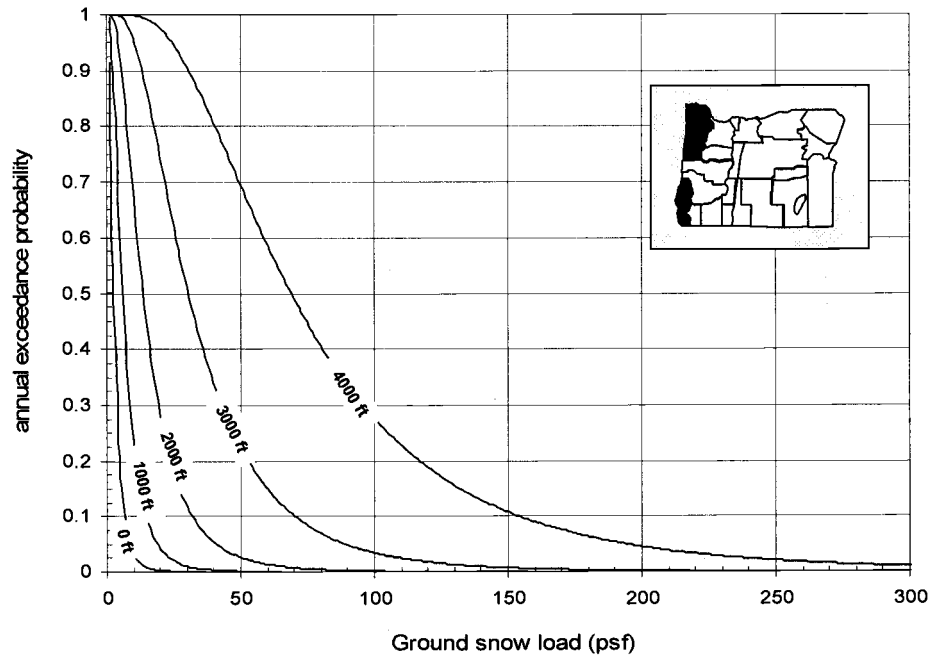


C.1(v) – Design ground snow load curves for P-02

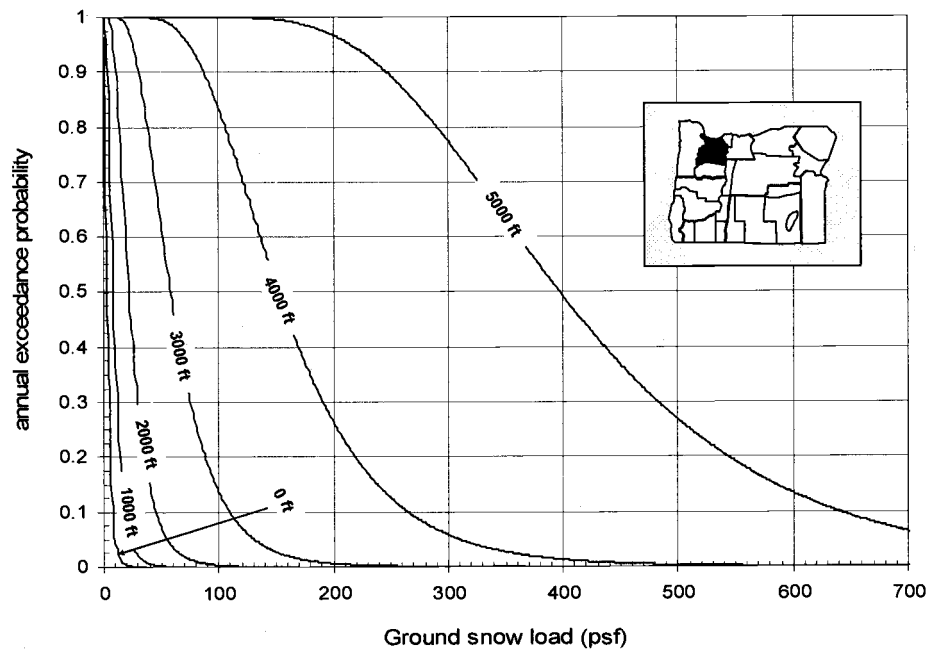


C.1(w) – Design ground snow load curves for G-23

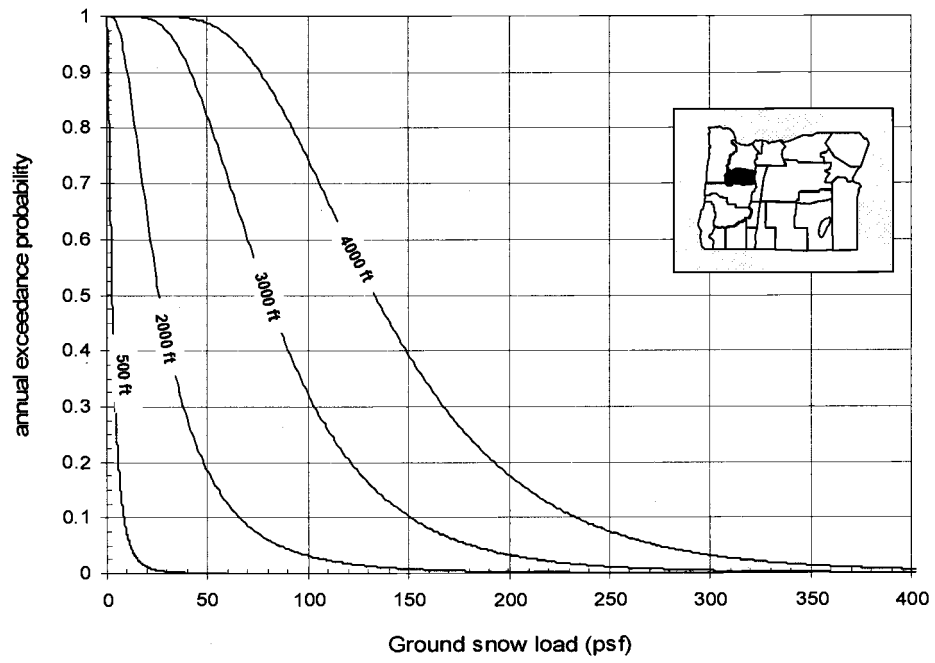
Appendix C.2 – Complete results for ground snow hazard curves for Oregon



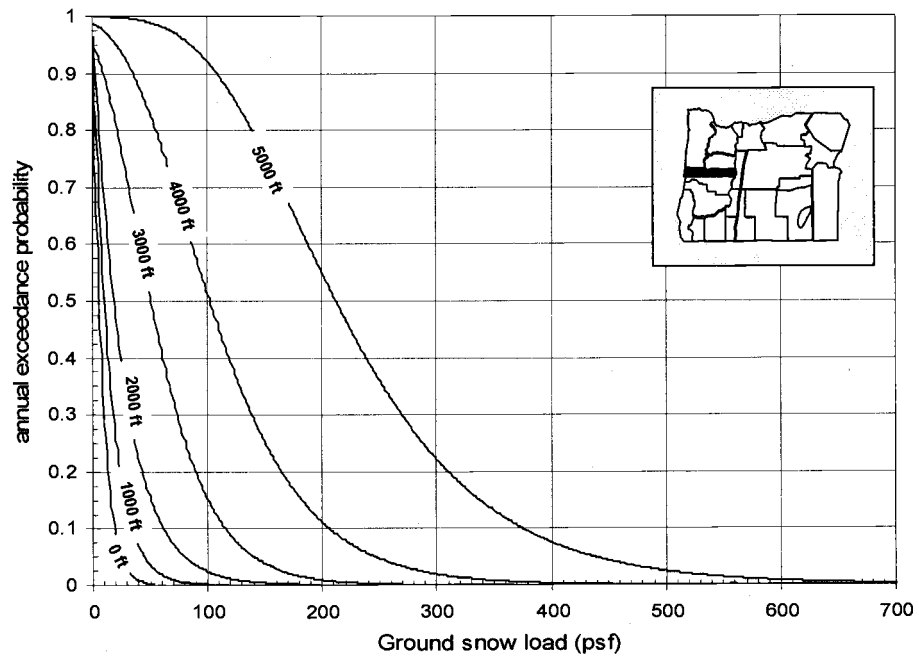
C.2(a) – Ground snow hazard curves for G-01



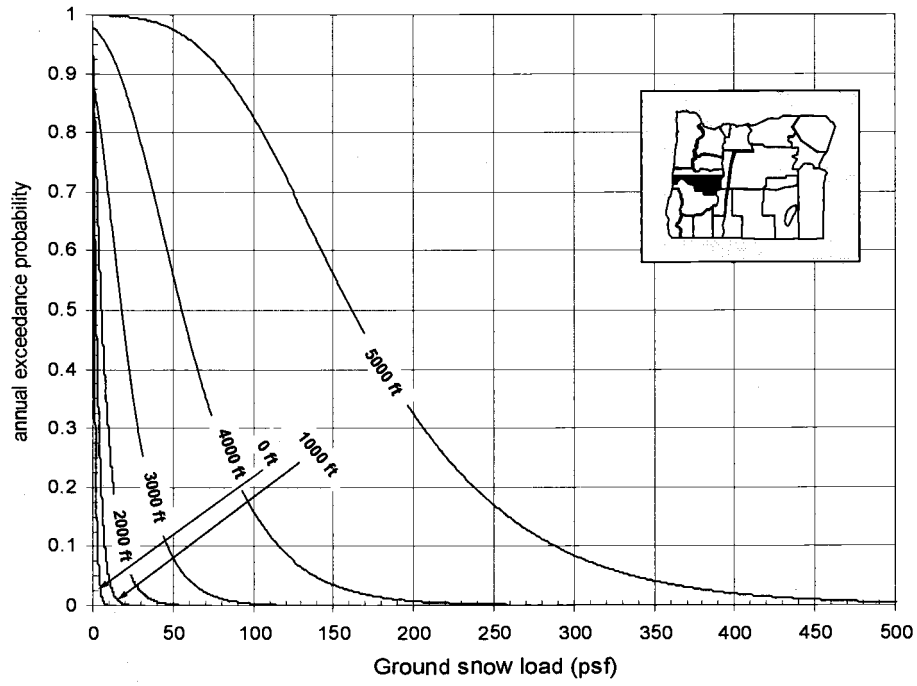
C.2(b) – Ground snow hazard curves for G-02



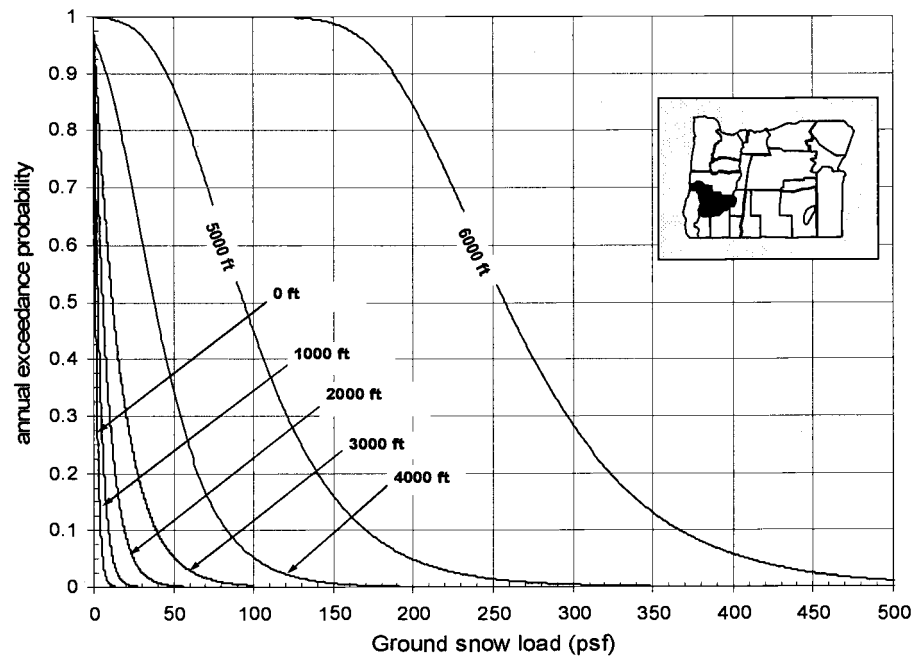
C.2(c) – Ground snow hazard curves for G-03



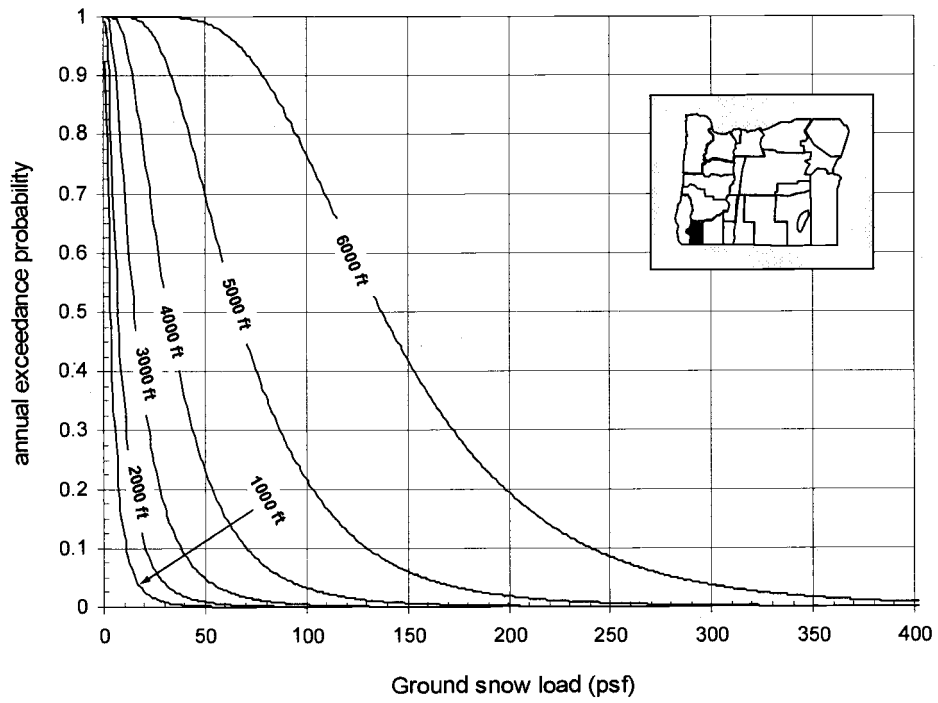
C.2(d) – Ground snow hazard curves for G-04 (North)



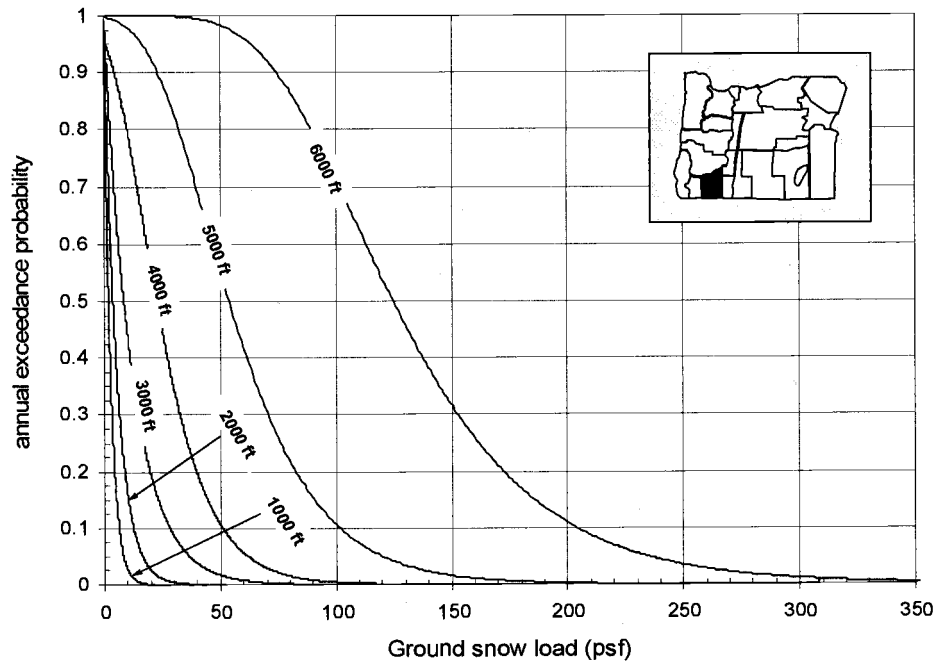
C.2(e) – Ground snow hazard curves for G-04 (South)



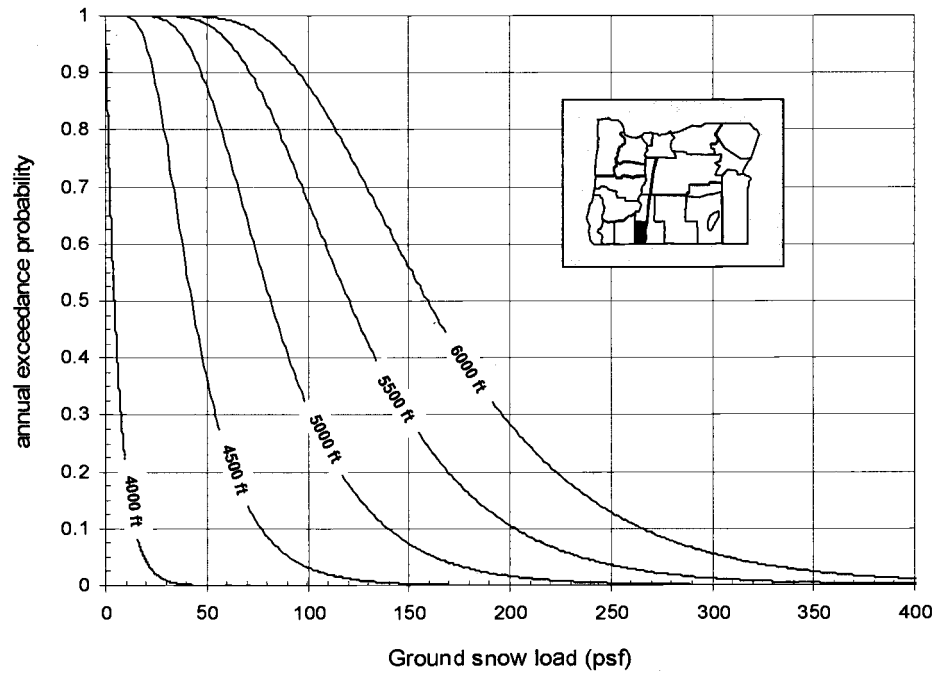
C.2(f) – Ground snow hazard curves for G-05



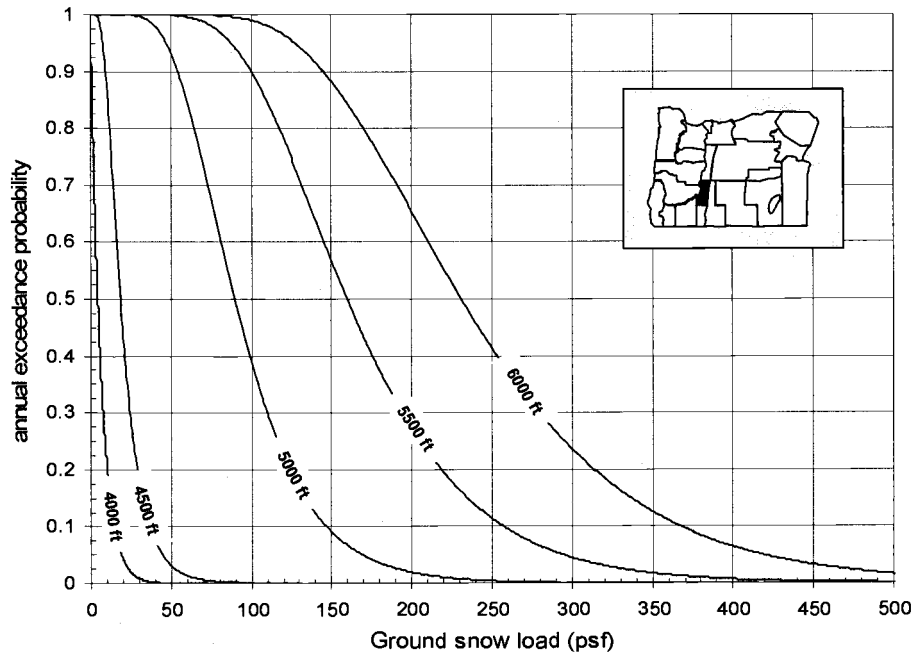
C.2(g) – Ground snow hazard curves for G-06



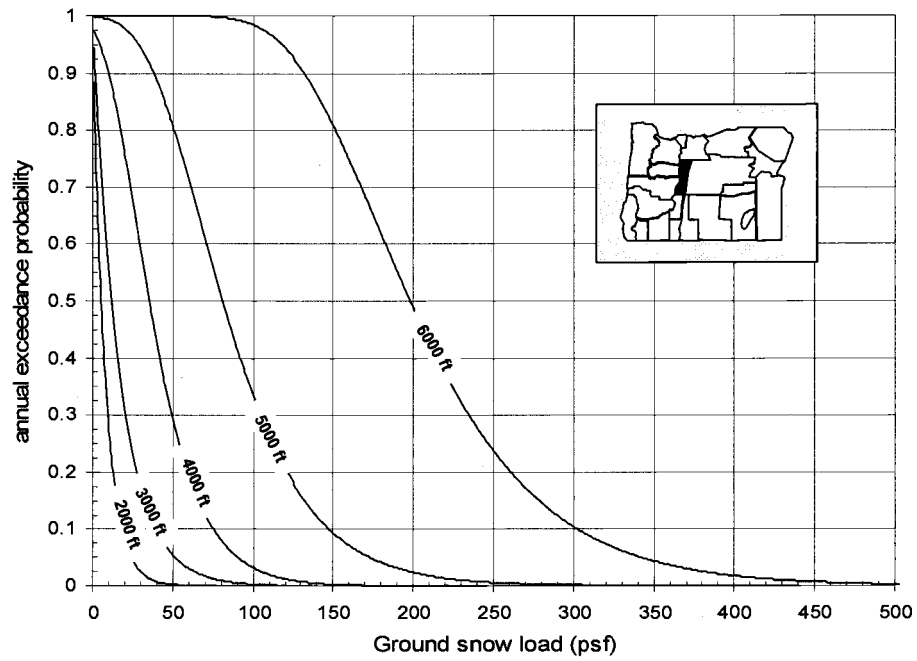
C.2(h) – Ground snow hazard curves for G-07



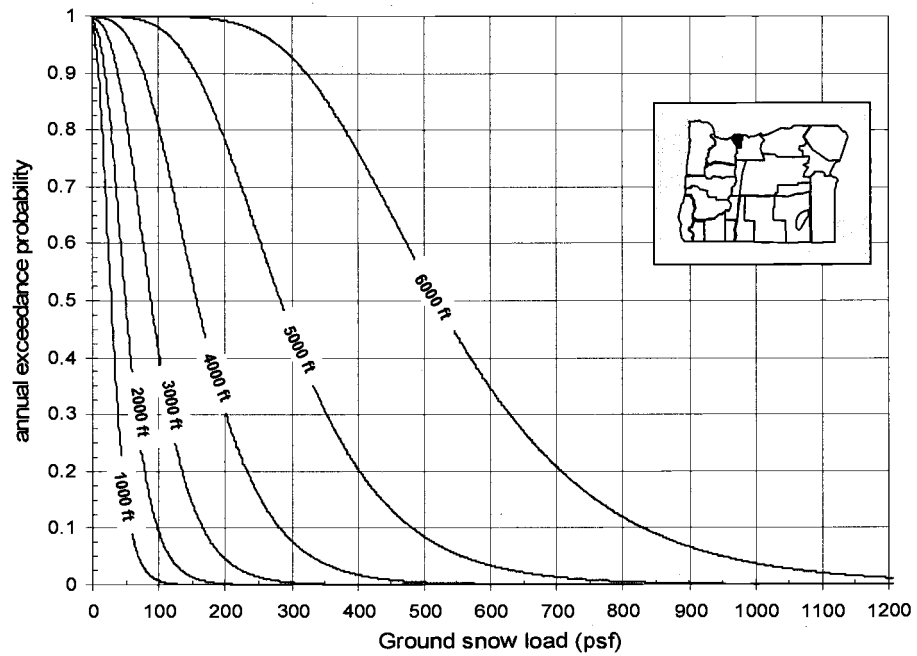
C.2(i) – Ground snow hazard curves for G-08



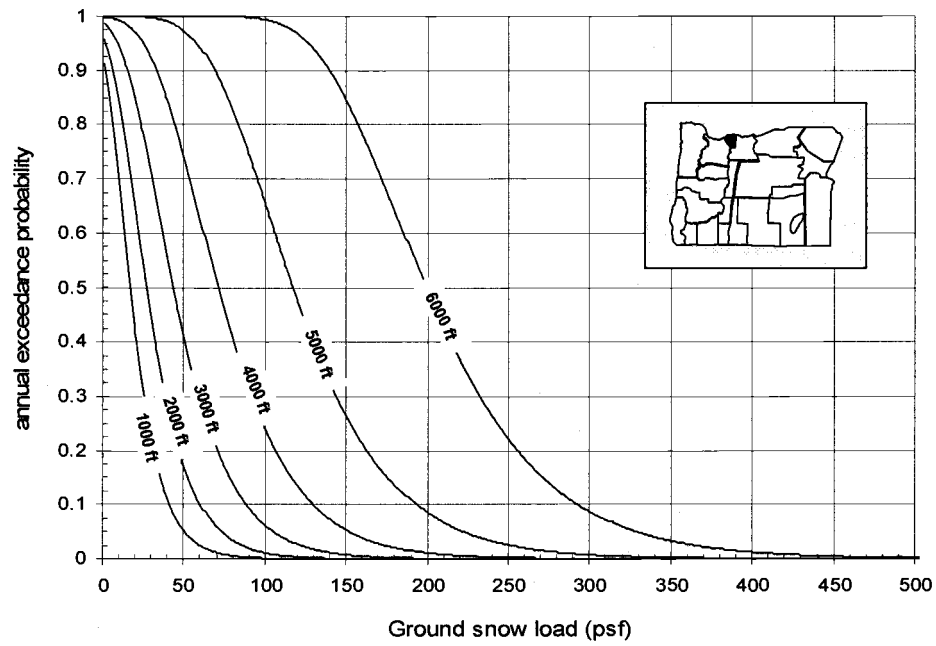
C.2(j) – Ground snow hazard curves for G-09



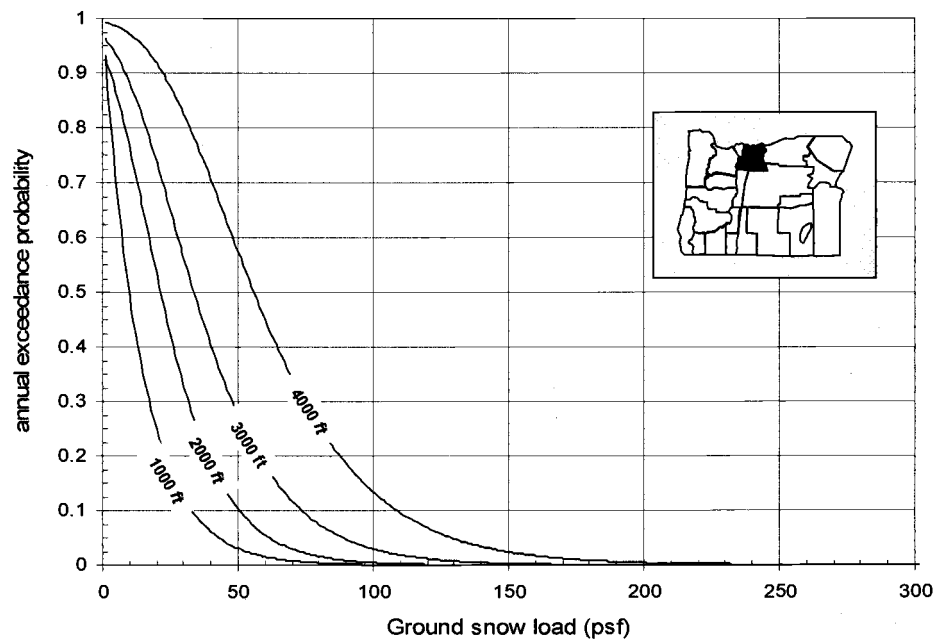
C.2(k) – Ground snow hazard curves for G-10



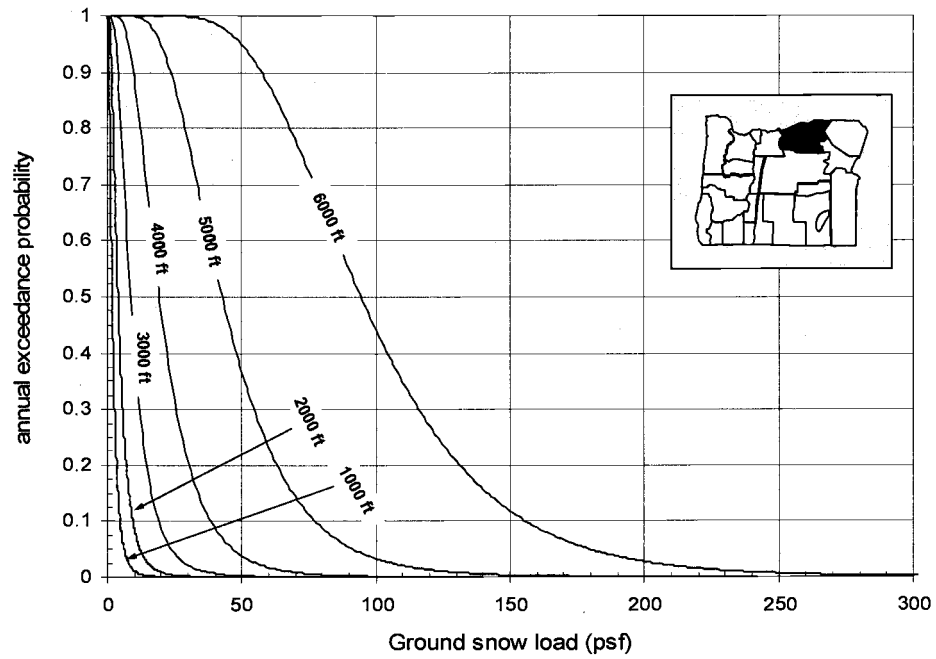
C.2(l) – Ground snow hazard curves for G-11 (Hood River County)



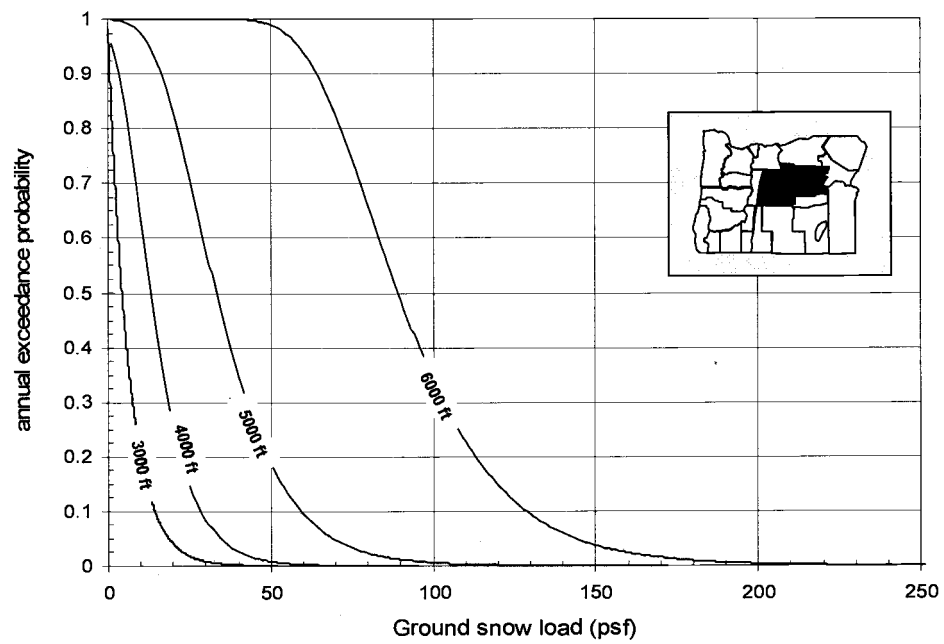
C.2(m) – Ground snow hazard curves for G-12
(Rain Shadow – Northeast of Mt. Hood only)



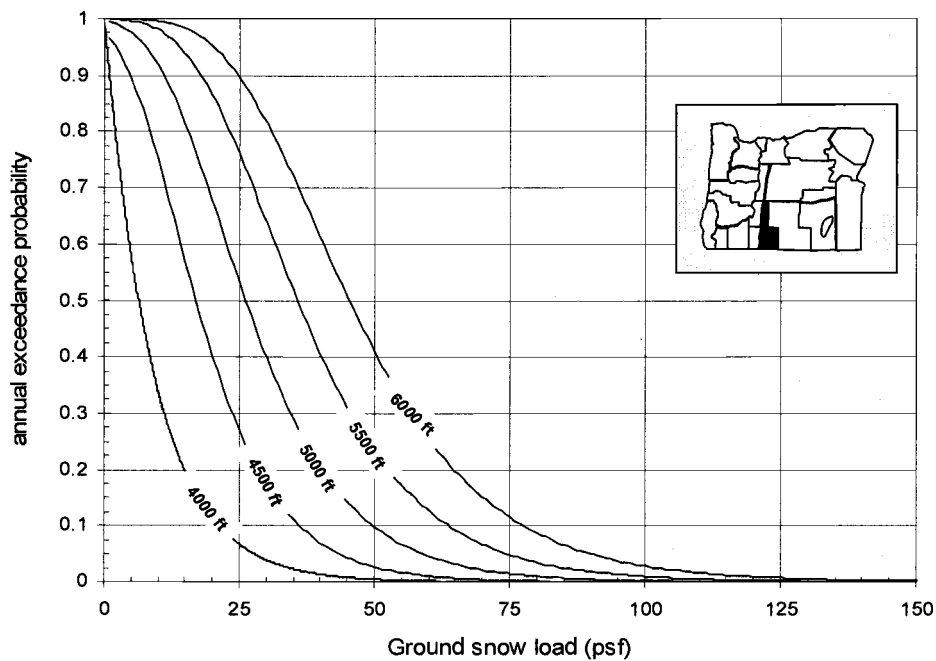
C.2(n) – Ground snow hazard curves for G-12



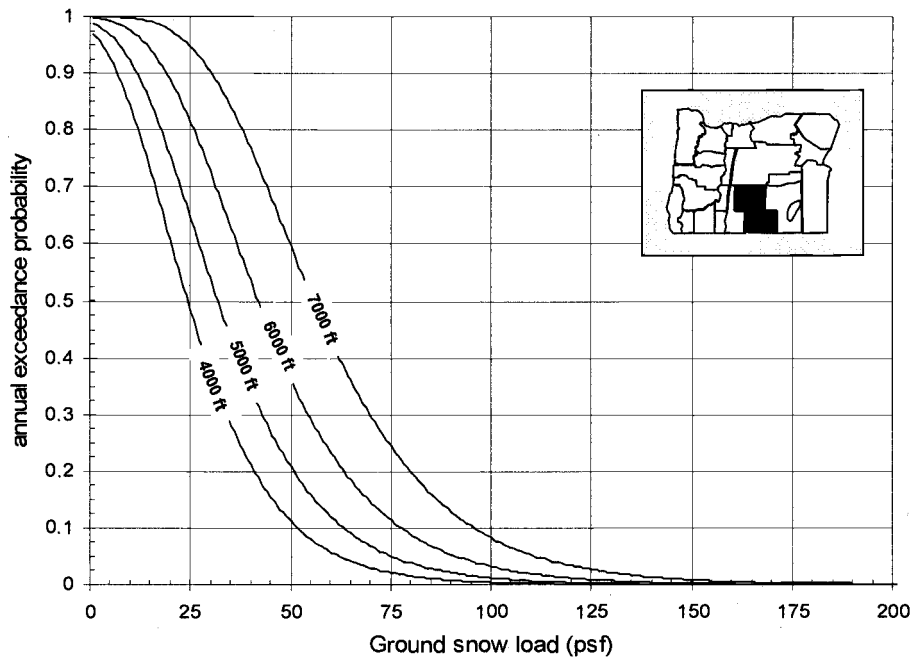
C.2 (o) – Ground snow hazard curves for G-13



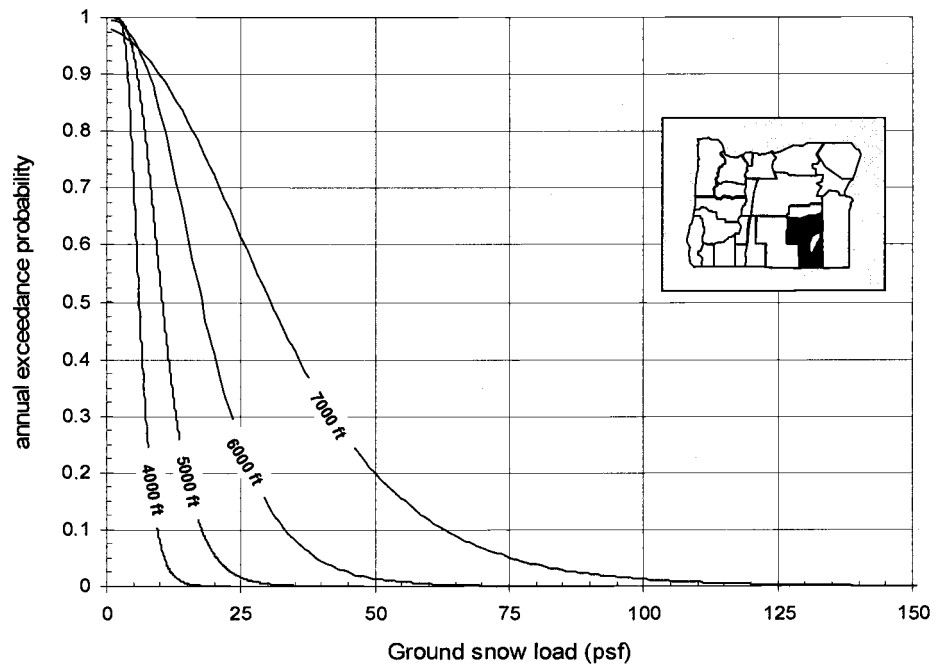
C.2 (p) – Ground snow hazard curves for G-14



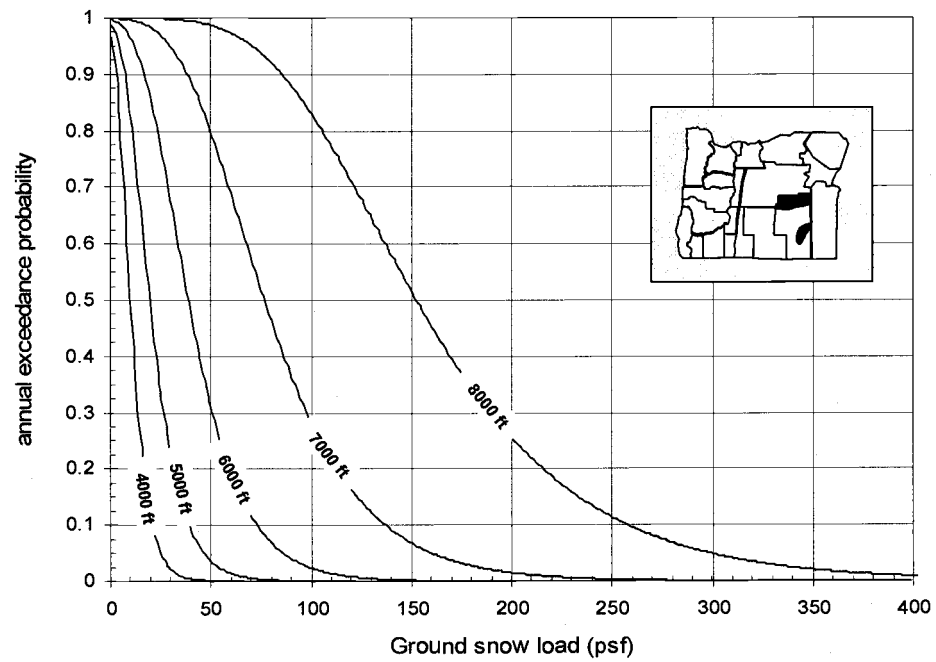
C.2 (q) – Ground snow hazard curves for G-15



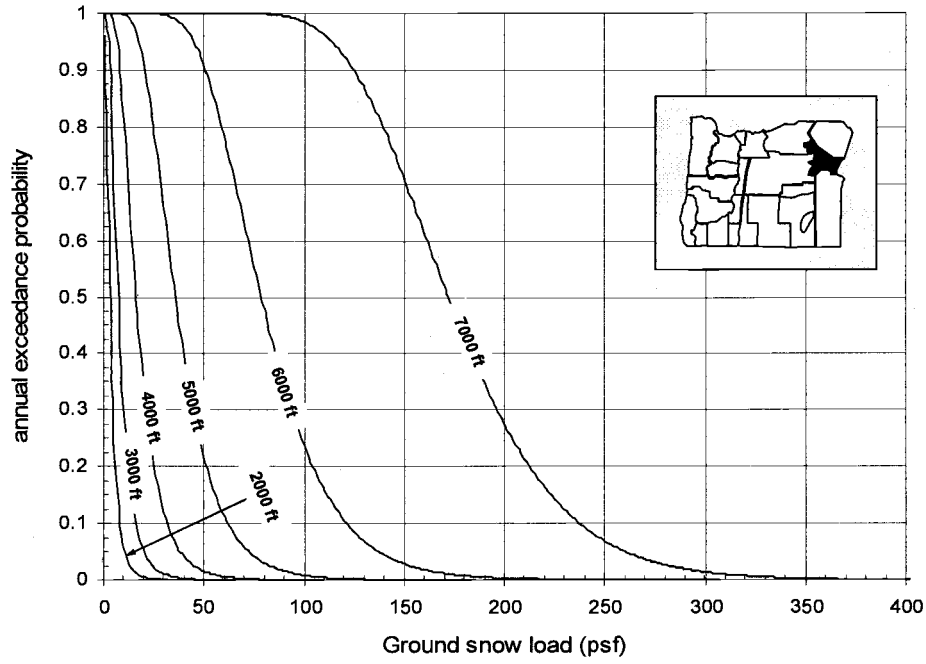
C.2 (r) – Ground snow hazard curves for G-16



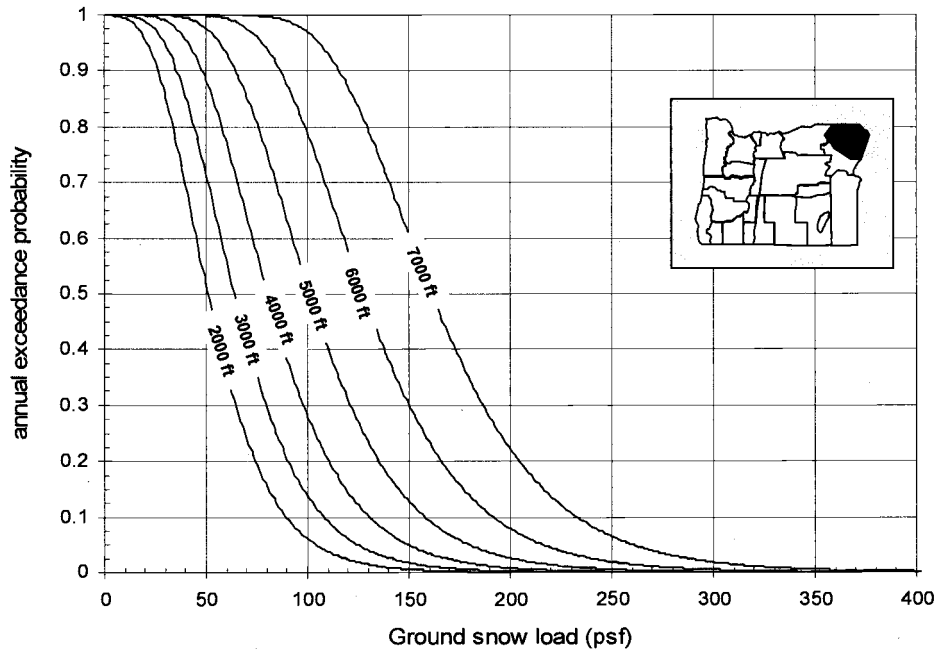
C.2(s) – Ground snow hazard curves for G-17



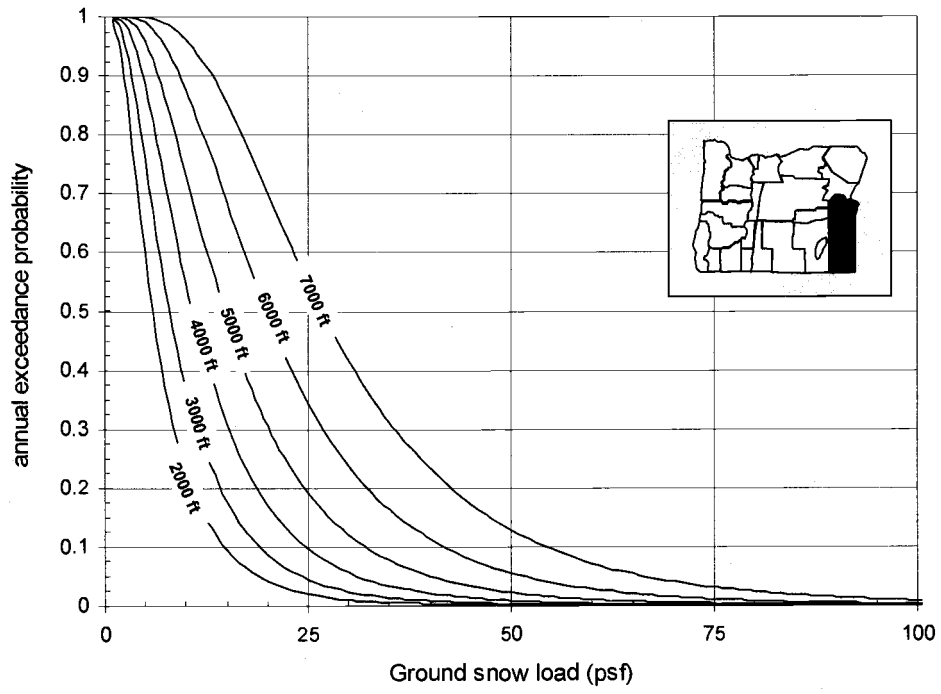
C.2(t) – Ground snow hazard curves for G-18



C.2(u) – Ground snow hazard curves for P-01

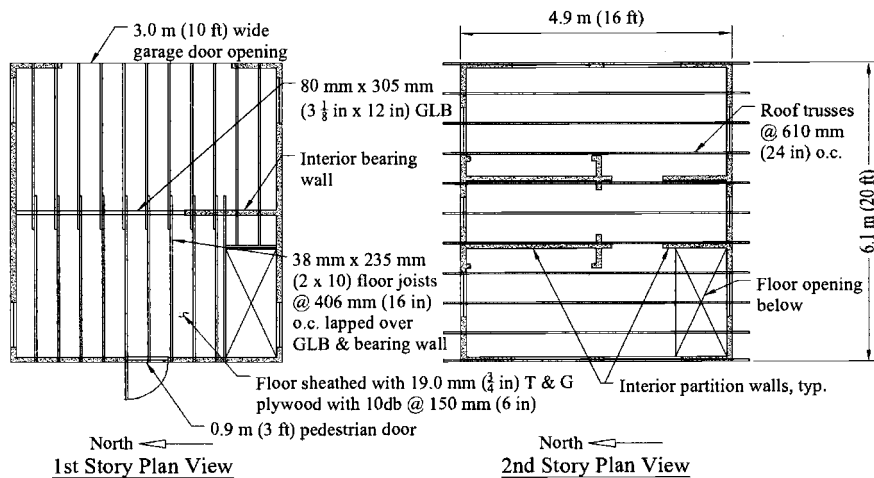
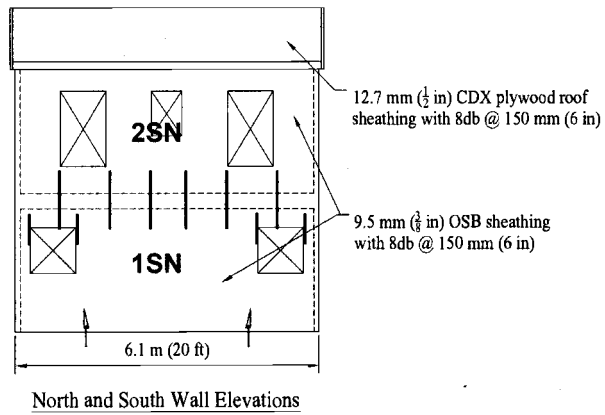
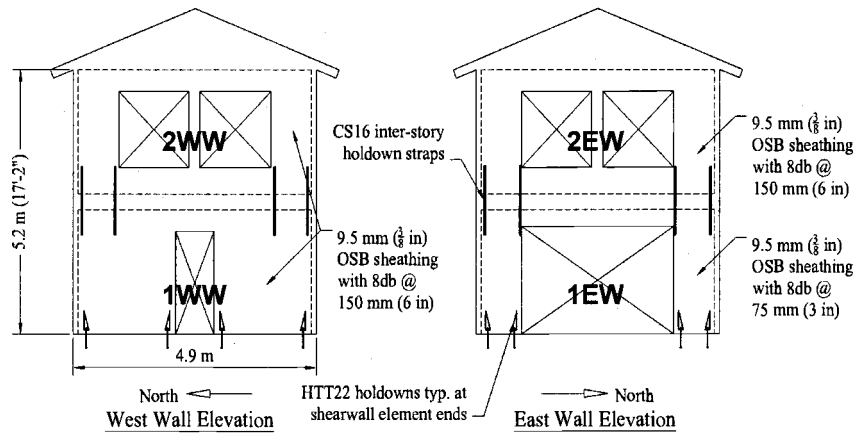


C.2(v) – Ground snow hazard curves for P-02



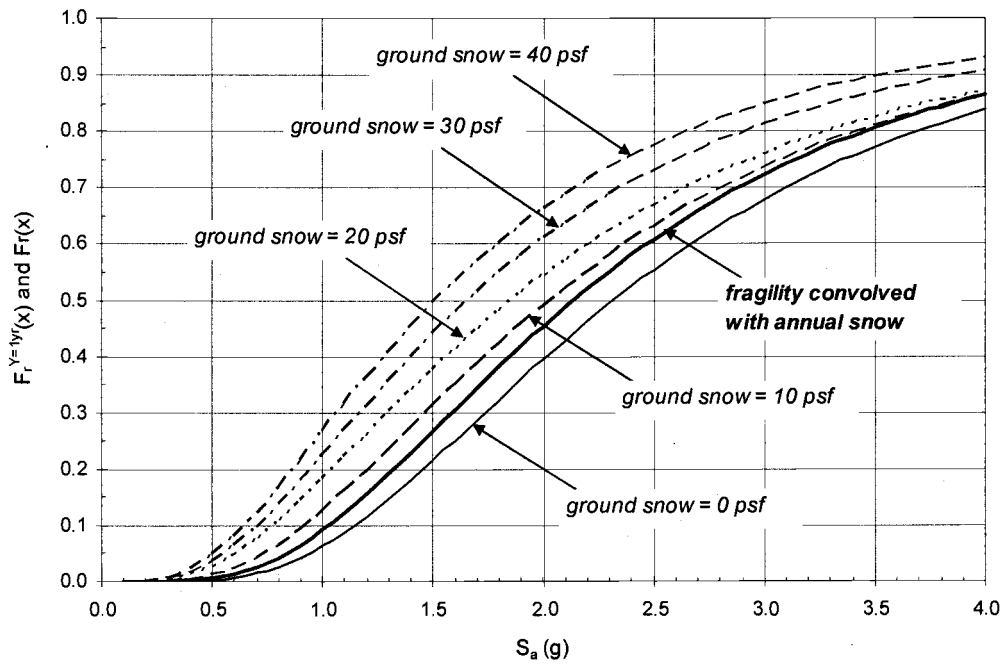
C.2(w) – Ground snow hazard curves for G-23

Appendix D.1 – Plan and section views for Type B Structure

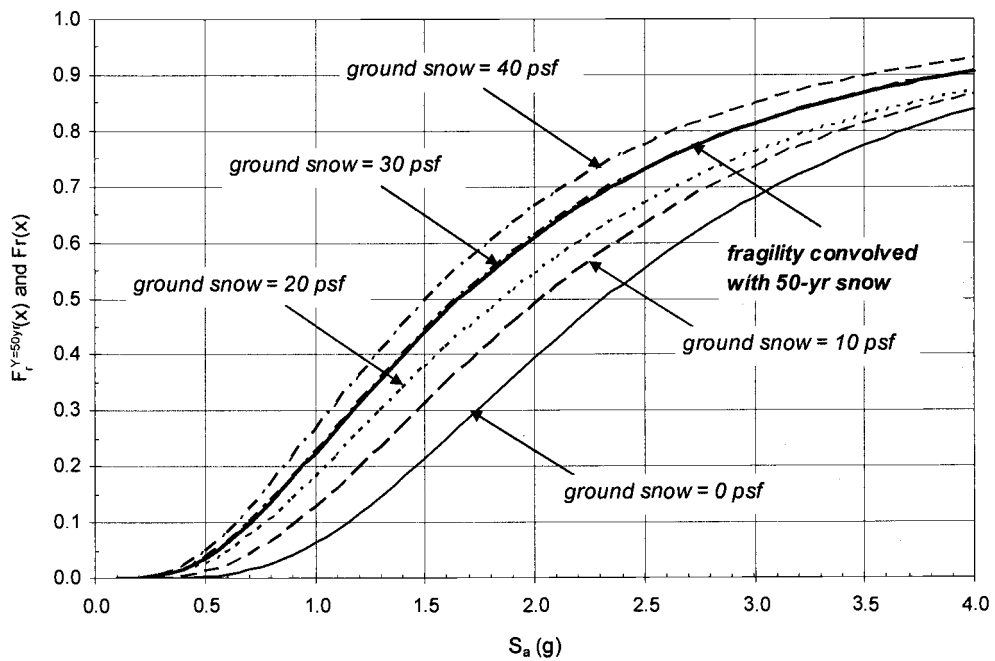


D.1 - Plan and section views for Type B Structure

Appendix D.2 – Comparisons of $F_r^{(Y=1yr)}(x)$ and $F_r^{(Y=50yr)}(x)$ with the fragility curves $F_r(x)$ in the case of Boston, MA



D.2(a) – Comparison of $F_r^{Y=1yr}(x)$ with $F_r(x)$
 [Type A building / Boston, MA / 2% drift limit]



D.2(b) – Comparison of $F_r^{Y=50yr}(x)$ with $F_r(x)$
 [Type A building / Boston, MA / 2% drift limit]